Gamma-Ray Bursts

Contents

1 Topics

- The “canonical” GRB: short vs long GRBs
- GRBs without SNe: binary mergers
- P-GRB dominated GRBs
- Prompt emission and X-ray flares: the clumpiness of CBM
- GRBs as distance indicators: the Amati relation
- The afterglow luminosity evolution over the EQTSs
- GRBs and SNe: the induced gravitational collapse

2 Participants

2.1 ICRANet participants

- David Arnett
- Maria Grazia Bernardini
- Carlo Luciano Bianco
- Pascal Chardonnet
- Valeri Chechetkin
- Massimo Della Valle
- Nino Panagia
- Elena Pian
- Remo Ruffini
- Gregory Vereshchagin
- She-Sheng Xue

2.2 Past collaborators

- Demetrios Christodoulou (ETH Zurich, Switzerland)
- Alessandra Corsi (INAF-IASF Roma, Italy)
- Thibault Damour (IHES, France)
- Federico Fraschetti (CEA Saclay, France)
- Vahe Gurzadyan (Yerevan Physics Institute, Armenia)
- Massimiliano Lattanzi (Oxford Astrophysics, UK)
- Giuliano Preparata (Università di Milano, Italy)
- Jay D. Salmonson (Livermore Lab, USA)
- Jim Wilson (Livermore Lab, USA)

2.3 Ongoing collaborations

- Alexey Aksenov (ITEP, Russia)
- Lorenzo Amati (INAF-IASF Bologna, Italy)
- Sabrina Casanova (MPIK, Germany)
- Alessandro Chieffi (INAF-IASF Roma, Italy)
- Guido Chincarini (Universit di Milano “BIcocca”, Italy)
- Stefano Covino (OAB, Italy)
- Filippo Frontera (Universit di Ferrara, Italy)
- Dafne Guetta (OAR, Italy)
- Cristiano Guidorzi (OAB, Italy)
- Stanislav Kelner (MEPhI, Russia, and MPIK, Germany)
- Marco Limongi (OAR, Italy)
- Vanessa Mangano (INAF-IASF Palermo, Italy)
- Susanna Vergani (Dunsink Observatory, Ireland)

2.4 Students

- Riccardo Belvedere (IRAP PhD, Italy)
- Letizia Caito (IRAP PhD, Italy)
- Maria Giovanna Dainotti (IRAP PhD, Italy)
- Gustavo de Barros (IRAP PhD, Brazil)
- Walter Ferrara (IRAP PhD, Italy)
- Roberto Guida (IRAP PhD, Italy)
- Barbara Patricelli (IRAP PhD, Italy)
- Luis Juracy Rangel Lemos (IRAP PhD, Brazil)
- Ivan Siutsou (IRAP PhD, Belarus)
- Wen-Biao Han (IRAP PhD, China)

3 Brief description

3.1 Highlights of the latest results

In the following highlights, out of the many thousands of GRBs, we focus on a special set of them, which are representative and can be considered prototypes for different families of sources. Contrary to the expectations, in fact, although the sources at first sight appear all different, after a closer theoretical analysis they can be divided in clear classes, of which we give in the following some prototypical examples. In particular, we are going to quote the results which have signed a discriminant between different theoretical model and have been essential in identifying the nature of GRB sources or their progenitors.

3.1.1 The "canonical" GRB: short vs long GRBs (GRB991216 and GRB 050315 as the prototypes)

Traditionally, GRBs are divided into two classes, "short" GRBs and "long" GRBs, arranged in a bimodal distribution with a separation around a duration $T_{90} \sim 2$s (Klebesadel, 1992; Dezalay et al., 1992). We recall that T_{90} is the time in which it is emitted the 90% of the energy of the event.

In Ruffini et al. (2001b) we proposed that both short and long GRBs are created by the same process of gravitational collapse to a black hole. The energy source is the $e^{\pm}$ plasma created in the process of the black hole formation, which reaches thermal equilibrium on a time scale on the order of $\sim 10^{-13}$ s (Aksenov et al., 2007) and then it expands as an optically thick and spherically symmetric "fireshell" with a constant width in the laboratory frame, i.e. the frame in which the black hole is at rest (Ruffini et al., 1999, 2000). There are only two free parameters characterizing the source within our model (Ruffini et al., 2000, 2001b, 2007a):

- the total energy $E^{tot}_{e^{\pm}}$ of the $e^{\pm}$ plasma forming the self-accelerating optically thick fireshell
- the fireshell baryon loading $B \equiv M_B c^2 / E^{tot}_{e^{\pm}}$, where M_B is the total baryons' mass.

These two parameters fully determine the optically thick self-acceleration phase of the fireshell, which lasts until the transparency condition is reached and the Proper-GRB (P-GRB) is emitted. After the transparency point the self-acceleration phase ends and it remains only an optically thin fireshell of baryonic matter ballistically expanding with an initially ultrarelativistic velocity and loosing its kinetic energy via the interaction with the CircumBurst Medium (CBM).

Therefore, we define a "canonical GRB" light curve with two sharply different components (see Fig. 3.1 and Ruffini et al., 2001b, 2007a; Bernardini et al., 2007; Bianco et al., 2008a,b):

- **The P-GRB**, which is emitted when the optically thick fireshell becomes transparent. It depends only on $E_{e^\pm}^{tot}$ and B. It has the imprint of the black hole formation, an harder spectrum and no spectral lag (Bianco et al., 2001; Ruffini et al., 2005d).
- **the afterglow**, which is due to the collision between the leftover optically thin fireshell and the CBM (Ruffini et al., 2001b, 2007a; Bianco and Ruffini, 2004, 2005b,a). It depends on $E_{e^\pm}^{tot}$ and B but its temporal structure depends also on the additional parameters describing the effective CBM distribution: its density n_{cbm} and the ratio $\mathcal{R} \equiv A_{eff}/A_{vis}$ between the effective emitting area of the fireshell A_{eff} and its total visible area A_{vis}. It presents a clear hard-to-soft spectral evolution in time and it is composed by a rising part, a peak and a decaying tail (Ruffini et al., 2002a, 2004b, 2005c; Bernardini et al., 2005a; Ruffini et al., 2006b; Dainotti et al., 2007).

A major effort is currently being made in clarifying what in the literature is called "prompt emission" which, within our theory, is composed by both the P-GRB and the peak of the afterglow (see Fig. 3.1).

The ratio between the total time-integrated luminosity of the P-GRB (namely, its total energy) and the corresponding one of the afterglow is the crucial quantity for the identification of GRBs' nature (Ruffini et al., 2001b):

- When $B \leq 10^{-5}$ we have a P-GRB dominated event (in the limit $B \to 0$ the afterglow vanishes).
- In the opposite limit, for $10^{-4} \leq B \leq 10^{-2}$ we have an afterglow dominated GRB, and this is indeed the case of most of the GRBs we have recently examined (see e.g. Fig. 3.2).

Our effort on this topic is currently threefold (see details in section H.1):

- The so-called "prompt emission" light curves of many GRBs present a small pulse preceding the main GRB event, with a lower peak flux and separated by this last one by a quiescent time. The nature of such GRB "precursors" is one of the most debated issues in the current literature (see Burlon et al., in press). Our aim is to show, by direct computations within our model of the temporal separation and intensity ratio

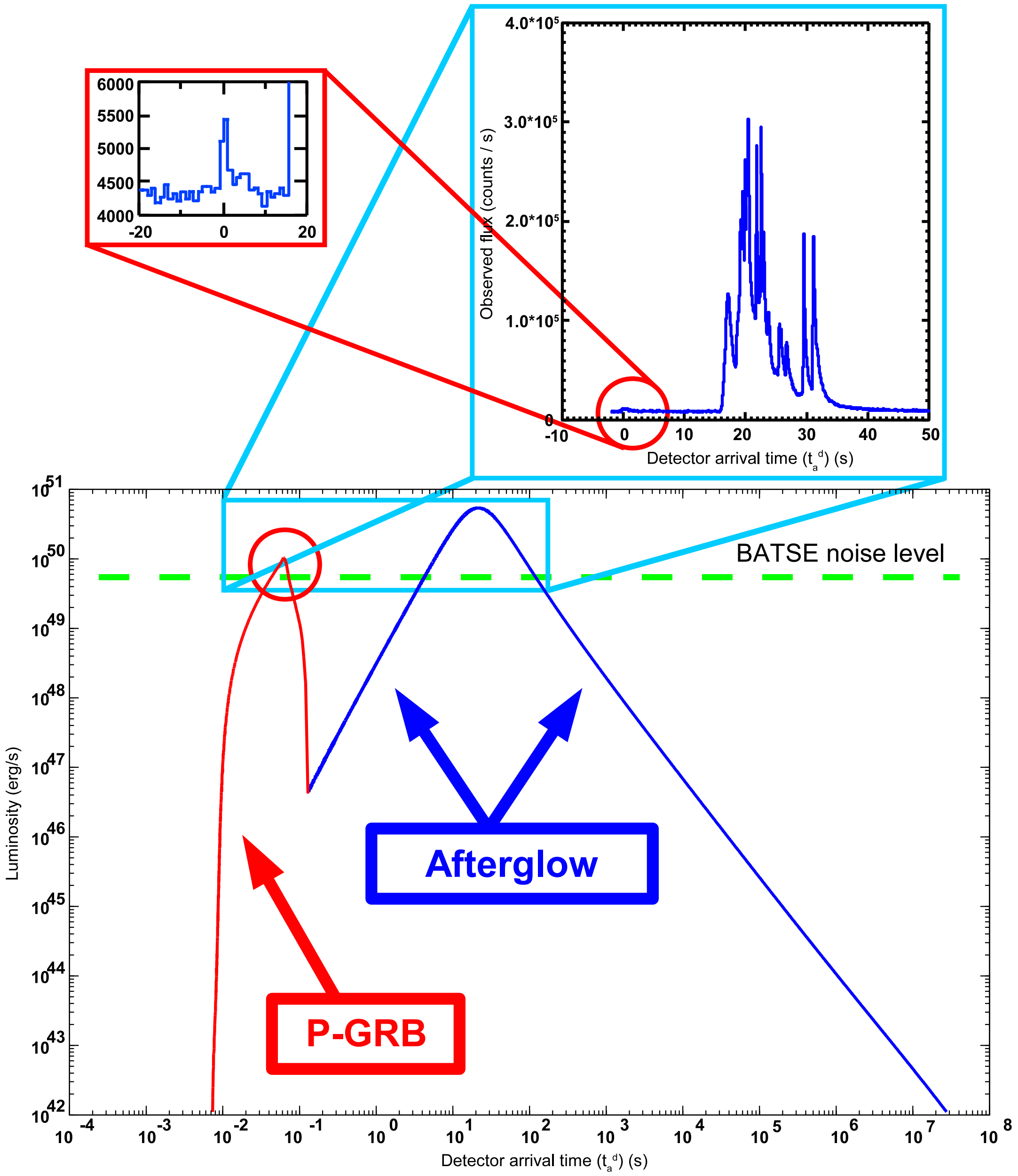

Figure 3.1: The "canonical GRB" light curve theoretically computed for GRB 991216. The prompt emission observed by BATSE is identified with the peak of the afterglow, while the small precursor is identified with the P-GRB. For this source we have $E_{e^\pm}^{tot} = 4.83 \times 10^{53}$ ergs, $B \simeq 3.0 \times 10^{-3}$ and $\langle n_{cbm} \rangle \sim 1.0$ particles/cm^3. Details in Ruffini et al. (2001b, 2002a, 2007a).

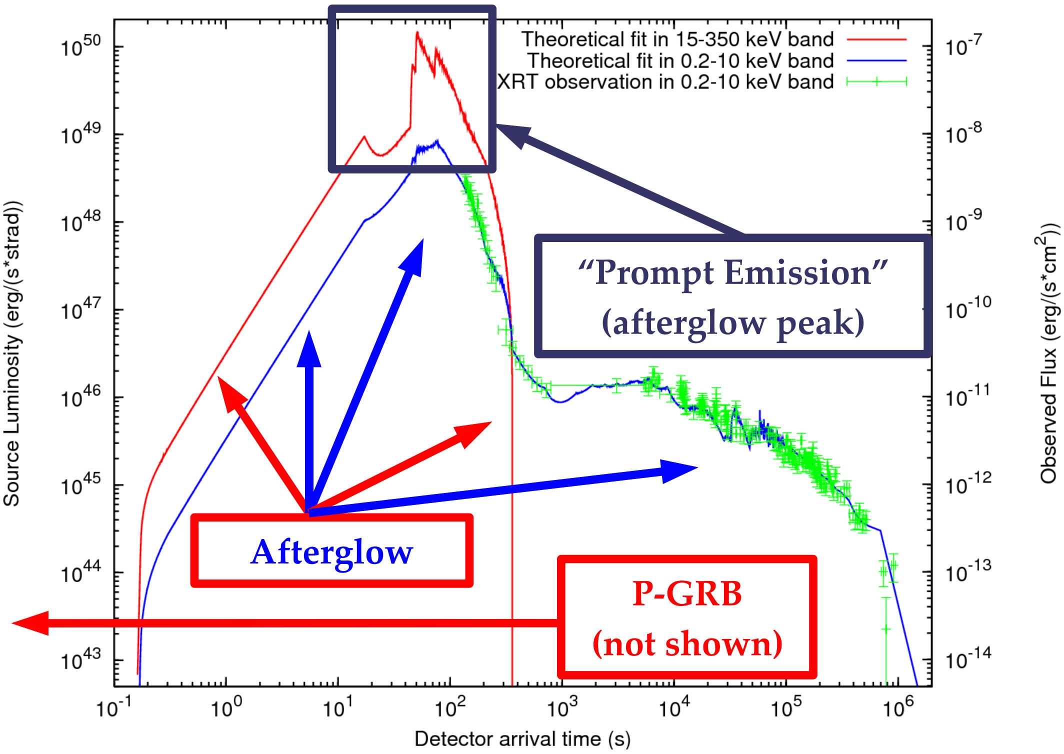

Figure 3.2: The theoretical light curves in the $15-150$ keV (red line) and $0.2-10$ kev (blue line) energy bands compared with XRT observations of GRB 050315. The P-GRB is outside the plot on the left, and the prompt emission is identified with the peak of the afterglow. Details in Vaughan et al. (2006).

between the P-GRB and the peak of the afterglow, that such precursors must be identified with the P-GRBs, as in the case of GRB 991216 (see Fig. 3.1).

- A major effort is currently being pursued to establish a new GRB classification based on the source physical properties and not on the mere measurement of the T_{90} duration. Within our framework, in fact, while the P-GRBs has a very well defined time scale due to the reaching of transparency, the long GRBs are simply identified with the peaks of the afterglow (see Figs. 3.1-3.2). As such, they cannot have an intrinsic time scale: their duration is just a function of the instrumental noise threshold (Ruffini et al., 2006a). This prediction has been strongly supported by the Swift observations (see e.g. the case of GRB 050315 reported in Fig. 3.3).
- Having so established that the so-called long GRBs class depends on the instrumental noise threshold and not on intrinsic properties of the source, we will see in the next report a clarification on the nature of the short GRBs made possible by the theoretical interpretation of a family of GRBs identified by Norris and Bonnell (2006) and characterized by "an occasional softer extended emission lasting tenths of seconds after an initial spikelike emission". The nature of these sources has been understood on the ground of fitting the fireshell model to GRB 970228 as a prototype (Bernardini et al., 2007) and confirmed in GRB 0606014.

3.1.2 GRBs without SNe: binary mergers (GRB 0606014 as the prototype)

A source which has represented the strongest challenge to the traditionally accepted GRB scenario is GRB 0606014 (Gehrels et al., 2006; Mangano et al., 2007, , see detailed analysis in section H.2), observed by Swift and VLT. The first remarkable peculiarity of this GRB is that it is the first nearby long duration GRB clearly not associated with a bright Type Ib/c supernova (SN) (Della Valle et al., 2006; Gal-Yam et al., 2006). This has infringed the commonly accepted collapsar scenario, according to which long duration GRBs ($T_{90} > 2$s) are thought to be produced by SN events during the collapse of massive stars in star forming regions (Woosley, 1993). The observations of broad-lined and bright type Ib/c SNe associated with GRBs are often reported to favor this scenario (Woosley and Bloom, 2006, and references therein). The *ansatz* has been advanced that every long GRB should have a SN associated with it (Zhang et al., 2006b). Consequently, in all nearby long GRBs ($z \leq 1$) the SN emission should be observed.

The second novelty of GRB 060614 is that it challenges the traditional separation between Long Soft GRBs and Short Hard GRBs, being a source of the

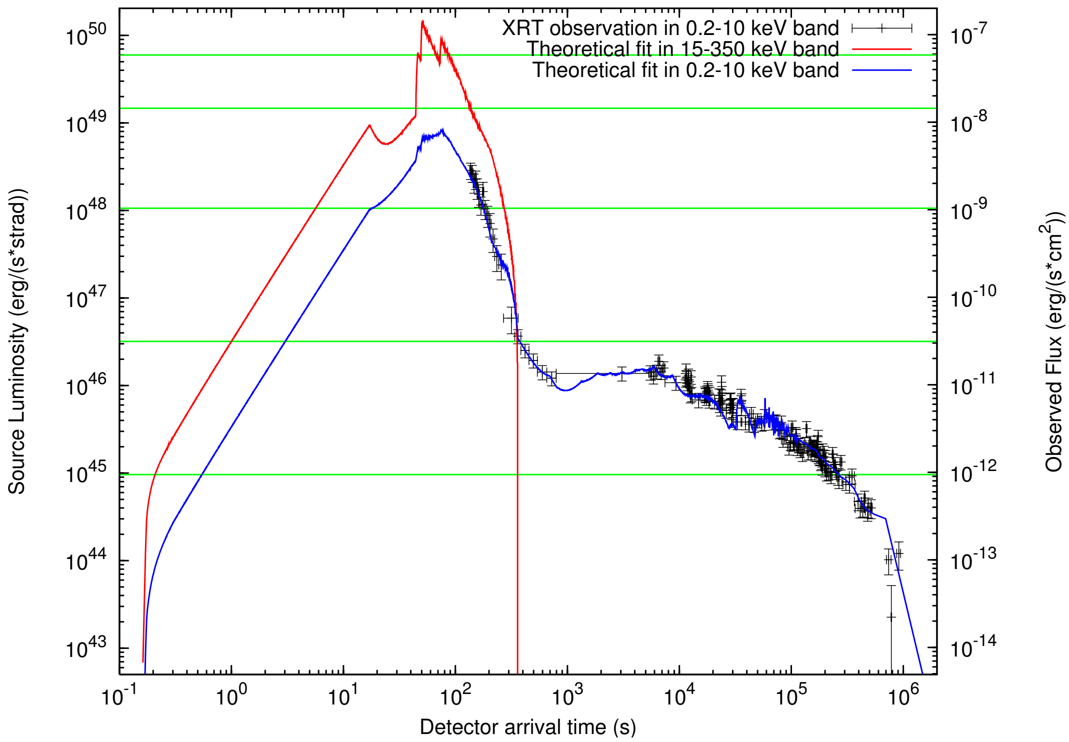

Figure 3.3: The theoretical light curves in the $15 - 150$ keV (red line) and $0.2 - 10$ kev (blue line) energy bands compared with XRT observations of GRB 050315 (Vaughan et al., 2006). The horizontal green lines correspond to different possible instrumental thresholds. It is clear that long GRB durations are just functions of the observational threshold. Details in Ruffini et al. (2006a).

Norris and Bonnell (2006) kind (see above section 3.1.1). In fact, in its15–150keV light curve it presents a short, hard and multi-peaked episode (about 5s). Such an episode is followed by a softer, prolonged emission that manifests a strong hard to soft evolution in the first 400s of data (Mangano et al., 2007).

The softer extended emission appears to have a peak luminosity smaller than the one of the initial spikelike emission. This has misled the understanding of the correct role of the afterglow. As we show in section H.2 (see also Bernardini et al., 2007), we have successfully identified the initial spikelike emission with the P-GRB and the softer extended emission with the peak of the afterglow (see Fig. 3.4). Within the fireshell model, we have performed the fit of the observed light curves in the 15–150keV energy band, corresponding to the γ-ray emission, and in the 0.2–10keV energy band, corresponding to the X-ray component. From the theoretical simulations we have derived the total initial energy $E_{tot}^{e^\pm}$ and the value of B (see section 3.1.1). Moreover, a very small average CBM density ($\sim 10^{-3}$particles/cm^{-3}), typical of galactic halos, has been inferred. Our analysis put forward three main results:

- GRB 060614 represents an additional fundamental progress in clarifying the role of the CBM density in determining the GRB morphology. It confirms the results presented in GRB970228 (Bernardini et al., 2007), that is the prototype of the new class of "fake" short GRBs, or, better, of canonical GRBs "disguised" as short ones. The sharp spiky emission corresponds to the P-GRB, and the softer extended emission to the peak of the afterglow.

- They correspond to canonical GRBs with a baryon loading $B > 10^{-3}$ and an afterglow emission energetically predominant with respect to the P-GRB one: as we have shown, the time-integrated afterglow luminosity is much larger than the P-GRB one.

- Moreover, the peak luminosity of the P-GRB is much larger than the afterglow one, due to the low average CBM density and it is neither intrinsic to the progenitor nor to the black hole.

We then conclude:

- The low value of the CBM density is compatible with a galactic halo environment.

- This result points to an old binary system as the progenitor of GRB 060614 and well justify the absence of an associated SN Ib/c event (see also Davies et al., 2007). Such a binary system departed from its original location in a star forming region and spiraled out in a low density region of the galactic halo (see e.g. Kramer, in press).

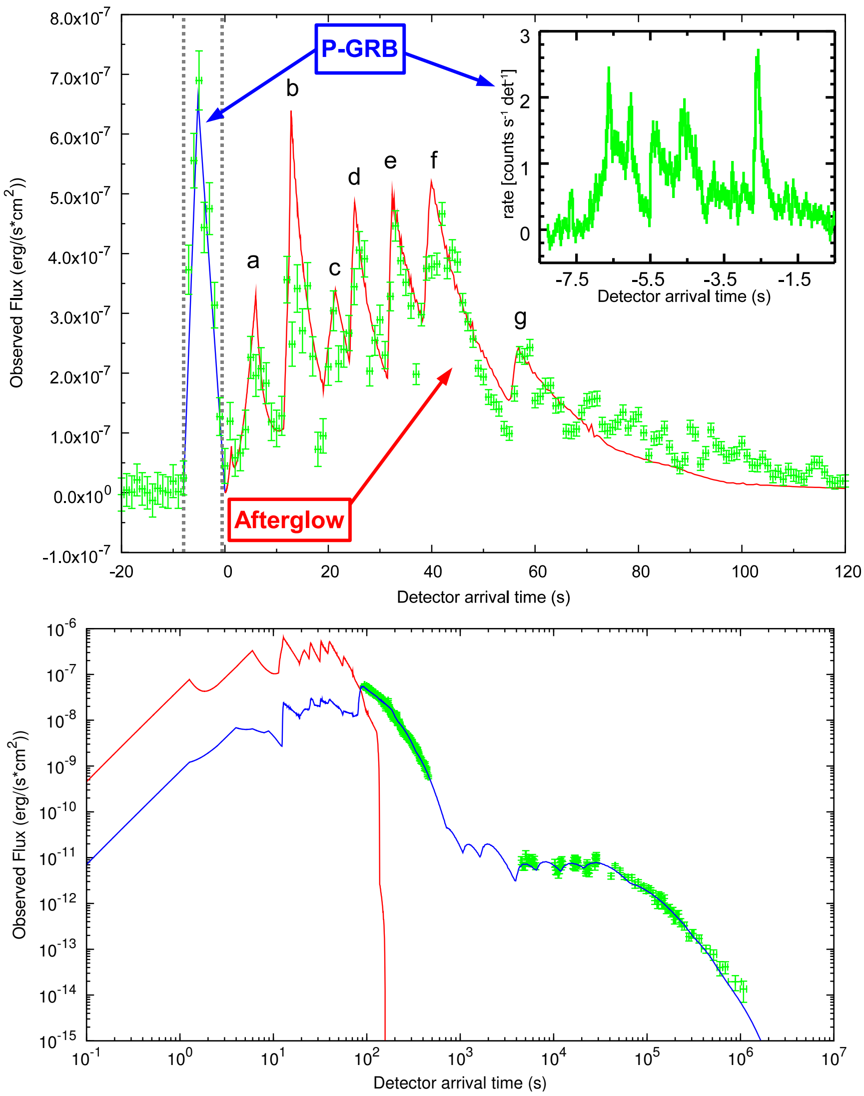

Figure 3.4: Upper panel: the BAT 15–150keV light curve (green points) at 1s time resolution is compared with the corresponding theoretical afterglow light curve we compute (red line). The onset of the afterglow is at the end of the P-GRB (qualitatively sketched in blue lines and delimited by dashed gray vertical lines). Therefore the zero of the temporal axis is shifted by 5.5s with respect to the BAT trigger time. In the upper right corner there is an enlargement of the P-GRB at 50ms time resolution (reproduced from Mangano et al., 2007), showing its structure. Lower panel: the XRT 0.2–10keV light curve (green points) is compared with the corresponding theoretical afterglow light curve we compute (blue line). Also in this case we have a good correspondence between data and theoretical results. For completeness, the red line shows again the theoretical afterglow light curve in the 15–150keV energy range.

- The energetic of this source is about two orders of magnitude smaller than the one of GRB970228 (Bernardini et al., 2007). A natural explanation is that instead of a neutron star - neutron star merging binary system we are in presence of a white dwarf - neutron star binary. This would explain also the variability of the P-GRB. The observations of GRB 060614 offers in fact the opportunity, for the first time, to analyze in detail the structure of a P-GRB lasting 5s. This feature can be directly linked to the physics of the gravitational collapse originating the GRB.

These result points to the possibility that the majority of GRBs declared as shorts (see e.g. Piro, 2005) are likely "disguised" short GRBs of the Norris and Bonnell (2006) kind. However, a possible exception to this is discussed in the next section.

3.1.3 P-GRB dominated GRBs (GRB 050509B as the prototype)

As we introduced in 3.1.1, the baryon loading is the key parameter to classify GRBs. If $B \leq 10^{-5}$ (this value slightly depends on the energy of the GRB, see section H.1.1 for details) we obtain a light curve that is "P-GRB dominated", since the total energy emitted in the whole afterglow is lower than the one emitted in the P-GRB (see Fig. 3.5). Our aim is to investigate if this is indeed the case of GRB 050509B (Gehrels et al., 2005). We performed two different analysis (see details in section H.3): first, we assume $B = 3.7 \times 10^{-3}$, then $B = 1.1 \times 10^{-4}$.

In the first analysis we identified the prompt emission of this GRB (BAT data) with our P-GRB and we fitted the afterglow to the other data in X-rays. In this case, we have the total energy of the GRB estimated in $E^{tot}_{e^\pm} = 2.11 \times 10^{48}$ erg. The P-GRB has an energy of $E_{P-GRB} = 1.6 \times 10^{47}$ erg, it means that more then 90% of the energy is released in the afterglow. Therefore in this case GRB 050509B is not a P-GRB dominated GRB.

In the second analysis we fit the BAT data as the peak of the afterglow. The P-GRB is very energetic $E_{P-GRB} = 3.30 \times 10^{49}$ erg in comparison with the afterglow, and we argue that it was not visible because its peak energy would be about 817 keV. In this case the energy of the GRB is $E^{tot}_{e^\pm} = 5.07 \times 10^{49}$ erg, and this implies that the energy emitted on the P-GRB is almost 60% of the total one. This means that this GRB is indeed a P-GRB dominated GRB but in this case the P-GRB was not detected since it was above the BAT limit (Bat sensitivity is up to 150 keV).

In order to distinguish between the two analyses we can use the Amati relation (Amati et al., 2002, see also 3.1.5). None of these two approaches to the study of GRB 050509B are in agreement with the Amati relation. As it is valid just for "long" GRBs (see section 3.1.5) we can conclude that the first interpretation is not correct.

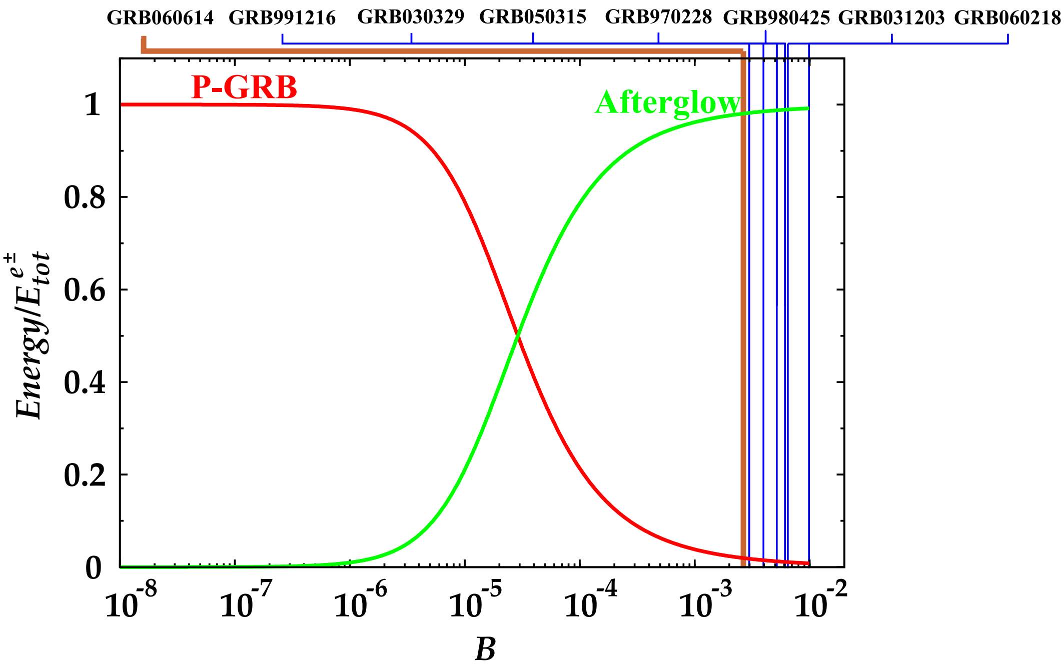

Figure 3.5: Here the energies emitted in the P-GRB (red line) and in the afterglow (green line), in units of the total energy of the plasma, are plotted as functions of the B parameter. When $B \leq 10^{-5}$, the P-GRB becomes predominant over the afterglow, giving rise to a P-GRB dominated GRB. In the figure are also marked in blue the values of the B parameters corresponding to some GRBs we analyzed, all belonging to the class of long GRBs, together with the GRB060614 one (thick brown line, see section 3.1.2).

- GRB 050509B is indeed a P-GRB dominated GRB, since it is out of the Amati relation (the expected peak energy for the P-GRB is 817 keV), like the other "short" GRBs (see 3.1.5). The new missions as *Fermi*-GLAST and AGILE looking at high energy emission from GRBs will be very important to observe P-GRB dominated GRBs and to understand the very new physics they can teach us.

3.1.4 Prompt emission and X-ray flares: the clumpiness of CBM (GRB 060607A as the prototype)

GRB 060607A is a very distant ($z = 3.082$ Ledoux et al., 2006) and energetic event ($E_{iso} \sim 10^{53}$ erg Molinari et al., 2007). Its BAT light curve shows a double-peaked structure with a duration of $T_{90} = (100 \pm 5)$ s (Tueller et al., 2006). The time-integrated spectrum over the T_{90} is best fit with a simple power-law model with an index $\Gamma = 1.45 \pm 0.08$ (Guidorzi, private communication). The XRT light curve shows a prominent flaring activity (at least three flares) superimposed to the normal afterglow decay (Page et al., 2006).

- GRB 060607A main peculiarity is that the peak of the near-infrared (NIR) afterglow has been observed with the REM robotic telescope (Molinari et al., 2007). Interpreting the NIR light curve as corresponding to the afterglow onset as predicted by the fireball forward shock model (Sari and Piran, 1999; Meszaros, 2006), it is possible to infer the initial Lorentz gamma factor of the emitting system that results to be $\Gamma_\circ \sim 400$ (Molinari et al., 2007; Covino et al., 2007; Jin and Fan, 2007). Moreover, these measurements seem to be consistent with an interstellar medium environment, ruling out the wind-like medium (Molinari et al., 2007; Jin and Fan, 2007).

- We analyze GRB 060607A (see the detailed analysis in section H.4) within the fireshell model (Ruffini et al., 2001c,b, 2007a). The initial Lorentz gamma factor of the fireshell obtained adopting the exact solutions of its equations of motions (Bianco and Ruffini, 2005a) and as initial condition the free parameters of the fireshell estimated is $\gamma_\circ = 328$.

- We deal only with the BAT and XRT observations, which are the basic contribution to the afterglow emission according to the fireshell model. We do not deal with the infrared emission that, on the contrary, is used in the current literature to estimate the dynamical quantities of the fireball in the forward external shock regime. Nevertheless, the initial value of Lorentz gamma factor we predict is compatible with the one deduced from the REM observations even under very different assumptions, $\Gamma_\circ \sim 400$ (Molinari et al., 2007; Covino et al., 2007; Jin and Fan, 2007).

- According to the "canonical GRB" scenario (Ruffini et al., 2001b, 2007a) we interpret the whole prompt emission as the peak of the afterglow emission, and the remaining part of the light curve with the decaying tail of the afterglow. We find from our theoretical computations (see 3.1.1) that the P-GRB total isotropic energy is $E_{P-GRB} = 1.9\% \, E_{e^\pm}^{tot} = 4.7 \times 10^{51}$ erg, hence the P-GRB results to be undetectable if we assume a duration $\Delta t_{p-grb} \gtrsim 10$ s. The theoretical light curves obtained are well in agreement with the observations in all the *Swift* BAT energy bands (15–25 keV, 25–50 keV, 50–100 keV, 100–150 keV, see Fig. 3.6).

- We then turn to the analysis of the GRB 060607A prompt emission time-integrated spectrum. As discussed in previous works (Ruffini et al., 2004b, 2005c; Bernardini et al., 2005a), even if the fireshell model assumes that the GRB spectrum is thermal in the comoving frame, the shape of the final spectrum in the laboratory frame is clearly non-thermal. In fact each single instantaneous spectrum is the result of a convolution of thermal spectra. In fact photons observed at the same arrival time are emitted at different comoving time (the so called EQTS, see also section 3.1.6 Bianco and Ruffini, 2004, 2005b), hence with different temperatures. This calculation produces a non-thermal instantaneous spectrum in the observer frame. This effect is enhanced if we calculate the time-integrated spectrum: we perform two different integrations, one on the observation time and one on the EQTS, and what we get is a typical non-thermal power-law spectrum which results to be in good agreement with the observations.

- We analyzed the X-ray flares observed by *Swift* XRT ($0.2 - 10$ keV) in the early part of the decaying phase of the afterglow. According to the fireshell model these flares have the same origin of the peaks observed in the prompt emission, namely they are produced by the interaction of the fireshell with overdense CBM. We found initially that our theoretical light curve is not compatible with the observations of the first flare while it is in agreement with the second one (see Fig. 3.6, lower right panel). This discrepancy is due to the simple modeling adopted, namely the CBM is arranged in spherical shells (Ruffini et al., 2002a). This approximation fails when the visible area of the fireshell is comparable with the size of the CBM clouds. This is indeed the case of the first flare, which is produced by the interaction with a CMB clump very small compared with the fireshell visible area. Following the results obtained for GRB 011121 (see A.10), we tried to fit the first flare accounting for the three-dimensional structure of the CBM clouds. We "cut" the emission at a certain angle θ_{cloud} from the line of sight corresponding to the transverse dimension of the CBM cloud which, we recall, is for the first flare very small ($d_{clump} = r_{clump} sin\theta_{clump} \sim 10^{15}$

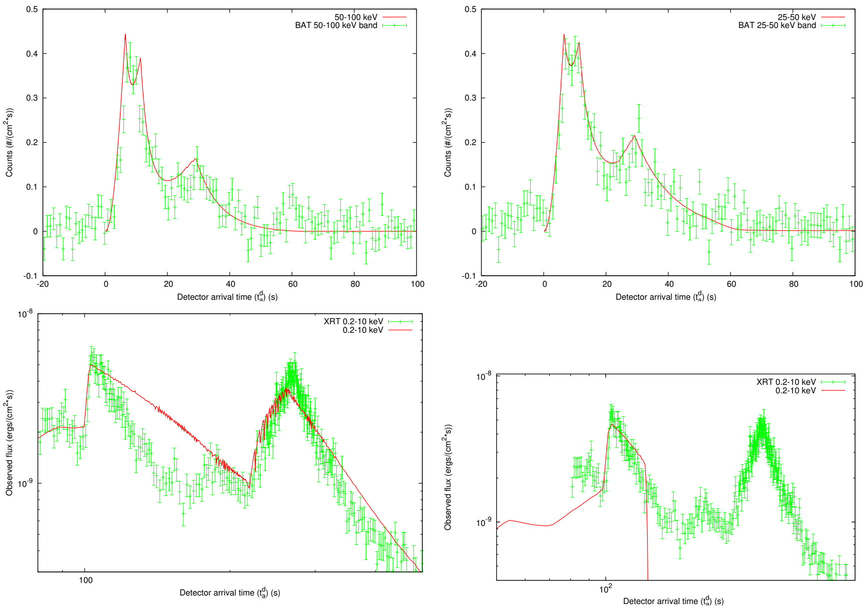

Figure 3.6: Upper panel: *Swift* BAT light curve (green points) in two energy bands (25–50 kev, right panel and 50–100 keV, left panel) compared with the theoretical one (red lines). Lower panel: *Swift* XRT (0.2–10 keV) light curve (green points) compared with, respectively, the theoretical one obtained assuming the CBM distributed in spherical shells (left panel), the theoretical one obtained imposing a finite transverse dimension for the CBM cloud (right panel).

cm $\sim 10^{-3} d_{fireshell}$, where d_{clump} and $d_{fireshell}$ are respectively the CMB clump and the fireshell transverse dimensions, and r_{clump} is the distance of the clump from the source). We obtain in this way a flare whose duration $\delta t / t_{tot}$ is compatible with the observation (see Fig. 3.6) and it is indeed a confirmation that it is possible to obtain arbitrarily short flares by the interaction with the CBM.

3.1.5 GRBs as distance indicators: the Amati relation

The very frequent detections of gamma-ray bursts (GRBs) up to very high redshifts ($z = 6.7$) make them essential as cosmological indicators, complementary to supernovae Ia, which are observed only up to small redshifts (z=1.7 Leibundgut, 2001; Riess et al., 2001).

One of the hottest topics on GRBs is indeed the possible existence of empirical relations between GRB observables, which may lead, if confirmed, to using GRBs as cosmological probes of models universe.

The first empirical relation, discovered when analyzing the *Beppo*SAX so-called "long" bursts with known redshift, was the "Amati relation". It was found that the isotropic-equivalent radiated energy of the prompt emission E_{iso} is correlated with the cosmological rest-frame νF_ν spectrum peak energy $E_{p,i}$: $E_{p,i} \propto (E_{iso})^a$, with $a = 0.52 \pm 0.06$. The existence of the Amati relation has been confirmed by studying a sample of GRBs discovered by Swift, with $a = 0.49^{+0.06}_{-0.05}$. Many others empirical relations exist, some are three parameters relations while others are constituted only by two parameter such as the Amati one. Among the two parameters correlations the following are worth noting $E_\gamma - E_{peak}$ (Ghirlanda et al., 2004, 2006), $L - E_{peak}$ (Schaefer, 2003), $L - \tau_{lag}$ (Norris et al., 2000), $L - V$ (Fenimore and Ramirez-Ruiz, 2000; Reichart et al., 2001), $L - \tau_{RT}$.
Some of them are purely phenomenological, such as $L - E_{peak}$ while others are based on assumptions and are dependent on models, basically the standard fireball model, such as for example $E_\gamma - E_{peak}$, $L - V$. Some correlations assume spherical symmetry, such as the Amati relation, while others assume collimated (jet) emission, such as $E_iso - E_p - t_b$. Moreover, three-parameter have also been proposed such as, e.g.,the $E_iso - E_p - t_b$ one
(Liang and Zhang, 2005) and that proposed by (Firmani et al., 2005, 2006). Among the crucial issues raised by the Amati relation as well as the others, there are their theoretical explanations and their possible dependence on the assumed cosmological model. A possible theoretical explanation of the Amati relation is given by (Guida et al., 2008) within the framework of the fireshell model (details in section H.5).

The basic statements of our approach are the following:

- Only the *entire* afterglow emission is considered in establishing our E_p - E_{aft} relation.

- From this assumption one derives, in a natural way, that the Amati relation holds only for long GRBs, where the P-GRB is negligible, and not for short GRBs.

- Finally the relation is independent of the assumed cosmological model.

The completion of the $E_p - E_{aft}$ relation has been made possible thanks to the Swift satellite, that has for the first time a high quality data in selected energy bands from the GRB trigger time all the way to the latest afterglow phases. This has given us the opportunity to apply our theoretical "fireshell" model, thereby obtaining detailed values for its two free parameters, namely for the total energy $E_{tot}^{e^\pm}$ and the baryon loading B of the fireshell, as well as for the effective density and filamentary structure of the CBM. From this we were able to compute multi-band light curves and spectra, both instantaneous and time-integrated, compared with selected GRB sources, such as GRB 050315.

We examined a set of "gedanken" GRBs, all at the same cosmological redshift of GRB 050315. Such a set assumes the same fireshell baryon loading and effective CBM distribution as GRB 050315 and each "gedanken" GRB differs from the others uniquely by the value of its total energy $E_{tot}^{e^\pm}$. We then considered a second set of "gedanken" GRBs, differing from the previous one by assuming a constant effective CBM density instead of the one inferred for GRB 050315. In both these sets, we looked for a relation between the isotropic-equivalent radiated energy of the *entire* afterglow E_{aft} and the corresponding time-integrated νF_ν spectrum peak energy E_p:

$$E_p \propto (E_{aft})^a \,. \tag{3.1.1}$$

Our relation extends over two orders of magnitude in energy, from 10^{51} to 10^{53} erg, and is well-fitted by a power law $E_p \propto (E_{aft})^a$ with $a = 0.45 \pm 0.01$ (see Fig. 3.7). We emphasize that such a power-law slope strictly agrees with the Amati relation, namely $E_{p,i} \propto (E_{iso})^a$, with $a = 0.49^{+0.06}_{-0.05}$. We recall that E_p is the observed peak energy; i.e., it is not rescaled for the cosmological redshift, because all the "gedanken" GRBs of the set are at the same redshift of GRB 050315, namely $z = 1.949$. The normalization is clearly different from the Amati one.

In the second set of "gedanken" GRBs, built assuming a constant effective CBM density ~ 1 particle/cm^3, instead of the one specifically inferred for GRB 050315, there in no relation between E_p and E_{aft}.

Let's now turn to the analogies and differences between our E_p-E_{aft} relation and the Amati one,

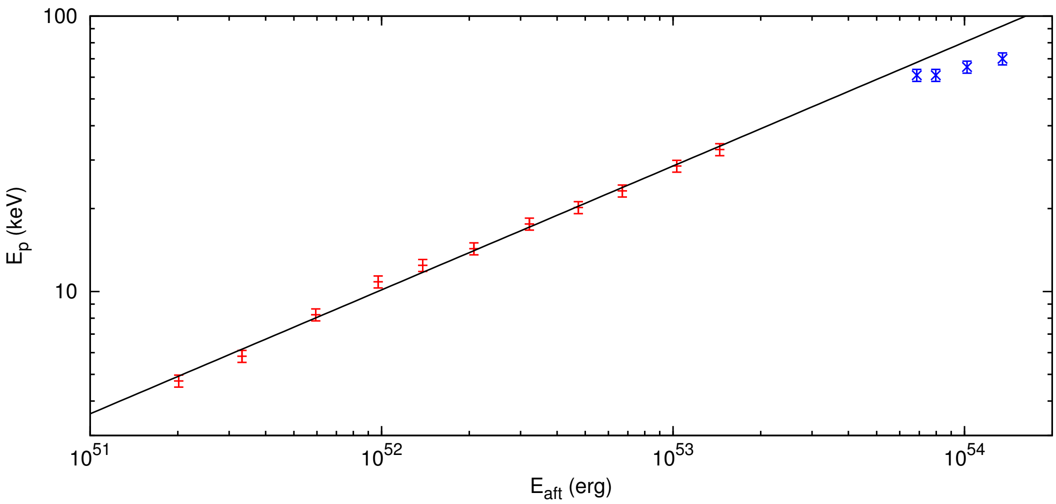

Figure 3.7: The $E_p - E_{aft}$ relation: the results of the simulations of the first set of "gedanken" GRBs (red points) are well-fitted by a power law (black line) $E_p \propto (E_{aft})^a$ with $a = 0.45 \pm 0.01$. The blue points are the results of the extension of the first set above 10^{53} erg.

- Our analysis excludes the P-GRB from the prompt emission, extends all the way to the latest afterglow phases.
- It is independent of the assumed cosmological model, since all "gedanken" GRBs are at the same redshift.
- The Amati relation, on the other hand, includes the P-GRB, focuses only on the prompt emission, being therefore influenced by the instrumental threshold that fixes the end of the prompt emission, and depends on the assumed cosmology. This might explain the intrinsic scatter observed in the Amati relation.

3.1.6 The afterglow luminosity evolution over the equitemporal surfaces

It is widely accepted that Gamma-Ray Burst (GRB) afterglows originate from the interaction of an ultrarelativistically expanding shell into the CircumBurst Medium (CBM). Differences exists on the detailed kinematics and dynamics of such a shell, as well as on the radiative regime involved (see e.g. Bianco and Ruffini, 2005a; Meszaros, 2006, and references therein).

Due to the ultrarelativistic velocity of the expanding shell (Lorentz gamma factor $\gamma \sim 102 - 103$), photons emitted at the same time in the laboratory frame (i.e. the one in which the center of the expanding shell is at rest) from the shell surface but at different angles from the line of sight do not reach the observer at the same arrival time. Therefore, what we would see if we were able to resolve spatially the GRB afterglows would be not the spherical surface of the shell but the EQuiTemporal Surface (EQTS), defined as the surface locus of points which are source of radiation reaching the observer at the same arrival time (see e.g. Sari, 1998; Panaitescu and Meszaros, 1998a; Granot et al., 1999; Bianco et al., 2001; Bianco and Ruffini, 2004, 2005b, and references therein).

The knowledge of the exact shape of the EQTSs is crucial, since any theoretical model must perform an integration over the EQTSs to compute any prediction for the observed quantities (see e.g. Gruzinov and Waxman, 1999; Bianco and Ruffini, 2004, 2005b; Meszaros, 2006; Huang et al., 2006, 2007, and references therein). One of the key problem is therefore the angular size of the visible region of each EQTS, as well as the distribution of the luminosity over such a visible region. In particular, if the luminosity is maximum along the line of sight, GRB afterglows would appear as point-like or circle-like sources in the sky, while, if it is maximum at the boundaries of the visible region, they would appear as rings (see e.g. Waxman, 1997; Sari, 1998; Panaitescu and Meszaros, 1998a; Granot et al., 1999; Waxman et al., 1998; Galama et al., 2003; Granot and Loeb, 2003; Taylor et al., 2004, and references therein). This is crucial also for the inferences on possible beaming angles (see e.g. Panaitescu, 2006; Bianco and Ruffini, 2006, and references therein).

In Bianco and Ruffini (2005a) there have been presented the analytic solutions of the equations of motion for Gamma-Ray Burst (GRB) afterglow, compared with the approximate solutions usually adopted in the current literature, both in the fully radiative and adiabatic regimes. In Bianco and Ruffini (2004, 2005b) there have been presented the corresponding analytic expressions for the EQTSs. Starting from these premises, we here present the distribution of the afterglow bolometric luminosity over the visible region of a single EQTSs within the fireshell model for GRBs (see the following report about "Relativistic effects in Physics and Astrophysics"for details and e.g. Ruffini et al., 2007a, and references therein). The computation is separately performed over different selected EQTSs encompassing all the afterglow regimes, from the prompt emission all the way to the latest phases. The temporal evolution of the luminosity distribution over the EQTSs' visible region is also therefore presented (see Fig. 3.8).

3.1.7 GRBs and SNe: the induced gravitational collapse

The *Collapsar model* (Woosley, 1993; Paczynski, 1998; MacFadyen and Woosley, 1999; Zhang et al., 2003) proposes that GRBs arise from the collapse of a single Wolf-Rayet star endowed with fast rotation. This idea is purported by the evidence that many GRBs are close to star-forming regions and that this suggests that GRBs are linked to cataclysmic deaths of massive stars ($M > 30M_{\odot}$). In

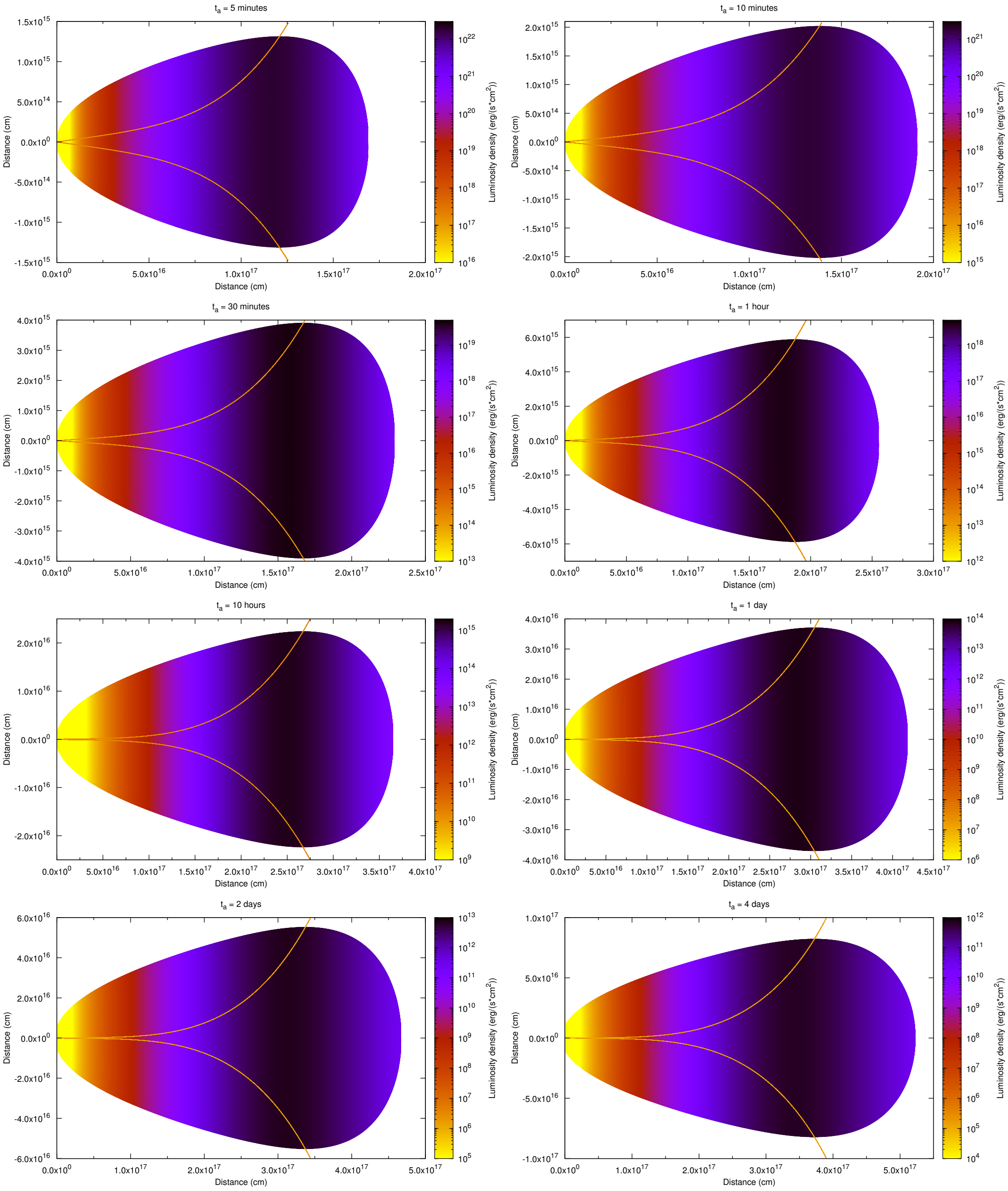

Figure 3.8: We plot the luminosity density over 8 different EQTSs, corresponding to arrival time values ranging from the early to the late afterglow phases. The orange lines represent the boundaries of the visible regions.

such a model very massive stars are able to fuse material in their centers all the way to iron, at which point a star cannot continue to generate energy by fusion and collapses, in this case, immediately forming a black hole. Matter from the star around the core rains down toward the center and (for rapidly rotating stars) swirls into a high-density accretion disk. The mass of the accretion disk is around 0.1 $M_\odot$. The infall of this material into the black hole is assumed to drive a pair of jets (with opening angles < 10 degrees) out along the rotational axis, where the matter density is much lower than in the accretion disk, toward the poles of the star at velocities approaching the speed of light, creating a relativistic shock wave at the front (Blandford and McKee, 1976). The processes of core collapse and of accretion along the polar column and the jet propagation through the stellar envelope all together last ~ 10 sec (MacFadyen and Woosley, 1999). The jet, as it passes through the star, is modulated by its interaction with the surrounding medium. In this way the Collapsar model attempts to explain the time structure of GRB prompt emission and to produce the variable Lorentz factor necessary for the internal shocks occurrence (Woosley and Bloom, 2006). Moreover it is a prediction of this model that the central engine remains active for a long time after the principal burst is over, potentially contributing to the GRB afterglow (Burrows et al., 2005b).

Three very special conditions are required for a star to evolve all the way to a gamma-ray burst according to this theory: the star should be very massive ($25M_\odot$ Woosley (1993), $35 - 40M_\odot$ on the main sequence Fryer et al. (1999)) to form a central black hole, the star rapidly rotates to develop an accretion torus capable of launching jets, and the star should have low metallicity in order to strip off its hydrogen envelope so the jets can reach the surface. As a result, gamma-ray bursts are far rarer than ordinary core-collapse supernovae, which only require the star to be massive enough to fuse all the way to iron.

The consensus and the difficulties for the Collapsar model can be simply summarized:

- Langer (2006) asserts that long gamma-ray bursts are found in systems with abundant recent star formation, low metallicity environment.

- The second evidence in favor of the Collapsar model is that there are several observed cases where a supernova is practical coeval with GRBs.

- However, strong evidence against the Collapsar model comes from the fact that there were recently discovered two nearby long gamma-ray bursts which lacked a signature of any type Ib/c supernova: both GRB 060614 (Della Valle et al., 2006; Gal-Yam et al., 2006, see also above section 3.1.2) and GRB 060505 (Fynbo et al., 2006) defied predictions that a supernova would emerge despite intense scrutiny from ground-based telescopes.

Within our fireshell model, we recall, the approach is drastically different, as already introduced in Ruffini et al. (2001a). In fact in this framework, the SN which is often observed in temporal and spatial coincidence with the GRB cannot be interpreted as its progenitor because of the high quantity of ejected matter from the supernova explosion would prevent the GRB occurrence. Moreover:

- It is very unlikely that a core collapse SN produces directly a black hole.
- GRBs originate from gravitational collapses to black holes (see section 3.1.1). The possible explanation for the GRB-SN connection proposed in Ruffini et al. (2001a) is that both the GRB and the supernova progenitors belong to a binary system. Under special conditions it is possible that the GRB emission triggers the supernova explosion of the companion star. Alternatively, it is possible that the process of gravitational collapse to a black hole producing the GRB is "induced" by the supernova Ib/c on a companion neutron star (see Fig. 3.9 and Ruffini et al., 2007b; Dainotti et al., 2007). The faintness of this GRB class could be in this case naturally explained by the formation of the smallest possible black hole, just over the critical mass of the neutron star (Ruffini, 2006). Moreover these systems occur in a low density CBM (10^{-2}–1 particle/cm^3. We are still working in collaboration with Professor Arnett on these possible scenarios in order to clarify the reliability of these proposals or, eventually, to trace an intermediate situation in which both the systems (GRB and SN) influence each other.
- Also the observation of the occurrence of "long" GRBs in star forming regions is explained by identifying the progenitor with a binary system formed by a neutron star and a star evolved out of the main sequence.

3.1.8 Fermi's approach to the study of hadronic interactions

The aim of this work is to determinate the total energy via gamma ray produced from proton-proton collisions in the scenario of the Gamma Ray burst (GRB).

The pp collision produces pions: π^+, π^- e π^0, where each π^0 decays in two photons gamma ($\pi^0 \rightarrow 2\gamma$, with probability of 98,798%). In order to achieve this production of gamma ray, we should before get the multiplicity of pions in function of the energy of incident proton.

We made the theoretical reconstruction of the work of Fermi H.6.1.1, where he made a detailed physical approach of the pion multiplicity via collision pp. Fermi used three stages and each with a physical tool: first, the dynamic of the relativistic particle in the center of mass (c.m.) frame of the system,

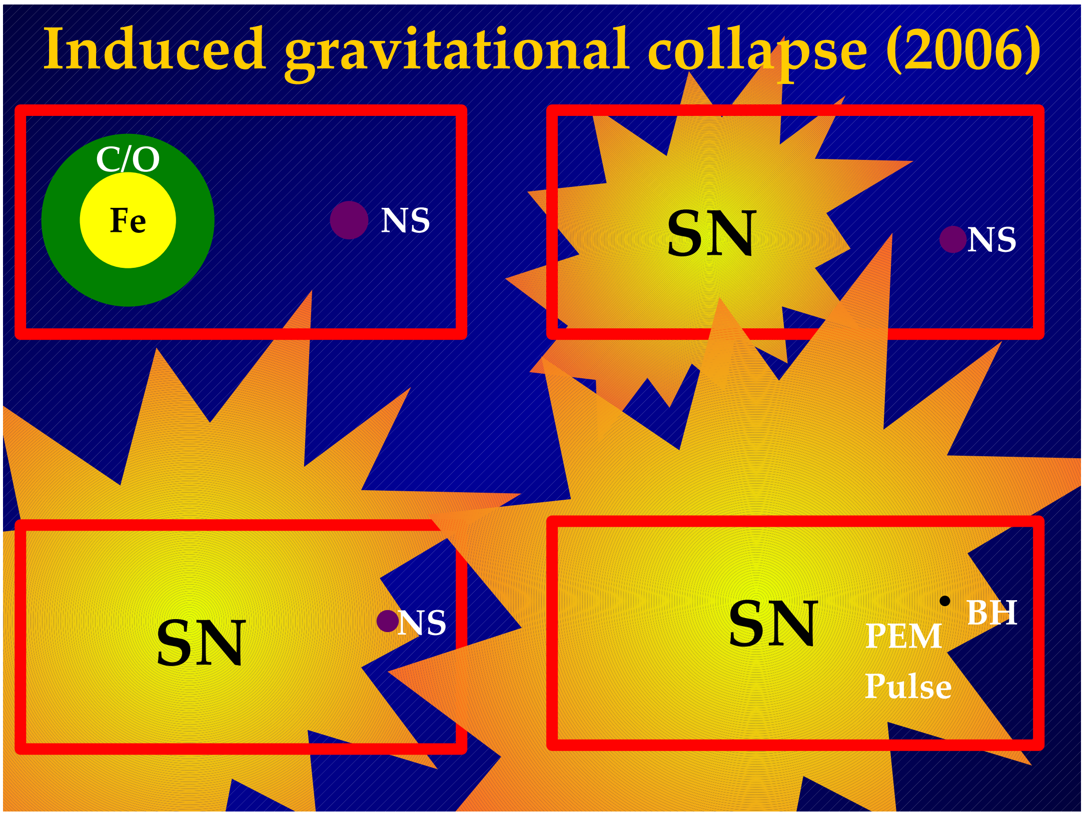

Figure 3.9: A sketch summarizing the induced gravitational collapse scenario.

second, a probabilistic approach of the pions production, and, third, he used the law of Black Body to get the pions multiplicities.

Although we have reconstructed the interesting physical approach of Fermi about the pp collisions, it was not still possible to explain this theoretical process, from the experimental data. The Fermi approach was basically classical/relativistic, because in that time the Quantum Electrodynamic (QED) and the Quantum Chromodynamic (QCD) had not been still developed. But even currently, after the knowledge of the QED and QCD, it is not possible to reproduce the experimental curves with theoretical ones.

In the Fermi approach, it has been considered the collision of a proton with relativistic velocity hitting a rest protonin the laboratory frame (LF). But by convenience, it has been made the entire mathematical approach in the center of mass frame. Fermi considered Ω being the volume of the system during the collision, therefore, all the protons and pions are inside of Ω in the instant of the collision. Fermi considered the radius of Ω equivalent to the Compton wavelength of the pion ($r = \lambda_{Compton}$), that is greater than the one of the proton. In our approach we made a small change: we inserted a parameter "a" multiplying the Compton wavelength of pion, resulting $r = a\lambda$. Where we know the experimental curves of the pions multiplicity, the parameter "a" help us to fit the theoretical curve with the experimental curve, and then to hypothesize a physical explanation of the Ω volume. In the c.m. frame, the two protons have the same velocity, but in opposite direction, then the protons have the same Lorentz factor γ_p. We obtain γ_p in function of the c.m. energy $\sqrt{s}$ by the Lorentz Invariance, that is defined by the square of the 4-momentum of the system is invariant in time and frame.

Then, Fermi made a probabilistic analysis of "n" particles inside of a volume Ω, obtaining the density of states of energies $G(s)$, the number of state $N_n(s)$ in a phase space with energy between $\sqrt{s}$ and $\sqrt{s} + d\sqrt{s}$ and the probability to form a state with "n" particles $S_n(s)$ (it is well known as statistical weights). This probabilistic analysis will be useful in the next, thermodynamic approach. Fermi assumed that the Ω system is an ensemble microcanonical, therefore, it is isolated, and he also assumed that all particles have the same probability of transition, so they have the temperature associate T, thus can be treated like a black body. Fermi used the Planck Law for the protons (bosons) and the Planck Law Modified for the pions (fermions), and also associated them Stefan-Boltzmann Laws. In this way, Fermi obtained the pions multiplicity in function of the incident proton energy. In our analysis, the aim is the multiplicity of the π^0, while Fermi did not study the multiplicity of each kind of pion singularly. To make this calculation, we assume that the transferred energy from the protons to the pions is divided equally among the three kind of pions, since the experimental data give multiplicities almost equal for the three kinds of pions. Fermi obtained expressions of multiplicity for intermediate energies of the incident proton (classical) and extremely high energies of incident protons (relativistic), where in the classical case he made the treatment in function of the kinetic energy T and in the other case he made the treatment of the relativistic energy.

The modern approach of the pp collisions, briefly, was to get the Monte Carlo code that give curves that is with the maximal of agreement with the experimental curves. In our case we use the SIBYLL code, more precisely the analytical parametrization of Kelner 2006, for the production of the particles and gamma rays via pp collisions. Kelner obtained expressions quite simple for the cross section and for the π^0 multiplicity.

From the comparison between the expressions obtained by Fermi and Kelner, it results that the best fit for the parameter of the radius of the volume Ω is $a = 5$, but even with this fit the two curves diverge for high energies of incident protons.

In the last section we calculate the production of gamma ray via pp collision in the case of Fireshell model, where we got that the production of gamma rays, in the GRB scenario, has inferior contribution than $10^{-10}\%$ of total energy of GRB.

3.2 Appendix: The "fireshell" model for GRBs

3.2.1 GRBs: Historical background

The basic steps leading to the birth of relativistic astrophysics are shortly outlined: from the understanding of the thermonuclear evolution of stars, to the discovery of neutron stars in pulsars and the observations of neutron stars and black holes in binary X-ray sources. We then recall the pioneering works of the discovery of Gamma-Ray Bursts (GRBs) and their theoretical explanation, predicting energetics on the order of 10^{54} ergs, in terms of the blackholic energy. Finally, we mention the early GRB classification into short and long GRBs, following the BATSE observations of the CGRO satellite, as well as the crucial role of the BeppoSAX satellite, leading to the optical identification and determination of the energetics of GRBs.

3.2.2 The three paradigms identifying the "canonical GRB"

Soon after the first attempt in the year 2000 of interpreting GRB 991216 in a consistent theoretical framework, our group became aware of the total conceptual new scenario presenting itself in the physics and astrophysics of GRBs. It was not just a problem of parameters' fitting in some already known theoretical framework. We were in presence of a new conceptual scenario, needing new paradigms to be developed. In three letters published on the same issue of *Astrophysical Journal Letters* in 2001, we introduced these three fundamental new paradigms (Ruffini et al., 2001c,b,a):

1. The Relative Space-Time Transformation (RSTT) paradigm (Ruffini et al., 2001c), linking the comoving time, the laboratory time and the time at the observer, necessary for the description of the GRB phenomenon.

2. The Interpretation of the Burst Structure (IBS) paradigm (Ruffini et al., 2001b), introducing the novel concept of the Proper-GRB (P-GRB) and separating it from the afterglow.

3. The GRB-Supernova Time Sequence (GSTS) paradigm (Ruffini et al., 2001a) introducing the novel concept of induced gravitational collapse.

3.2.3 The optically thick "fireshell"

The fireshell in the Livermore code In appendix "The fireshell in the Livermore code" we recall the basic hydrodynamics and rate equation for the electron-positron plasma. Then we outline the numerical code used to evolve the spherically symmetric general relativistic hydrodynamic equations starting from the dyadosphere. Such a code was not used by us but had already been developed independently for more general astrophysical scenarios by Jim Wilson and Jay Salmonson at the Lawrence Livermore National Laboratory (see Wilson et al., 1998a,b). In our collaboration, the Livermore code has been used in order to validate the correct choice among a variety of different semi-analytic models developed at the University of Rome "La Sapienza".

The fireshell in the Rome code In appendix "The fireshell in the Rome code" we first recall the co-variant energy-momentum tensor and the thermodynamic quantities used to describe the electron-positron plasma as well as their expression as functions of Fermi integrals. The thermodynamic equilibrium of the photons and the electron-positron pairs is initially assumed at temperature larger than e^+e^- pairs creation threshold ($T > 1$ MeV). The numerical code implementing entropy and energy conservations as well as the rate equation for the electron-positron pairs is outlined. We recall, as well, the simulation of different geometries assumed for the fireshell and the essential role of the Livermore code in selecting the correct one among these different possibilities for the dynamics of this plasma composed uniquely of electron, positron and photons (PEM pulse). The correct solution resulted to be the following: the fireshell is expanding in its comoving frame but its thickness is kept constant in the laboratory frame due to the balancing effect of the Lorentz contraction. We then examine the equations for the engulfment of the baryon loading as well as the further expansion of the fireshell composed by electron, positron, photons and baryon (PEMB pulse) up to the transparency point. We again point out the special role of the Livermore code in validating our results. Quite in addition of this validation procedures, the

Livermore code has been essential in evidencing an instability occurring at a critical value of the baryon loading parameter $B = 10^{-2}$ (Ruffini et al., 2000).

3.2.4 The optically thin "fireshell": the afterglow

In appendix "The optically thin "fireshell": the afterglow" we write the energy and momentum conservation equations for the interaction between the Accelerated Baryonic Matter (ABM) pulse and the CircumBurst Medium (CBM) in a finite difference formalism. We then express these same equations in a differential formalism to compare our approach with the ones in the current literature. We write the exact analytic solutions of such differential equations both in the fully radiative and in the adiabatic regimes.

3.2.5 The "canonical GRB" bolometric light curve

In the appendix "The "canonical GRB" bolometric light curve" we derive the expression for the bolometric luminosity of the GRB afterglow and we address the general issue of the possible explanation of the observed substructures in the GRB prompt emission as due to CBM inhomogeneities. On this topic there exist in the literature two extreme points of view: the one by Fenimore and collaborators (see e.g. Fenimore et al., 1996, 1999; Fenimore, 1999) and Piran and collaborators (see e.g. Sari and Piran, 1997; Piran, 1999, 2000, 2001) on one side and the one by Dermer and collaborators (Dermer, 1998; Dermer et al., 1999; Dermer and Mitman, 1999) on the other. Fenimore and collaborators have emphasized the relevance of a specific signature to be expected in the collision of a relativistic expanding shell with the CBM, what they call a fast rise and exponential decay (FRED) shape. This feature is confirmed by our analysis. However they also conclude, sharing the opinion by Piran and collaborators, that the variability observed in GRBs is inconsistent with causally connected variations in a single, symmetric, relativistic shell interacting with the ambient material ("external shocks", Fenimore et al., 1999). In their opinion the solution of the short time variability has to be envisioned within the protracted activity of an unspecified "inner engine" (Sari and Piran (1997); see as well Rees and Meszaros (1994); Panaitescu and Meszaros (1998b); Mészáros and Rees (2001); Mészáros (2002)). On the other hand, Dermer and collaborators, by considering an idealized process occurring at a fixed $\gamma = 300$, have reached the opposite conclusions and they purport that GRB light curves are tomographic images of the density distributions of the medium surrounding the sources of GRBs (Dermer and Mitman, 1999). By applying the exact formulas derived in previous appendices, we show that Dermer's conclusions are correct, and we identify that the "tomography" purported by Dermer and Mitman (1999) leads to CBM clouds consistently on the order of $\sim 10^{14}$ cm. Apparent superluminal effects are introduced. In our treatment we have adopted a simple spherically symmetric approximation for the CBM distribution. We show that the agreement of this approximation with the observations is excellent for Lorentz gamma factors $\gamma > 150$ since the relativistic beaming angle introduced in the previous appendices provides an effective cut-off to the visible CBM structure. For lower Lorentz gamma factors, a three dimensional description of the CBM would be needed and the corresponding treatment is currently in preparation.

We then define the "canonical GRB" light curve with two sharply different components: the Proper-GRB (P-GRB), emitted when the optically thick fireshell of electron-positron plasma originating the phenomenon reaches the transparency, and the afterglow, emitted due to the collision between the remaining optically thin fireshell and the CBM. Our "canonical GRB" scenario puts a special emphasis on the discrimination between "genuine" and "fake" short GRBs:

- The **"genuine" short GRBs** inherit their features from an intrinsic property of their sources. The very small fireshell baryon loading, in fact, implies that the afterglow time-integrated luminosity is negligible with respect to the P-GRB one.

- The **"fake" short GRBs**, instead, inherit their features from the environment. The very small CBM density, in fact, implies that the afterglow peak luminosity is lower than the P-GRB one, even if the afterglow total time-integrated luminosity is higher. This deflated afterglow peak can be observed as a "soft bump" following the P-GRB spike, as in GRB 970228 (Bernardini et al., 2007, 2008), GRB 060614 (Caito et al., 2008), and the sources analyzed by Norris and Bonnell (2006).

3.2.6 The spectra of the afterglow

In appendix "The spectra of the afterglow", having shown in the previous appendices a general agreement between the observed luminosity variability and our treatment of the bolometric luminosity, we have further developed the model in order to explain:
a) the details of the observed luminosity in fixed energy bands, which are the ones actually measured by the detectors on the satellites;
b) the instantaneous as well as the average spectral distribution in the entire afterglow and;
c) the hard to soft drift observed in GRB spectra.
The fundamental assumption is introduced that the X and gamma ray radiation during the entire afterglow phase has a thermal spectrum in the comoving frame. The ratio $\mathcal{R} = A_{eff}/A_{vis}$ between the "effective emitting area" A_{eff} of the ABM pulse and its full visible area A_{vis} is introduced. Due to the CBM inhomogeneities, composed of clouds with filamentary structure, the

ABM emitting region is in fact far from being homogeneous. We have justified the existence of this thermal emission by considering the CBM filamentary structure and its optical thickness (see Ruffini et al., 2005c). The theoretical prediction for the observed spectra starting from these premises has been by far the most complex and, in our opinion, the most elegant aspect of the entire GRB model. In order to compute the luminosity in a fixed energy band at a given value of the arrival time it is necessary to perform a convolution over the given EQuiTemporal Surface (EQTS, see Bianco and Ruffini, 2004, 2005b, and the following report about "Relativistic effects in Physics and Astrophysics") of an infinite number of elementary contributions, each one characterized by a different value of Lorentz and Doppler factors. Therefore, each observed instantaneous spectrum is theoretically predicted to be the result of a convolution of an infinite number of thermal spectra, each one with a different temperature, over the given EQTS and its shape is theoretically predicted to be non-thermal. Moreover, the observed time-integrated spectra depart even more from a thermal shape, being the convolution over the observation time of an infinite number of non-thermal instantaneous spectra. We confirm in this work the qualitative suggestion advanced by Blinnikov et al. (1999). We then examine the issue of the possible presence or absence of jets in GRBs in the case of GRB 991216. We compare and contrast our theoretically predicted afterglow luminosity in the 2–10 keV band for spherically symmetric versus collimated emission. At these wavelengths the collimated emission can be excluded and data analysis confirms spherical symmetry. In fact, the actual afterglow luminosity in fixed energy bands, in spherical symmetry, does not have a simple power law dependence on arrival time. This circumstance has been erroneously interpreted, in the usual presentation in the literature, as a broken power-law supporting the existence of jet-like structures in GRBs.

3.2.7 On the GRB-SN association

In appendix "On the GRB-SN association" we apply our theoretical framework to the analysis of all the GRBs associated with Supernovae (SNe). We proceed first to GRB 980425; we go then to GRB 030329; finally, we discuss the late time emission of GRB 031203 observed by XMM and Chandra. We summarize the general results of these GRBs associated with SNe and we make some general conclusions on the relations between GRBs, SNe and the URCA sources. We finally present some novel considerations about our third paradigm and the concept of induced gravitational collapse.

3.2.8 Application to GRB 031203

In appendix "Application to GRB 031203" we show how we are able to predict the whole dynamics of the process which originates the GRB 031203 emission fixing univocally the two free parameters of the model, $E_{e^\pm}^{tot}$ and B. Moreover, it is possible to obtain the exact temporal structure of the prompt emission taking into account the effective CBM filamentary structure. The important point we like to emphasize is that we can get both the luminosity emitted in a fixed energy band and the photon number spectrum starting from the hypothesis that the radiation emitted in the GRB process is thermal in the co-moving frame of the expanding pulse. We obtain a good agreement of our prediction with the photon number spectrum observed by INTEGRAL and, in addition, we predict a specific hard-to-soft behavior in the instantaneous spectra. Due to the possibility of reaching a precise identification of the emission process in GRB afterglows by the observations of the instantaneous spectra, it is hoped that further missions with larger collecting area and higher time resolving power be conceived and a systematic attention be given to closer-by GRB sources. Despite this GRB is often considered as "unusual" (Watson et al., 2004; Soderberg et al., 2004), in our treatment we are able to explain its low gamma-ray luminosity in a natural way, giving a complete interpretation of all its spectral features. In agreement to what has been concluded by Sazonov et al. (2004a), it appears to us as a under-energetic GRB ($E_{e^\pm}^{tot} \approx 10^{50}$ erg), well within the range of applicability of our theory, between 10^{48} erg for GRB 980425 (Ruffini et al., 2004a, 2007b) and 10^{54} erg for GRB 991216 (Ruffini et al., 2003).

3.2.9 Application to GRB 050315

Having used GRB 991216 as a prototype, we were constrained by the absence of data in the time range between ~ 36 s and ~ 3500 s. This same situation was encountered, even more extremely, in all the other sources, like e.g. GRB 970228, GRB 980425, GRB 030329, etc. Fortunately, the launch of the *Swift* mission changed drastically and positively this situation. We could obtain a continuous set of data from the prompt emission to the latest afterglow phases in multiple energy bands.

In appendix "Application to GRB 050315" we discuss how before the *Swift* data, our model could not be directly fully tested. With GRB 050315, for the first time, we have obtained a good match between the observational data and our predicted intensities, in 5 energy bands, with continuous light curves near the beginning of the GRB event, including the "prompt emission", all the way to the latest phases of the afterglow. This certainly supports our model and opens a new phase of using it to identify the astrophysical scenario underlying the GRB phenomena. In particular:

1. We have confirmed that the "prompt emission" is not necessarily due

to the prolonged activity of an "inner engine", but corresponds to the emission at the peak of the afterglow.

2. We have a clear theoretical prediction, fully confirmed from the observations, on the total energy emitted in the P-GRB $E_{P-GRB} = 1.98 \times 10^{51}$ erg and on its temporal separation from the peak of the afterglow $\Delta t_a^d = 51$ s. To understand the physics of the inner engine more observational and theoretical attention should be given to the analysis of the P-GRB.

3. We have uniquely identified the basic parameters characterizing the GRB energetics: the total energy of the electron-positron plasma $E_{e^\pm}^{tot} = 1.46 \times 10^{53}$ erg and the baryon loading parameter $B = 4.55 \times 10^{-3}$.

4. The "canonical behavior" in almost all the GRB observed by *Swift*, showing an initial very steep decay followed by a shallow decay and finally a steeper decay, as well as the time structure of the "prompt emission" have been related to the fluctuations of the CBM density and of the $\mathcal{R}$ parameter.

5. The theoretically predicted instantaneous photon number spectrum shows a very clear hard-to-soft behavior continuously and smoothly changing from the "prompt emission" all the way to the latest afterglow phases.

After the analysis of the above two sources, only the earliest part of the afterglow we theoretically predicted, which corresponds to a bolometric luminosity monotonically increasing with the photon detector arrival time, preceding the "prompt emission", still remains to be checked by direct observations. We hope in the near future to find an intense enough source, observed by the *Swift* satellite, to verify this still untested theoretical prediction.

As a byproduct of the above results, we could explain one of the long lasting unanswered puzzles of GRBs: the light curves in the "prompt emission" show very strong temporal substructures, while they are remarkably smooth in the latest afterglow phases. The explanation follows from three factors: 1) the value of the Lorentz γ factor, 2) the EQTS structure and 3) the coincidence of the "prompt emission" with the peak of the afterglow. For $\gamma \sim 200$, at the peak of the afterglow, the diameter of the EQTS visible area due to relativistic beaming is small compared to the typical size of an CBM cloud. Consequently, any small inhomogeneity in such a cloud produces a marked variation in the GRB light curve. On the other hand, for $\gamma \to 1$, in the latest afterglow phases, the diameter of the EQTS visible area is much bigger than the typical size of an CBM cloud. Therefore, the observed light curve is a superposition of the contribution of many different clouds and inhomogeneities, which produces on average a much smoother light curve (details in Ruffini et al., 2002a, 2003)).

3.2.10 Application to GRB 011121

A flare is a large scale activity in excess on the underlying light curve that manifests as a bump in luminosity rather intense and sharp in the decaying phase of the afterglow. When the first flare was detected by BeppoSAX, on the X-Ray light curve of GRB 011121, it was assumed as an extremely peculiar phenomenon. However, by the advent of the Swift Mission, many flares have been discovered in the light curves of about the 50% of the total amount of X-Ray afterglows observed: it was clear that flares are a very typical feature of GRBs phenomenon.

In our theory the multiwavelenght emission is entirely due to the fully inelastic collisions of the baryonic remnants of the fireshell with the CBM. Flares also, as characteristic parts of the afterglow, can be naturally explained in this context. We realized a first attempt to check this idea analyzing the burst with the first flare observed: GRB 011121.

3.2.11 Application to GRB 060218

GRB060218 is the best example of a Gamma-Ray Burst (GRB) associated with a Supernova (SN) Ib/c (Campana et al., 2006a). Its extremely long duration is unusual, with the longest T_{90} ever observed ($T_{90} \sim 2100$ s). This source is also interesting since it represents a discriminant between existing GRB theories: it has been pointed out by Soderberg et al. (2006b) and Fan et al. (2006) that it is impossible to explain the X- and radio afterglows within the traditional synchrotron model. They attempted to fit only the late radio data after $\sim 10^3$ s and they attributed the nature of the prompt emission to an as yet undetermined "inner engine" (see Soderberg et al., 2006b), possibly a magnetar (Mazzali et al., 2006).

Here we present a detailed fit of the entire X- and γ-ray light curves including the prompt emission: there is no need here for the prolonged activity of an inner engine. Therefore we explain the unusually high values of the observed T_{90} by our "fireshell" model.

The initial total energy of the electron-positron plasma $E_{e^\pm}^{tot} = 2.32 \times 10^{50}$ erg has a particularly low value, similar to the other GRBs associated with SNe. For the first time, we observe a baryon loading $B = 10^{-2}$ which coincides with the upper limit for the dynamical stability of the fireshell. The effective CBM density shows a radial dependence $n_{cbm} \propto r^{-\alpha}$ with $1.0 \lesssim \alpha \lesssim 1.7$ and monotonically decreases from 1 to 10^{-6} particles/cm^3. This behavior is interpreted as being due to a fragmentation in the fireshell. Analogies with the fragmented density and filling factor characterizing Novae are outlined. The fit presented is particularly significant in view of the complete data set available for GRB060218 and of the fact that it fulfills the Amati relation.

3.2.12 Application to GRB 970228

The discovery by *Swift* and HETE-2 of an afterglow emission associated possibly with short GRBs opened the new problematic of their nature and classification. The observations of GRB 060614 (Gehrels et al., 2006; Mangano et al., 2007) challenged the standard GRB classification scheme (Klebesadel, 1992; Dezalay et al., 1992) in which the gamma events are branched into two classes: "short" GRBs (events which last less than $\sim$ 2s) and "long" GRBs (events which last more than $\sim$ 2s). GRB 060614, indeed, "reveals a first short, hard-spectrum episode of emission (lasting 5 s) followed by an extended and somewhat softer episode (lasting $\sim$ 100 s)": a "two-component emission structure" (Gehrels et al., 2006). Moreover, stringent upper limits on the luminosity of the Supernova possibly associated with GRB 060614 have been established (Della Valle et al., 2006; Gal-Yam et al., 2006). Gehrels et al. (2006) concluded that "it is difficult to determine unambiguously which category GRB 060614 falls into" and that, then, GRB 060614, due to its "hybrid" observational properties, "opens the door on a new GRB classification scheme that straddles both long and short bursts" (Gehrels et al., 2006).

These observations motivated Norris and Bonnell (2006) to reanalyze the BATSE catalog identifying a new GRB class with "an occasional softer extended emission lasting tenths of seconds after an initial spikelike emission" (Norris and Bonnell, 2006). In some cases, "the strength of the extended emission converts an otherwise short burst into one with a duration that can be tens of seconds, making it appear to be a long burst" (Norris and Bonnell, 2006). Hence, Norris and Bonnell (2006) suggested that the standard "long-short" GRB classification scheme "is at best misleading" (Norris and Bonnell, 2006).

In this appendix we will propose GRB 970228 (Costa et al., 1997; Frontera et al., 1998, 2000) as the prototype of these "hybrid" sources, since it shares the same morphology and observational features. We will show that such "hybrid" sources are indeed explainable within our "canonical GRB" scenario in terms of a peculiarly small average value of the CBM density, compatible with a galactic halo environment (see also Bernardini et al., 2007, 2008, and sec. A.5.2 for details).

We analyze *Beppo*SAX data on GRB 970228 within the "fireshell" model and we find that GRB 970228 is a "canonical GRB" as defined in sec. A.5.2, with the main peculiarity of a particularly low average density of the CBM $\langle n_{cbm} \rangle \sim 10^{-3}$ particles/cm^3, consistent with a galactic halo environment. We also simulate the light curve corresponding to a rescaled CBM density profile with $\langle n_{cbm} \rangle = 1$ particle/cm^3. From such a comparison it follows that the total time-integrated luminosity is a faithful indicator of the nature of GRBs, contrary to the peak luminosity which is merely a function of the CBM density.

Moreover, we investigate how GRB 970228 unveils another peculiarity of this class of GRBs: they do not fulfill the "Amati relation". We provide a theoretical explanation within the fireshell model for the apparent absence of such correlation for the GRBs belonging to this new class.

4 Selected publications before 2005

4.1 Refereed journals

1. D. Christodoulou, R. Ruffini; "Reversible Transformations of a Charged Black Hole"; Physical Review D, 4, 3552 (1971).

   A formula is derived for the mass of a black hole as a function of its "irreducible mass", its angular momentum, and its charge. It is shown that 50% of the mass of an extreme charged black hole can be converted into energy as contrasted with 29% for an extreme rotating black hole.

2. T. Damour, R. Ruffini; "Quantum electrodynamical effects in Kerr-Newman geometries"; Physical Review Letters, 35, 463 (1975).

   Following the classical approach of Sauter, of Heisenberg and Euler and of Schwinger the process of vacuum polarization in the field of a "bare" Kerr-Newman geometry is studied. The value of the critical strength of the electromagnetic fields is given together with an analysis of the feedback of the discharge on the geometry. The relevance of this analysis for current astrophysical observations is mentioned.

3. G. Preparata, R. Ruffini, S.-S. Xue; "The dyadosphere of black holes and gamma-ray bursts"; Astronomy & Astrophysics, 338, L87 (1999).

   The "dyadosphere" has been defined as the region outside the horizon of a black hole endowed with an electromagnetic field (abbreviated to EMBH for "electromagnetic black hole") where the electromagnetic field exceeds the critical value, predicted by Heisenberg & Euler for $e^{\pm}$ pair production. In a very short time ($\sim O(\hbar/mc^2)$) a very large number of pairs is created there. We here give limits on the EMBH parameters leading to a Dyadosphere for $10M_{\odot}$ and $10^5M_{\odot}$ EMBH's, and give as well the pair densities as functions of the radial coordinate. We here assume that the pairs reach thermodynamic equilibrium with a photon gas and estimate the average energy per pair as a function of the EMBH mass. These data give the initial conditions for the analysis of an enormous pair-electromagnetic-pulse or "P.E.M. pulse" which naturally leads to relativistic expansion. Basic energy requirements for gamma ray bursts (GRB), including GRB971214 recently observed at z=3.4, can be accounted for by processes occurring in the dyadosphere. In this letter we do not address the problem of forming either the EMBH or the dyadosphere: we establish some inequalities which must be satisfied during their formation process.

4. R. Ruffini, J.D. Salmonson, J.R. Wilson, S.-S. Xue; "On the pair electromagnetic pulse of a black hole with electromagnetic structure"; Astronomy & Astrophysics, 350, 334 (1999).

   We study the relativistically expanding electron-positron pair plasma formed by the process of vacuum polarization around an electromagnetic black hole (EMBH). Such processes can occur for EMBH's with mass all the way up to $6 \times 10^5 M_\odot$. Beginning with a idealized model of a Reissner-Nordstrom EMBH with charge to mass ratio $\xi = 0.1$, numerical hydrodynamic calculations are made to model the expansion of the pair-electromagnetic pulse (PEM pulse) to the point that the system is transparent to photons. Three idealized special relativistic models have been compared and contrasted with the results of the numerically integrated general relativistic hydrodynamic equations. One of the three models has been validated: a PEM pulse of constant thickness in the laboratory frame is shown to be in excellent agreement with results of the general relativistic hydrodynamic code. It is remarkable that this precise model, starting from the fundamental parameters of the EMBH, leads uniquely to the explicit evaluation of the parameters of the PEM pulse, including the energy spectrum and the astrophysically unprecedented large Lorentz factors (up to 6×10^3 for a $10^3 M_\odot$ EMBH). The observed photon energy at the peak of the photon spectrum at the moment of photon decoupling is shown to range from 0.1 MeV to 4 MeV as a function of the EMBH mass. Correspondingly the total energy in photons is in the range of 10^{52} to 10^{54} ergs, consistent with observed gamma-ray bursts. In these computations we neglect the presence of baryonic matter which will be the subject of forthcoming publications.

5. R. Ruffini, J.D. Salmonson, J.R. Wilson, S.-S. Xue; "On the pair-electro magnetic pulse from an electromagnetic black hole surrounded by a baryonic remnant"; Astronomy & Astrophysics, 359, 855 (2000).

   The interaction of an expanding Pair-Electromagnetic pulse (PEM pulse) with a shell of baryonic matter surrounding a Black Hole with electromagnetic structure (EMBH) is analyzed for selected values of the baryonic mass at selected distances well outside the dyadosphere of an EMBH. The dyadosphere, the region in which a super critical field exists for the creation of e+e- pairs, is here considered in the special case of a Reissner-Nordstrom geometry. The interaction of the PEM pulse with the baryonic matter is described using a simplified model of a slab of constant thickness in the laboratory frame (constant-thickness approximation) as well as performing the integration of the general relativistic hydrodynamical equations. Te validation of the constant-thickness approximation, already presented in a previous paper Ruffini et al. (1999) for a PEM pulse in vacuum, is here generalized to the presence of baryonic matter. It is found that for a baryonic shell of mass-energy less than 1% of the total energy of the dyadosphere, the constant-thickness approximation is in excellent agreement with full general relativistic computations. The approximation breaks down for larger values of the baryonic shell mass, however such cases are of less interest for observed Gamma Ray Bursts (GRBs). On the basis of numerical computations of the slab model for PEM pulses, we describe (i) the properties of relativistic evolution of a PEM pulse colliding with a baryonic shell; (ii) the details of the expected emission energy and observed temperature of the associated GRBs for a given value of the EMBH mass; $10^3 M_\odot$, and for baryonic mass-energies in the range 10^{-8} to 10^{-2} the total energy of the dyadosphere.

6. C.L. Bianco, R. Ruffini, S.-S. Xue; "The elementary spike produced by a pure e+e- pair-electromagnetic pulse from a Black Hole: The PEM Pulse"; Astronomy & Astrophysics, 368, 377 (2001).

   In the framework of the model that uses black holes endowed with electromagnetic structure (EMBH) as the energy source, we study how an elementary spike appears to the detectors. We consider the simplest possible case of a pulse produced by a pure e^+e^- pair-electro-magnetic plasma, the PEM pulse, in the absence of any baryonic matter. The resulting time profiles show a *Fast-Rise-Exponential-Decay* shape, followed by a power-law tail. This is obtained without any special fitting procedure, but only by fixing the energetics of the process taking place in a given EMBH of selected mass, varying in the range from 10 to 10^3 $M_\odot$ and considering the relativistic effects to be expected in an electron-positron plasma gradually reaching transparency. Special attention is given to the contributions from all regimes with Lorentz γ factor varying from $\gamma = 1$ to $\gamma = 10^4$ in a few hundreds of the PEM pulse travel time. Although the main goal of this paper is to obtain the elementary spike intensity as a function of the arrival time, and its observed duration, some qualitative considerations are also presented regarding the expected spectrum and on its departure from the thermal one. The results of this paper will be comparable, when data will become available, with a subfamily of particularly short GRBs not followed by any afterglow. They can also be propedeutical to the study of longer bursts in presence of baryonic matter currently observed in GRBs.

7. R. Ruffini, C.L. Bianco, P. Chardonnet, F. Fraschetti, S.-S. Xue; "Relative spacetime transformations in Gamma-Ray Bursts"; The Astrophysical Journal, 555, L107 (2001).

   The GRB 991216 and its relevant data acquired from the BATSE experiment and RXTE and Chandra satellites are used as a prototypical case to test the theory linking the origin of gamma ray bursts (GRBs) to the process of vacuum polarization occurring during the formation phase of a black hole endowed with electromagnetic structure (EMBH). The relative space-time transformation paradigm (RSTT paradigm) is presented. It relates the observed signals of GRBs to their past light cones, defining the events on the worldline of the source essential for the interpretation of the data. Since GRBs present regimes with unprecedently large Lorentz γ factor, also sharply varying with time, particular attention is given to the constitutive equations relating the four time variables: the comoving time, the laboratory time, the arrival time at the detector, duly corrected by the cosmological effects. This paradigm is at the very foundation of any possible interpretation of the data of GRBs.

8. R. Ruffini, C.L. Bianco, P. Chardonnet, F. Fraschetti, S.-S. Xue; "On the interpretation of the burst structure of Gamma-Ray Bursts"; The Astrophysical Journal, 555, L113 (2001).

   Given the very accurate data from the BATSE experiment and RXTE and Chandra satellites, we use the GRB 991216 as a prototypical case to test the EMBH theory linking the origin of the energy of GRBs to the electromagnetic energy of black holes. The fit of the afterglow fixes the only two free parameters of the model and leads to a new paradigm for the interpretation of the burst structure, the IBS paradigm. It leads as well to a reconsideration of the relative roles of the afterglow and burst in GRBs by defining two new phases in this complex phenomenon: a) the injector phase, giving rise to the proper-GRB (P-GRB), and b) the beam-target phase, giving rise to the extended afterglow peak emission (E-APE) and to the afterglow. Such differentiation leads to a natural possible explanation of the bimodal distribution of GRBs observed by BATSE. The agreement with the observational data in regions extending from the horizon of the EMBH all the way out to the distant observer confirms the uniqueness of the model.

9. R. Ruffini, C.L. Bianco, P. Chardonnet, F. Fraschetti, S.-S. Xue; "On a possible Gamma-Ray Burst-Supernova time sequence"; The Astrophysical Journal, 555, L117 (2001).

   The data from the Chandra satellite on the iron emission lines in the afterglow of GRB 991216 are used to give further support for the EMBH theory, which links the origin of the energy of GRBs to the extractable energy of electromagnetic black holes (EMBHs), leading to an interpretation of the GRB-supernova correlation. Following the relative space-time transformation (RSTT) paradigm and the interpretation of the burst structure (IBS) paradigm, we introduce a paradigm for the correlation between GRBs and supernovae. The following sequence of events is shown as kinematically possible and consistent with the available data: a) the GRB-progenitor star P_1 first collapses to an EMBH, b) the proper GRB (P-GRB) and the peak of the afterglow (E-APE) propagate in interstellar space until the impact on a supernova-progenitor star P_2 at a distance $\leq 2.69 \times 10^{17}$ cm, and they induce the supernova explosion, c) the accelerated baryonic matter (ABM) pulse, originating the afterglow, reaches the supernova remnants 18.5 hours after the supernova explosion and gives rise to the iron emission lines. Some considerations on the dynamical implementation of the paradigm are presented. The concept of induced supernova explosion introduced here specifically for the GRB-supernova correlation may have more general application in relativistic astrophysics.

10. R. Ruffini, C.L. Bianco, P. Chardonnet, F. Fraschetti, S.-S. Xue; "On the physical processes which lie at the bases of time variability of GRBs"; Il Nuovo Cimento B, 116, 99 (2001).

    The relative-space-time-transformation (RSTT) paradigm and the interpretation of the burst-structure (IBS) paradigm are applied to probe the origin of the time variability of GRBs. Again GRB 991216 is used as a prototypical case, thanks to the precise data from the CGRO, RXTE and Chandra satellites. It is found that with the exception of the relatively inconspicuous but scientifically very important signal originating from the initial "proper gamma ray burst" (P-GRB), all the other spikes and time variabilities can be explained by the interaction of the accelerated-baryonic-matter pulse with inhomogeneities in the interstellar matter. This can be demonstrated by using the RSTT paradigm as well as the IBS paradigm, to trace a typical spike observed in arrival time back to the corresponding one in the laboratory time. Using these paradigms, the identification of the physical nature of the time variablity of the GRBs can be made most convincingly. It is made explicit the dependence of a) the intensities of the afterglow, b) the spikes amplitude and c) the actual time structure on the Lorentz gamma factor of the accelerated-baryonic-matter pulse. In principle it is possible to read off from the spike structure the detailed density contrast of the interstellar medium in the host galaxy, even at very high redshift.

11. R. Ruffini, C.L. Bianco, P. Chardonnet, F. Fraschetti, S.-S. Xue; "On the structures in the afterglow peak emission of gamma ray bursts"; The Astrophysical Journal, 581, L19 (2002).

    Using GRB 991216 as a prototype, it is shown that the intensity substructures observed in what is generally called the "prompt emission" in gamma ray bursts (GRBs) do originate in the collision between the accelerated baryonic matter (ABM) pulse with inhomogeneities in the interstellar medium (ISM). The initial phase of such process occurs at a Lorentz factor $\gamma \sim 310$. The crossing of ISM inhomogeneities of sizes $\Delta R \sim 10^{15}$ cm occurs in a detector arrival time interval of ~ 0.4 s implying an apparent superluminal behavior of $\sim 10^5 c$. The long lasting debate between the validity of the external shock model vs. the internal shock model for GRBs is solved in favor of the first.

12. R. Ruffini, C.L. Bianco, P. Chardonnet, F. Fraschetti, S.-S. Xue; "On the structure of the burst and afterglow of Gamma-Ray Bursts I: the radial approximation"; International Journal of Modern Physics D, 12, 173 (2003).

    We have recently proposed three paradigms for the theoretical interpretation of gamma-ray bursts (GRBs). (1) The relative space-time transformation (RSTT) paradigm emphasizes how the knowledge of the entire world-line of the source from the moment of gravitational collapse is a necessary condition in order to interpret GRB data. (2) The interpretation of the burst structure (IBS) paradigm differentiates in all GRBs between an injector phase and a beam-target phase. (3) The GRB-supernova time sequence (GSTS) paradigm introduces the concept of *induced supernova explosion* in the supernovae-GRB association. In the introduction the RSTT and IBS paradigms are enunciated and illustrated using our theory based on the vacuum polarization process occurring around an electromagnetic black hole (EMBH theory). The results are summarized using figures, diagrams and a complete table with the space-time grid, the fundamental parameters and the corresponding values of the Lorentz gamma factor for GRB 991216 used as a prototype. In the following sections the detailed treatment of the EMBH theory needed to understand the results of the three above letters is presented. We start from the considerations on the dyadosphere formation. We then review the basic hydrodynamic and rate equations, the equations leading to the relative space-time transformations as well as the adopted numerical integration techniques. We then illustrate the five fundamental eras of the EMBH theory: the self acceleration of the e^+e^- pair-electromagnetic plasma (PEM pulse), its interaction with the baryonic remnant of the progenitor star, the further self acceleration of the e^+e^- pair-electroma--gnetic radiation and baryon plasma (PEMB pulse). We then study the approach of the PEMB pulse to transparency, the emission of the proper GRB (P-GRB) and its relation to the "short GRBs". Particular attention is given to the free parameters of the theory and to the values of the thermodynamical quantities at transparency. Finally the three different regimes of the afterglow are described within the fully radiative and radial approximations: the ultrarelativistic, the relativistic and the nonrelativistic regimes. The best fit of the theory leads to an unequivocal identification of the "long GRBs" as extended emission occurring at the afterglow peak (E-APE). The relative intensities, the time separation and the hardness ratio of the P-GRB and the E-APE are used as distinctive observational test of the EMBH theory and the excellent agreement between our theoretical predictions and the observations are documented. The afterglow power-law indexes in the EMBH theory are compared and contrasted with the ones in the literature, and no beaming process is found for GRB 991216. Finally, some preliminary results relating the observed time variability of the E-APE to the inhomogeneities in the interstellar medium are presented, as well as some general considerations on the EMBH formation. The issue of the GSTS paradigm will be the object of a forthcoming publication and the relevance of the iron-lines observed in GRB 991216 is shortly reviewed. The general conclusions are then presented based on the three fundamental parameters of the EMBH theory: the dyadosphere energy, the baryonic mass of the remnant, the interstellar medium density. An in depth discussion and comparison of the EMBH theory with alternative theories is presented as well as indications of further developments beyond the radial approximation, which will be the subject of paper II in this series. Future needs for specific

GRB observations are outlined.

13. R. Ruffini, C.L. Bianco, P. Chardonnet, F. Fraschetti, V. Gurzadyan, S.-S. Xue; "On the instantaneous spectrum of gamma ray bursts"; International Journal of Modern Physics D, 13, 843 (2004).

    A theoretical attempt to identify the physical process responsible for the afterglow emission of Gamma-Ray Bursts (GRBs) is presented, leading to the occurrence of thermal emission in the comoving frame of the shock wave giving rise to the bursts. The determination of the luminosities and spectra involves integration over an infinite number of Planckian spectra, weighted by appropriate relativistic transformations, each one corresponding to a different viewing angle in the past light cone of the observer. The relativistic transformations have been computed using the equations of motion of GRBs within our theory, giving special attention to the determination of the equitemporal surfaces. The only free parameter of the present theory is the "effective emitting area" in the shock wave front. A self consistent model for the observed hard-to-soft transition in GRBs is also presented. When applied to GRB 991216 a precise fit $\left(\chi^2 \simeq 1.078\right)$ of the observed luminosity in the 2–10 keV band is obtained. Similarly, detailed estimates of the observed luminosity in the 50–300 keV and in the 10–50 keV bands are obtained.

4.2 Conference proceedings

1. R. Ruffini; "Beyond the critical mass: The dyadosphere of black holes"; in "Black Holes and High Energy Astrophysics", H. sato, N. Sugiyama, Editors; p. 167; Universal Academy Press (Tokyo, Japan, 1998).

   The "dyadosphere" (from the Greek word "duas-duados" for pairs) is here defined as the region outside the horizon of a black hole endowed with an electromagnetic field (abbreviated to EMBH for "electromagnetic black hole") where the electromagnetic field exceeds the critical value, predicted by Heisenberg and Euler for e^+e^- pair production. In a very short time ($\sim O(\hbar/mc^2)$), a very large number of pairs is created there. I give limits on the EMBH parameters leading to a Dyadosphere for $10M_\odot$ and $10^5M_\odot$ EMBH's, and give as well the pair densities as functions of the radial coordinate. These data give the initial conditions for the analysis of an enormous pair-electromagnetic-pulse or "PEM-pulse" which naturally leads to relativistic expansion. Basic energy requirements for gamma ray bursts (GRB), including GRB971214 recently observed at $z = 3.4$, can be accounted for by processes occurring in the dyadosphere.

2. R. Ruffini, C.L. Bianco, P. Chardonnet, F. Fraschetti, L. Vitagliano, S.-S. Xue; "New perspectives in physics and astrophysics from the theoretical understanding of Gamma-Ray Bursts"; in "COSMOLOGY AND

GRAVITATION: Xth Brazilian School of Cosmology and Gravitation; 25th Anniversary (1977-2002)", Proceedings of the Xth Brazilian School on Cosmology and Gravitation, Mangaratiba, Rio de Janeiro (Brazil), July - August 2002, M. Novello, S.E. Perez Bergliaffa, Editors; AIP Conference Proceedings, 668, 16 (2003).

If due attention is given in formulating the basic equations for the Gamma-Ray Burst (GRB) phenomenon and in performing the corresponding quantitative analysis, GRBs open a main avenue of inquiring on totally new physical and astrophysical regimes. This program is very likely one of the greatest computational efforts in physics and astrophysics and cannot be actuated using shortcuts. A systematic approach is needed which has been highlighted in three basic new paradigms: the relative space-time transformation (RSTT) paradigm, the interpretation of the burst structure (IBS) paradigm, the GRB-supernova time sequence (GSTS) paradigm. From the point of view of fundamental physics new regimes are explored: (1) the process of energy extraction from black holes; (2) the quantum and general relativistic effects of matter-antimatter creation near the black hole horizon; (3) the physics of ultrarelativisitc shock waves with Lorentz gamma factor $\gamma > 100$. From the point of view of astronomy and astrophysics also new regimes are explored: (i) the occurrence of gravitational collapse to a black hole from a critical mass core of mass $M \gtrsim 10M_{\odot}$, which clearly differs from the values of the critical mass encountered in the study of stars "catalyzed at the endpoint of thermonuclear evolution" (white dwarfs and neutron stars); (ii) the extremely high efficiency of the spherical collapse to a black hole, where almost 99.99% of the core mass collapses leaving negligible remnant; (iii) the necessity of developing a fine tuning in the final phases of thermonuclear evolution of the stars, both for the star collapsing to the black hole and the surrounding ones, in order to explain the possible occurrence of the "induced gravitational collapse". New regimes are as well encountered from the point of view of nature of GRBs: (I) the basic structure of GRBs is uniquely composed by a proper-GRB (P-GRB) and the afterglow; (II) the long bursts are then simply explained as the peak of the afterglow (the E-APE) and their observed time variability is explained in terms of inhomogeneities in the interstellar medium (ISM); (III) the short bursts are identified with the P-GRBs and the crucial information on general relativistic and vacuum polarization effects are encoded in their spectra and intensity time variability. A new class of space missions to acquire information on such extreme new regimes are urgently needed.

3. R. Ruffini, C.L. Bianco, P. Chardonnet, F. Fraschetti, S.-S. Xue; "The EMBH Model in GRB 991216 and GRB 980425"; in Proceedings of "Third Rome Workshop on Gamma-Ray Burst in the Afterglow Era", 17-20 September 2002; M. Feroci, F. Frontera, N. Masetti, L. Piro, Editors; ASP Conference Series, 312, 349 (2004).

This is a summary of the two talks presented at the Rome GRB meeting by C.L. Bianco and R. Ruffini. It is shown that by respecting the Relative Space-Time Transformation (RSTT) paradigm and the Interpretation of the Burst Structure (IBS) paradigm, important inferences are possible: a) in the new physics occurring in the energy sources of GRBs, b) on the structure of the bursts and c) on the composition of the interstellar matter surrounding the source.

4. M.G. Bernardini, C.L. Bianco, P. Chardonnet, F. Fraschetti, R. Ruffini, S.-S. Xue; "A New Astrophysical 'Triptych': GRB030329/SN2003dh/ URCA-2"; in "GAMMA-RAY BURSTS: 30 YEARS OF DISCOVERY", Proceedings of the Los Alamos "Gamma Ray Burst Symposium", Santa Fe, New Mexico, 8 12 September 2003, E.E. Fenimore, M. Galassi, Editors; AIP Conference Proceedings, 727, 312 (2004).

   We analyze the data of the Gamma-Ray Burst/Supernova GRB030329/ SN2003dh system obtained by HETE-2, R-XTE, XMM and VLT within our theory for GRB030329. By fitting the only three free parameters of the EMBH theory, we obtain the luminosity in fixed energy bands for the prompt emission and the afterglow. Since the Gamma-Ray Burst (GRB) analysis is consistent with a spherically symmetric expansion, the energy of GRB030329 is $E = 2.1 \times 10^{52}$ erg, namely $\sim 2 \times 10^3$ times larger than the Supernova energy. We conclude that either the GRB is triggering an induced-supernova event or both the GRB and the Supernova are triggered by the same relativistic process. In no way the GRB can be originated from the supernova. We also evidence that the XMM observations, much like in the system GRB980425/SN1998bw, are not part of the GRB afterglow, as interpreted in the literature, but are associated to the Supernova phenomenon. A dedicated campaign of observations is needed to confirm the nature of this XMM source as a newly born neutron star cooling by generalized URCA processes.

5. F. Fraschetti, M.G. Bernardini, C.L. Bianco, P. Chardonnet, R. Ruffini, S.-S. Xue; "The GRB980425-SN1998bw Association in the EMBH Model"; in "GAMMA-RAY BURSTS: 30 YEARS OF DISCOVERY", Proceedings of the Los Alamos "Gamma Ray Burst Symposium", Santa Fe, New Mexico, 8 12 September 2003, E.E. Fenimore, M. Galassi, Editors; AIP Conference Proceedings, 727, 424 (2004).

   Our GRB theory, previously developed using GRB 991216 as a prototype, is here applied to GRB 980425. We fit the luminosity observed in the 40–700 keV, 2–26 keV and 2–10 keV bands by the BeppoSAX satellite. In addition the supernova SN1998bw is the outcome of an "induced gravitational collapse" triggered by GRB 980425, in agreement with the GRB-Supernova Time Sequence (GSTS) paradigm. A further outcome of this astrophysically exceptional sequence of events is the formation of a young neutron star generated by the SN1998bw event. A coordinated observational activity is recommended to further enlighten the underlying scenario of this most unique astrophysical system.

6. A. Corsi, M.G. Bernardini, C.L. Bianco, P. Chardonnet, F. Fraschetti, R. Ruffini, S.-S. Xue; "GRB 970228 Within the EMBH Model"; in "GAMMA-RAY BURSTS: 30 YEARS OF DISCOVERY", Proceedings of the Los Alamos "Gamma Ray Burst Symposium", Santa Fe, New Mexico, 8 12 September 2003, E.E. Fenimore, M. Galassi, Editors; AIP Conference Proceedings, 727, 428 (2004).

   We consider the gamma-ray burst of 1997 February 28 (GRB 970228) within the ElectroMagnetic Black Hole (EMBH) model. We first determine the value of the two free parameters that characterize energetically the GRB phenomenon in the EMBH model, that is to say the dyadosphere energy, $E_{dya} = 5.1 \times 10^{52}$ ergs, and the baryonic remnant mass M_B in units of E_{dya}, $B = M_B c^2 / E_{dya} = 3.0 \times 10^{-3}$. Having in this way estimated the energy emitted during the beam-target phase, we evaluate the role of the InterStellar Medium (ISM) number density (n_{ISM}) and of the ratio $\mathcal{R}$ between the effective emitting area and the total surface area of the GRB source, in reproducing the observed profiles of the GRB 970228 prompt emission and X-ray (2-10 keV energy band) afterglow. The importance of the ISM distribution three-dimensional treatment around the central black hole is also stressed in this analysis.

5 Publications (2005–2008)

5.1 Refereed journals

1. R. Ruffini, C.L. Bianco, P. Chardonnet, F. Fraschetti, V. Gurzadyan, S.-S. Xue; "Emergence of a filamentary structure in the fireball from GRB spectra"; International Journal of Modern Physics D, 14, 97 (2005).

   It is shown that the concept of a fireball with a definite filamentary structure naturally emerges from the analysis of the spectra of Gamma-Ray Bursts (GRBs). These results, made possible by the recently obtained analytic expressions of the equitemporal surfaces in the GRB afterglow, depend crucially on the single parameter R describing the effective area of the fireball emitting the X-ray and gamma-ray radiation. The X-ray and gamma-ray components of the afterglow radiation are shown to have a thermal spectrum in the comoving frame of the fireball and originate from a stable shock front described self-consistently by the Rankine-Hugoniot equations. Precise predictions are presented on a correlation between spectral changes and intensity variations in the prompt radiation verifiable, e.g., by the Swift and future missions. The highly variable optical and radio emission depends instead on the parameters of the surrounding medium. The GRB 991216 is used as a prototype for this model.

2. R. Ruffini, M.G. Bernardini, C.L. Bianco, P. Chardonnet, F. Fraschetti, V. Gurzadyan, M. Lattanzi, L. Vitagliano, S.-S. Xue; "Extracting energy from black holes: 'long' and 'short' GRBs and their astrophysical settings"; Il Nuovo Cimento C, 28, 589 (2005).

   The introduction of the three interpretational paradigms for Gamma-Ray Bursts (GRBs) and recent progress in understanding the X- and gamma-ray luminosity in the afterglow allow us to make assessments about the astrophysical settings of GRBs. In particular, we evidence the distinct possibility that some GRBs occur in a binary system. This subclass of GRBs manifests itself in a "tryptich": one component formed by the collapse of a massive star to a black hole, which originates the GRB; a second component by a supernova and a third one by a young neutron star born in the supernova event. Similarly, the understanding of the physics of quantum relativistic processes during the gravitational collapse makes possible precise predictions about the structure of short GRBs.

3. M.G. Bernardini, C.L. Bianco, P. Chardonnet, F. Fraschetti, R. Ruffini, S.-S. Xue; "Theoretical interpretation of luminosity and spectral properties of GRB 031203"; The Astrophysical Journal, 634, L29 (2005).

   The X-ray and gamma-ray observations of the source GRB 031203 by INTEGRAL are interpreted within our theoretical model. In addition to a complete spacetime parameterization of the GRB, we specifically assume that the afterglow emission originates from a thermal spectrum in the comoving frame of the expanding baryonic matter shell. By determining the two free parameters of the model and estimating the density and filamentary structure of the ISM, we reproduce the observed luminosity in the 20-200 keV energy band. As in previous sources, the prompt radiation is shown to coincide with the peak of the afterglow, and the luminosity substructure is shown to originate in the filamentary structure of the ISM. We predict a clear hard-to-soft behavior in the instantaneous spectra. The time-integrated spectrum over 20 s observed by INTEGRAL is well fitted. Despite the fact that this source has been considered "unusual", it appears to us to be a normal low-energy GRB.

4. R. Ruffini, M.G. Bernardini, C.L. Bianco, P. Chardonnet, F. Fraschetti, S.-S. Xue; Evidence for isotropic emission in GRB991216; Advances in Space Research, 38, 1291 (2006).

   The issue of the possible presence or absence of jets in GRBs is here re-examined for GRB991216. We compare and contrast our theoretically predicted afterglow luminosity in the 2–10 keV band for spherically symmetric versus jetted emission. At these wavelengths the jetted emission can be excluded and data analysis confirms spherical symmetry. These theoretical fits are expected to be improved by the forthcoming data of the Swift mission.

5. R. Ruffini, M.G. Bernardini, C.L. Bianco, P. Chardonnet, F. Fraschetti, R. Guida, S.-S. Xue; "GRB 050315: A step toward understanding the uniqueness of the overall GRB structure"; The Astrophysical Journal, 645, L109 (2006).

   Using the Swift data of GRB 050315, we are making progress toward understanding the uniqueness of our theoretically predicted gamma-ray burst (GRB) structure, which is composed of a proper GRB (P-GRB), emitted at the transparency of an electron-positron plasma with suitable baryon loading, and an afterglow comprising the so-called prompt emission due to external shocks. Thanks to the Swift observations, the P-GRB is identified, and for the first time we can theoretically fit detailed light curves for selected energy bands on a continuous timescale ranging over 106 s. The theoretically predicted instantaneous spectral distribution over the entire afterglow is presented, confirming a clear hard-to-soft behavior encompassing, continuously, the "prompt emission" all the way to the latest phases of the afterglow.

6. C.L. Bianco, L. Caito, R. Ruffini; "Theoretical interpretation of GRB 011121"; Il Nuovo Cimento B, 121, 1441 (2006).

   GRB011121 is analyzed as a prototype to understand the "flares" recently observed by Swift in the afterglow of many GRB sources. Detailed theoretical computation of the GRB011121 light curves in selected energy bands are presented and compared and contrasted with observational BeppoSAX data.

7. R. Ruffini, M.G. Bernardini, C.L. Bianco, P. Chardonnet, F. Fraschetti, R. Guida, S.-S. Xue; "GRB 050315: A step toward the uniqueness of the overall GRB structure"; Il Nuovo Cimento B, 121, 1367 (2006).

   Using the *Swift* data of GRB 050315, we progress on the uniqueness of our theoretically predicted Gamma-Ray Burst (GRB) structure as composed by a proper-GRB (P-GRB), emitted at the transparency of an electron-positron plasma with suitable baryon loading, and an afterglow comprising the so called "prompt emission" as due to external shocks. Thanks to the *Swift* observations, we can theoretically fit detailed light curves for selected energy bands on a continuous time scale ranging over 10^6 seconds. The theoretically predicted instantaneous spectral distribution over the entire afterglow confirms a clear hard-to-soft behavior encompassing, continuously, the "prompt emission" all the way to the latest phases of the afterglow. Consequences of the instrumental threshold on the definition of "short" and "long" GRBs are discussed.

8. M.G. Bernardini, C.L. Bianco, L. Caito, P. Chardonnet, A. Corsi, M.G. Dainotti, F. Fraschetti, R. Guida, R. Ruffini, S.-S. Xue; GRB970228 as a prototype for short GRBs with afterglow; Il Nuovo Cimento B, 121, 1439 (2006).

   GRB970228 is analyzed as a prototype to understand the relative role of short GRBs and their associated afterglows, recently observed by Swift and HETE-II. Detailed theoretical computation of the GRB970228 light curves in selected energy bands are presented and compared with observational BeppoSAX data.

9. M.G. Dainotti, M.G. Bernardini, C.L. Bianco, L. Caito, R. Guida, R. Ruffini; "GRB060218 and GRBs associated with Supernovae Ib/c"; Astronomy & Astrophysics, 471, L29 (2007).

   Context: The *Swift* satellite has given continuous data in the range 0.3–150 keV from 0 s to 10^6 s for GRB060218 associated with SN2006aj. This Gamma-Ray Burst (GRB) which has an unusually long duration ($T_{90} \sim 2100$ s) fulfills the Amati relation. These data offer the opportunity to probe theoretical models for GRBs connected with Supernovae (SNe).
   Aims: We plan to fit the complete γ- and X-ray light curves of this long duration GRB, including the prompt emission, in order to clarify the nature of the progenitors and the astrophysical scenario of the class of GRBs associated with SNe Ib/c.

Methods: We apply our "fireshell" model based on the formation of a black hole, giving the relevant references. It is characterized by the precise equations of motion and equitemporal surfaces and by the role of thermal emission.
Results: The initial total energy of the electron-positron plasma $E_{e^\pm}^{tot} = 2.32 \times 10^{50}$ erg has a particularly low value, similar to the other GRBs associated with SNe. For the first time, we observe a baryon loading $B = 10^{-2}$ which coincides with the upper limit for the dynamical stability of the fireshell. The effective CircumBurst Medium (CBM) density shows a radial dependence $n_{cbm} \propto r^{-\alpha}$ with $1.0 \lesssim \alpha \lesssim 1.7$ and monotonically decreases from 1 to 10^{-6} particles/cm^3. This behavior is interpreted as being due to a fragmentation in the fireshell. Analogies with the fragmented density and filling factor characterizing Novae are outlined. The fit presented is particularly significant in view of the complete data set available for GRB060218 and of the fact that it fulfills the Amati relation.
Conclusions: We fit GRB060218, usually considered as an X-Ray Flash (XRF), as a "canonical GRB" within our theoretical model. The smallest possible black hole, formed by the gravitational collapse of a neutron star in a binary system, is consistent with the especially low energetics of the class of GRBs associated with SNe Ib/c. We provide the first evidence for a fragmentation in the fireshell. This fragmentation is crucial in explaining both the unusually large T_{90} and the consequently inferred abnormally low value of the CBM effective density.

10. M.G. Bernardini, C.L. Bianco, L. Caito, M.G. Dainotti, R. Guida, R. Ruffini; "GRB970228 and a class of GRBs with an initial spikelike emission"; Astronomy & Astrophysics, 474, L13 (2007).

Context: The discovery by *Swift* and HETE-2 of an afterglow emission associated possibly with short GRBs opened the new problematic of their nature and classification. This issue has been further enhanced by the observation of GRB060614 and by a new analysis of the BATSE catalog which led to the identification of a new class of GRBs with "an occasional softer extended emission lasting tenths of seconds after an initial spikelike emission".
Aims: We plan a twofold task: a) to fit this new class of "hybrid" sources within our "canonical GRB" scenario, where all GRBs are generated by a "common engine" (i.e. the gravitational collapse to a black hole); b) to propose GRB970228 as the prototype of the above mentioned class, since it shares the same morphology and observational features.
Methods: We analyze *Beppo*SAX data on GRB970228 within the "fireshell" model and we determine the parameters describing the source and the CircumBurst Medium (CBM) needed to reproduce its light curves in the 40–700 keV and 2–26 keV energy bands.
Results: We find that GRB970228 is a "canonical GRB", like e.g. GRB050315, with the main peculiarity of a particularly low average density of the CBM $\langle n_{cbm} \rangle \sim 10^{-3}$ particles/cm^3. We also simulate the light curve corresponding

to a rescaled CBM density profile with $\langle n_{cbm} \rangle = 1$ particle/cm^3. From such a comparison it follows that the total time-integrated luminosity is a faithful indicator of the nature of GRBs, contrary to the peak luminosity which is merely a function of the CBM density.
Conclusions: We call attention on discriminating the short GRBs between the "genuine" and the "fake" ones. The "genuine" ones are intrinsically short, with baryon loading $B \lesssim 10^{-5}$, as stated in our original classification. The "fake" ones, characterized by an initial spikelike emission followed by an extended emission lasting tenths of seconds, have a baryon loading $10^{-4} \lesssim B \leq 10^{-2}$. They are observed as such only due to an underdense CBM consistent with a galactic halo environment which deflates the afterglow intensity.

11. R. Guida, M.G. Bernardini, C.L. Bianco, L. Caito, M.G. Dainotti, R. Ruffini; "The Amati relation in the "fireshell" model"; Astronomy & Astrophysics, 487, L37 (2008).

    Context: The cosmological origin of gamma-ray bursts (GRBs) has been firmly established, with redshifts up to $z = 6.29$. They are possible candidates for use as "distance indicators" for testing cosmological models in a redshift range hardly achievable by other cosmological probes. Asserting the validity of the empirical relations among GRB observables is now crucial for their calibration.
    Aims: Motivated by the relation proposed by Amati and collaborators, we look within the "fireshell" model for a relation between the peak energy E_p of the νF_ν total time-integrated spectrum of the afterglow and the total energy of the afterglow E_{aft}, which in our model encompasses and extends the prompt emission.
    Methods: The fit within the fireshell model, as for the "canonical" GRB050315, uses the complete arrival time coverage given by the Swift satellite. It is performed simultaneously, self-consistently, and recursively in the four BAT energy bands (15–25 keV, 25–50 keV, 50–100 keV, and 100-150 keV), as well as in the XRT one (0.2–10 keV). It uniquely determines the two free parameters characterizing the GRB source, the total energy $E_{tot}^{e^\pm}$ of the $e^\pm$ plasma and its baryon loading B, as well as the effective CircumBurst Medium (CBM) distribution. We can then build two sets of "gedanken" GRBs varying the total energy of the electron-positron plasma $E_{tot}^{e^\pm}$ and keeping the same baryon loading B of GRB050315. The first set assumes the one obtained in the fit of GRB050315 for the effective CBM density. The second set assumes instead a constant CBM density equal to the average value of the GRB050315 prompt phase.
    Results: For the first set of "gedanken" GRBs we find a relation $E_p \propto (E_{aft})^a$, with $a = 0.45 \pm 0.01$, whose slope strictly agrees with the Amati one. Such a relation, in the limit $B \to 10^{-2}$, coincides with the Amati one. Instead, no correlation is found in the second set of "gedanken" GRBs.
    Conclusions: Our analysis excludes the proper GRB (P-GRB) from the prompt emission, extends all the way to the latest afterglow phases, and is independent of the assumed cosmological model, since all "gedanken" GRBs are at

the same redshift. The Amati relation, on the other hand, includes the P-GRB, focuses only on the prompt emission, being therefore influenced by the instrumental threshold that fixes the end of the prompt emission, and depends on the assumed cosmology. This might explain the intrinsic scatter observed in the Amati relation.

12. L. Caito, M.G. Bernardini, C.L. Bianco, M.G. Dainotti, R. Guida, R. Ruffini; "GRB060614: a "fake" short GRB from a merging binary system"; Astronomy & Astrophysics, submitted to.

    Context: GRB060614 observations by VLT and by Swift have infringed the traditionally accepted Gamma-Ray Burst (GRB) collapsar scenario that purports the origin of all long duration GRBs from supernovae. GRB060614 is the first nearby long duration GRB clearly not associated to a bright Ib/c supernova. Moreover, its duration ($T_{90} \sim 100$s) makes it hardly classifiable as a short GRB. It presents strong similarities with GRB970228, the prototype of the new class of "fake" short GRBs that appear to originate from the coalescence of binary neutron stars or white dwarfs spiraled out into the galactic halo. *Aims*: Within the "canonical" GRB scenario based on the "fireshell" model, we test if GRB060614 can be a "fake", or, better, "disguised" short GRB. We model the traditionally called "prompt emission" and discriminate the signal originating from the gravitational collapse leading to the GRB from the process occurring in the CircumBurst Medium (CBM). *Methods*: We fit GRB060614 light curves in Swift's BAT ($15-150$keV) and XRT ($0.2-10$keV) energy bands. Within the fireshell model, light curves are formed by two well defined and different components: the Proper-GRB (P-GRB), emitted at the fireshell transparency, and the afterglow, due to the interaction between the leftover accelerated baryonic shell and the CBM. *Results*: We determine the two free parameters describing the GRB source within the fireshell model: the total $e^\pm$ plasma energy ($E_{tot}^{e^\pm} = 2.94 \times 10^{51}$erg) and baryon loading ($B = 2.8 \times 10^{-3}$). A small average CBM density $\sim 10^{-3}$particles/cm^3 is inferred, typical of galactic halos. The first spikelike emission is identified with the P-GRB and the following prolonged emission with the peak of the afterglow. We obtain very good agreement in the BAT ($15-150$keV) energy band, in what is traditionally called "prompt emission", and in the XRT ($0.2-10$keV) one. *Conclusions*: The *anomalous* GRB060614 finds a natural interpretation within our canonical GRB scenario: it is a "disguised" short GRB. The total time-integrated afterglow luminosity is greater than the P-GRB one, but its peak luminosity is smaller since it is deflated by the peculiarly low average CBM density of galactic halos. This result points to an old binary system, likely formed by a white dwarf and a neutron star, as the progenitor of GRB060614 and well justify the absence of an associated supernova Ib/c. Particularly important for further studies of the final merging process are the temporal structures in the P-GRB down to 0.1s.

5.2 Conference proceedings

1. R. Ruffini, M.G. Bernardini, C.L. Bianco, P. Chardonnet, F. Fraschetti, V. Gurzadyan, L. Vitagliano, S.-S. Xue; "The Blackholic energy: long and short Gamma-Ray Bursts (New perspectives in physics and astrophysics from the theoretical understanding of Gamma-Ray Bursts, II)"; in Proceedings of the XIth Brazilian School on Cosmology and Gravitation, Mangaratiba, Rio de Janeiro (Brazil), July August 2004, M. Novello, S.E. Perez Bergliaffa, Editors; AIP Conference Proceedings, 782, 42 (2005).

   We outline the confluence of three novel theoretical fields in our modeling of Gamma-Ray Bursts (GRBs): 1) the ultrarelativistic regime of a shock front expanding with a Lorentz gamma factor ~ 300; 2) the quantum vacuum polarization process leading to an electron-positron plasma originating the shock front; and 3) the general relativistic process of energy extraction from a black hole originating the vacuum polarization process. There are two different classes of GRBs: the long GRBs and the short GRBs. We here address the issue of the long GRBs. The theoretical understanding of the long GRBs has led to the detailed description of their luminosities in fixed energy bands, of their spectral features and made also possible to probe the astrophysical scenario in which they originate. We are specially interested, in this report, to a subclass of long GRBs which appear to be accompanied by a supernova explosion. We are considering two specific examples: GRB980425/SN1998bw and GRB030329/SN2003dh. While these supernovae appear to have a standard energetics of 10^{49} ergs, the GRBs are highly variable and can have energetics 10^4 – 10^5 times larger than the ones of the supernovae. Moreover, many long GRBs occurs without the presence of a supernova. It is concluded that in no way a GRB can originate from a supernova. The precise theoretical understanding of the GRB luminosity we present evidence, in both these systems, the existence of an independent component in the X-ray emission, usually interpreted in the current literature as part of the GRB afterglow. This component has been observed by Chandra and XMM to have a strong decay on scale of months. We have named here these two sources respectively URCA-1 and URCA-2, in honor of the work that George Gamow and Mario Shoenberg did in 1939 in this town of Urca identifying the basic mechanism, the Urca processes, leading to the process of gravitational collapse and the formation of a neutron star and a supernova. The further hypothesis is considered to relate this X-ray source to a neutron star, newly born in the Supernova. This hypothesis should be submitted to further theoretical and observational investigation. Some theoretical developments to clarify the astrophysical origin of this new scenario are outlined. We turn then to the theoretical developments in the short GRBs: we first report some progress in the understanding the dynamical phase of collapse, the mass-energy formula and the extraction of blackholic energy which have been motivated by the analysis of the short GRBs. In this context progress has also been accomplished on establishing an absolute lower limit to the irreducible mass of the black hole as well as on some critical considerations about the relations of general relativity and the second law of thermodynamics. We recall how this last issue has been one of the most debated in theoretical physics in the past thirty years due to the work of Bekenstein and Hawking. Following these conceptual progresses we analyze the vacuum polarization process around an overcritical collapsing shell. We evidence the existence of a separatrix and a dyadosphere trapping surface in the dynamics of the electron-positron plasma generated during the process of gravitational collapse. We then analyze, using recent progress in the solution of the Vlasov-Boltzmann-Maxwell system, the oscillation regime in the created electron-positron plasma and their rapid convergence to a thermalized spectrum. We conclude by making precise predictions for the spectra, the energy fluxes and characteristic time-scales of the radiation for short-bursts. If the precise luminosity variation and spectral hardening of the radiation we have predicted will be confirmed by observations of short-bursts, these systems will play a major role as standard candles in cosmology. These considerations will also be relevant for the analysis of the long-bursts when the baryonic matter contribution will be taken into account.

2. R. Ruffini, M.G. Bernardini, C.L. Bianco, P. Chardonnet, F. Fraschetti, V. Gurzadyan, L. Vitagliano, S.-S. Xue; "Black hole physics and astrophysics: The GRB-Supernova connection and URCA-1 URCA-2"; in Proceedings of the Tenth Marcel Grossmann Meeting on General Relativity, Rio de Janeiro, Brazil, July 2003, M. Novello, S.E. Perez-Bergliaffa, Editors; p. 369; World Scientific, (Singapore, 2006).

   We outline the confluence of three novel theoretical fields in our modeling of Gamma-Ray Bursts (GRBs): 1) the ultrarelativistic regime of a shock front expanding with a Lorentz gamma factor ~ 300; 2) the quantum vacuum polarization process leading to an electron-positron plasma originating the shock front; and 3) the general relativistic process of energy extraction from a black hole originating the vacuum polarization process. There are two different classes of GRBs: the long GRBs and the short GRBs. We here address the issue of the long GRBs. The theoretical understanding of the long GRBs has led to the detailed description of their luminosities in fixed energy bands, of their spectral features and made also possible to probe the astrophysical scenario in which they originate. We are specially interested, in this report, to a subclass of long GRBs which appear to be accompanied by a supernova explosion. We are considering two specific examples: GRB980425/SN1998bw and GRB030329/SN2003dh. While these supernovae appear to have a standard energetics of 10^{49} ergs, the GRBs are highly variable and can have energetics 10^4 – 10^5 times larger than the ones of the supernovae. Moreover, many long GRBs occurs without the presence of a supernova. It is concluded that in no way a

GRB can originate from a supernova. The precise theoretical understanding of the GRB luminosity we present evidence, in both these systems, the existence of an independent component in the X-ray emission, usually interpreted in the current literature as part of the GRB afterglow. This component has been observed by Chandra and XMM to have a strong decay on scale of months. We have named here these two sources respectively URCA-1 and URCA-2, in honor of the work that George Gamow and Mario Shoenberg did in 1939 in this town of Urca identifying the basic mechanism, the Urca processes, leading to the process of gravitational collapse and the formation of a neutron star and a supernova. The further hypothesis is considered to relate this X-ray source to a neutron star, newly born in the Supernova. This hypothesis should be submitted to further theoretical and observational investigation. Some theoretical developments to clarify the astrophysical origin of this new scenario are outlined.

3. M.G. Bernardini, C.L. Bianco, P. Chardonnet, F. Fraschetti, R. Ruffini, S.-S. Xue; "General features of GRB 030329 in the EMBH model"; in Proceedings of the Tenth Marcel Grossmann Meeting on General Relativity, Rio de Janeiro, Brazil, July 2003, M. Novello, S.E. Perez-Bergliaffa, Editors; p. 2459; World Scientific, (Singapore, 2006).

   GRB 030329 is considered within the EMBH model. We determine the three free parameters and deduce its luminosity in given energy bands comparing it with the observations. The observed substructures are compared with the predictions of the model: by applying the result that substructures observed in the extended afterglow peak emission (E-APE) do indeed originate in the collision of the accelerated baryonic matter (ABM) pulse with the inhomogeneities in the interstellar medium around the black-hole, masks of density inhomogeneities are considered in order to reproduce the observed temporal substructures. The induced supernova concept is applied to this system and the general consequences that we are witnessing are the formation of a cosmological thriptych of a black hole originating the GRB 030329, the supernova SN2003dh and a young neutron star. Analogies to the system GRB 980425–SN1998bw are outlined.

4. R. Ruffini, M.G. Bernardini, C.L. Bianco, P. Chardonnet, A. Corsi, F. Fraschetti, S.-S. Xue; "GRB 970228 and its associated Supernova in the EMBH model"; in Proceedings of the Tenth Marcel Grossmann Meeting on General Relativity, Rio de Janeiro, Brazil, July 2003, M. Novello, S.E. Perez-Bergliaffa, Editors; p. 2465; World Scientific, (Singapore, 2006).

   The γ-ray burst of 1997 February 28 is analyzed within the Electromagnetic Black Hole model. We first estimate the value of the total energy deposited in the dyadosphere, E_{dya}, and the amount of baryonic matter left over by the EMBH progenitor star, $B = M_B c^2 / E_{dya}$. We then consider the role of the interstellar medium number density n_{ISM} and of the ratio R between the effective emitting area and the total surface area of the γ-ray burst source, in reproducing the prompt emission and the X-ray afterglow of this burst. Some considerations are also done concerning the possibility of explaining, within the theory, the observed evidence for a supernova in the optical afterglow.

5. F. Fraschetti, M.G. Bernardini, C.L. Bianco, P. Chardonnet, R. Ruffini, S.-S. Xue; "Inferences on the ISM structure around GRB980425 and GRB980425-SN1998bw association in the EMBH Model"; in Proceedings of the Tenth Marcel Grossmann Meeting on General Relativity, Rio de Janeiro, Brazil, July 2003, M. Novello, S.E. Perez-Bergliaffa, Editors; p. 2451; World Scientific, (Singapore, 2006).

   We determine the four free parameters within the EMBH model for GRB 980425 and deduce its luminosity in given energy bands, its spectra and its time variability in the prompt radiation. We compute the basic kinematical parameters of GRB 980425. In the extended afterglow peak emission the Lorentz γ factor is lower than the critical value 150 which has been found in Ruffini et al. (2002) to be necessary in order to perform the tomography of the ISM surrounding the GRB as suggested by Dermer & Mitman (1999). The detailed structure of the density inhomogeneities as well as the effects of radial apparent superluminal effects are evaluated within the EMBH model. Under the assumption that the energy distribution of emitted radiation is thermal in the comoving frame, time integrated spectra of EMBH model for prompt emission are computed. The induced supernova concept is applied to this system and general consequences on the astrophysical and cosmological scenario are derived.

6. R. Ruffini, M.G. Bernardini, C.L. Bianco, P. Chardonnet, F. Fraschetti, R. Guida, S.-S. Xue; "GRB 050315: A step in the proof of the uniqueness of the overall GRB structure"; in "GAMMA-RAY BURSTS IN THE SWIFT ERA: Sixteenth Maryland Astrophysics Conference", Washington, DC, USA, November 29th December 2nd 2005, Stephen S. Holt, Neil Gehrels, John A. Nousek, Editors; AIP Conference Proceedings, 836, 103 (2006).

   Using the Swift data of GRB 050315, we progress in proving the uniqueness of our theoretically predicted Gamma-Ray Burst (GRB) structure as composed by a proper-GRB, emitted at the transparency of an electron-positron plasma with suitable baryon loading, and an afterglow comprising the "prompt radiation" as due to external shocks. Detailed light curves for selected energy bands are theoretically fitted in the entire temporal region of the Swift observations ranging over 10^6 seconds.

7. R. Ruffini, M.G. Bernardini, C.L. Bianco, P. Chardonnet, F. Fraschetti, S.-S. Xue; "Theoretical Interpretation of GRB 031203 and URCA-3"; in "Relativistic Astrophysics and Cosmology - Einsteins Legacy", B. As-

chenbach, V. Burwitz, G. Hasinger, B. Leibundgut, Editors; Springer-Verlag (2007).

8. R. Ruffini, M.G. Bernardini, C.L. Bianco, L. Caito, P. Chardonnet, M.G. Dainotti, F. Fraschetti, R. Guida, M. Rotondo, G. Vereshchagin, L. Vitagliano, S.-S. Xue; "The Blackholic energy and the canonical Gamma-Ray Burst"; in Proceedings of the XIIth Brazilian School on Cosmology and Gravitation, Mangaratiba, Rio de Janeiro (Brazil), September 2006, M. Novello, S.E. Perez Bergliaffa, Editors; AIP Conference Proceedings, 910, 55 (2007).

Gamma-Ray Bursts (GRBs) represent very likely "the" most extensive computational, theoretical and observational effort ever carried out successfully in physics and astrophysics. The extensive campaign of observation from space based X-ray and γ-ray observatory, such as the *Vela*, CGRO, BeppoSAX, HETE-II, INTEGRAL, *Swift*, R-XTE, *Chandra*, XMM satellites, have been matched by complementary observations in the radio wavelength (e.g. by the VLA) and in the optical band (e.g. by VLT, Keck, ROSAT). The net result is unprecedented accuracy in the received data allowing the determination of the energetics, the time variability and the spectral properties of these GRB sources. The very fortunate situation occurs that these data can be confronted with a mature theoretical development. Theoretical interpretation of the above data allows progress in three different frontiers of knowledge: **a)** the ultrarelativistic regimes of a macroscopic source moving at Lorentz gamma factors up to ~ 400; **b)** the occurrence of vacuum polarization process verifying some of the yet untested regimes of ultrarelativistic quantum field theories; and **c)** the first evidence for extracting, during the process of gravitational collapse leading to the formation of a black hole, amounts of energies up to 10^{55} ergs of blackholic energy — a new form of energy in physics and astrophysics. We outline how this progress leads to the confirmation of three interpretation paradigms for GRBs proposed in July 2001. Thanks mainly to the observations by *Swift* and the optical observations by VLT, the outcome of this analysis points to the existence of a "canonical" GRB, originating from a variety of different initial astrophysical scenarios. The communality of these GRBs appears to be that they all are emitted in the process of formation of a black hole with a negligible value of its angular momentum. The following sequence of events appears to be canonical: the vacuum polarization process in the dyadosphere with the creation of the optically thick self accelerating electron-positron plasma; the engulfment of baryonic mass during the plasma expansion; adiabatic expansion of the optically thick "fireshell" of electron-positron-baryon plasma up to the transparency; the interaction of the accelerated baryonic matter with the interstellar medium (ISM). This leads to the canonical GRB composed of a proper GRB (P-GRB), emitted at the moment of transparency, followed by an extended afterglow. The sole parameters in this scenario are the total energy of the dyadosphere E_{dya}, the fireshell baryon loading M_B defined by the dimensionless parameter $B \equiv M_B c^2 / E_{dya}$, and the ISM filamentary distribution around the source. In the limit $B \to 0$ the total energy is radiated in the P-GRB with a vanishing contribution in the afterglow. In this limit, the canonical GRBs explain as well the short GRBs. In these lecture notes we systematically outline the main results of our model comparing and contrasting them with the ones in the current literature. In both cases, we have limited ourselves to review already published results in refereed publications. We emphasize as well the role of GRBs in testing yet unexplored grounds in the foundations of general relativity and relativistic field theories.

9. R. Ruffini, M.G. Bernardini, C.L. Bianco, L. Caito, P. Chardonnet, M.G. Dainotti, F. Fraschetti, R. Guida, G. Vereshchagin, S.-S. Xue; "The role of GRB 031203 in clarifying the astrophysical GRB scenario"; in Proceedings of the 6^{th} Integral Workshop - The Obscured Universe, Moscow, (Russia), July 2006, S. Grebenev, R. Sunyaev, C. Winkler, A. Parmar, L. Ouwehand, Editors; ESA Special Publication, SP-622, 561 (2007).

   The luminosity and the spectral distribution of the afterglow of GRB 031203 have been presented within our theoretical framework, which envisages the GRB structure as composed by a proper-GRB, emitted at the transparency of an electron-positron plasma with suitable baryon loading, and an afterglow comprising the "prompt emission" as due to external shocks. In addition to the GRB emission, there appears to be a prolonged soft X-Ray emission lasting for 10^6–10^7 seconds followed by an exponential decay. This additional source has been called by us URCA-3. It is urgent to establish if this component is related to the GRB or to the Supernova (SN). In this second case, there are two possibilities: either the interaction of the SN ejecta with the interstellar medium or, possibly, the cooling of a young neutron star formed in the SN 2003lw process. The analogies and the differences between this triptych GRB 031203 / SN 2003lw / URCA-3 and the corresponding ones GRB 980425 / SN 1998bw / URCA-1 and GRB 030329 / SN 2003dh / URCA-2, as well as GRB 060218 / SN 2006aj are discussed.

10. M.G. Bernardini, C.L. Bianco, L. Caito, M.G. Dainotti, R. Guida, R. Ruffini; "GRB970228 and the class of GRBs with an initial spikelike emission: do they follow the Amati relation?"; in Relativistic Astrophysics Proceedings of the 4^{th} Italian-Sino Workshop, Pescara (Italy), July 2007, C.L. Bianco, S.-S. Xue, Editors; AIP Conference Proceedings, 966, 7 (2008).

    On the basis of the recent understanding of GRB050315 and GRB060218, we return to GRB970228, the first Gamma-Ray Burst (GRB) with detected afterglow. We proposed it as the prototype for a new class of GRBs with "an occasional softer extended emission lasting tenths of seconds after an initial spikelike emission". Detailed theoretical computation of the GRB970228 light curves in selected energy bands for the prompt emission are presented and compared with observational *Beppo*SAX data. From our analysis we conclude that GRB970228 and likely the ones of the above mentioned new class of GRBs are "canonical GRBs" have only one peculiarity: they exploded in a galactic environment, possibly the halo, with a very low value of CBM density. Here we investigate how GRB970228 unveils another peculiarity of this class of GRBs: they do not fulfill the "Amati relation". We provide a theoretical explanation within the fireshell model for the apparent absence of such correlation for the GRBs belonging to this new class.

11. C.L. Bianco, M.G. Bernardini, L. Caito, M.G. Dainotti, R. Guida, R. Ruffini; "The "Fireshell" Model and the "Canonical" GRB Scenario; in Relativistic Astrophysics Proceedings of the 4^{th} Italian-Sino Workshop, Pescara (Italy), July 2007, C.L. Bianco, S.-S. Xue, Editors; AIP Conference Proceedings, 966, 12 (2008).

    In the "fireshell" model we define a "canonical GRB" light curve with two sharply different components: the Proper-GRB (P-GRB), emitted when the optically thick fireshell of electron-positron plasma originating the phenomenon reaches transparency, and the afterglow, emitted due to the collision between the remaining optically thin fireshell and the CircumBurst Medium (CBM). We outline our "canonical GRB" scenario, originating from the gravitational collapse to a black hole, with a special emphasis on the discrimination between "genuine" and "fake" short GRBs.

12. L. Caito, M.G. Bernardini, C.L. Bianco, M.G. Dainotti, R. Guida, R. Ruffini; "GRB 060614: A Progress Report"; in Relativistic Astrophysics Proceedings of the 4^{th} Italian-Sino Workshop, Pescara (Italy), July 2007, C.L. Bianco, S.-S. Xue, Editors; AIP Conference Proceedings, 966, 16 (2008).

    The explosion of GRB 060614, detected by the Swift satellite, produced a deep break in the GRB scenario opening new horizons of investigation, because it can't be traced back to any traditional scheme of classification. In fact, it manifests peculiarities both of long bursts and of short bursts. Above all, it is the first case of long duration near GRB without any bright Ib/c associated Supernova. We will show that, in our canonical GRB scenario, this "anomalous" situation finds a natural interpretation and allows us to discuss a possible variation to the traditional classification scheme, introducing the distinction between "genuine" and "fake" short bursts.

13. M.G. Dainotti, M.G. Bernardini, C.L. Bianco, L. Caito, R. Guida, R. Ruffini; "GRB 060218 and the Binaries as Progenitors of GRB-SN Systems"; in Relativistic Astrophysics Proceedings of the 4^{th} Italian-Sino Workshop, Pescara (Italy), July 2007, C.L. Bianco, S.-S. Xue, Editors; AIP Conference Proceedings, 966, 25 (2008).

    We study the Gamma-Ray Burst (GRB) 060218: a particularly close source at $z = 0.033$ with an extremely long duration, namely $T_{90} \sim 2000$ s, related to SN 2006aj. This source appears to be a very soft burst, with a peak in the spectrum at 4.9 keV, therefore interpreted as an X-Ray Flash (XRF). It fullfills the Amati relation. I present the fitting procedure, which is time consuming. In order to show its sensitivity I also present two examples of fits with the same value of B and different value of $E^{tot}_{e^{\pm}}$. We fit the X- and γ-ray observations by *Swift* of GRB 060218 in the 0.1–150 keV energy band during the entire time of observations from 0 all the way to 10^6 s within a unified theoretical model. The free parameters of our theory are only three, namely the total energy $E^{tot}_{e\pm}$ of the $e^{\pm}$ plasma, its baryon loading $B \equiv M_B c^2 / E^{tot}_{e\pm}$, as well as the CircumBurst Medium (CBM) distribution. We justify the extremely long duration of this GRB by a total energy $E^{tot}_{e\pm} = 2.32 \times 10^{50}$ erg, a very high value of the baryon loading $B = 1.0 \times 10^{-2}$ and the effective CircumBurst Medium (CBM) density which shows a radial dependence $n_{cbm} \propto r^{-\alpha}$ with $1.0 \leq \alpha \leq 1.7$ and monotonically decreases from 1 to 10^{-6} particles/cm^3. We recall that this value of the B parameter is the highest among the sources we have analyzed and it is very close to its absolute upper limit expected. By our fit we show that there is no basic differences between XRFs and more general GRBs. They all originate from the collapse process to a black hole and their difference is due to the variability of the three basic parameters within the range of full applicability of the theory. We also think that the smallest possible black hole, formed by the gravitational collapse of a neutron star in a binary system, is consistent with the especially low energetics of the class of GRBs associated with SNe Ib/c.

14. R. Guida, M.G. Bernardini, C.L. Bianco, L. Caito, M.G. Dainotti, R. Ruffini; "The Amati Relation within the Fireshell Model"; in Relativistic Astrophysics Proceedings of the 4^{th} Italian-Sino Workshop, Pescara (Italy), July 2007, C.L. Bianco, S.-S. Xue, Editors; AIP Conference Proceedings, 966, 46 (2008).

    In this work we show the existence of a spectral-energy correlation within our "fireshell" model for GRBs. The free parameters of the model are the total energy $E^{e\pm}_{tot}$ of the $e^{\pm}$ plasma and its baryon loading $B \equiv M_B\, c^2 / E^{e\pm}_{tot}$, characterizing the source, and the parameters describing the effective CircumBurst medium (CBM) distribution, namely its particle number density ρ and its effective emitting area R. We build a sample of pseudo-GRBs, i.e. a set of theoretically simulated light curves, varying the total energy of the electron-positron plasma $E^{e\pm}_{tot}$ and keeping the same baryon loading; the parametrization used to describe the distribution of the CircumBurst medium is the same as well for all the pseudo-GRBs. The values of these parameters (B, ρ and R) used in this work are equal to the ones assumed to fit GRB050315, a *Swift* burst representing a good example of what in the literature has been addressed as "canonical light curve". For each GRB of the sample we calculate the νF_ν spectrum integrating the theoretically computed light curve over the total time, namely from our T_0, the end of the Proper-GRB (P-GRB), up to the end of our afterglow phase, when the fireshell Lorentz gamma factor is close to unity; we exclude the P-GRB from this spectral computation because, following our "canonical"

GRB scenario, this component of the GRB emission is physically different from the other component, that is our afterglow component, so one should take care in no mixing them. We find that the maximum of this spectrum, that is the observed peak energy $E_{p,tot}$, correlates with the initial electron-positron plasma energy $E^{e\pm}_{tot}$ in a way very similar to the Amati one: $E_{p,tot} \propto (E^{e\pm}_{tot})^{0.5}$.

15. R. Guida, M.G. Bernardini, C.L. Bianco, L. Caito, M.G. Dainotti, R. Ruffini; "Theoretical interpretation of the Amati relation within the fireshell model"; in GAMMA-RAY BURSTS 2007: Proceedings of the Santa Fe Conference, Santa Fe (NM, USA), November 2007, M. Galassi, D. Palmer, E. Fenimore, Editors; AIP Conference Proceedings, 1000, 60 (2008).

    We discuss within our theoretical "fireshell" model for Gamma-Ray Bursts (GRBs) the theoretical interpretation of the phenomenological correlation between the isotropic-equivalent radiated energy of the prompt emission E_{iso} and the cosmological rest-frame νF_{ν} spectrum peak energy E_p observed by Amati and collaborators. Possible reasons for some of the outliers of this relation are given.

16. L. Caito, M.G. Bernardini, C.L. Bianco, M.G. Dainotti, R. Guida, R. Ruffini; "GRB 060614: a Fake Short Gamma-Ray Burst"; in GAMMA-RAY BURSTS 2007: Proceedings of the Santa Fe Conference, Santa Fe (NM, USA), November 2007, M. Galassi, D. Palmer, E. Fenimore, Editors; AIP Conference Proceedings, 1000, 301 (2008).

    The explosion of GRB 060614 produced a deep break in the GRB scenario and opened new horizons of investigation because it can't be traced back to any traditional scheme of classification. In fact, it manifests peculiarities both of long bursts and of short bursts and, above all, it is the first case of long duration near GRB without any bright Ib/c associated Supernova. We will show that, in our canonical GRB scenario, this "anomalous" situation finds a natural interpretation and allows us to discuss a possible variation to the traditional classification scheme, introducing the distinction between "genuine" and "fake" short bursts.

17. C.L. Bianco, M.G. Bernardini, L. Caito, M.G. Dainotti, R. Guida, R. Ruffini; "Short and canonical GRBs"; in GAMMA-RAY BURSTS 2007: Proceedings of the Santa Fe Conference, Santa Fe (NM, USA), November 2007, M. Galassi, D. Palmer, E. Fenimore, Editors; AIP Conference Proceedings, 1000, 305 (2008).

    Within the "fireshell" model for the Gamma-Ray Bursts (GRBs) we define a "canonical GRB" light curve with two sharply different components: the Proper-GRB (P-GRB), emitted when the optically thick fireshell of electron-positron plasma originating the phenomenon reaches transparency, and the afterglow, emitted due to the collision between the remaining optically thin fireshell and the CircumBurst Medium (CBM). We outline our "canonical GRB" scenario, with a special emphasis on the discrimination between "genuine" and "fake" short GRBs.

18. C.L. Bianco, M.G. Bernardini, L. Caito, M.G. Dainotti, R. Guida, R. Ruffini, G. Vereshchagin, S.-S. Xue; "The Equations of motion of the "fireshell""; in OBSERVATIONAL EVIDENCE FOR BLACK HOLES IN THE UNIVERSE: Proceedings of the 2^{nd} Kolkata Conference, Kolkata (India), February 2008, S.K. Chakrabarti, A.S. Majumdar, Editors; AIP Conference Proceedings, 1053, 259 (2008).

    The Fireshell originating a Gamma-Ray Burst (GRB) encompasses an optically thick regime followed by an optically thin one. In the first one the fireshell self-accelerates from a Lorentz gamma factor equal to 1 all the way to 200-300. The physics of this system is based on the continuous annihilation of electron-positron pairs in an optically thick e^+e^- plasma with a small baryon loading. In the following regime, the optically thin fireshell, composed by the baryons left over after the transparency point, ballistically expands into the Circum-Burst Medium (CBM). The dynamics of the fireshell during both regimes will be analyzed. In particular we will re-examine the validity of the constant-index power-law relation between the fireshell Lorentz gamma factor and its radial coordinate, usually adopted in the current literature on the grounds of an "ultrarelativistic" approximation. Such expressions are found to be mathematically correct but only approximately valid in a very limited range of the physical and astrophysical parameters and in an asymptotic regime which is reached only for a very short time, if any.

19. M.G. Bernardini, C.L. Bianco, L. Caito, M.G. Dainotti, R. Guida, R. Ruffini; "The "Canonical" GRBs within the fireshell model"; in OBSERVATIONAL EVIDENCE FOR BLACK HOLES IN THE UNIVERSE: Proceedings of the 2^{nd} Kolkata Conference, Kolkata (India), February 2008, S.K. Chakrabarti, A.S. Majumdar, Editors; AIP Conference Proceedings, 1053, 267 (2008).

    Within the fireshell model we define a "canonical" GRB light curve with two sharply different components: the Proper-GRB (P-GRB), emitted when the optically thick fireshell of electron-positron plasma originating the phenomenon reaches transparency, and the afterglow, emitted due to the collision between the remaining optically thin fireshell and the CircumBurst Medium (CBM). On the basis of the recent understanding of GRB970228 as the prototype for a new class of GRBs with "an occasional softer extended emission lasting tenths of seconds after an initial spikelike emission" we outline our "canonical" GRB scenario, originating from the gravitational collapse to a black hole, with a special emphasis on the discrimination between short GRBs and the ones appearing as such due to their peculiar astrophysical setting.

20. M.G. Dainotti, M.G. Bernardini, C.L. Bianco, L. Caito, R. Guida, R. Ruffini; "GRB 060218: the density mask and its peculiarity compared to the

other sources"; in OBSERVATIONAL EVIDENCE FOR BLACK HOLES IN THE UNIVERSE: Proceedings of the 2^{nd} Kolkata Conference, Kolkata (India), February 2008, S.K. Chakrabarti, A.S. Majumdar, Editors; AIP Conference Proceedings, 1053, 283 (2008).

The Swift satellite has given continuous data in the range 0.3150 keV from 0 s to 106 s for GRB060218 associated with SN2006aj. It has an unusually long duration ($T_{90} \sim 2100$ s). We plan to fit the complete γ- and X-ray light curves of this long duration GRB, including the prompt emission and we give peculiar attention to the afterglow lightcurve in order to better constrain the density mask. We apply our "fireshell" model based on the formation of a black hole, giving the relevant references. The initial total energy of the electron-positron plasma $E^{tot}_{e^{\pm}} == 2.32 \times 10^{50}$ erg has a particularly low value similarly to the other GRBs associated with SNe. For the first time we observe a baryon loading $B = 10^{-2}$ which coincides with the upper limit for the dynamical stability of the fireshell. The effective CircumBurst Medium (CBM) density shows a radial dependence $n_{cbm} \propto r^{-a}$ with $1.0 \leq a \leq 1.7$ and monotonically decreases from 1 to 10^{-6} particles/cm^3. Such a behavior is interpreted as due to a fragmentation in the fireshell. Such a fragmentation is crucial in explaining both the unusually large T_{90} and the consequently inferred abnormal low value of the CBM effective density. We present the comparison between the density mask of this source and the ones of a normal GRB 050315 and a fake short, GRB 970228, making some assumptions on the CBM behaviour in the surrounding of the Black hole.

21. L. Caito, M.G. Bernardini, C.L. Bianco, M.G. Dainotti, R. Guida, R. Ruffini; "GRB 060614 in the canonical fireshell model"; in OBSERVATIONAL EVIDENCE FOR BLACK HOLES IN THE UNIVERSE: Proceedings of the 2^{nd} Kolkata Conference, Kolkata (India), February 2008, S.K. Chakrabarti, A.S. Majumdar, Editors; AIP Conference Proceedings, 1053, 291 (2008).

    Gamma-Ray Burst (GRB) 060614 is the first nearby long duration GRB clearly not associated to any bright Ib/c Supernova. The explosion of this burst undermines one of the fundamental assumptions of the standard scenario and opens new horizons and hints of investigation. GRB 060614, hardly classifiable as a short GRB, is not either a "typical" long GRB since it occurs in a low star forming region. Moreover, it presents deep similarities with GRB 970228, which is the prototype of the "fake" short bursts, or better canonical GRBs disguised as short ones. Within the "fireshell" model, we test if this "anomalous" source can be a disguised short GRB.

22. L.J. Rangel Lemos, S. Casanova, R. Ruffini, S.S. Xue; "Fermis approach to the study of pp interactions"; in OBSERVATIONAL EVIDENCE FOR BLACK HOLES IN THE UNIVERSE: Proceedings of the 2^{nd} Kolkata Conference, Kolkata (India), February 2008, S.K. Chakrabarti, A.S. Majumdar, Editors; AIP Conference Proceedings, 1053, 275 (2008).

The physics of hadronic interactions found much difficulties for explain the experimental data. In this work we study the approach of Fermi (1950) about the multiplicity of pions emitted in pp interactions and in follow we compare with the modern approach

23. M.G. Bernardini, C.L. Bianco, L. Caito, M.G. Dainotti, R. Guida, R. Ruffini; "Preliminary analysis of GRB060607A within the fireshell model"; in 2008 NANJING GAMMA-RAY BURST CONFERENCE; Proceedings of the 2008 Nanjing Gamma-Ray Burst Conference, Nanjing (China), June 2008, Y.-F. Huang, Z.-G. Dai, B. Zhang, Editors; AIP Conference Proceedings, 1065, in press.

    GRB060607A is a very distant ($z = 3.082$) and energetic event ($E_{iso} \sim 10^{53}$ erg). Its main peculiarity is that the peak of the near-infrared afterglow has been observed with the REM robotic telescope, allowing to infer the initial Lorentz gamma factor of the emitting system. We present a preliminary analysis of the spectra and light curves of GRB060607A prompt emission within the fireshell model. We show that the N(E) spectrum of the prompt emission, whose behavior is usually described as "simple power-law", can also be fitted in a satisfactory way by a convolution of thermal spectra as predicted by the model we applied. The theoretical time-integrated spectrum of the prompt emission as well as the light curves in the BAT and XRT energy band are in good agreement with the observations, enforcing the plausibility of our approach. Furthermore, the initial value of Lorentz gamma factor we predict is compatible with the one deduced from the REM observations.

24. C.L. Bianco, M.G. Bernardini, L. Caito, M.G. Dainotti, R. Guida, R. Ruffini; "The "fireshell" model and the "canonical GRB" scenario"; in 2008 NANJING GAMMA-RAY BURST CONFERENCE; Proceedings of the 2008 Nanjing Gamma-Ray Burst Conference, Nanjing (China), June 2008, Y.-F. Huang, Z.-G. Dai, B. Zhang, Editors; AIP Conference Proceedings, 1065, in press.

    The Swift observation of GRB 060614, as well as the catalog analysis by Norris and Bonnell (2006), opened the door "on a new Gamma-Ray Bursts (GRBs) classification scheme that straddles both long and short bursts" (Gehrels et al., 2006). Within the "fireshell" model for the Gamma-Ray Bursts (GRBs) we define a "canonical GRB" light curve with two sharply different components: the Proper-GRB (P-GRB), emitted when the optically thick fireshell of electron-positron plasma originating the phenomenon reaches transparency, and the afterglow, emitted due to the collision between the remaining optically thin fireshell and the CircumBurst Medium (CBM). We here outline our "canonical GRB" scenario, which implies three different GRB classes: the "genuine" short GRBs, the "fake" or "disguised" short GRBs and the other (so-called "long") GRBs. We also outline some implications for the theoretical interpretation of the Amati relation.

25. G. De Barros, M.G. Bernardini, C.L. Bianco, L. Caito, M.G. Dainotti, R. Guida, R. Ruffini; "Is GRB 050509b a genuine short GRB?"; in 2008 NANJING GAMMA-RAY BURST CONFERENCE; Proceedings of the 2008 Nanjing Gamma-Ray Burst Conference, Nanjing (China), June 2008, Y.-F. Huang, Z.-G. Dai, B. Zhang, Editors; AIP Conference Proceedings, 1065, in press.

    Within our "fireshell" model we introduced a "canonical" GRB scenario which differentiates physically the "proper GRB" (P-GRB) emission when photons decouple, and the afterglow emission due to interaction of the accelerated baryons with the CircumBurst Medium (CBM). The ratio between energetics of the two components is ruled by the baryon loading of the fireshell. We here analyse the possibility that GRB050509b is the first case of a "genuine" short GRB the ones with smaller baryon loading. In such a case, the GRB050509b "prompt emission" would be dominated by the "proper GRB" and, moreover, the P-GRB total energy would be greater than the afterglow one. Our fit of the afterglow data and of the P-GRB energetics indicates that this source present the smallest baryon loading we ever encountered so far, being on the order of 10^{-4}.

26. R. Ruffini, A.G. Aksenov, M.G. Bernardini, C.L. Bianco, L. Caito, M.G. Dainotti, G. De Barros, R. Guida, G.V. Vereshchagin, S.-S. Xue; "The canonical Gamma-Ray Bursts and their "precursors""; in 2008 NANJING GAMMA-RAY BURST CONFERENCE; Proceedings of the 2008 Nanjing Gamma-Ray Burst Conference, Nanjing (China), June 2008, Y.-F. Huang, Z.-G. Dai, B. Zhang, Editors; AIP Conference Proceedings, 1065, in press.

    The fireshell model for Gamma-Ray Bursts (GRBs) naturally leads to a canonical GRB composed of a proper-GRB (P-GRB) and an afterglow. P-GRBs, introduced by us in 2001, are sometimes considered "precursors" of the main GRB event in the current literature. We show in this paper how the fireshell model leads to the understanding of the structure of GRBs, with precise estimates of the time sequence and intensities of the P-GRB and the of the afterglow. It leads as well to a natural classification of the canonical GRBs which overcomes the traditional one in short and long GRBs.

H.1 The “fireshell” model and the “canonical GRB” scenario

GRB 060614 (Gehrels et al., 2006; Mangano et al., 2007) has infringed the traditionally accepted Gamma-Ray Burst (GRB) classification scheme (Klebesadel, 1992; Dezalay et al., 1992), in which GRBs originate from “Hypernovae” and are branched into two classes: “short” GRBs (lasting less than $\sim$ 2 s) and “long” GRBs (lasting more than $\sim$ 2 s up to $\sim$ 1000 s). Stringent upper limits on the luminosity of the Type Ib/c Supernova (SN) possibly associated with GRB 060614 have been established (Della Valle et al., 2006; Gal-Yam et al., 2006). Moreover, GRB 060614 “reveals a first short, hard-spectrum episode of emission (lasting 5 s) followed by an extended and somewhat softer episode (lasting $\sim$ 100 s)”: a “two-component emission structure”. GRB 060614 appears as a long burst, lasting more than $\sim$ 100 s, but shares some spectral properties with the short ones as the absence of a spectral lag (Gehrels et al., 2006). The authors conclude that “it is difficult to determine unambiguously which category GRB 060614 falls into” and then GRB 060614, due to its “hybrid” observational properties, “opens the door on a new GRB classification scheme that straddles both long and short bursts” (Gehrels et al., 2006).

Some months before, reanalyzing the BATSE, HETE-II and Swift catalogs, Norris and Bonnell (2006) had identified a new GRB class with “an occasional softer extended emission lasting tenths of seconds after an initial spikelike emission”. A two-component emission structure which is “similar” to the one then observed in GRB 060614 (Gehrels et al., 2006). Norris and Bonnell (2006) had suggested that the traditional GRB classification scheme “is at best misleading” (Norris and Bonnell, 2006).

We are going to show that such problems of the traditional GRB classification scheme find a natural solution within the “canonical” GRB scenario implied by the “fireshell” model. Within the “fireshell” model all GRBs, both “long” and “short”, originate from the formation of a black hole, either occurring in a single process of gravitational collapse, possibly induced in a binary system, or in a merging binary system composed by neutron stars and/or white dwarfs in all possible combinations (Ruffini et al., 2001b, 2007a; Bernardini et al., 2007). The occurrence of an associated SN, rather than a necessity, is more likely an exception linked to the process of “induced” gravitational collapse (Ruffini et al., 2007b; Dainotti et al., 2007). The $e^{\pm}$ plasma created in the process of the black hole formation reaches thermal equilibrium on a time scale on the order of $\sim 10^{-13}$ s (Aksenov et al., 2007). Then it expands

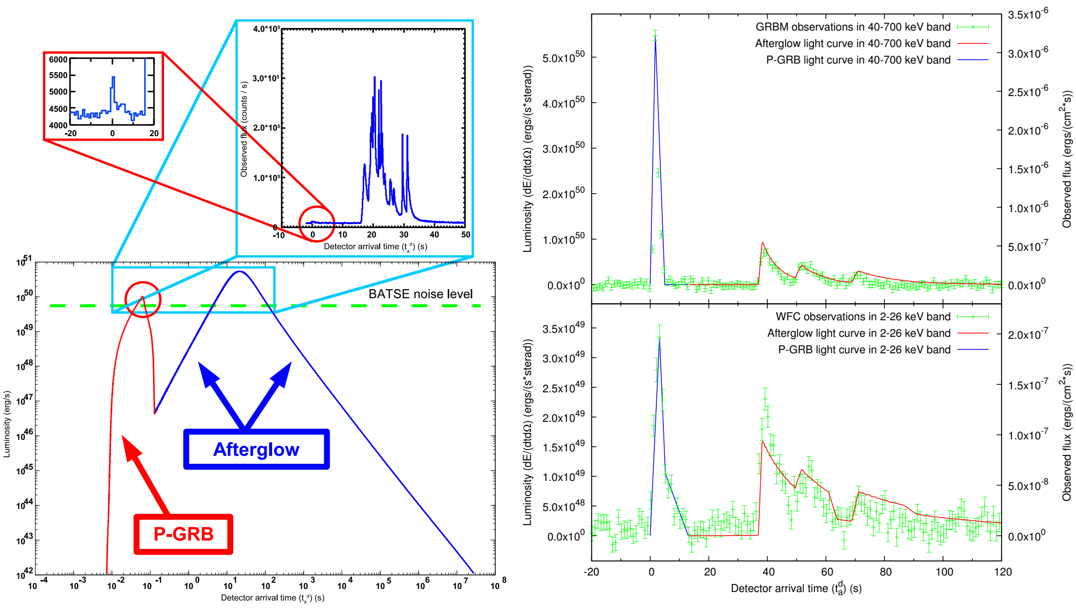

Figure H.1.1: Left: The "canonical GRB" light curve theoretically computed for GRB 991216. The prompt emission observed by BATSE is identified with the peak of the afterglow, while the small precursor is identified with the P-GRB. For this source we have $E_{e^\pm}^{tot} = 4.83 \times 10^{53}$ ergs, $B \simeq 3.0 \times 10^{-3}$ and $\langle n_{cbm} \rangle \sim 1.0$ particles/cm^3. Details in Ruffini et al. (2001b, 2002a, 2007a). **Right:** The "canonical GRB" light curve theoretically computed for the prompt emission of GRB 970228. *Beppo*SAX GRBM (40–700 keV, above) and WFC (2–26 keV, below) light curves (data points) are compared with the afterglow peak theoretical ones (solid lines). The onset of the afterglow coincides with the end of the P-GRB (represented qualitatively by the dotted lines). For this source we have $E_{e^\pm}^{tot} = 1.45 \times 10^{54}$ ergs, $B \simeq 5.0 \times 10^{-3}$ and $\langle n_{cbm} \rangle \sim 10^{-3}$ particles/cm^3. Details in Bernardini et al. (2007, 2008).

as an optically thick and spherically symmetric "fireshell" with a constant width in the laboratory frame, i.e. the frame in which the black hole is at rest (Ruffini et al., 1999, 2000). There are only two free parameters characterizing the source (Ruffini et al., 2001b, 2007a): the total energy $E_{e^\pm}^{tot}$ of the $e^\pm$ plasma forming the self-accelerating optically thick fireshell and its baryon loading $B \equiv M_B c^2 / E_{e^\pm}^{tot}$, where M_B is the total baryons' mass (Ruffini et al., 2000). These two parameters fully determine the optically thick acceleration phase of the fireshell, which lasts until the transparency condition is reached and the Proper-GRB (P-GRB) is emitted (Ruffini et al., 2001b, 2007a, see also Ruffini et al. contribution in this volume).

We define a "canonical GRB" light curve with two sharply different components (see Fig. H.1.1) (Ruffini et al., 2001b, 2007a; Bernardini et al., 2007; Bianco et al., 2008a,b):

- **The Proper GRB (P-GRB)**, which is emitted when the optically thick fireshell becomes transparent. It depends only on $E_{e^\pm}^{tot}$ and B. It has the imprint of the black hole formation, an harder spectrum and no spectral lag (Bianco et al., 2001; Ruffini et al., 2005d). It does not fulfill the "Amati" (Amati et al., 2002; Amati, 2006) relation (Bernardini et al., 2008; Guida et al., 2008).

- **the afterglow**, which is due to the collision between the remaining optically thin fireshell and the CircumBurst Medium (CBM) (Ruffini et al., 2001b, 2007a; Bianco and Ruffini, 2004, 2005b,a). It depends on $E_{e^\pm}^{tot}$ and B but its temporal structure depends also on the additional parameters describing the effective CBM distribution: its density n_{cbm} and the ratio $\mathcal{R} \equiv A_{eff}/A_{vis}$ between the effective emitting area of the fireshell A_{eff} and its total visible area A_{vis}. It presents a clear hard-to-soft spectral evolution in time and which is composed by a rising part, a peak and a decaying tail (Ruffini et al., 2002a, 2004b, 2005c; Bernardini et al., 2005a; Ruffini et al., 2006b; Dainotti et al., 2007). It fulfills the "Amati" (Amati et al., 2002; Amati, 2006) relation (Bernardini et al., 2008; Guida et al., 2008).

What in the current literature (see e.g. Refs. Piran, 2005; Meszaros, 2006, and references therein) is usually called the "prompt emission" neglects all the above analysis; in fact, it comprises the P-GRB together with the rising part and the peak of the afterglow. What is usually called the "afterglow" is just its decaying tail (see e.g. Bernardini et al., 2005a; Ruffini et al., 2006b, 2007a; Dainotti et al., 2007; Bernardini et al., 2007; Bianco et al., 2008a). Within our approach there is no separation between the end of the "prompt emission" and the beginning of the decaying tail of the afterglow. Moreover, within our framework one derives, in a natural way, that the "Amati" relation is observed to hold (Amati, 2006) only for long GRBs, where the P-GRB is negligible, and not for short GRBs (Bernardini et al., 2008; Guida et al., 2008).

The ratio between the total time-integrated luminosity of the P-GRB (namely, its total energy) and the corresponding one of the afterglow is the crucial quantity for the identification of GRBs' nature. Such a ratio, as well as the temporal separation between the corresponding peaks, is a function of the B parameter (see Fig. H.1.2, Ref. Ruffini et al., 2001b, as well as Ruffini et al. contribution in this volume). When $B \lesssim 10^{-5}$, the P-GRB is the leading contribution to the emission and the afterglow is negligible: we have a "genuine" short GRB (Ruffini et al., 2001b). When $10^{-4} \lesssim B \lesssim 10^{-2}$, instead, the afterglow contribution is generally predominant (for the existence of the upper limit $B \lesssim 10^{-2}$ see Ref. Ruffini et al., 2000). Still, this last case presents two distinct possibilities: the afterglow peak luminosity can be either larger or smaller than the P-GRB one (Bernardini et al., 2007; Bianco et al., 2008a,b).

The simultaneous occurrence of an afterglow with total time-integrated luminosity larger than the P-GRB one, but with a smaller peak luminosity, is

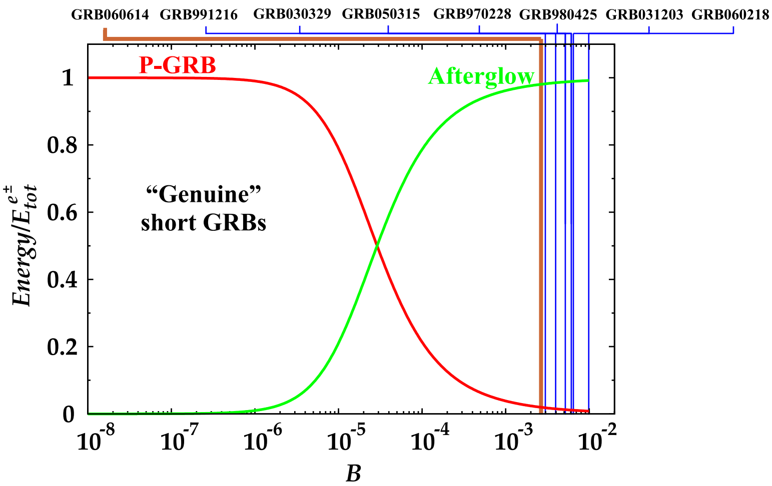

Figure H.1.2: The energy radiated in the P-GRB (solid line) and in the afterglow (dashed line), in units of $E^{tot}_{e^\pm}$, are plotted as functions of the B parameter. This plot has been made assuming a fixed value for $E^{tot}_{e^\pm} = 4.83 \times 10^{53}$ ergs. For further details see Ruffini et al. contribution in this volume. Also represented are the values of the B parameter computed for GRB 991216, GRB 030329, GRB 980425, GRB 970228, GRB 050315, GRB 031203, GRB 060218. Remarkably, they are consistently smaller than, or equal to in the special case of GRB 060218, the absolute upper limit $B \lesssim 10^{-2}$ (Ruffini et al., 2000). The "genuine" short GRBs have a P-GRB predominant over the afterglow: they occur for $B \lesssim 10^{-5}$ (Ruffini et al., 2001b; Bernardini et al., 2007).

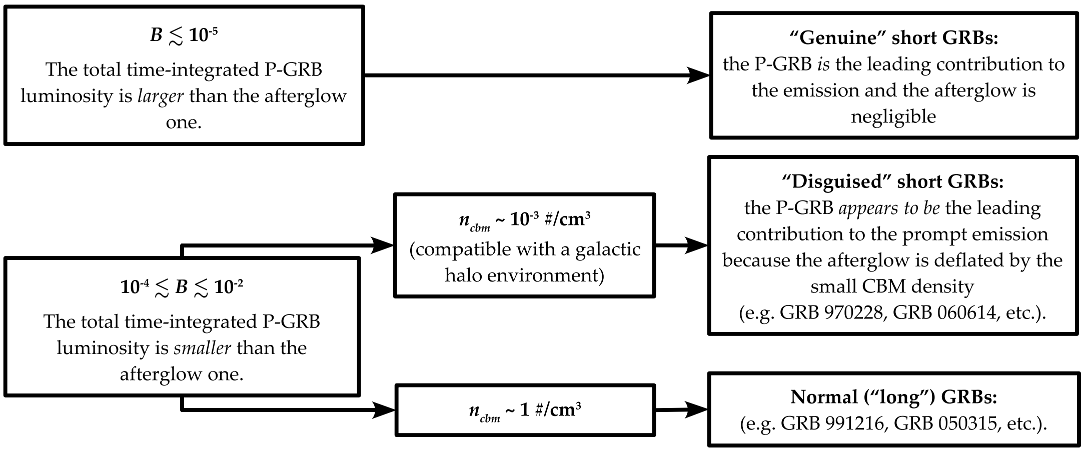

Figure H.1.3: A sketch summarizing the "canonical GRB" scenario.

indeed explainable in terms of a peculiarly small average value of the CBM density ($n_{cbm} \sim 10^{-3}$ particles/cm^3), compatible with a galactic halo environment. Such a small average CBM density "deflates" the afterglow peak luminosity (see Fig. H.1.1 and Refs. Bernardini et al., 2007, 2008). Of course, such a deflated afterglow lasts longer, since the total time-integrated luminosity in the afterglow is fixed by the value of the B parameter (see above, Fig. H.1.2 and Refs. Bernardini et al., 2007; Bianco et al., 2008a,b). Therefore, GRBs belonging to this new class, characterized by a high value of the B parameter and a very small CBM density, inherit their peculiar features from the external environment and not from the intrinsic nature of the source. In this sense, they are only "fake" short GRBs or, better, canonical GRBs "disguised" as short ones (Bernardini et al., 2007; Bianco et al., 2008a,b). Such a class is the one identified by Norris and Bonnell (2006), includes GRB 060614 and has GRB 970228 as a prototype (see Fig. H.1.1 and Refs. Bernardini et al., 2007; Bianco et al., 2008a,b). The whole "canonical GRB" scenario is depicted in Fig. H.1.3. Actually, all GRBs we analyzed appears to be canonical ones with $B > 10^{-3}$ (see Fig. H.1.2).

H.1.1 The canonical Gamma-Ray Bursts and their "precursors"

The so-called "prompt emission" light curves of many GRBs present a small pulse preceding the main GRB event, with a lower peak flux and separated by this last one by a quiescent time. The nature of such GRB "precursors" is one of the most debated issues in the current literature (see Burlon et al., in press). Already in 2001 (Ruffini et al., 2001b), within the "fireshell" model, we proposed that GRB "precursors" are the P-GRBs emitted when the fireshell becomes transparent, and we gave precise estimates of the time sequence and intensities of the P-GRB and the of the afterglow.

We have recently shown (Aksenov et al., submitted to) that a thermal spectrum still occurs in presence of $e^{\pm}$ pairs and baryons. By solving the rate equation we have evaluated the evolution of the temperature during the fireshell expansion, all the way up to when the transparency condition is reached (Ruffini et al., 1999, 2000). In the upper panel of Fig. H.1.4 we plot, as a function of B, the fireshell temperature $T_\circ$ at the transparency point, i.e. the temperature of the P-GRB radiation. The plot is drawn for four different values of $E^{tot}_{e^\pm}$ in the interval $[10^{49}, 10^{55}]$ ergs, well encompassing GRBs' observed isotropic energies. We plot both the value in the co-moving frame $T^{com}_\circ$ and the one Doppler blue-shifted toward the observed $T^{obs}_\circ = (1+\beta_\circ)\gamma_\circ T^{com}_\circ$, where $\beta_\circ$ is the fireshell speed at the transparency point in units of c (Ruffini et al., 2000).

In the middle panel of Fig. H.1.4 we plot, as a function of B, the fireshell Lorentz gamma factor at the transparency point $\gamma_\circ$. The plot is drawn for the same four different values of $E^{tot}_{e^\pm}$ of the upper panel. Also plotted is the asymptotic value $\gamma_\circ = 1/B$, which corresponds to the condition when the entire initial internal energy of the plasma $E^{tot}_{e^\pm}$ has been converted into kinetic energy of the baryons (Ruffini et al., 2000). We see that such an asymptotic value is approached for $B \rightarrow 10^{-2}$. We see also that, if $E^{tot}_{e^\pm}$ increases, the maximum values of $\gamma_\circ$ are higher and they are reached for lower values of B.

In the lower panel of Fig. H.1.4 we plot the same Fig. H.1.2 but for the same four different values of $E^{tot}_{e^\pm}$ of the upper panel. We saw in the previous section that for $B \lesssim 10^{-5}$ the total energy emitted in the P-GRB is always larger than the one emitted in the afterglow: we have what we call a "genuine" short GRB (Ruffini et al., 2001b; Bernardini et al., 2007; Bianco et al., 2008b, see also Bianco et al. contribution in this volume). On the other hand, for $3.0 \times 10^{-4} \lesssim B < 10^{-2}$ the total energy emitted in the P-GRB is always smaller than the one emitted in the afterglow. If it is not below the instrumental threshold and if $n_{cbm} \sim 1$ particle/cm^3 (see Fig. H.1.3), the P-GRB can be observed in this case as a small pulse preceding the main GRB event (which coincides with the peak of the afterglow), i.e. as a GRB "precursor" (Ruffini et al., 2001b, 2003; Bianco et al., 2008b).

Particularly relevant for the new era of the *Agile* and *GLAST* satellites is that for $B < 10^{-3}$ the P-GRB emission has an observed temperature up to 10^3 keV or higher. This high-energy emission has been unobservable by the *Swift* satellite.

In Fig. H.1.5 we plot, as a function of B, the arrival time separation Δt_a between the P-GRB and the peak of the afterglow measured in the cosmological rest frame of the source. Such a time separation Δt_a is the "quiescent time" between the precursor (i.e. the P-GRB) and the main GRB event (i.e. the peak of the afterglow). The plot is drawn for the same four different values

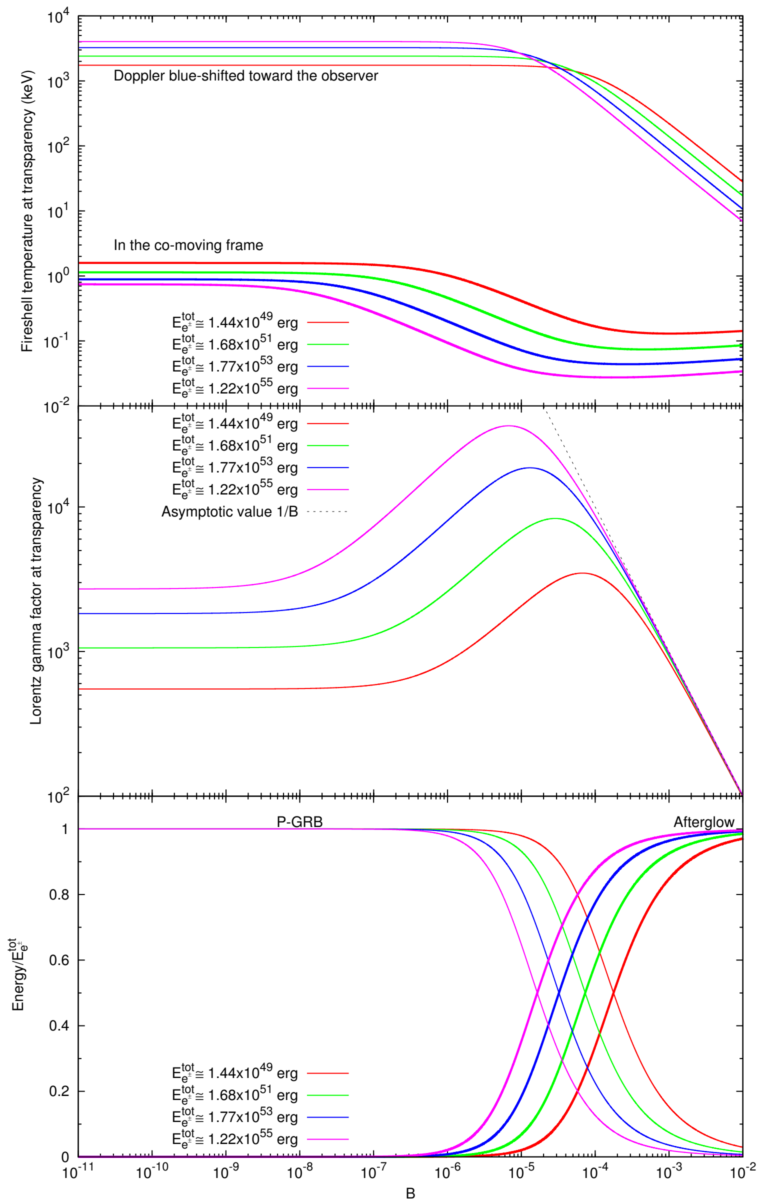

Figure H.1.4: At the fireshell transparency point, for 4 different values of $E^{tot}_{e^\pm}$, we plot as a function of B: **(Above)** The fireshell temperature in the co-moving frame $T^{com}_\circ$ (thicker lines) and the one Doppler blue-shifted along the line of sight toward the observer in the source cosmological rest frame $T^{obs}_\circ$ (thinner lines); **(Middle)** The fireshell Lorentz gamma factor $\gamma_\circ$ together with the asymptotic value $\gamma_\circ = 1/B$; **(Below)** The energy radiated in the P-GRB (thinner lines, rising when B decreases) and the one converted into baryonic kinetic energy and later emitted in the afterglow (thicker lines, rising when B increases), in units of $E^{tot}_{e^\pm}$.

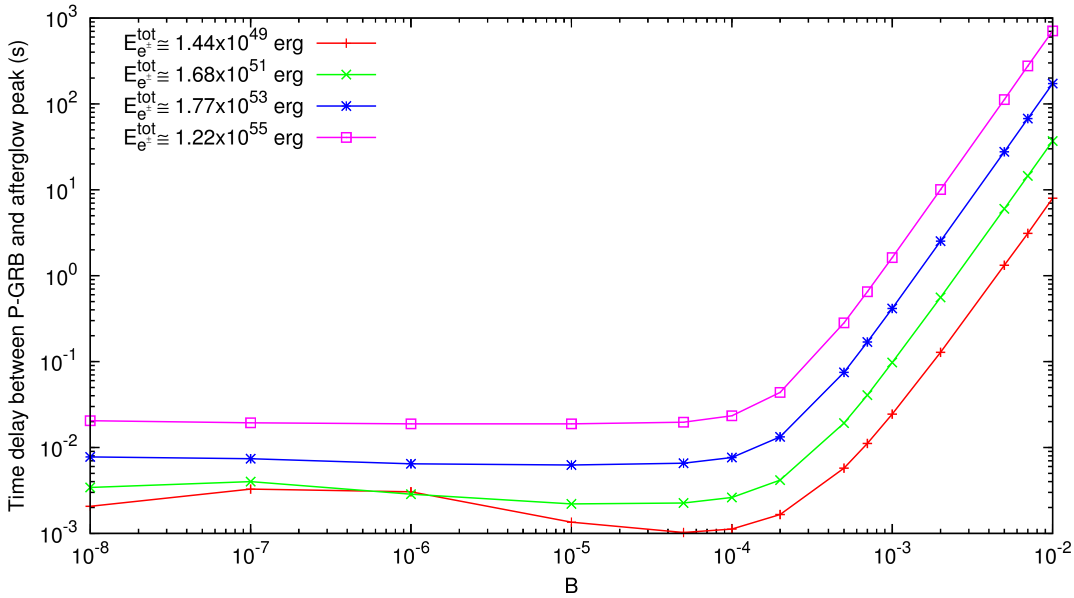

Figure H.1.5: For 4 different values of $E_{e^\pm}^{tot}$, we plot as a function of B the arrival time separation Δt_a between the P-GRB and the peak of the afterglow (i.e. the "quiescent time between the "precursor" and the main GRB event), measured in the source cosmological rest frame. This computation has been performed assuming a constant CBM density $n_{cbm} = 1.0$ particles/cm^3. The points represents the actually numerically computed values, connected by straight line segments.

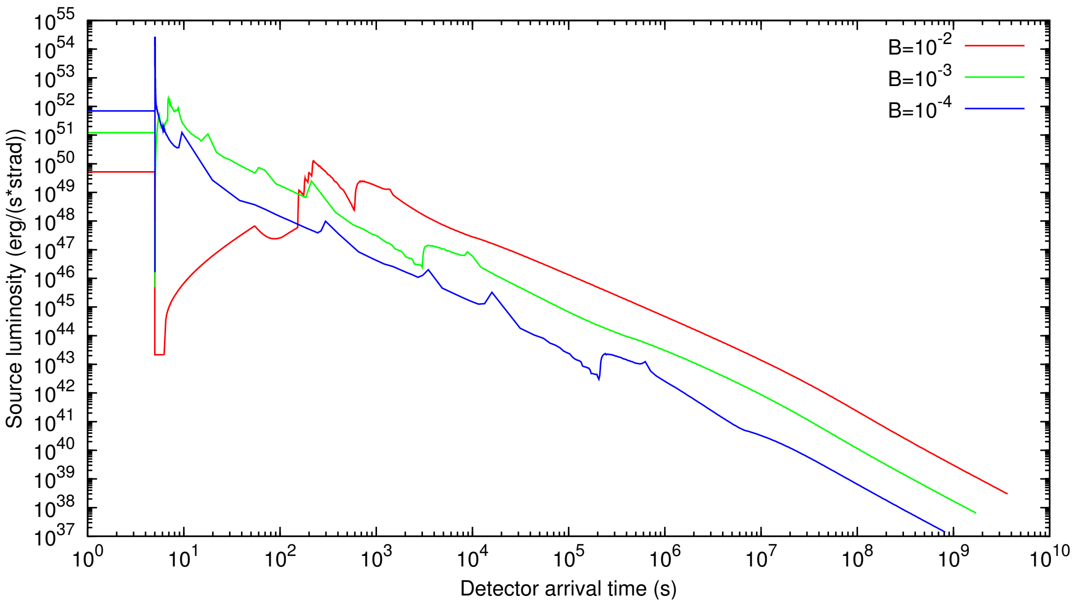

Figure H.1.6: We plot three theoretical afterglow bolometric light curves together with the corresponding P-GRB peak luminosities (the horizontal segments). The computations have been performed assuming the same $E^{tot}_{e^\pm}$ and CBM structure of GRB991216 and three different values of B. The P-GRBs have been assumed to have the same duration in the three cases, i.e. 5 s. For B decreasing, the afterglow light curve squeezes itself on the P-GRB.

of $E^{tot}_{e^\pm}$ of Fig. H.1.4. The arrival time of the peak of the afterglow emission depends on the detailed profile of the CBM density. In this plot it has been assumed a constant CBM density $n_{cbm} = 1.0$ particles/cm^3. We can see that, for $3.0 \times 10^{-4} \lesssim B < 10^{-2}$, which is the condition for P-GRBs to be "precursors" (see above), Δt_a increases both with B and with $E^{tot}_{e^\pm}$. We can have $\Delta t_a > 10^2$ s and, in some extreme cases even $\Delta t_a \sim 10^3$ s. For $B \lesssim 3.0 \times 10^{-4}$, instead, Δt_a presents a behavior which qualitatively follows the opposite of $\gamma_\circ$ (see middle panel of Fig. H.1.4).

Finally, in Fig. H.1.6 we present three theoretical afterglow bolometric light curves together with the corresponding P-GRB peak luminosities for three different values of B. The duration of the P-GRBs has been assumed to be the same in the three cases (i.e. 5 s). The computations have been performed assuming the same $E^{tot}_{e^\pm}$ and the same detailed CBM density profile of GRB991216 (Ruffini et al., 2003). In this picture we clearly see how, for B decreasing, the afterglow light curve "squeezes" itself on the P-GRB and the P-GRB peak luminosity increases.

Before closing, we like to mention that, using the diagrams represented in Figs. H.1.4-H.1.5, in principle one can compute the two free parameters of the fireshell model, namely $E^{tot}_{e^\pm}$ and B, from the ratio between the total energies of the P-GRB and of the afterglow and from the temporal separation between the peaks of the corresponding bolometric light curves. None of these quantities depends on the cosmological model. Therefore, one can in principle use this method to compute the GRBs' intrinsic luminosity and make GRBs the best cosmological distance indicators available today. The increase of the number of observed sources, as well as the more accurate knowledge of their CBM density profiles, will possibly make viable this procedure to test cosmological parameters, in addition to the Amati relation (Amati et al., 2008; Guida et al., 2008).

H.2 GRB 060614: another example of fake short burst

GRB 060614 (Gehrels et al., 2006; Mangano et al., 2007) has imposed to the general attention of the Gamma-Ray Burst's (GRB's) scientific community because it is the first clear example of a near, long GRB not associated with a bright Ib/c Supernova (SN) (Della Valle et al., 2006; Gal-Yam et al., 2006). It has been estimated that, if present, the SN-component should be about 200 times fainter than the archetypal SN 1998bw associated to GRB980425; moreover, it would also be fainter (at least 30 times) than any stripped-envelope Supernova ever observed (Richardson et al., 2006). In the standard scenario, long duration GRBs ($T_{90} > 2$s) are thought to be produced by SN events during the collapse of massive stars in star forming regions (Woosley, 1993). The observations of broad-lined and bright type Ib/c SNe associated with GRBs are often reported to favor this scenario (Woosley and Bloom, 2006, and references therein). The *ansatz* has been advanced that every long GRB should have a SN associated with it (Zhang et al., 2006b). Consequently, in all nearby long GRBs ($z \leq 1$) the SN emission should be observed. To account for the revolutionary situation of GRB 060614 some obvious hypothesis have been proposed and ruled out: the chance superposition with a galaxy at low redshift (Gal-Yam et al., 2006) and the strong dust obscuration and extinction (Fynbo et al., 2006). Appeal has been made to the possible occurrence of an unusually low luminosity stripped-envelope core-collapse SN (Della Valle et al., 2006).

The second novelty of GRB 060614 is that it challenges the traditional separation between Long Soft GRBs and Short Hard GRBs. Traditionally (Klebesadel, 1992; Dezalay et al., 1992), the "short" GRBs have $T_{90} < 2$s, present an harder spectrum and negligible spectral lag, and are assumed to originate from merging of two compact objects. i.e. two neutron stars or a neutron star and a black hole (see e.g. Blinnikov et al., 1984; Paczynski, 1986; Goodman, 1986; Eichler et al., 1989; Piran, 2005; Meszaros, 2006, and references therein). GRB 060614 is a near long GRB, its redshift is $z = 0.125$ and it lasts about one hundred seconds ($T_{90} = (102 \pm 5)$s; Gehrels et al., 2006) and it fulfills the $E_p^{rest} - E_{iso}$ correlation (Amati et al., 2007). However, its morphology is different from typical long GRBs, similar to the one of GRB050724, classified as a short GRB (Zhang et al., 2006b; Piro, 2005). Also its optical afterglow luminosity is intermediate between the traditional long ones and the traditional short ones (Kann et al., 2008). Its 15–150keV light curve presents a short, hard and multi-peaked episode (about 5s). Such an episode is followed by a softer, prolonged emission that manifests a strong hard to soft evolution in the first 400s of data (Mangano et al., 2007). The total fluence in the 15–150keV energy band is $F = (2.17 \pm 0.04) \times 10^{-5}$erg/cm^2, the 20% emitted during the initial spikelike emission, where the peak luminosity reaches the value of 300keV before decreasing until 8keV during the BAT-XRT overlap time (about 80s). Moreover, its host galaxy has a moderate specific star formation rate ($R_{Host} \approx 2M_s y^{-1}(L^*)^{-1}$, $M_{vHost} \approx -15.5$; Fynbo et al., 2006; Della Valle et al., 2006). The spectral lag in its light curves is very small or absent (Gehrels et al., 2006). All these features are typical of the short GRBs.

This apparent contradiction finds a natural explanation in the framework of our "fireshell" model. There, the origin of all GRBs is traced back to the formation of a black hole, either occurring in a single process of gravitational collapse, or induced in a binary system (Ruffini et al., 2001a), or in a merging binary system composed by neutron stars and/or white dwarfs in all possible combinations. In the fireshell model, the occurrence of a GRB-SN is not a necessity. It is only a possibility linked, for example, to the process of "induced" gravitational collapse (Ruffini et al., 2007b; Dainotti et al., 2007). The "canonical" GRB light curve is there formed by a P-GRB (often labeled as "precursor"), emitted at the fireshell transparency, and an extended afterglow (whose peak is often labeled as "prompt emission"), whose luminosity is very sensitive to the average CBM density. In the case of GRB 060614 the P-GRB is identified with the $\approx$ 5s multipeaked spike of "hard" emission. As discussed in Sect. 2, the relative energetics of the P-GRB and the afterglow is ruled by a dimensionless parameter: the fireshell baryon loading B. In the limit of $B \to 0$ all the GRB energy is emitted in the P-GRB: these are the "genuine" short GRBs (Ruffini et al., 2001b). The "genuine" short GRBs are the limiting case of canonical GRBs for a pure $e^{\pm}$ plasma with negligible baryonic contamination. The difference between short and long GRBs, or, better, between short and generic canonical GRBs (see Sect. 2), within our approach, is not related to different progenitors: it is linked to the value of the fireshell baryon loading. The crucial quantity to understand GRB nature is the time-integrated luminosity of the P-GRB vs. the afterglow one. The comparison of the corresponding peak luminosities can be indeed misleading, as clearly shown in the present case of GRB 060614 and in the prototypical case of GRB970228 (Bernardini et al., 2007).

Here we address the issue of the novel class of GRBs with "an occasional softer extended emission lasting tenths of seconds after an initial spikelike emission" (Norris and Bonnell, 2006). The softer extended emission appears to have a peak luminosity smaller than the one of the initial spikelike emission. This has misled the understanding of the correct role of the afterglow. As we show in the following (see also Bernardini et al., 2007), we have successfully identified the initial spikelike emission with the P-GRB and the softer extended emission with the peak of the afterglow. We show explic-

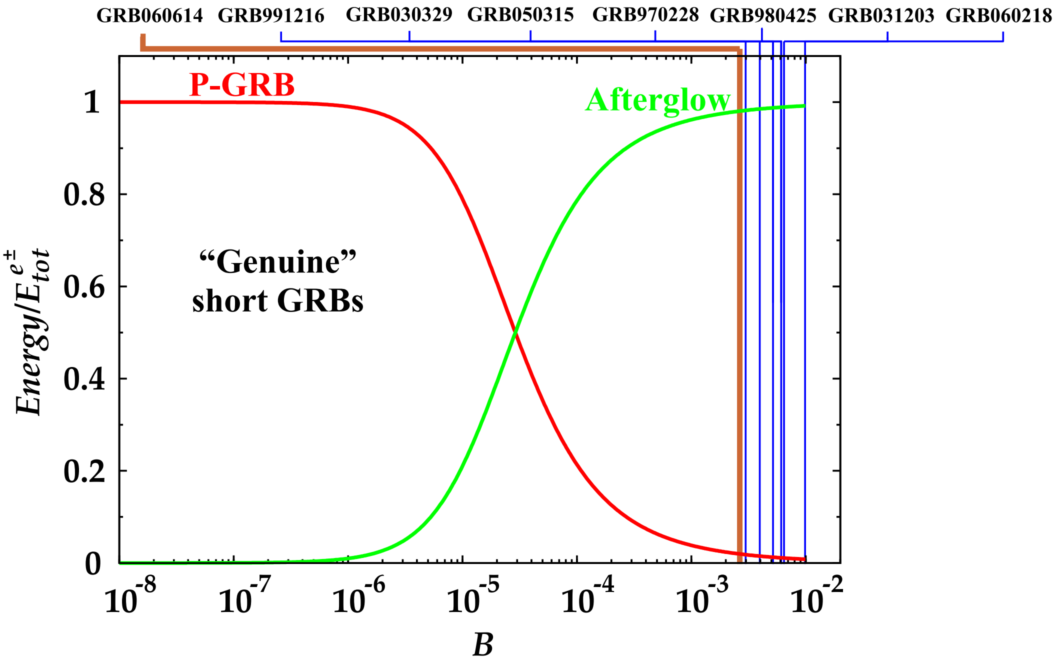

Figure H.2.1: Here the energies emitted in the P-GRB (red line) and in the afterglow (green line), in units of the total energy of the plasma, are plotted as functions of the B parameter. When $B \leq 10^{-5}$, the P-GRB becomes predominant over the afterglow, giving rise to a "genuine" short GRB. In the figure are also marked in blue the values of the B parameters corresponding to some GRBs we analyzed, all belonging to the class of long GRBs, together with the GRB 060614 one (thick brown line).

itly that the integrated afterglow luminosity is much larger than the P-GRB one, as expected in a canonical GRB with $B > 10^{-3}$. As we will show, the peculiarity of the low afterglow luminosity and of its much longer time evolution is not intrinsic to the progenitor nor to the black hole, but it uniquely depends on the peculiarly low value of the CBM density, typical of galactic halos, $\sim 10^{-3}$particles/cm^3. Therefore, GRBs belonging to this novel class are only "fake" short GRBs, or, better, canonical GRBs "disguised" as short ones, and have GRB970228 as a prototype (Bernardini et al., 2007).

H.2.1 The fit of the observed luminosity

We have performed the analysis of the observed light curves in the 15–150keV energy band, corresponding to the γ-ray emission observed by the BAT instrument on the Swift satellite, and in the 0.2–10keV energy band, corresponding to the X-ray component from the XRT instrument on Swift satellite. We do not address in this Letter the issue of the optical emission, that represent less than 10% of the total energy of the GRB. From this fit (see Figs. H.2.2, H.2.4) we have derived the total initial energy $E_{tot}^{e^\pm}$, the value of B as well as the effective CBM distribution (see Fig. H.2.3). We find $E_{tot}^{e^\pm} = 2.94 \times 10^{51}$erg, that accounts for the bolometric emission of both the P-GRB and the afterglow. Such a value is compatible with the observed $E_{iso} \simeq 2.5 \times 10^{51}$erg (Gehrels et al., 2006). The value of B is $B = 2.8 \times 10^{-3}$, that corresponds to the lowest one of all the GRBs we have examined (see Fig. H.2.1). It corresponds to a canonical GRB with a very clear afterglow predominance over the P-GRB. From the model, having determined $E_{tot}^{e^\pm}$ and B, we can compute the theoretical expected P-GRB energetics E_{P-GRB} (Ruffini et al., 2001b). We obtain $E_{P-GRB} \simeq 1.15 \times 10^{50}$erg, that is in good agreement with the observed one $E_{iso,1p} \simeq 1.18 \times 10^{50}$erg (Gehrels et al., 2006). The Lorentz Gamma Factor at the transparency results to be $\gamma_\circ = 346$, one of the highest of all the GRBs we have examined.

In Fig. H.2.2 we plot the comparison between the BAT observational data of the GRB0606014 prompt emission in the 15–150keV energy range and the P-GRB and afterglow light curved computed within our model. The temporal variability of the afterglow peak emission is due to the inhomogeneities in the effective CBM density (see Figs. H.2.2, H.2.3). Toward the end of the BAT light curve, the good agreement between the observations and the fit is affected by the Lorentz gamma factor decrease and the corresponding increase of the maximum viewing angle. The source visible area becomes larger than the typical size of the filaments. This invalidates the radial approximation we use for the CBM description. To overcome this problem it is necessary to introduce a more detailed three-dimensional CBM description, in order to avoid an over-estimated area of emission and, correspondingly, to describe the sharpness of some observed light curves. We are still working on this issue (Ruffini et al., 2002a; Caito et al., in press; Bianco et al., 2006a; Guida et al., in press). We turn now to the crucial determination of the CBM density, which is derived from the fit. At the transparency point it resulted to be $n_{CBM} = 4.8 \times 10^{-3}$particles/cm^3 (see Fig. H.2.3). This density is compatible with the typical values of the galactic halos. During the peak of the afterglow emission the effective average CBM density decreases reaching $\langle n_{CBM} \rangle = 2.25 \times 10^{-5}$particles/cm^3, possibly due to an occurring fragmentation of the shell (Dainotti et al., 2007) or due to a fractal structure in the CBM. The $\mathcal{R}$ value resulted to be on average $\langle R \rangle = 1.72 \times 10^{-8}$. It is interesting to emphasize the striking analogy of the numerical value and the overall radial dependence of the CBM density in the present case of GRB 060614 when compared and contrasted with the ones of GRB970228 (Bernardini et al., 2007).

Concerning the 0.2–10keV light curve of the decaying phase of the afterglow, observed by the XRT instrument, we have also reproduced very satisfactorily both the hard decrease in the slope and the plateau of the light curve keeping constant the effective CBM density and changing only $\mathcal{R}$. The result

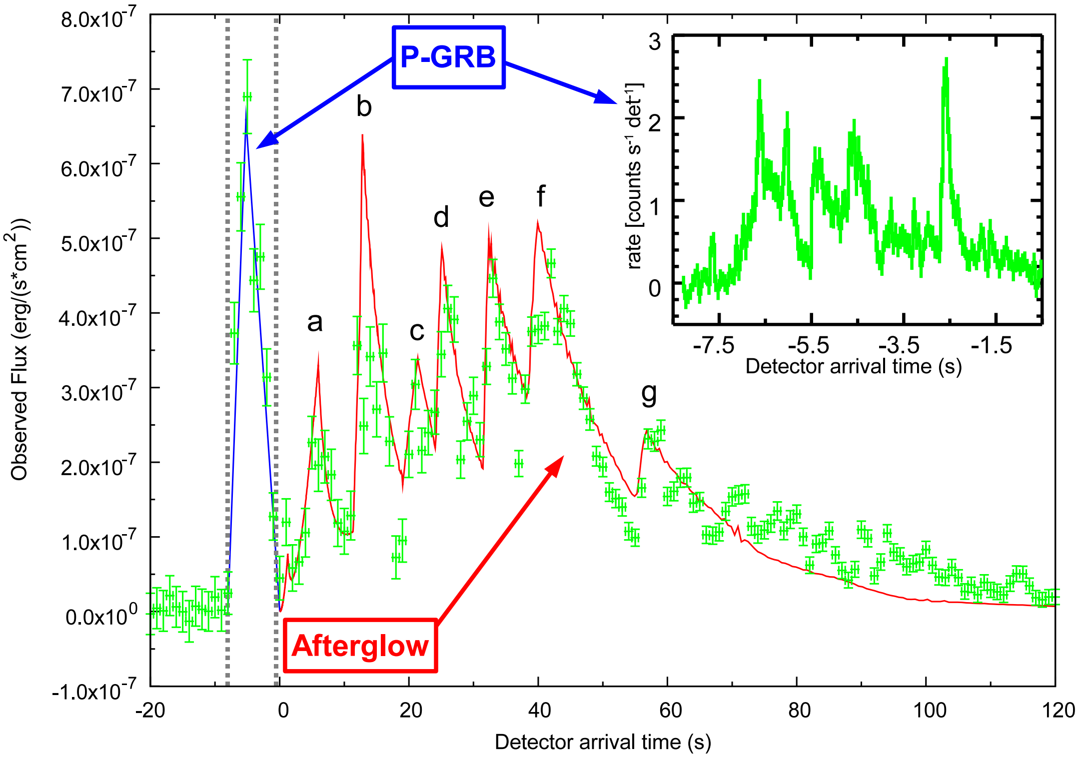

Figure H.2.2: The BAT 15–150keV light curve (green points) at 1s time resolution is compared with the corresponding theoretical afterglow light curve we compute (red line). The onset of the afterglow is at the end of the P-GRB (qualitatively sketched in blue lines and delimited by dashed gray vertical lines). Therefore the zero of the temporal axis is shifted by 5.5s with respect to the BAT trigger time. The peaks of the afterglow light curves are labeled to match them with the corresponding CBM density peak in Fig. H.2.3. In the upper right corner there is an enlargement of the P-GRB at 50ms time resolution (reproduced from Mangano et al., 2007), showing its structure.

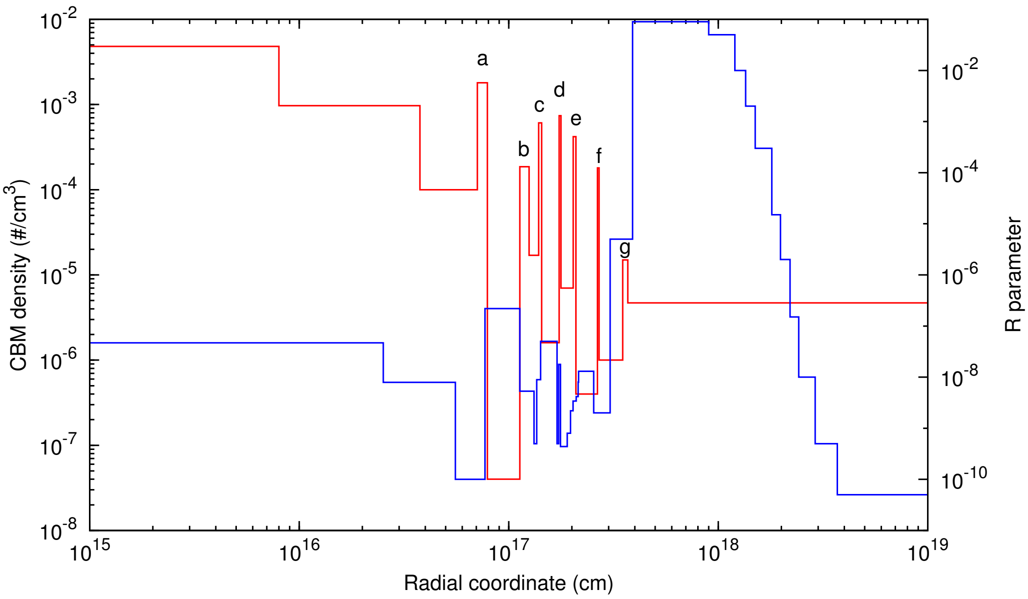

Figure H.2.3: Here are the plot of the effective CBM density (red line) and of the $\mathcal{R}$ parameter (blue line) versus the radial coordinate of the shell. The CBM density peaks are labeled to match them with the corresponding afterglow light curve peaks in Fig. H.2.2. They corresponds to filaments of characteristic size $\Delta r \sim 10^{15}$cm and density contrast $\Delta n_{CBM}/\langle n_{CBM}\rangle \sim 20$ particles/cm^3.

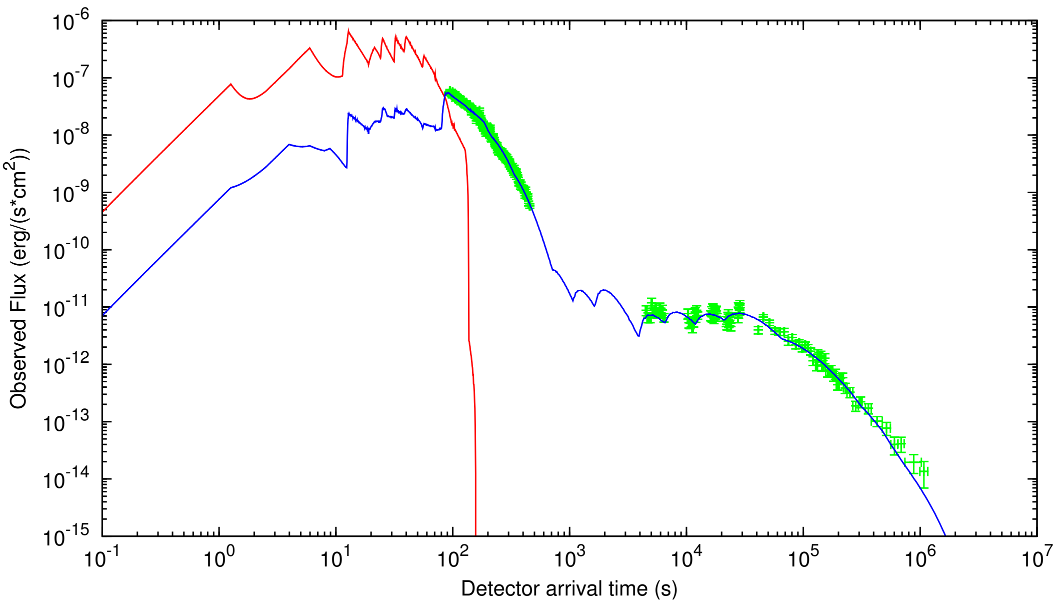

Figure H.2.4: The XRT 0.2–10keV light curve (green points) is compared with the corresponding theoretical afterglow light curve we compute (blue line). Also in this case we have a good correspondence between data and theoretical results. For completeness, the red line shows again the theoretical afterglow light curve in the 15–150keV energy range presented in Fig. H.2.2.

of this analysis is reported in Fig. H.2.4. We put in this phase $n_{CBM} = 4.70 \times 10^{-6}$particles/cm^{-3}. The average value of the $\mathcal{R}$ parameter is $\langle R \rangle = 1.27 \times 10^{-2}$. The drastic enhancement in the $\mathcal{R}$ parameter with respect to the values at the peak of the afterglow is conforming to what happens for other sources we have studied: GRB060218 presents a bump of five orders of magnitude (Dainotti et al., 2007), in GRB060710 the bump is of about four order of magnitude (see Guida et al., in preparation) while in GRB050315 there is a three order of magnitude bump (Ruffini et al., 2006b). In these last two cases, we found the occurrence of the enhancement of $\mathcal{R}$ between r=2 $\times$ 10^{17}cm and r=3 $\times$ 10^{17}cm, just like for GRB 060614, for which we have the bump at r=3.5 $\times$ 10^{17}cm. The time of the bump approximately corresponds to the appearance of the optical emission observed in GRB 060614 and, more in general, to the onset of the second component of the Willingale et al. (2007) scheme for GRBs.

H.2.2 Conclusions

Since the earliest days of GRBs, the attention has been focused on the classification between short and long GRBs (Klebesadel, 1992; Dezalay et al., 1992). One of the major outcome of the Swift observation of, e.g., GRB050315

(Vaughan et al., 2006; Ruffini et al., 2006b) has been the confirmation that long GRB duration is not intrinsic to the source but is merely a function of the instrumental noise threshold (Ruffini et al., 2006a). Such a concept had been introduced in Ruffini et al. (2001b), where the coincidence of long GRBs with the peaks of the afterglows was proposed. GRB 060614 represents an additional fundamental progress in clarifying the role of the CBM density in determining the GRB morphology. It confirms the results presented in GRB970228 (Bernardini et al., 2007), that is the prototype of the new class of "fake" short GRBs, or, better, of canonical GRBs "disguised" as short ones. The sharp spiky emission corresponds to the P-GRB. They correspond to canonical GRBs with an afterglow emission energetically predominant with respect to the P-GRB one and a baryon loading $B > 10^{-3}$. As recalled above, the comparison of the peak luminosity of the P-GRB and of the afterglow is indeed misleading: it follows from the low average CBM density and it is neither intrinsic to the progenitor nor to the black hole. This result points to the possibility that the majority of GRBs declared as shorts (see e.g. Piro, 2005) are likely "disguised" short GRBs.

The observations of GRB 060614 offer the opportunity, for the first time, to analyze in detail the structure of a P-GRB lasting 5s. This feature is directly linked to the physics of the gravitational collapse originating the GRB. Recently, there has been a crucial theoretical physics result, showing that the characteristic time constant for the thermalization for an $e^{\pm}$ plasma is on the order of 10^{-13}s (Aksenov et al., 2007). Such a time scale still applies for an $e^{\pm}$ plasma with a baryon loading on the order of the one observed in GRBs (Aksenov et al., 2008). The shortness of such a time scale, as well as the knowledge of the dynamical equations of the optically thick phase preceding the P-GRB emission (Bianco et al., 2006b), implies that the structure of the P-GRB is a faithful representation of the gravitational collapse process leading to the formation of the black hole (Ruffini et al., 2005d). In this respect, it is indeed crucial that the Swift data on the P-GRB observed in GRB 060614 (see Fig. H.2.2) appear to be highly structured all the way to time scale of 0.1s. This opens a new field of research: the study of the P-GRB structure in relation to the process of gravitational collapse leading to the GRB.

The low value of the CBM density is compatible with a galactic halo environment. This result points to an old binary system as the progenitor of GRB 060614 and well justify the absence of an associated SN Ib/c event (see also Davies et al., 2007). Such a binary system departed from its original location in a star forming region and spiraled out in a low density region of the galactic halo (see e.g. Kramer, in press). The energetic of this source is about two orders of magnitude smaller than the one of GRB970228 (Bernardini et al., 2007). A natural explanation is that instead of a neutron star - neutron star merging binary system we are in presence of a white dwarf - neutron star binary. The structure of the gravitational collapse of a binary system to a black hole is certainly more complex than the direct collapse of a star into a black hole. In principle, the nature of the white dwarf, with typical radius on the order of 10^3km, as opposed to the one of the neutron star, typically on the order of 10km, may manifest itself in characteristic signatures in the structure of the P-GRB (see Fig. H.2.2). We therefore agree, for different reasons, with the identification proposed by Davies et al. (2007) for the progenitor of this source. GRB 060614 must necessarily fulfill, and indeed it does, the Amati relation. This happens even taking into account the entire prompt emission mixing together P-GRB and afterglow (Amati et al., 2007), due to the above recalled energetic predominance of the afterglow (see also Guida et al., 2008).

H.3 Application to GRB 050509B

The baryon loading is the key parameter to classify GRBs: if they are on the left part of the crossing $B \leq 10^{-5}$ we call them "genuine" short (see section H.1). To investigate if this is the case of GRB 050509B (Gehrels et al., 2005) we did two different analysis, the first one has a big B and is represented by the line on the right side of the crossing. The second analysis have a small B and is the line on the left side of the cross (see Fig. H.3.1).

H.3.1 Data analysis

H.3.1.1 Analysis 1

We identify the prompt emission of this GRB see figure H.3.2 with our P-GRB. Then the afterglow fits the other data in X-rays, see Fig. H.3.3. In this case, we have the total energy of the GRB estimated in 2.11 x 10^{48} erg (which is a low energy for GRBs) and the baryon loading is $B = 3.7$ x 10^{-3}. The P-GRB has an energy of $E_{P-GRB} = 1.638$ x 10^{47} erg, it means that more then 90% of the energy is released in the afterglow, so this is not a short GRB at all. It has emitted much more energy after the 40 ms detected by BAT, but the energy was below its threshold and before the beginning of data collection by XRT (which has the first data after 100 seconds).

H.3.1.2 Analysis 2

We did an alternative analysis looking for a case in which this GRB is "genuine" short. In this analysis we fit the first data (see figure H.3.2) with the peak of the afterglow. The P-GRB is very energetic $E_{P-GRB} = 3.30$ x 10^{49} erg in comparison with the afterglow, but it was not visible because its peak energy would be about 817 KeV. The peak emission of the afterglow, would be the emission observed, see figure H.3.4. In this case the energy of the GRB is 5.07 x 10^{49} erg, the baryon loading is $B = 1.1$ x 10^{-4}, and this implies that the energy emitted on the P-GRB is almost 60% of the total one. This means that this GRB is a "genuine" short; but it was not "observed".

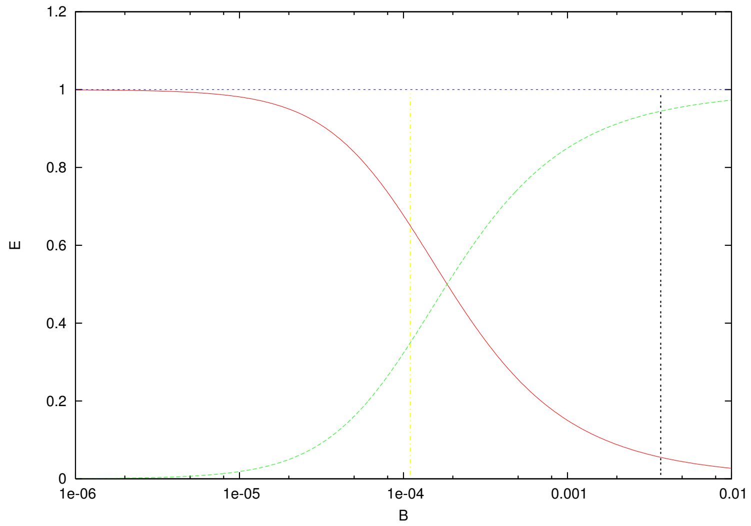

Figure H.3.1: Energy emitted in: the P-GRB (red line) and afterglow (green line), in function of the B parameter. The blue line is the sum of the two lines. In black is the B parameter of our first analysis and in yellow is our second analysis which results to be a "genuine" short. Details in section H.1.

H.3.2 GRB 050509B within the Amati relation

None of our two analysis are compatible with the Amati relation as you can see in figure H.3.5. As the Amati relation is valid just for long GRBs we can conclude that the first analysis is wrong and so we remain with the second analysis. So we have 050509B as a "genuine" short GRB, it is out of the Amati relation, like the other short GRBs. We expect so, from our fit (see figure H.3.4), a very hard emission, mainly in the P-GRB but also in the afterglow. The P-GRB have photon emission until 817 kev, very above the BAT trigger which is less then 350 kev. Is very important to have satellites looking to high energy emission from GRBs, because only with then we can observe the "genuine" short GRBs.

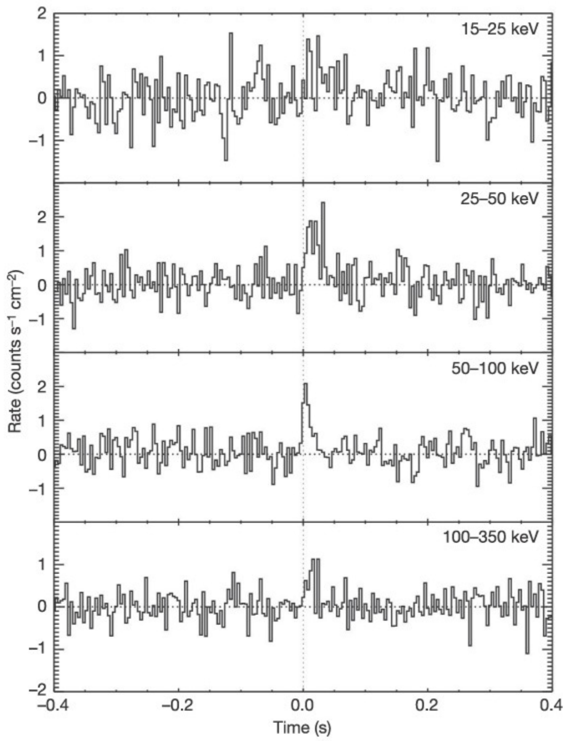

Figure H.3.2: Data detected by BAT, figure from 2005Natur.437..851G.

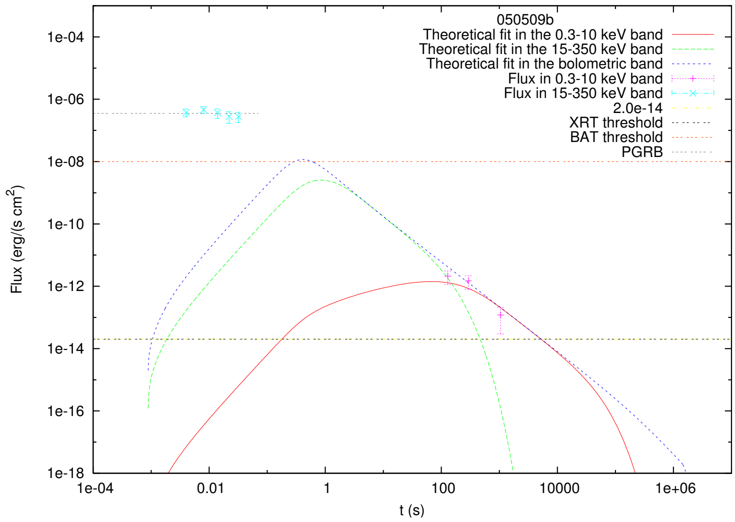

Figure H.3.3: Our fit where the BAT data is the P-GRB with a peak energy observe above 600 kev. And the afterglow which have a total energy that is eight times larger then the P-GRB.

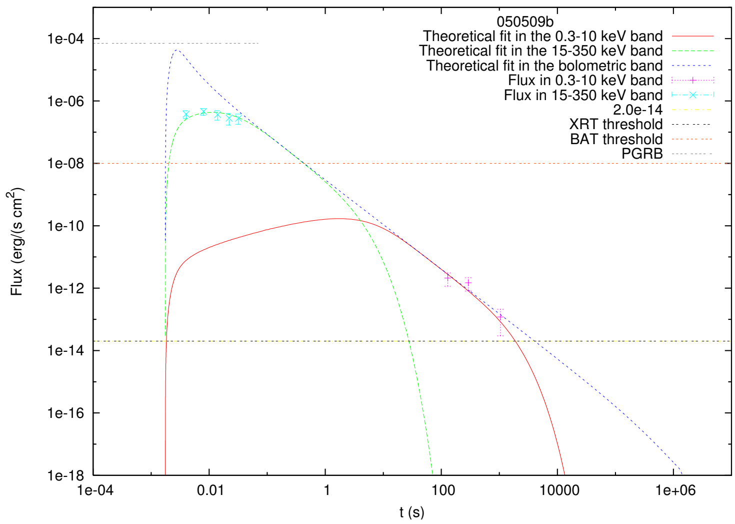

Figure H.3.4: Our fit where the BAT data is the afterglow emission and the P-GRB is above the trigger. In this case the P-GRB is more then twice the afterglow, but is too hard to be observed.

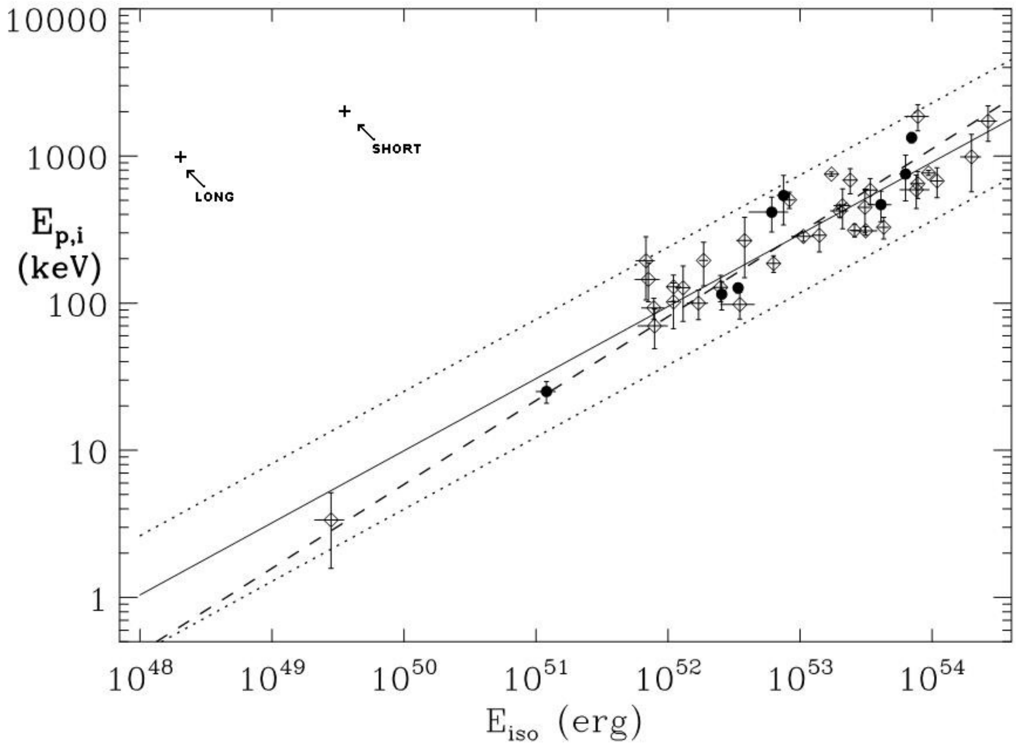

Figure H.3.5: Our two fits are out of this relation. We know that this relation is valid just for long GRBs and that short GRBs are harder in the peak energy emission. So our fit like a short GRB can be true.

H.4 GRB 060607A: a complete analysis of the prompt emission and X-ray flares.

GRB 060607A is a very distant ($z = 3.082$ Ledoux et al., 2006) and energetic event ($E_{iso} \sim 10^{53}$ erg Molinari et al., 2007). Its BAT light curve shows a double-peaked structure with a duration of $T_{90} = (100 \pm 5)$ s (Tueller et al., 2006). The time-integrated spectrum over the T_{90} is best fit with a simple power-law model with an index $\Gamma = 1.45 \pm 0.08$ (Guidorzi, private communication). The XRT light curve shows a prominent flaring activity (at least three flares) superimposed to the normal afterglow decay (Page et al., 2006).

The GRB 060607A main peculiarity is that the peak of the near-infrared (NIR) afterglow has been observed with the REM robotic telescope (Molinari et al., 2007). Interpreting the NIR light curve as corresponding to the afterglow onset as predicted by the fireball forward shock model (Sari and Piran, 1999; Meszaros, 2006), it is possible to infer the initial Lorentz gamma factor of the emitting system that results to be $\Gamma_\circ \sim 400$ (Molinari et al., 2007; Covino et al., 2007; Jin and Fan, 2007). Moreover, these measurements seem to be consistent with an interstellar medium environment, ruling out the wind-like medium (Molinari et al., 2007; Jin and Fan, 2007).

We analyze GRB 060607A within the fireshell model (Ruffini et al., 2001c,b, 2007a). We show how GRB 060607A cannot be a "fake" short GRB, or better a GRB disguised as short (Bernardini et al., 2007) with realistic values of the fireshell and CBM parameters, but is a normal long GRB. We show also that within this interpretation the N(E) spectrum of the prompt emission can be fitted in a satisfactory way by a convolution of thermal spectra as predicted by the model we applied (Ruffini et al., 2004b, 2005c; Bernardini et al., 2005a). The theoretical spectrum and light curve in the BAT energy band obtained are in good agreement with the observations, enforcing the plausibility of our approach. Moreover, in analogy with the case of GRB 011121 (see A.10), we propose an interpretation of the observed X-ray flares as produced by overdense CBM clouds, in analogy with the gamma-ray light curve.

In this preliminary analysis we deal only with the BAT and XRT observations, which are the basic contribution to the afterglow emission according to the fireshell model. We do not deal with the infrared emission that, on the contrary, is used in the current literature to estimate the dynamical quanti-

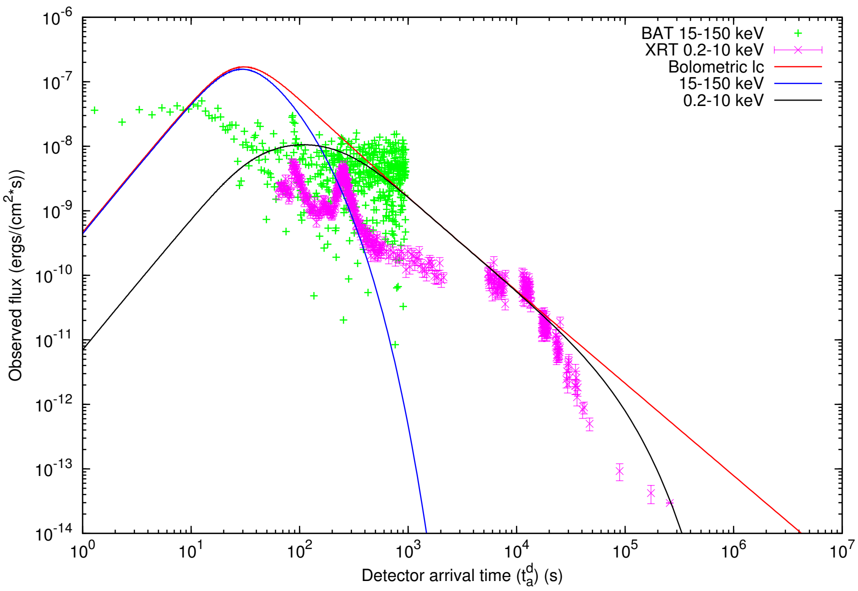

Figure H.4.1: *Swift* BAT (15–150 keV, green points) and XRT (0.3–10 keV, pink points) light curves compared with the theoretical light curves in the same energy bands (blue and black lines respectively) as well as the bolometric one (red line), obtained assuming that GRB 060607A is a "fake" short GRB. The discrepancy among them is evident.

ties of the fireball in the forward external shock regime. Nevertheless, the initial value of Lorentz gamma factor we predict is compatible with the one deduced from the REM observations even under very different assumptions.

H.4.1 GRB 060607A as a "fake" short GRB.

Since the BAT light curve behavior resembles the GRB 970228 one (see A.12), we attempt to fit GRB 060607A as a "fake" short GRB, or better as a long GRB disguised as short (Bernardini et al., 2007). We consider the first pulse as the P-GRB and the rest of the prompt emission as the peak of the afterglow. The temporal variability of the light curves has been reproduced assuming overdense spherical CBM regions (Ruffini et al., 2002a).

We therefore obtain for the two parameters of the fireshell $E_{e^\pm}^{tot} = 4.1 \times 10^{53}$ erg and $B = 3.0 \times 10^{-4}$ and for the CBM $\langle \mathcal{R} \rangle = 1.0 \times 10^{-9}$ and $\langle n_{cbm} \rangle = 4.0 \times 10^{-9}$ particles/cm^3. By comparing these values with the ones obtained for GRB 970228 (see A.12) we can recognize that the baryon loading in this case is too small to be a long GRB and, more important, the density of the CBM is completely unreliable. Hence we can conclude that, despite its appearance, GRB 060607A cannot be a long GRB disguised as short.

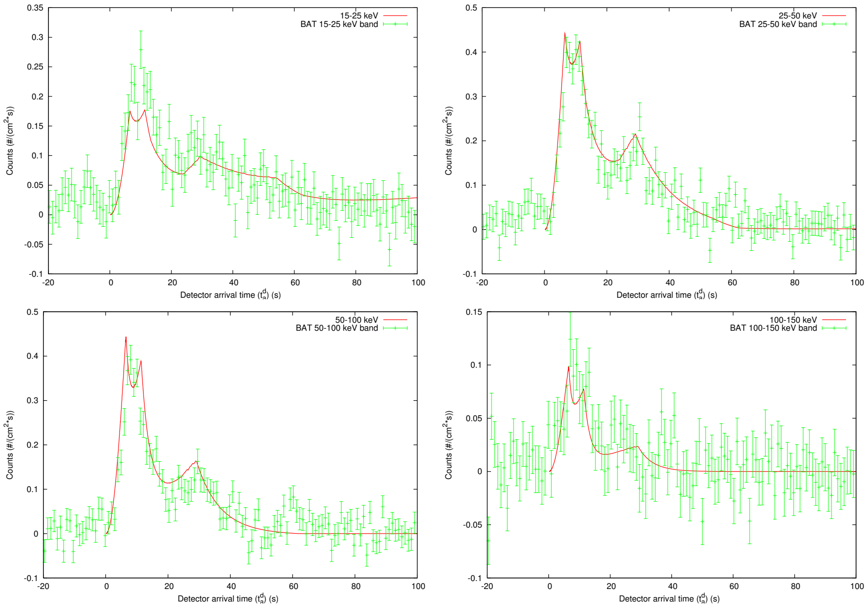

Figure H.4.2: *Swift* BAT (15–25 keV, 25–50 keV, 50–100 keV, 100–150 keV) light curves (green points) compared with the theoretical ones (red lines).

H.4.2 GRB 060607A prompt emission

H.4.2.1 Light curves

In Fig. H.4.2 we present the theoretical fit of *Swift* BAT light curves in different energy bands (15–25 keV, 25–50 keV, 50–100 keV, 100–150 keV) of GRB 060607A. We identify the whole prompt emission with the peak of the afterglow emission, and the remaining part of the light curve with the decaying tail of the afterglow, according to our "canonical GRB" scenario (Ruffini et al., 2001b, 2007a). The temporal variability of the light curves has been reproduced assuming overdense spherical CBM regions (Ruffini et al., 2002a). The detailed structure of the CBM adopted is presented in Fig. H.4.3.

We therefore obtain for the two parameters characterizing the source in our model $E_{e^\pm}^{tot} = 2.5 \times 10^{53}$ erg and $B = 3.0 \times 10^{-3}$. This implies an initial $e^\pm$ plasma with a total number of $e^\pm$ pairs $N_{e^\pm} = 2.6 \times 10^{58}$ and an initial temperature $T = 1.7$ MeV. The theoretically estimated total isotropic energy emitted in the P-GRB is $E_{P-GRB} = 1.9\% \, E_{e^\pm}^{tot} = 4.7 \times 10^{51}$ erg, hence the P-GRB results to be undetectable if we assume a duration $\Delta t_{p-grb} \gtrsim 10$ s.

After the transparency point at $r_0 = 1.4 \times 10^{14}$ cm from the progenitor, the initial Lorentz gamma factor of the fireshell is $\gamma_\circ = 328$. This value has been obtained adopting the exact solutions of the equations of motions of the fireshell (Bianco and Ruffini, 2005a) and using as initial conditions the two free parameters ($E_{e^\pm}^{tot}$ and B) estimated from the simultaneous analysis of the BAT and XRT light curves.

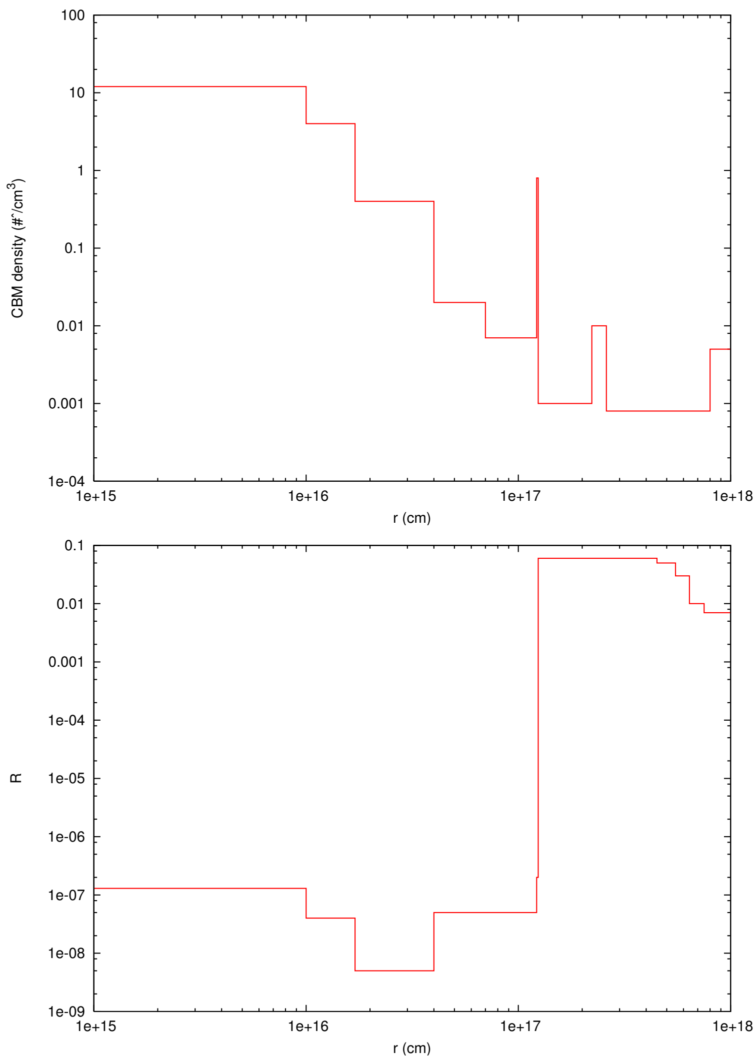

Figure H.4.3: Detailed structure of the CBM adopted: particle number density n_{cbm} (upper panel) and fraction effective emitting area $\mathcal{R}$ (lower panel) versus distance from the progenitor. The two X-ray flares corresponds in the upper panel to the huge increases in the CBM density that departs from the roughly power-law decrease observed. In the lower panel, the X-ray flares produce an increase of the emitting area which is not real but due to the lack of a complete 3-dimensional treatment of the interaction between the fireshell and the CBM (see text).

H.4.2.2 Time-integrated spectra

We turn now to the analysis of the GRB 060607A prompt emission time-integrated spectrum. As discussed in previous works (Ruffini et al., 2004b, 2005c; Bernardini et al., 2005a), even if the fireshell model assumes that the GRB spectrum is thermal in the comoving frame, the shape of the final spectrum in the laboratory frame is clearly non-thermal. In fact each single instantaneous spectrum is the result of a convolution of thermal spectra. In fact photons observed at the same arrival time are emitted at different comoving time (the so called EQTS Bianco and Ruffini, 2004, 2005b), hence with different temperatures. This calculation produces a non-thermal instantaneous spectrum in the observer frame. This effect is enhanced if we calculate the time-integrated spectrum: we perform two different integrations, one on the observation time and one on the EQTS, and what we get is a typical non-thermal power-law spectrum which results to be in good agreement with the observations (see Fig. H.4.4).

H.4.3 The X-ray flares.

We analyze now the X-ray flares observed by *Swift* XRT ($0.2 - 10$ keV) in the early part of the decaying phase of the afterglow. According to the fireshell model these flares have the same origin of the prompt emission, namely they are produced by the interaction of the fireshell with overdense CBM. As we can see in the upper panel in Fig. H.4.5, the result obtained is compatible with the observations only for the second flare but not for the first one since its duration is longer. This discrepancy is due to the simple modeling adopted, namely the CBM is arrangen in shperical shells (Ruffini et al., 2002a). This approximetion fails when the visible area of the fireshell is comparable with the size of the CBM clouds.

To solve this problem, following the results obtained for GRGB 011121 (see A.10), we tried to account for the three-dimensional structure of the CBM clouds by "cutting" the emission at a certain angle θ_{cloud} from the line of sight, corresponding to the transverse dimension of the CBM cloud, until the duration of the flare $\delta t / t_{tot}$ is compatible with the observation (see Fig. H.4.5 middle and lower panels). It is worth to observe that with this procedure we kee the value of R constant during the flare. Hence the increase in R that we obtained in our previous analysis (see Fig. H.4.3) is not real but it compensates the fact that spherical approximation is not valid at this stage.

This procedure affects the dynamics of the fireshell, so the light curve after the "cut" is meaningless. Nevertheless, it is a confirmation that it is possible to obtain arbitrarily short flares by the interaction with the CBM.

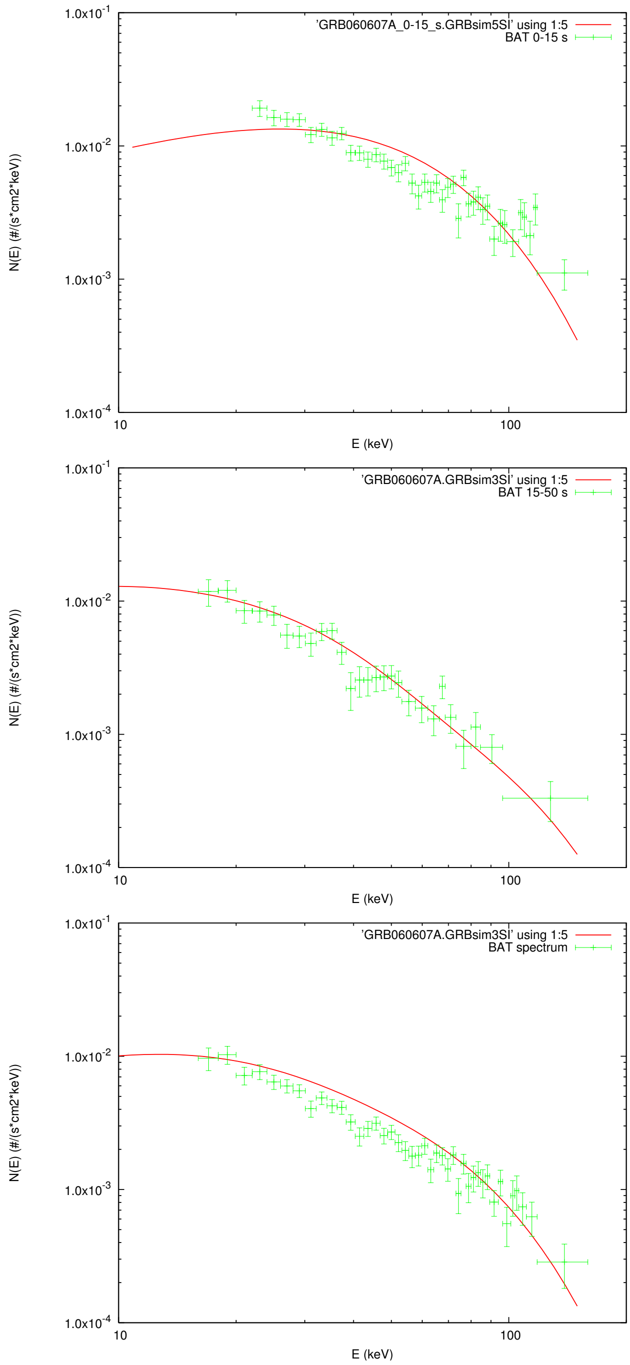

Figure H.4.4: Theoretically predicted time-integrated photon number spectrum $N(E)$ corresponding to the $0 - 15$ s (upper panel), $15 - 50$ s (middle panel), and to the whole duration ($T_{90} = 100$ s, lower panel) of the prompt emission (solid lines) compared with the observed spectra integrated in the same intervals.

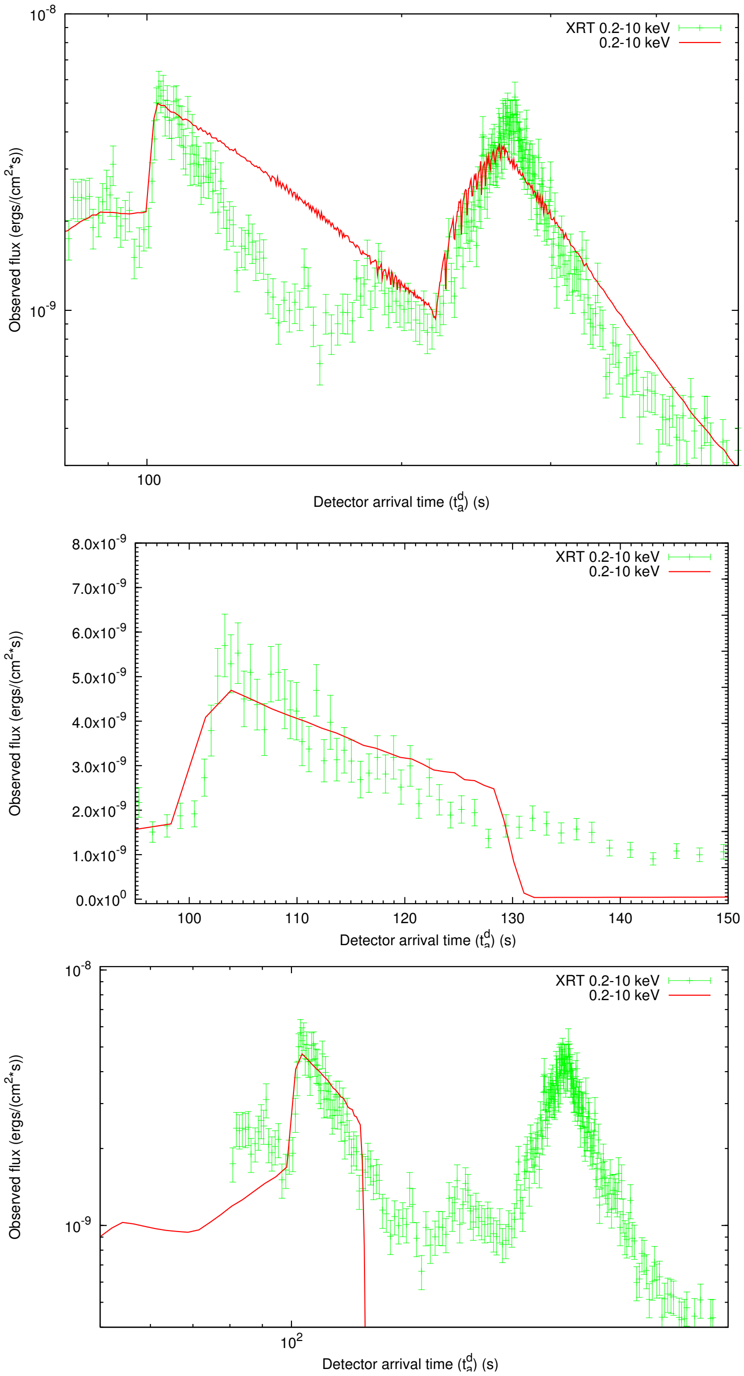

Figure H.4.5: *Swift* XRT (0.2–10 keV) light curve (green points) compared with, respectively, the theoretical one obtained assuming the CBM distributed in spherical shells (upper panel), the theoretical one obtained imposing a finite transverse dimension for the CBM cloud (middle panel) and the same theoretical curve il logarithmic scale (lower panel).

H.4.4 Conclusions

We presented the analysis of GRB 060607A within the fireshell model (Ruffini et al., 2001c,b, 2007a). We verified that, despite its appearance, GRB 060607A cannot be a long GRB disgiused as short as, for example, GRB 970228 (see A.12) with realistic values of the CBM parameters. Hence, according to the "canonical GRB" scenario (Ruffini et al., 2001b, 2007a) we interpreted the whole prompt emission as the peak of the afterglow emission, and the remaining part of the light curve with the decaying tail of the afterglow. We found in this second case that the P-GRB is too faint to be detected, as we expected from our interpretation. The theoretical light curves obtained are well in agreement with the observations in all the *Swift* BAT energy bands.

Furthermore, the initial Lorentz gamma factor of the fireshell, obtained adopting the exact solutions of its equations of motions (Bianco and Ruffini, 2005a) and as initial condition the free parameters of the fireshell estimated by the simultaneous analysis of the BAT and XRT light curves, is $\gamma_\circ = 328$. In this preliminary analysis we deal only with the BAT and XRT observations, which are the basic contribution to the afterglow emission according to the fireshell model. We do not deal with the infrared emission that, on the contrary, is used in the current literature to estimate the dynamical quantities of the fireball in the forward external shock regime. Nevertheless, the initial value of Lorentz gamma factor we predict is compatible with the one deduced from the REM observations even under very different assumptions, $\Gamma_\circ \sim 400$ (Molinari et al., 2007; Covino et al., 2007; Jin and Fan, 2007).

We investigated also the GRB 060607A prompt emission spectra integrated in different time intervals assuming a thermal spectrum in the comoving frame. The results obtained show clearly that, after the correct space-time transformations, both the instantaneous and the time-integrated spectra in the observer frame have nothing to do with a Planckian distribution, but they have a power-law shape, thus confirming our previous analyses (Bernardini et al., 2005a; Ruffini et al., 2006b).

Finally we analyzed the X-ray flares observed by *Swift* XRT ($0.2 - 10$ keV) in the early part of the decaying phase of the afterglow. According to the fireshell model these flares have the same origin of the prompt emission, namely they are produced by the interaction of the fireshell with overdense CBM. We found that our theoretical light curve is not compatible with the observations since in such regime the one-dimensional approximation fails. Following the results obtained for GRGB 011121 (see A.10), we tried to account for the three-dimensional structure of the CBM clouds by "cutting" the emission at a certain angle θ_{cloud} from the line of sight, corresponding to the transverse dimension of the CBM cloud. We obtain in this way a flare whose duration $\delta t / t_{tot}$ is compatible with the observation.

H.5 Theoretical background for GRBs' empirical correlations

The detection of gamma-ray bursts (GRBs) up to very high redshifts (up to $z = 6.7$, see Greiner et al., 2008), their high observed rate of one every few days, and the progress in the theoretical understanding of these sources all make them useful as cosmological tools, complementary to supernovae Ia, which are observed only up to $z = 1.7$ (Leibundgut, 2001; Riess et al., 2001). One of the hottest topics on GRBs is the possible existence of empirical relations between GRB observables (Amati et al., 2002; Ghirlanda et al., 2004; Yonetoku et al., 2004; Liang and Zhang, 2005; Firmani et al., 2006; Amati et al., 2008), which may lead, if confirmed, to using GRBs as tracers of models of universe. The first empirical relation, discovered when analyzing the *BeppoSAX* so-called "long" bursts with known redshift, was the "Amati relation" (Amati et al., 2002). It was found that the isotropic-equivalent radiated energy of the prompt emission E_{iso} is correlated with the cosmological rest-frame νF_ν spectrum peak energy $E_{p,i}$: $E_{p,i} \propto (E_{iso})^a$, with $a = 0.52 \pm 0.06$ (Amati et al., 2002). The existence of the Amati relation has been confirmed by studying a sample of GRBs discovered by Swift, with $a = 0.49^{+0.06}_{-0.05}$ (Sakamoto et al., 2006b; Amati, 2006).

Swift has for the first time made it possible to obtain high quality data in selected energy bands from the GRB trigger time all the way to the latest afterglow phases (Gehrels et al., 2004). This has given us the opportunity to apply our theoretical "fireshell" model, thereby obtaining detailed values for its two free parameters, namely for the total energy $E_{tot}^{e^\pm}$ and the baryon loading B of the fireshell, as well as for the effective density and filamentary structure of the CircumBurst Medium (CBM). From this we were able to compute multi-band light curves and spectra, both instantaneous and time-integrated, compared with selected GRB sources, such as GRB 050315.

In the "fireshell" model, $E_{tot}^{e^\pm}$ comprises two different components: (i) the proper GRB (P-GRB) with energy E_{P-GRB}, emitted at the moment when the e^+e^--driven accelerating baryonic matter reaches transparency, and (ii) the following afterglow phase with energy E_{aft}, with the decelerating baryons interacting with the CBM (Ruffini et al., 2001b). These two phases are clearly distinguishable by their relative intensity and temporal separation in arrival time. We have

$$E_{tot}^{e^\pm} = E_{P-GRB} + E_{aft}\,. \tag{H.5.0.1}$$

What is usually called the "prompt emission" corresponds within the fireshell model to the P-GRB together with the peak of the afterglow (see below, e.g. Ruffini et al., 2001b, 2006b, 2007a; Dainotti et al., 2007; Bernardini et al., 2007; Caito et al., 2008; Bianco et al., 2008a, and references therein).

Among the crucial issues raised by the Amati relation, there are its theoretical explanation and its possible dependence on the assumed cosmological model. We examined a set of "gedanken" GRBs, all at the same cosmological redshift of GRB 050315. Such a set assumes the same fireshell baryon loading and effective CBM distribution as GRB 050315 (Ruffini et al., 2006b, see also section A.9) and each "gedanken" GRB differs from the others uniquely by the value of its total energy $E_{tot}^{e^\pm}$. We then considered a second set of "gedanken" GRBs, differing from the previous one by assuming a constant effective CBM density instead of the one inferred for GRB 050315. In both these sets, we looked for a relation between the isotropic-equivalent radiated energy of the *entire* afterglow E_{aft} and the corresponding time-integrated νF_ν spectrum peak energy E_p:

$$E_p \propto (E_{aft})^a \,. \tag{H.5.0.2}$$

In this chapter, after briefly recalling the various spectral-energy correlations mentioned above, we present the derivation of the $E_p - E_{aft}$ relation for the two sets of "gedanken" GRBs.

H.5.1 Spectral-energy correlations

Many empirical spectral-energy correlations exist, some are purely phenomenological and assumption free while others are based on assumptions and are dependent on model, basically the standard fireball model (Piran, 1999). Some correlations assume spherical symmetry while others assume collimated (jet) emission. This last case was triggered by the observation by Frail et al. (2001) that the collimation corrected energetics of those GRBs of know jet aperture angles clustered into a narrow distribution, $E_\gamma = (1 - \cos\theta_j)E_{iso} \sim 10^{51}$ erg. The opening angle of the jet is estimated within the standard model as

$$\begin{aligned} \theta_{\rm j} &= 0.161 \left(\frac{t_{\rm jet,d}}{1+z}\right)^{3/8} \left(\frac{n\,\eta_\gamma}{E_{\rm iso,52}}\right)^{1/8}; \quad \mathrm{H} \\ \theta_{\rm j} &= 0.2016 \left(\frac{t_{\rm jet,d}}{1+z}\right)^{1/4} \left(\frac{\eta_\gamma\, A_*}{E_{\rm iso,52}}\right)^{1/4}; \quad \mathrm{W} \end{aligned} \tag{H.5.1.1}$$

where $t_{\rm jet,d}$ is the break time measured in days and z is the redshift. The efficiency η_γ relates the isotropic kinetic energy of the fireball $E_{\rm k,iso}$ to the prompt emitted energy $E_{\rm iso}$: $E_{\rm k,iso} = E_{\rm iso}/\eta_\gamma$. Usually, it is assumed a constant value for all bursts, i.e. $\eta_\gamma = 0.2$ (after its first use by Frail et al. (2001), following the estimate of this parameter in GRB 970508 Frail et al. (2000)). In the homogeneous (H) case, n is the CircumBurst density, independent from the radial coordinate; for the wind (W) case, the density is a function of the radial coordinate, $n(r) = A\, r^{-2}$ and A_* is the value of A ($A = \dot{M}_w/(4\pi v_w) = 5 \times 10^{11}\, A_*$ g cm^{-1}) when setting the wind mass loss rate to $\dot{M}_w = 10^{-5} M_\odot yr^{-1}$ and the wind velocity to $v_w = 10^3$ km s^{-1}. Usually, a constant value (i.e. $A_* = 1$) is adopted for all bursts.

The most important spectral-energy correlations are:

- **The Amati relation:** It was historically the first correlation discovered, considering *BeppoSAX* bursts (Amati et al., 2002). It was found that the isotropic-equivalent radiated energy of the prompt emission E_{iso} is correlated with the cosmological rest-frame νF_ν spectrum peak energy $E_{p,i}$: $E_{p,i} \propto E_{iso}^{0.5}$. This correlation, recently updated (Amati, 2006) to a larger sample, holds for all but two long bursts, while no short burst satisfies it. The long burst outliers are GRB 980425 and the debated GRB 031203 (Watson et al., 2006b). As far as short bursts are concerned, there are two cases: the burst with an initial spike-like emission followed by a soft bump (short burst with afterglow) and the short burst with no afterglow. The burst belonging to the first class are what we named (Bernardini et al., 2007) "fake" short GRBs, while the ones belonging to the second case are the "genuine" short GRBs. Both classes, as already said above, does not follow the Amati relation, but, if one excludes the initial spike-like emission and considers only the soft later part of the bursts in the first class, then the Amati relation is recovered (Amati, 2007; Bernardini et al., 2008).

- **The Yonetoku correlation:** Yonetoku et al. (2004) showed that also the peak luminosity $L_{p,iso}$ of the prompt emission correlates with E_p, in the same way as E_{iso}: $E_p \propto L_{p,iso}^{1/2}$. The scatter is similar to the scatter of the Amati correlation, and the outliers are the same as well.

- **The Ghirlanda correlation:** Assuming a collimated emission, Ghirlanda et al. (2004) found that the collimation corrected (by a factor $(1 - \cos\theta_j)$) energy, E_γ, is tightly correlated with E_p. The correlation is $E_{p,i} \propto E_\gamma^{0.7}$. As outlined above, this relation is based on a theoretical model needed to calculate θ_j, that in turns relies on the assumptions adopted for the efficiency and the CircumBurst density and profile.

- **The Liang & Zhang correlation:** To find the jet angle θ_j, as explained above, one needs a model and some assumptions; the Liang and Zhang (2005) correlation instead is entirely phenomenological, so model independent and assumptions free. It involves three observables (plus the redshift) and it is of the form $E_{iso} \propto E_p^2 t_{jet}^{-1}$. It is consistent (Nava et al., 2006) with the Ghirlanda correlation, and has similar spread.

- **The Firmani correlation:** The Firmani et al. (2006) correlation links three quantities of the prompt emission: the bolometric isotropic peak luminosity $L_{\rm p}$, the peak energy $E_{\rm p,iso}$ of the time integrated spectrum, and a characteristic time: $T_{0.45}$, which is the time interval spanned by the brightest 45% of the total light curve counts above the background. This time is used to characterize the variability properties of the prompt emission (Reichart et al., 2001). The correlation is of the form: $L_{\rm p,iso} \propto E_{\rm p}^{3/2} T_{0.45}^{-1/2}$. Also this relation is model independent and assumption free.

H.5.2 The $E_p - E_{aft}$ relation

In our approach, only the *entire* afterglow emission is considered in establishing our $E_p - E_{aft}$ relation. From this assumption one derives, in a natural way, that the Amati relation holds only for long GRBs, where the P-GRB is negligible, and not for short GRBs (Amati et al., 2007).

We can compute the "instantaneous" spectrum of GRB 050315 at each value of the detector arrival time during the entire afterglow emission. Such a spectrum sharply evolves in the arrival time, presenting a typical hard-to-soft behavior (Ruffini et al., 2006b). We then computed the νF_ν time-integrated spectrum over the total duration of our afterglow phase, that is, from the end of the P-GRB up to when the fireshell reaches a Lorentz gamma factor close to unity. We can then define the energy E_p as the energy of the peak of this νF_ν time-integrated spectrum, and we look at its relation with the total energy E_{aft} of the afterglow.

We construct two sets of "gedanken" GRBs at a fixed cosmological redshift, therefore independently of the cosmological model. The first set assumes the same fireshell baryon loading and effective CBM distribution as GRB 050315 (see Fig. H.5.1) and each "gedanken" GRB differs from the others uniquely by the value of its total energy $E_{tot}^{e^\pm}$. The second set assumes a constant effective CBM density ~ 1 particle/cm^3 instead of the one inferred for GRB 050315.

In our model, E_{aft} is a fixed value determined by $E_{tot}^{e^\pm}$ and B, so clearly there are no errors associated to it. Instead, E_p is evaluated from the numerically calculated spectrum, and its determination is therefore affected by the numerical resolution. Choosing a 5% error on E_p, which is consistent with our numerical resolution, we checked that this value is reasonable looking at each spectrum. Figure H.5.2 shows the time-integrated spectrum corresponding to $E_{tot}^{e^\pm} = 3.40 \times 10^{51}$ erg with the error around E_p.

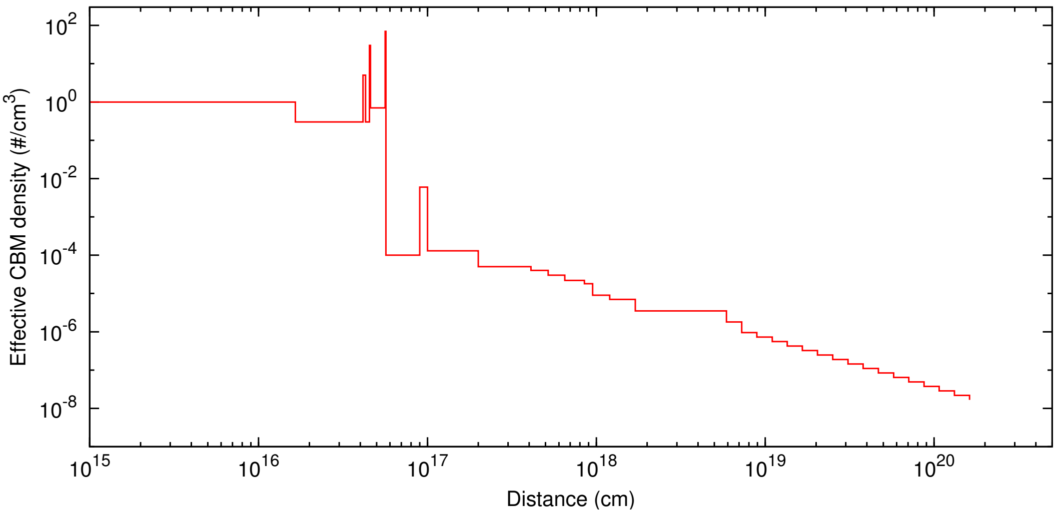

Figure H.5.1: The effective CBM number density inferred from the theoretical analysis of GRB 050315. Details in Ruffini et al. (2006b) and in section A.9.

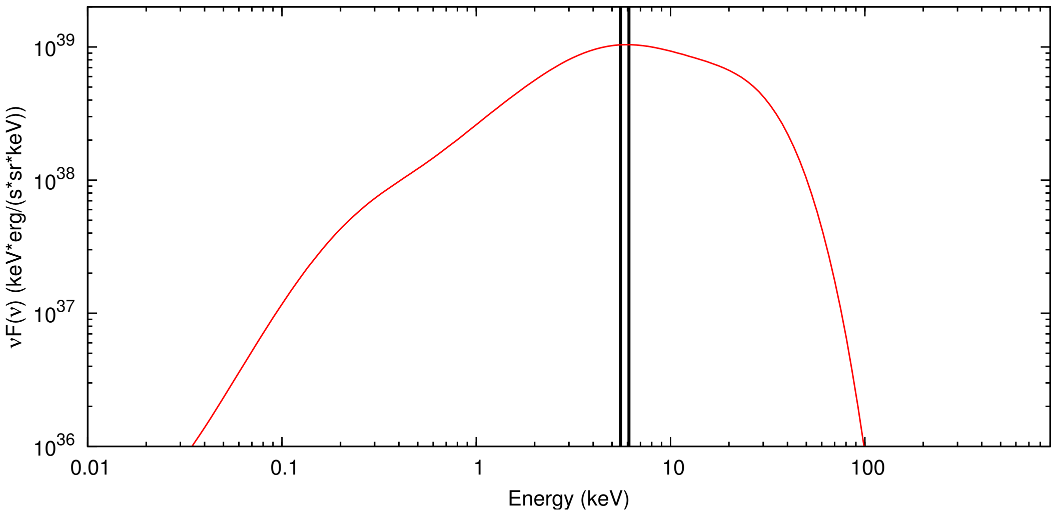

Figure H.5.2: The νF_ν time-integrated spectrum over the total duration of our afterglow phase for the "gedanken" GRB of the first set with total energy $E_{tot}^{e^\pm} = 3.40 \times 10^{51}$. The two vertical lines constrain the 5% error region around the peak. We determine $E_p = 5.82$ keV $\pm 5\%$.

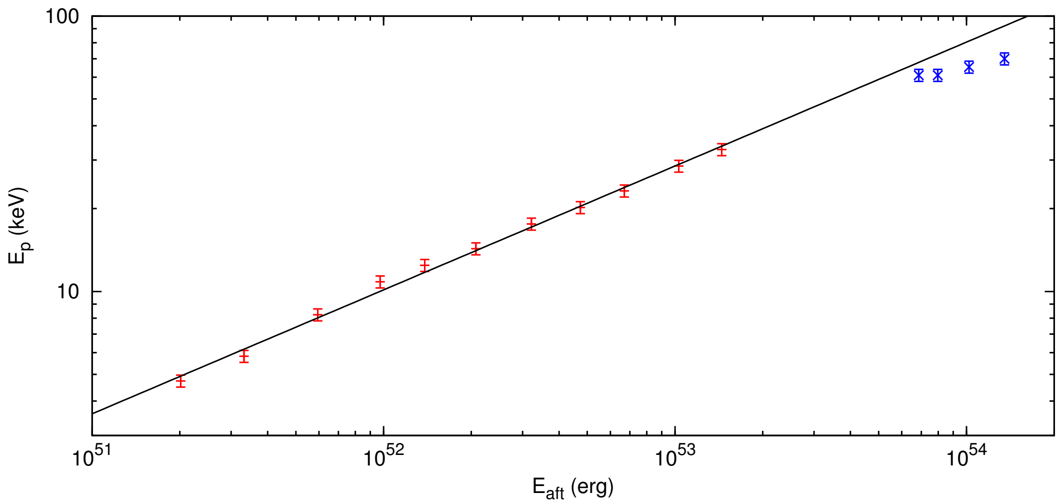

Figure H.5.3: The $E_p - E_{aft}$ relation: the results of the simulations of the first set of "gedanken" GRBs (red points) are well-fitted by a power law (black line) $E_p \propto (E_{aft})^a$ with $a = 0.45 \pm 0.01$. The blue points are the results of the extension of the first set above 10^{53} erg.

H.5.3 Results and discussion

Figure H.5.3 shows the $E_p - E_{aft}$ relation of the "gedanken" GRBs belonging to the first set (red points). It extends over two orders of magnitude in energy, from 10^{51} to 10^{53} erg, and is well-fitted by a power law $E_p \propto (E_{aft})^a$ with $a = 0.45 \pm 0.01$. We emphasize that such a power-law slope strictly agrees with the Amati relation, namely $E_{p,i} \propto (E_{iso})^a$, with $a = 0.49^{+0.06}_{-0.05}$ (Amati, 2006). We recall that E_p is the observed peak energy; i.e., it is not rescaled for the cosmological redshift, because all the "gedanken" GRBs of the set are at the same redshift of GRB 050315, namely $z = 1.949$ (Vaughan et al., 2006). The normalization is clearly different from the Amati one.

If we try to extend the first sample of "gedanken" GRBs below 10^{51} erg, the relevant CBM distribution would be for $r \lesssim 10^{16}$ cm, where no data are available from the GRB 050315 observations. If we try to extend the first set of "gedanken" GRBs above 10^{53} erg, we notice that for $E_{tot}^{e^\pm} \gtrsim 10^{54}$ erg the small "bump", which can be noticed between 0.2 and 1.0 keV in the spectrum of Fig. H.5.2, evolves into a low-energy second spectral peak that is even higher than the high-energy one (see Fig. H.5.4). We are currently investigating whether this low-energy second peak is a real, theoretically predicted spectral feature that may be observed in the future in highly energetic sources. There is also the other possibility that the low-energy and late part of our GRB 050315 fit is not enough constrained by the XRT observational data so that this effect is magnified by the $E_{tot}^{e^\pm}$ rescaling.

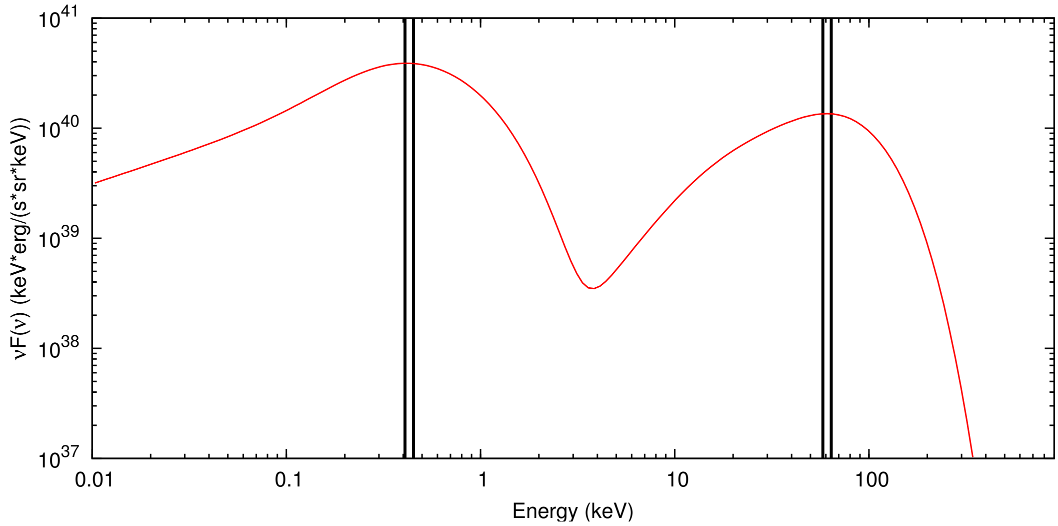

Figure H.5.4: The νF_ν time-integrated spectrum over the total duration of our afterglow phase for the "gedanken" GRB of the extended first set with total energy $E^{e^\pm}_{tot} = 6.95 \times 10^{53}$ erg. The vertical lines constrain the 5% error region around each peak.

The high-energy spectral peak is due to the emission at the peak of the afterglow, and therefore due to the so-called "prompt emission". The low-energy one is due to late-time soft X-ray emission. Therefore, the high-energy spectral peak is the relevant one for the Amati relation. We find indeed that such a high-energy spectral peak still fulfills the $E_p - E_{aft}$ relation for $E^{e^\pm}_{tot} \sim 10^{54}$ erg, with a possible saturation for $E^{e^\pm}_{tot} > 10^{54}$ erg (see Fig. H.5.3).

Figure H.5.5 clearly shows that in the second set of "gedanken" GRBs, built assuming a constant effective CBM density ~ 1 particle/cm^3, instead of the one specifically inferred for GRB 050315, there in no relation between E_p and E_{aft}.

H.5.4 Conclusions

The high-quality Swift data, for the first time giving gapless and multiwavelength coverage from the GRB trigger all the way to the latest afterglow phases, have led to a complete fit of the GRB 050315 multiband light curves based on our fireshell model. We fixed the free parameters describing the source and determined the instantaneous and time-integrated spectra during the entire afterglow.

Starting from this, we examined two sets of "gedanken" GRBs, constructed at a fixed cosmological redshift. The first set assumes the same fireshell baryon loading and effective CBM distribution as GRB 050315, and each "gedanken"

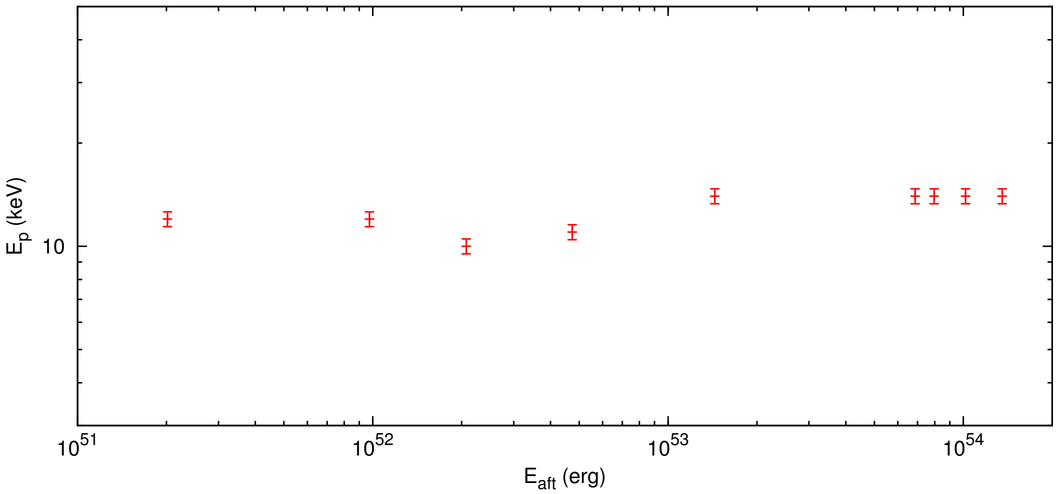

Figure H.5.5: The second set of "gedanken" GRBs. Clearly, in this case there in no relation between E_p and E_{aft}.

GRB differs from the others uniquely by the value of its total energy $E^{e^\pm}_{tot}$. The second set assumes a constant effective CBM density $\sim$ 1 particle/cm^3 instead of the one inferred for GRB 050315.

Recalling that the "canonical" GRB light curve in the fireshell model is composed of two well-separated components, the P-GRB, and the entire afterglow, we looked for a relation in both sets between the isotropic-equivalent radiated energy of the *entire* afterglow E_{aft} and the corresponding time-integrated νF_ν spectrum peak energy E_p: $E_p \propto (E_{aft})^a$. In doing so, we assumed that the Amati relation is directly linked to the interaction between the accelerated baryons and the CBM. The P-GRBs, which originate from the fireshell transparency, do not fulfill the Amati relation in our approach. Consequently, the short GRBs, which have a vanishing afterglow with respect to the P-GRB, should also not fulfill the Amati relation. This last point is supported by the observational evidence (Amati, 2006).

We notice that the first set of "gedanken" GRBs fulfills the $E_p \propto (E_{aft})^a$ relation very well with $a = 0.45 \pm 0.01$. This slope strongly agrees with the Amati relation. In contrast, no relation between E_p and E_{aft} seems to hold for the second set. We conclude that the Amati relation originates from the detailed structure of the effective CBM.

Turning now to the analogies and differences between our $E_p - E_{aft}$ relation and the Amati one, our analysis excludes the P-GRB from the prompt emission, extends all the way to the latest afterglow phases, and is independent of the assumed cosmological model, since all "gedanken" GRBs are at the same redshift. The Amati relation, on the other hand, includes the P-GRB, focuses only on the prompt emission, being therefore influenced by the instrumental threshold that fixes the end of the prompt emission, and depends on the assumed cosmology. This might explain the intrinsic scatter observed in the Amati relation (Amati, 2006). Our theoretical work is a first unavoidable step toward supporting the use of the empirical Amati relation for measuring the cosmological parameters.

H.6 Fermi's approach to the study of hadronic interactions

The knowledge of the radiation mechanisms is crucial for the correct understanding of many astronomical observations. In particular in gamma ray astronomy the observational data can be often explained by two or more production mechanisms. It is therefore important to model correctly the different interactions producing gamma rays. Among all mechanisms producing gamma rays hadronic interactions between nucleons which produce pions, which in turn decay into photons and neutrinos, are the most difficult to model. In fact, high energy collisions of nucleons cannot be treated perturbatively because of the large value of the interaction constant in nuclear interactions. Many authors have occupied themselves with this problem and already in 1950 Fermi developed a statistical method for computing the multiple production of particles in collisions of high energetic protons. In the meantime a very large set of data has been acquired from high energy accelerators. The aim of the paper is 1. to reduce the Fermi theoretical equations, 2. to compare them to the experimental data and 3. to outline novel theoretical approach.

H.6.1 Fermi's approach to the study of hadronic interactions

In treating high energy collisions of nucleons, Fermi made the assumption that the possible final configurations of the system are determined by the statistical weights of the various possible final configurations and accordingly developed a statistical method to determine the final particles produced (Fermi, 1950). First of all one might think of many different final configurations for the system after the collision, but conservation laws of charge and of momentum, as well as the feasibly of the processes, have to be taken into account. Transitions in Yukawa's theory, in which charged and neutral pions are emitted, are therefore the most probable processes taking place. So during the collisions of high energetic hadrons a large amount of energy is released in a small volume around the hadrons and used to form pions. In view of the strong interactions between these pions, one can imagine that the energy available in the small volume will be rapidly distributed to the different pions having different energies. In other words the energy will be statistically distributed among all degrees of freedom of the system. Fermi himself said: "When two nucleons collide with very great energy in their center of mass system this energy will be suddenly released in a small volume surrounding the two nucleons. The event is a collision in which the nucleons with their surrounding retinue of pions hit against each other so that all the portion of space occupied by the nucleons and by their surrounding pion field will be suddenly loaded with a very great amount of energy. Since the interactions of the pion field are strong we may expect that rapidly this energy will be distributed among the various degrees of freedom present in this volume according to statistical laws. One can then compute statistically the probability that in this tiny volume a certain number of pions will be created with a given energy distribution. It is then assumed that the concentration of energy will rapidly dissolve and that the particles into which the energy has been converted will fly out in all directions."

Fermi's method resembles somehow Heisenberg's approach (Heisenberg, 1949) to treat high energy collisions of nucleons, with the difference that Heisenberg used qualitative ideas of turbulence whereas, Fermi believed that in high energetic processes statistical equilibrium is reached.

According to Fermi the process proceeds as follows: in the laboratory frame a very energetic proton scatters off a proton target. For convenience the process is examined in the center of mass of the system. The only parameter which has to be tuned in Fermi's theory is the volume in which the energy is dumped. The value of this parameter can be modified to improve the agreement with the experiments. Fermi defined Ω being the volume at rest in the laboratory frame that contain the energy of the colliding particles, but we will call this volume by Ω Fermi volume. Since the particles mediating the Yukawa interactions are the pions, the volume is taken as a sphere with radius of order of the pion Compton wavelength $\lambda_\pi^c = \hbar/m_\pi c$ ($\Delta x \Delta p \geq \hbar/2 \Rightarrow \Delta x = \hbar/\Delta p \Rightarrow \lambda_\pi^c = \hbar/m_\pi c$).

We will use the index "0" for indicate that it is in the c.m. frame, and when do not the index, mean it is in the laboratory frame. Analogous, we use the index $'$ for indicate after the collision, and without the index say before of the collision.

We always will work in c.m. frame, where we define the volume Ω_0 containing the energy of the colliding particles in c.m. frame. The relation between the Fermi volume in the L.F. (Ω) and in the c.m. frame (Ω_0) is given by Lorentz contracted,

$$\Omega_0 = \frac{1}{\gamma}\Omega, \tag{H.6.1.1}$$

where

$$\Omega = \frac{4}{3}\pi R^3, \tag{H.6.1.2}$$

and

$$R = a\lambda_\pi^c \qquad \text{and} \qquad \breve{\ }^{\mathrm{c}}_{\text{ß}} = \frac{\hbar}{\mathrm{m}_{\text{ß}}\mathrm{c}} = 1.4 \times 10^{-13}\,\mathrm{cm}, \tag{H.6.1.3}$$

where λ_π^c is the Compton wavelength of the pion $\lambda_\pi^c = h/m_\pi c$, $\hbar$ the Planck constant, c the light speed, $\gamma = (1 - v^2/c^2)^{-1/2}$ is the Lorentz factor and $\vec{v}$ the velocity of proton in rest in c.m. frame and a a parameter that to fit the radius of the Fermi volume. Fermi didn't use the parameter a, but he said that the volume Ω could be parameterizable, then we will use the parameter a because we don't know exactly the radius of the Fermi volume.

Fermi obtained the Lorentz factor of Eq. (H.6.1.1) as $\gamma = \sqrt{s}/2m_pc^2$, where $\sqrt{s}$ is the total energy of the system in the c.m. frame (or only c.m. energy), Fermi in his work indicated by "W" the c.m. energy, but we will use $\sqrt{s}$ because it is the standard notation. We here derive his formula for the Lorentz factor.

Conform the Lorentz invariance, the square of 4-momentum of the system obtain the square of the c.m. energy, frame invariance, then

$$s = 2m_pc^2(E_p + m_pc^2) = (2E_{0p})^2, \tag{H.6.1.4}$$

where E_{0p} is the energy of each proton (the same energy) no c.m. frame. Note that E_{0p} can be wrote as

$$E_{0p} = \gamma m_pc^2, \tag{H.6.1.5}$$

where γ is the same Lorentz factor from Eq. (H.6.1.1).

Substituting Eq. (H.6.1.5) in Eq. (H.6.1.4), we obtain the Lorentz factor that fermi obtained,

$$\gamma = \frac{\sqrt{s}}{2m_pc^2}. \tag{H.6.1.6}$$

Note that the velocity $\vec{v}$ of the proton 'at rest' in c.m. frame is the same as the velocity of the c.m. in the laboratory frame. According to Landau and Lifshitz (1975), in this case the velocity of the c.m. is $\vec{v} = \vec{p}_{tot}c^2/E_{tot} = \vec{p}_1c^2/(E_p + m_pc^2)$. It is possible to get Eq. (H.6.1.6) using Eq. (H.6.1.4) and this definition of velocity of c.m. Landau and Lifshitz (1975).

Substituting Eq. (H.6.1.6) in Eq. (H.6.1.1), we get the expression of Fermi for the Lorentz contraction of the volume Ω

$$\Omega_0 = \frac{2m_pc^2}{\sqrt{s}}\Omega. \tag{H.6.1.7}$$

Note that if the c.m. energy $\sqrt{s}$ increase, the volume Ω_0 decreases, as is predicted in special relativity. The parameter volume will be therefore energy dependent. Fermi calculated also the cross-section as the area available for collisions around the pion cloud

$$\sigma_{tot} = \pi R^2. \tag{H.6.1.8}$$

Substituting λ_π^c of Eq. (H.6.1.3) in Eq. (H.6.1.8), we get $\sigma_{tot} = 6 \times 10^{-26}\,\text{cm}^2$, where $\hbar = 1.054 \times 10^{-27}$ erg.s and $c = 2.9979 \times 10^{10}$ cm/s a value close to the modern experimental value.

The probability to find n particles in a volume Ω inside of the possible physical volume V of the 'container' is

$$P_n = \left(\frac{\Omega}{V}\right)^n, \tag{H.6.1.9}$$

where n is also the degrees of freedom number.

If $\sqrt{s}$ is the total energy of the system, the density of states of energies possible is

$$G(\sqrt{s}) = \frac{d\mathcal{N}(\sqrt{s})}{d\sqrt{s}}, \tag{H.6.1.10}$$

where $d\mathcal{N}(\sqrt{s})$ is the number of states in the phase space lying between the energies $\sqrt{s}$ and $\sqrt{s} + d\sqrt{s}$. It is knowledge that in the case of a particle, the number of states in a phase space with energy $\sqrt{s}$ is gave by $\mathcal{N}_1(\sqrt{s}) = d^3\vec{r}_1 d^3\vec{p}_1/h^3$. But for '$n$' particles we have (Reif, 1965)

$$\mathcal{N}_n(\sqrt{s}) \propto \int_{\sqrt{s}}^{\sqrt{s}+\delta\sqrt{s}} \frac{d^3\vec{r}_1 ... d^3\vec{r}_n d^3\vec{p}_1 ... d^3\vec{p}_n}{(h^3)^n}. \tag{H.6.1.11}$$

where the numerator is the volume of the phase space of particles, and the denominator '$(h^3)^n$' is the element of volume in phase space (according uncertainty principle of Heisenberg). Note that $\mathcal{N}$ is dimensionless. Since each integral over $\vec{r}_i$ extends over the volume V of the container, $\int d^3\vec{r}_i = V$, but there are n such integrals. Then Eq. (H.6.1.11) becomes,

$$\mathcal{N}_n(\sqrt{s}) = \left(\frac{V}{8\pi^3\hbar^3}\right)^n Q_n(\sqrt{s}), \tag{H.6.1.12}$$

where $Q_n(\sqrt{s}) \propto \int_{\sqrt{s}}^{\sqrt{s}+\delta\sqrt{s}} d^3\vec{p}_1 ... d^3\vec{p}_n$, independent of V, is the sum over all possible state in the momentum space. This case describes n completely independent particles.

Substituting Eq. (H.6.1.12) in Eq. (H.6.1.10),

$$G_n(\sqrt{s}) = \left(\frac{V}{8\pi^3\hbar^3}\right)^n \frac{dQ_n(\sqrt{s})}{d\sqrt{s}}. \tag{H.6.1.13}$$

The probability to form this state $S_n(\sqrt{s})$ (it is knowledge how statistical weights) is given via product of the probability P_n (Eq. H.6.1.9) with the density of states $G_n(\sqrt{s})$ (H.6.1.13).

$$S_n(\sqrt{s}) = P_n G_n(\sqrt{s}),$$
$$S(n) = \left(\frac{\Omega}{8\pi^3\hbar^3}\right)^n \frac{dQ_n(\sqrt{s})}{d\sqrt{s}} \tag{H.6.1.14}$$

For the case of two particles ($n = 1$), which produce no pion, we have that the volume of momentum space is $Q = \frac{4}{3}\pi p^3$. In the classical case we have $T' = p^2/2\mu$ (kinetic energy), where μ is the reduced mass of the two protons, $\mu = m_p m_p/(m_p + m_p) = m_p/2$, then $p = \sqrt{m_p T'}$.

The number of constraints is 1, due to the fact that the impulse in the c.m. is zero. The classical case, Eq. (H.6.1.14), is rewrite,

$$S_{n=1} = \frac{\Omega m_p^{3/2}}{4\pi^2\hbar^3}\sqrt{T'} \tag{H.6.1.15}$$

where $T' = \sqrt{s} - 2m_p c^2$. In the case of extremely high energy $p = \frac{1}{c}\sqrt{s - m_p^2 c^4} \simeq \sqrt{s}/c$ (because $\sqrt{s} \gg m_p c^2$), then $Q = \frac{4}{3}\pi(\sqrt{s}/c)^3$, and

$$S_{n=1} = \frac{\Omega}{2\pi^2\hbar^3 c^3} s. \tag{H.6.1.16}$$

To account for $n + 1$ particles, the statistical weights of the classical and relativistic cases, respectively, are

$$S_n = \frac{(m_1 m_2 ... \mathrm{m_n})^{3/2} \blacksquare^{\mathrm{n}}}{2^{3n/2}\pi^{3n/2}\hbar^{3n}} \frac{T'^{3n/2-1}}{(3n/2-1)!}, \tag{H.6.1.17}$$
$$S_n = \frac{\Omega^n}{\pi^{2n}\hbar^{3n}c^{3n}} \frac{\sqrt{s}^{3n-1}}{(3n-1)!}. \tag{H.6.1.18}$$

It can be verified that considering $n = 1$ in Eq. (H.6.1.17) and (H.6.1.18) we get, respectively, the Eqs. (H.6.1.15) and (H.6.1.16), where $(1/2)! = \sqrt{2}/2$ (property of Gamma Function). The factors $\pi^{3n/2}(3n/2-1)!$ and $\pi^{2n}(3n-1)!$ are from the dimension of the sphere, it is analog of the factor $4\pi/3$ in the volume of an ordinary sphere. In treating the collisions of extremely high energy nucleons Fermi make use of thermodynamic laws, instead of considering a detailed statistical treatment. The energy density around the colliding nucleons is so high that multiple pions will be produced.

From Planck law, the spectral intensity (dimension $I_\nu(\nu, T) \to dE/dt\, dA\, d\Omega\, d\nu$) of the black body is given as

$$I_\nu(\nu, T) = \frac{2h\nu^3}{c^2}\frac{1}{e^{h\nu/kT} - 1}, \tag{H.6.1.19}$$

where k is the Boltzmann constant, ν the frequency and T the temperature.

From Stefan-Boltzmann law of the black-body (radiation flux $R(T) = \sigma T^4$, dimension $dE/dt\,dA$), the energy density $\rho(T)$ (dimension dE/dV) is

$$I(T) = \int_0^\infty I_\nu(\nu, T)d\nu = \frac{c}{4\pi}\rho(T) = \frac{1}{\pi}R(T) \Rightarrow$$

$$\rho(T) = \frac{4\pi}{c}\int_0^\infty I_\nu(\nu, T)d\nu = \frac{4}{c}\sigma T^4, \tag{H.6.1.20}$$

$$\rho(T) = \left(\frac{\pi^2}{15c^3\hbar^3}\right)(kT)^4 = \left(\frac{6.494}{\pi^2 c^3\hbar^3}\right)(kT)^4, \tag{H.6.1.21}$$

where $\pi^4/15 = 6\sum_{n=1}^{\infty} 1/n^4 = 6.494$ (from Gamma and Riemann Zeta functions, respectively, $\Gamma(z)$ and $\zeta(s)$), σ is the Stefan-Boltzmann constant and $I(T)$ the spectral intensity integer in all frequency of the black-body. According to Fermi: "Consequently the Stefan's law for the pions will be quite similar to the ordinary Stefan's law of the black-body radiation. The difference is only in a statistical weight factor. For the photons the statistical wight is the factor, 2, because of the two polarization directions. If we assume that the pions have spin zero and differ only by their charge $\pm e$ or 0, their statistical weight will be 3. Consequently, the energy density of the pions will be obtained by multiplying the energy density of the ordinary Stefan's law by the factor 3/2." Then, multiplying the energy density (H.6.1.21) by 3/2, the energy density via pions is

$$\rho_\pi(T) = \frac{3}{2}\rho(T) = \frac{3 \times 6.494}{2\pi^2\hbar^3 c^3}(kT)^4. \tag{H.6.1.22}$$

The total energy of the system (Eq. H.6.1.4) is divided among pions, protons and anti-protons. Then it is necessary to get the energy density via protons and anti-protons. In this case is used Planck law modified (for fermions) as

$$I_{fermion}(E, T) = \frac{2}{h^2c^2}\frac{E^3}{e^{E/kT} + 1}, \tag{H.6.1.23}$$

and

$$\rho_{fermion}(T) = \frac{4\pi}{c}\int_0^\infty I_{fermion}(E, T)\frac{dE}{h}. \tag{H.6.1.24}$$

It is necessary to use the Planck law modified because the protons and anti-protons are fermions, where they obey Fermi-Dirac statistical. According to Fermi: "The contribution of the nucleons and anti-nucleons to the energy density is given by a similar formula. The differences are that the statistical weight of the nucleons is eight since we have four different types of nucleons and anti-nucleons and for each, two spin orientations. A further difference is due to the fact that these particles obey the Pauli principle." Then it is necessary to multiply the Stefan-Boltzmann law by fermions to 8/2. The process is $pp \rightarrow \pi + X$, where "X" represent the protons and anti-protons, then the energy density via protons and anti-protons is

$$\rho_X(T) = \frac{8}{2}\rho_{fermion}(T) = \frac{4 \times 5.682}{\pi^2\hbar^3c^3}(kT)^4 \tag{H.6.1.25}$$

where $6\sum_{n=1}^{\infty}(-1)^{n+1}/n^4 = 5.682$.

The total energy density ρ_{tot} of the system during the collision is given by sum $\rho_{tot} = \rho_\pi + \rho_X$, but also it is the energy of c.m. divided per volume, $\rho_{tot} = \sqrt{s}/\Omega_0$. Then

$$\rho_{tot} = \frac{\sqrt{s}}{\Omega_0} = \rho_\pi + \rho_X. \tag{H.6.1.26}$$

Substituting Eqs. (H.6.1.22) and (H.6.1.25) in Eq. (H.6.1.26)

$$\rho_{tot} = \frac{\sqrt{s}}{\frac{2m_pc^2}{\sqrt{s}}\Omega} = \frac{3 \times 6.494}{2\pi^2\hbar^3c^3}(kT)^4 + \frac{4 \times 5.682}{\pi^2\hbar^3c^3}(kT)^4,$$

$$(kT)^4 = 0.152\frac{\hbar^3c^3s}{m_pc^2\Omega}. \tag{H.6.1.27}$$

Note that the energy density is frame invariant, $\rho_{tot} = E_{0tot}/\Omega_0 = E_{tot}/\Omega$, because cancel the Lorentz factors.

In the classical case to use the kinetics energy T',

$$T' = \sqrt{s} - 2m_pc^2. \tag{H.6.1.28}$$

Analogously Eq. (H.6.1.27), it is possible to get the classical case (similar Eqs. H.6.1.15 and H.6.1.16)

$$(kT)^4 = 0.152\frac{\hbar^3c^3T'^2}{m_pc^2\Omega}. \tag{H.6.1.29}$$

Analogous to the Eqs. (H.6.1.19) and (H.6.1.20) it has the definition of numerical density of the black-body radiation is (see Landau and Lifshitz, 1980)

$$n(T) = \frac{4\pi}{c}\int_0^\infty \frac{I_\nu(\nu,T)}{h\nu}d\nu = \frac{8\pi}{c^3}\int_0^\infty \frac{\nu^2 d\nu}{e^{h\nu/kT}-1} \Rightarrow$$

$$n(T) = \frac{1}{\pi^2}\left(\frac{kT}{c\hbar}\right)^3\int_0^\infty \frac{x^2dx}{e^x-1} = \frac{\Gamma(3)\zeta(3)}{\pi^2}\left(\frac{kT}{c\hbar}\right)^3,$$

$$n(T) = 0.243576\frac{(kT)^3}{\hbar^3c^3}, \tag{H.6.1.30}$$

where $x = h\nu/kT$. In the case of pions, $(\frac{\#\text{pions}}{\text{volume}})$, it is necessary multiply the last equation by $3/2$ (analogous Eq. H.6.1.22), as

$$n_\pi(T) = \frac{3}{2}n(T) = 0.365\frac{(kT)^3}{\hbar^3 c^3}, \tag{H.6.1.31}$$

where Fermi /citeFermi got also the last expression.

Substituting Eq. (H.6.1.27) and (H.6.1.29) in Eq. (H.6.1.30), we get, respectively, for the relativistic and classical cases,

$$n_\pi^{HE}(\sqrt{s}) = 0.0888\left(\frac{s}{\hbar c\, m_p c^2 \Omega}\right)^{3/4}, \tag{H.6.1.32}$$

$$n_\pi^{ME}(T') = 0.0888\left(\frac{T'^2}{\hbar c\, m_p c^2 \Omega}\right)^{3/4}. \tag{H.6.1.33}$$

We can define the multiplicity of pions per collision ($N_\pi^{HE} \rightarrow \#\,\text{pions}$), for high energy, being (using Eq. H.6.1.7)

$$n_\pi^{HE} = \frac{N_\pi^{HE}}{\Omega_0} \Rightarrow N_\pi^{HE} = \frac{2m_p c^2}{\sqrt{s}}\Omega n_\pi^{HE}. \tag{H.6.1.34}$$

Substituting Ep. (H.6.1.32) in Eq. (H.6.1.34)

$$N_\pi^{HE}(\sqrt{s}) = 0.1777\left(\frac{m_p c^2 \Omega^{LF} s}{\hbar^3 c^3}\right)^{1/4}. \tag{H.6.1.35}$$

According Eqs. (H.6.1.2) and (H.6.1.3),

$$\Omega = \frac{4\pi a^3 \hbar^3 c^3}{3(m_\pi c^2)^3}. \tag{H.6.1.36}$$

Substituting Eq. (H.6.1.36) in Eq. (H.6.1.35)

$$N_\pi^{HE}(\sqrt{s}) = 0.25422\left[\frac{m_p c^2 a^3 s}{(m_\pi c^2)^3}\right]^{1/4}. \tag{H.6.1.37}$$

The pions rest mass are different, $m_{\pi^0}c^2 = 0.135\,\text{GeV}$ and $m_{\pi^\pm}c^2 = 0.139\,\text{GeV}$. Fermi got that when considerer the conservation of angular momentum, it has the effect of reduction the numbers of pions and nucleons, then he found a factor obtained numerically of 0.51. The total energy via pions is divided approximately equal among π^0, π^- and π^+, then multiplying and dividing

Eq. (H.6.1.37) per, respectively, 0.51 and 3, it gets the π^0 and $\pi^{\pm}$ multiplicities

$$N_{\pi^0}^{HE}(\sqrt{s}) = 0.0432 \left[\frac{m_p c^2 a^3 s}{(m_{\pi^0} c^2)^3}\right]^{1/4}, \tag{H.6.1.38}$$

$$\tag{H.6.1.39}$$

Doing $m_{\pi^0} c^2 = 0.14385 m_p c^2$ and $m_{\pi^{\pm}} c^2 = 0.14875 m_p c^2$ in the lest two equations,

$$N_{\pi^0}^{HE}(\sqrt{s}) = 0.185 a^{3/4} \sqrt{\frac{\sqrt{s}}{m_p c^2}}, \tag{H.6.1.40}$$

$$N_{\pi^{\pm}}^{HE}(\sqrt{s}) = 0.180 a^{3/4} \sqrt{\frac{\sqrt{s}}{m_p c^2}}, \tag{H.6.1.41}$$

$$N_{\pi\, total}^{HE}(\sqrt{s}) = 0.546 a^{3/4} \sqrt{\frac{\sqrt{s}}{m_p c^2}}, \tag{H.6.1.42}$$

where $N_{\pi\, total}^{HE} = 2N_{\pi^{\pm}}^{HE} + N_{\pi^0}^{HE}$, can note that the lest value is the same in Fermi (Fermi, 1950).

The center of mass energy is according Eq. (H.6.1.4). Substituting Eq. (H.6.1.4) in Eq. (H.6.1.37), we get the equation of Fermi to the π^0 multiplicity for extreme high energies

$$N_{\pi^0}^{HE}(E_p) = 0.777 a^{3/4} \left(1 + \frac{E_p}{m_p c^2}\right)^{1/4}. \tag{H.6.1.43}$$

For the intermediate energy range (H.6.1.33), classical treatment. Doing the same procedure from Eq. (H.6.1.34) to (H.6.1.40),

$$N_{\pi^0}^{ME}(\sqrt{s}) = 0.6533 a^{3/4} \frac{(\sqrt{s}/m_p c^2 - 2)^{3/2}}{\sqrt{s}/m_p c^2}. \tag{H.6.1.44}$$

Substituting Eq. (H.6.1.4) in Eq. (H.6.1.44), we get the equation of Fermi to the multiplicity of pions in intermediate energy range,

$$N_{\pi^0}^{ME}(E_p) = 0.777 a^{3/4} \frac{\left(\sqrt{1 + E_p/m_p c^2} - \sqrt{2}\right)^{3/2}}{\sqrt{1 + E_p/m_p c^2}}. \tag{H.6.1.45}$$

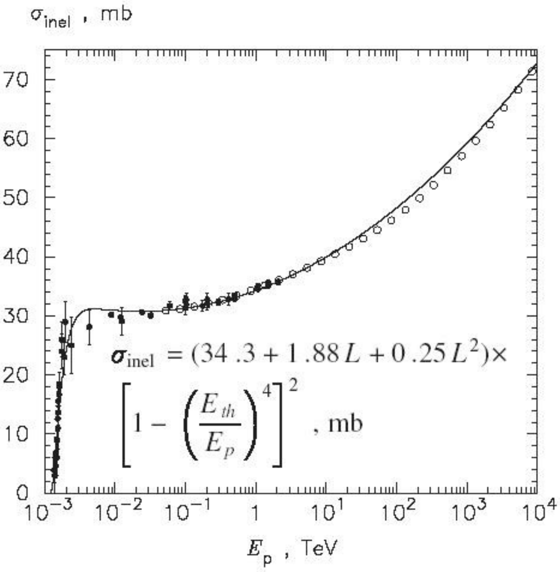

Figure H.6.1: The graphic compares the experimental data (black points) with the SIBYLL code (open points) and with the Kelner's expression (Kelner et al., 2006) for the cross section (solid curve).

H.6.2 Modern approach

Currently the modeling of pp interactions is done through computational codes, Monte Carlo codes such as SIBYLL, PHYTHIA, Dpmjet. Kelner (Kelner et al., 2006) presented new parameterizations of energy spectra of secondary particles, π and η mesons, gamma rays, electrons, and neutrinos produced in inelastic proton-proton collisions based on the SIBYLL code by Lipari (Fletcher et al., 1994). These parameterizations have very good accuracy in the energy range above 100 GeV (see figure H.6.1 and H.6.2).

The fit to the pp cross section obtained by Kelner et al. (2006) is

$$\sigma_{pp}(E_p) = (34.3 + 1.88L + 0.25L^2)\left[1-\left(\frac{E_{th}}{E_p}\right)^4\right]^2 \text{ mb}, \qquad \text{(H.6.2.1)}$$

where E_p is the incident proton energy in laboratory frame (the same that E_p in the last section), $L = \ln[E_p(TeV)]$ and E_{th} is the minimum threshold energy of the incident proton for production of a pion ($E_{th} = 1.22\,\text{GeV}$) and $1\,\text{mb} = 1\,\text{mbarn} = 10^{-27}\,\text{cm}^2$.

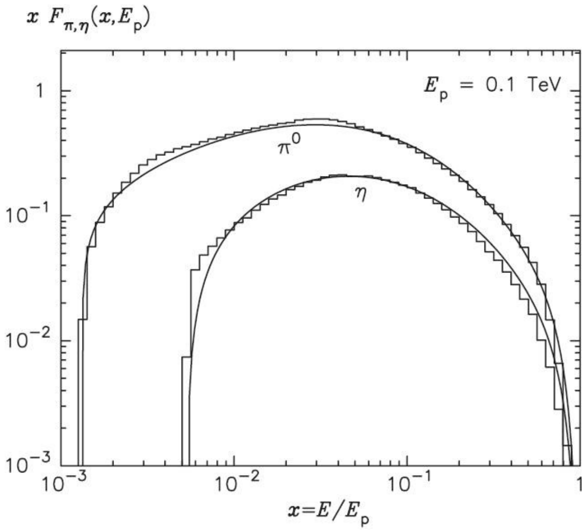

Figure H.6.2: Energy spectra of π and η mesons from the numerical simulations of the SIBYLL code (histograms) and from the analytical presentations given by Eqs. (H.6.2.3) and (H.6.2.4) for energy 0.1 TeV.

The function that Kelner got for the multiplicity of pions "N_π" is given as

$$dN_\pi \equiv F_\pi(x, E_p)dx, \tag{H.6.2.2}$$

$$F_\pi(x, E_p) = \frac{d}{dx}\phi(x, E_p), \tag{H.6.2.3}$$

$$\phi_{SIBYLL} = -B_\pi \left(\frac{1 - x^{\beta_\gamma}}{1 + k_\gamma x^{\beta_\gamma}(1 - x^{\beta_\gamma})} \right)^4, \tag{H.6.2.4}$$

where E_π is the total energy via neutral pions productions (secondary pions mesons), $x = E_\pi/E_p$, and B_π, β^γ and k^γ are functions dependent only of E_p in the Kelner parametrization (Kelner et al., 2006, see graphic H.6.2). Figure H.6.2 shows the spectrum distribution $xF_\pi(x, E_p)$ of π^0 production as a function of $x = E_\pi/E_p$, which is the percentage of incident proton energy transferred to the pions. Note in Fig. H.6.2 shoes the small probabilities of the π^0 productions at small energy transformation $x \leq 0.0015$ and large energy transformation $1 \geq x \geq 0.7\ E_p$. The maximum probability is at $x = 0.03$, indicating the approximate 3% of incident proton energy is transferred via neutral pion π^0. Since the experimental data show that the production of neutral pions π^0 is practically the same as the productions of positive π^+ and negative π^- charged pions, then we get that approximate 10% of incident proton energy E_p is transferred via pions (E_π).

Integrating Eq. (H.6.2.2) over x, Kelner obtained (Kelner et al., 2006) the

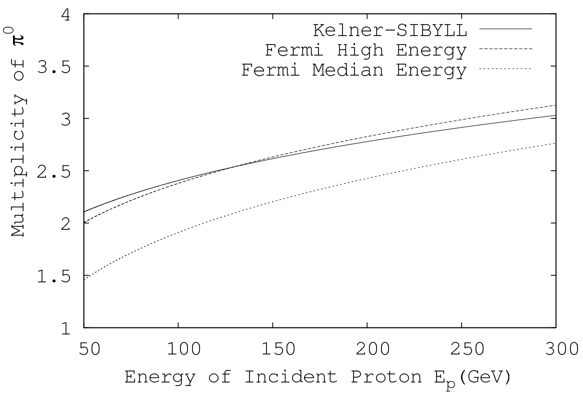

Figure H.6.3: The multiplicity of neutral pions π^0 in function of incident proton energy E_p for intermediate energy range $50 \leq E_p \leq 300$ GeV. We compared three results: Kelner-SIBYLL, Fermi approaches in median energy and high energy for $a = 5$.

multiplicity (number) of π^0 per pp collision as a function of E_p

$$N_{\pi}^{KS}(E_p) = 3.92 + 0.83L + 0.075L^2. \tag{H.6.2.5}$$

H.6.3 Comparison between Fermi's and Kelner-SIBYLL's approaches

We compared the multiplicities of neutral pions production (π^0) obtained the Fermi theoretical approach (Eqs. H.6.1.43 and H.6.1.45) and the Kelner analytical parametrization (Eq. H.6.2.5) to the SIBYLL code (Fletcher et al., 1994). The analytical parametrization of Kelner has good agreement with the SIBYLL code for energy $E_p > 100GeV$.

In the figure H.6.3 we compare the Fermi results in high-energy region (Eq. H.6.1.43) and median-energy region (Eq. H.6.1.45) with the description of Kelner-SIBYLL in intermediate energy range $50 - 300$ GeV. We used parameter $a = 5$, which give a very good agreement between Fermi result in high energy and Kelner-SIBYLL result in the range $100 - 300$ GeV. But Fermi result in median energy Eq. (H.6.1.45) gives lower multiplicity of π^0 in this energy range.

In the figure H.6.4, we use $a = 5$ and compare the Fermi result for high energy (H.6.1.43) with Kelner-SIBYLL result in the energy range $300 - 1000$ GeV. We find that Fermi result is about 8% larger than Kelner-SIBYLL result, this indicates that the validity of the Fermi approach in extremal high-energy range is in question. Because the cross-section grows with E_p (see Figure 1), and the a parameter by its definition should become larger with larger as the cross-section grows in this energy range. This makes that Fermi result

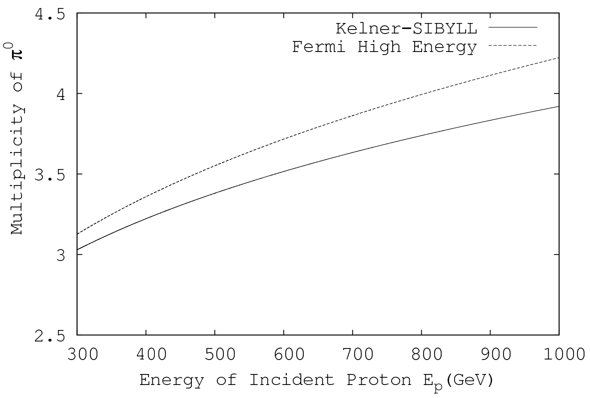

Figure H.6.4: The multiplicity of neutral pions π^0 in function of incident proton energy E_p for high energy range $300 \leq E_p \leq 1000$ GeV. We compared two results obtained respectively by Kelner-SIBYLL and Fermi Eq. (H.6.1.43) for $a = 5$.

further deviate from Kelner-SIBYLL result. One of reasons could probably be the fact that more particles, e.g.,gluons and quarks, are exited and participate the thermalization in the Fermi volume Ω, as a result, the energy transferred to π-productions is smaller than that estimated by Fermi with three particles proton, neutron and pion.

H.6.4 Gamma ray flux from GRB 061007

In this section we will obtain the quantity of gamma energy produced via pp collision in the GRB 061007. The dates that we have about this GRB are

$$\begin{cases} \text{Dyadosphere energy} & E_{dya} = 2.16 \times 10^{54}\,\text{erg} \\ \text{Barionic loading} & B = 2.15 \times 10^{-3} \\ \text{Redshift} & z = 1.262, \\ \text{Lorentz factor} & \gamma = 500. \end{cases} \tag{H.6.4.1}$$

We believe that all particles possess the same energy ($\gamma = 500$) for two reasons, $1 -$ we believe that all particles have the same probability of collision (or transition), $2 -$ if the particles possessed energy different, would not form a shell with a little thickness. Through the dates (H.6.4.1), we obtain (using 1 TeV = 1.602 erg)

$$\begin{cases} E_{shell} = (1+B)E_{dya} = 2.16 \times 10^{54} & \text{erg}, \\ N_p = \frac{E_{shell}}{E_p} = 2.88 \times 10^{54} & \text{protons}, \end{cases} \tag{H.6.4.2}$$

where $E_p = \gamma\, m_p c^2 \simeq 0.5$TeV.

The mean free path of a particle in a gas with particle density "n" and cross section "σ" is given as

$$t = (n\sigma c)^{-1}. \tag{H.6.4.3}$$

In the case of a relativistic shell (4.9×10^{53} proton) interacting against a ISM whoso density and cross section are,

$$\begin{cases} n_{ism} = 1, & \frac{\#\ protons}{cm^3}, \\ \sigma = 40 \ \text{ mb} = 4 \times 10^{-26} & \text{cm}^2. \end{cases} \tag{H.6.4.4}$$

Then with the lest dates, we can obtain the number of collisions (interactions) per seconds,

$$N_i = 3.45 \times 10^{39} \qquad \frac{\text{collisions}}{\text{second}}. \tag{H.6.4.5}$$

H.6.5 Summary

We study pions productions via the high-energy proton-proton collisions in Fermi scenario. Fermi assumes that during the collision, all particles interact are thermalized in a volume (we call Fermi volume) spherical Ω, whose size is order of pion Compton length which Fermi allowed to be parameterizable the radius, he assumed radius equal to the Compton wavelength of pion (meson π). The Fermi volume made up of the all particles involved in the collision, which Fermi assume that from the collision have only: protons, anti-protons and charged and neutral pions. Fermi made the mathematical analysis in the center of mass frame (c.m.).

In this work we started doing detailed discussion of the main points of the Fermi article (Fermi, 1950), we follow showing a brief argument of analytical parametrization of Kelner for the SIBYLL code and in the lest section we compared the Fermi approach with the parametrization of Kelner.

We initiated the fermi approach demonstrating the Lorentz factor of the particles (which they are the same for the two particles) in the center of mass frame for in follow to obtain the expression of Fermi volume between the c.m. and the LF, which to have the Lorentz contraction. We rebuilt the statistical analysis that Fermi obtained, which for he obtain the statistical weight S_n (for "n" collisions), Fermi had to get before P_n (probability of occur "n" collisions inside of a volume V), $G_n(\sqrt{s})$ (density of states of energies possible) and $N_n(\sqrt{s})$ (number of states in the phase space). Following, we rebuilt the Fermi calculus with details to obtain the pions multiplicity for a collision, for Fermi get its, he used the Planck Law for the black-body (modified and no-modified) for obtain the energy density of pions (bosons) and protons and anti-protons (fermions). But we accrescent the letter "a" to parametrize the curve of SIBYLL code, "a" is to parametrize the size of the Fermi volume, it gives the number of times of the Compton wavelength.

In the modern approach we show the parametrizations of Kelner for the SIBYLL code, the parametrization of the cross section and multiplicity of pions. Kelner obtained very good agreement with the SIBYLL code.

In the final section we compared the Fermi results with the parametrization of Kelner. We made two graphics for different ranges of energy of incident proton, in the intermediate energy range ($50 \leq E_p \leq 300$) we found good agreement for $a = 5$, but in the high energy range ($300 \leq E_p \leq 1000$) we found that Fermi result is about 8% larger than Kelner-SIBYLL result for $a = 5$, then indicate that the validity of our approach is in question in this range. Conform the first figure, the cross section of pp interactions increase with the increasing of the energy, then the Fermi volume also would should increase with the energy, but the "a" parameter is lower with the energy.

H.6.6 Appendix: Maximum and minimum energy of the Pions

In this section we will show the energy limits of the pions created via pp interactions and we will apply the limits in the work of Blattnig et al. (2000).

The energy of a pion in the laboratory frame (LF) in function of its energy in center of mass (c.m.) frame, is as

$$E_\pi = \gamma(E_{0\pi} + vp_{0\pi}cos\theta), \tag{H.6.6.1}$$

where γ is the Lorentz factor, "v" the velocity of the pion, $E_{0\pi}$ the pion energy in the c.m. frame and $p_{0\pi}$ the pion momentum in the c.m. frame (the index "0" inform c.m. frame and without the index "0" give in the LF). We will consider $c = 1$. If $cos\theta = 1$ the pion energy is maximum (E_π^{max}), and if $cos\theta = -1$ the pion energy is minimum (E_π^{min}). Then the maximum and minimum energy of the pion is,

$$E_\pi^{\frac{max}{min}} = \gamma(E_{0\pi} \pm vp_{0\pi}). \tag{H.6.6.2}$$

Developing the calculus we obtain the maximum and minimum energy of the pions,

$$E_\pi^{max} = \frac{1}{4m_p}(2m_pE_p - 2m_p^2 + m_\pi^2 + R_p), \tag{H.6.6.3}$$

$$E_\pi^{min} = \begin{cases} \frac{1}{4m_p}\left(2m_pE_p - 2m_p^2 + m_\pi^2 - R_p\right), & \text{if} \quad \mathrm{E_p} > \mathrm{E_p^*} \\ m_\pi, & \text{if} \quad \mathrm{E_p} \leq \mathrm{E_p^*}, \end{cases} \tag{H.6.6.4}$$

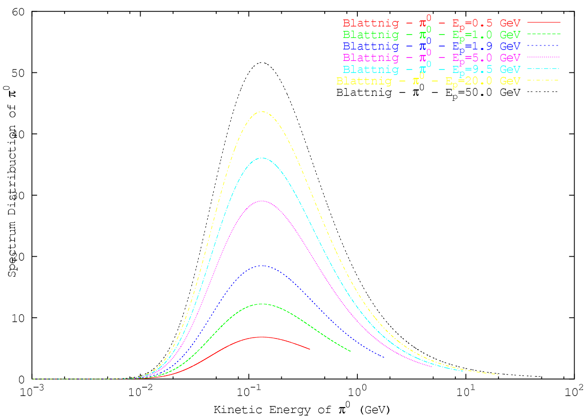

Figure H.6.5

where

$$R_p = \sqrt{\frac{(E_p - m_p)[(2m_pE_p - 2m_p^2 - m_\pi^2)^2 - 16m_p^2m_\pi^2]}{E_p + m_p}}. \tag{H.6.6.5}$$

$$E_p^* = \frac{2m_p^2 + 2m_pm_\pi - m_\pi^2}{2(m_p - m_\pi)} \simeq 1.242 \qquad \text{GeV}. \tag{H.6.6.6}$$

where E_p^* is the limit (threshold) of energy in the case that $E_\pi = m_\pi$.

A.1 GRBs: Historical background

A.1.1 Introduction

The last century was characterized by three great successes in the field of astrophysics, each one linked to a different energy source:

1. Jean Perrin (1920) and Arthur Eddington (1920) were the first to point out, independently, that the nuclear fusion of four hydrogen nuclei into one helium nucleus could explain the energy production in stars. This idea was put on a solid theoretical base by Atkinson and Houtermans (1929a,b) using George Gamow's quantum theory of barrier penetration (Gamow and Houtermans, 1929) further developed by C.F. von Weizsäckr (1937, 1938). The monumental theoretical work by Hans Bethe (1939), and later by Burbidge et al. (1957), completed the understanding of the basic role of nuclear energy generated by fusion processes in explaining the energy source of main sequence stars (Schwarzschild, 1965).

2. Pulsars, especially NP0532 at the center of the Crab nebula, were discovered by Jocelyn Bell and Tony Hewish (Bell and Hewish, 1967), and many theorists were actively trying to explain them as rotating neutron stars (see Gold, 1968, 1969; Pacini, 1968; Finzi and Wolf, 1968). These had already been predicted by George Gamow using Newtonian physics (Gamow, 1938) and by Robert Julius Oppenheimer and students using General Relativity (Oppenheimer and Serber, 1938; Oppenheimer and Snyder, 1939; Oppenheimer and Volkoff, 1939). The crucial evidence confirming that pulsars were neutron stars came when their energetics was understood (Finzi and Wolf, 1968). The following relation was established from the observed pulsar period P and its always positive first derivative dP/dt:

$$\left(\frac{dE}{dt}\right)_{obs} \simeq 4\pi^2 \frac{I_{NS}}{P^3}\frac{dP}{dt}\,, \tag{A.1.1.1}$$

where $\left(\frac{dE}{dt}\right)_{obs}$ is the observed pulsar bolometric luminosity, I_{NS} is its moment of inertia derived from the neutron star theory. This has to be related to the observed pulsar period. This equation not only identifies the role of neutron stars in explaining the nature of pulsars, but clearly indicates the rotational energy of neutron star as the pulsar energy source.

3. The birth of X-ray astronomy thanks to Riccardo Giacconi and his group (see e.g. Giacconi et al., 1978) led to a still different energy source, originating from the accretion of matter onto a star which has undergone a complete gravitational collapse process: a black hole (see e.g. Ruffini and Wheeler, 1971). In this case, the energetics is dominated by the radiation emitted in the accretion process of matter around an already formed black hole. Luminosities up to 10^4 times the solar luminosity, much larger then the ones of pulsars, could be explained by the release of energy in matter accreting in the deep potential well of a black hole (Leach and Ruffini, 1973). This allowed to probe for the first time the structure of circular orbits around a black hole computed by Ruffini and Wheeler (see e.g. Landau and Lifshitz, 1980). This result was well illustrated by the theoretical interpretation of the observations of Cygnus-X1, obtained by the Uhuru satellite and by the optical and radio telescopes on the ground (see Fig. A.1.1).

These three results clearly exemplify how the identification of the energy source is the crucial factor in reaching the understanding of any astrophysical or physical phenomenon.

The discovery of Gamma-Ray Bursts (GRBs) may well sign a further decisive progress. GRBs can give in principle the first opportunity to probe and observe a yet different form of energy: the extractable energy of the black hole introduced in 1971 (Christodoulou and Ruffini, 1971), which we shall refer in the following as the blackholic energy[1]. The blackholic energy, expected to be emitted during the dynamical process of gravitational collapse leading to the formation of the black hole, generates X- and γ-ray luminosities 10^{21} times larger than the solar luminosity, which manifest themselves in the GRB phenomenon. In the very short time they last, GRBs are comparable with the full electromagnetic luminosity of the entire visible universe.

A.1.2 The discovery of GRBs and the early theoretical works

We recall how GRBs were detected and studied for the first time using the *Vela* satellites, developed for military research to monitor the non-violation of the Limited Test Ban Treaty signed in 1963 (see e.g. Strong, 1975). It was clear from the early data of these satellites, which were put at $150,000$ miles from the surface of Earth, that the GRBs originated neither on the Earth nor

[1] This name is the English translation of the Italian words "energia buconerale", introduced by Iacopo Ruffini, December 2004, here quoted by his kind permission.

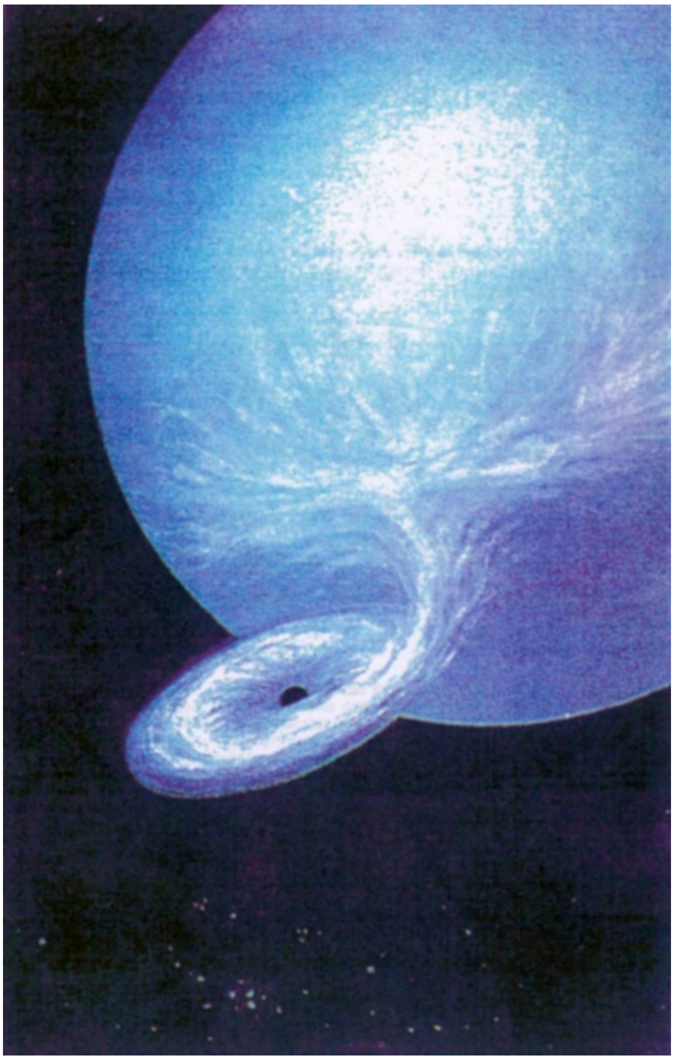

Figure A.1.1: Cygnus X-1, here represented in a artist view, offered the possibility of identifying the first black hole in our galaxy (Leach and Ruffini, 1973). The luminosity Φ of 10^4 solar luminosities points to the accretion process into a neutron star or a black hole as the energy source. The absence of pulsation is naturally explained either by a non-magnetized neutron star or a Kerr-Newman black hole, which has necessarily to be axially symmetric. What identifies the black hole unambiguously is that the mass of Cygnus X-1, observed to be larger than $9M_{\odot}$, exceeds the absolute upper limit of the neutron star mass, estimated at $3.2M_{\odot}$ by Rhoades and Ruffini (1974).

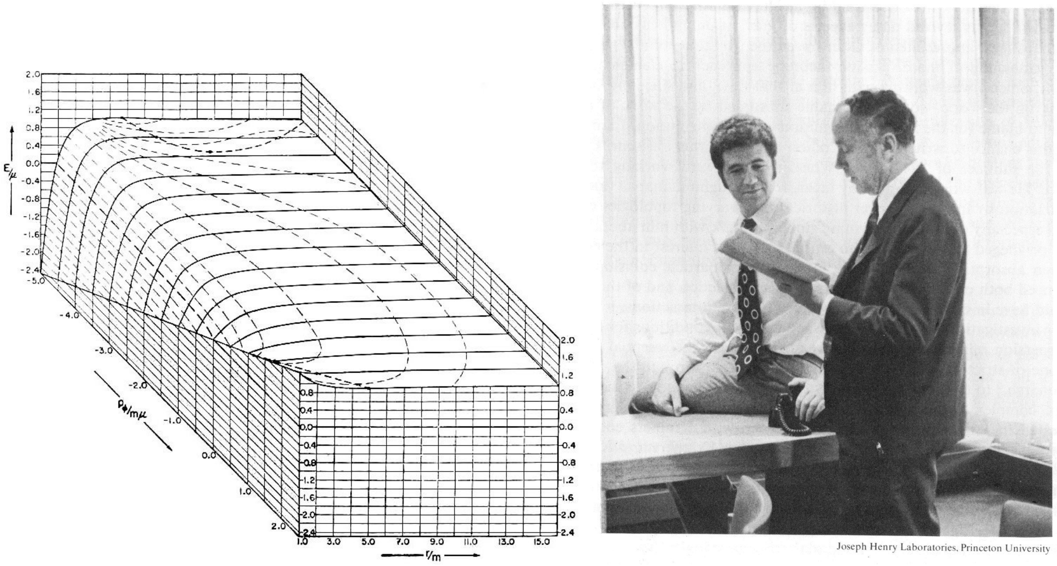

Figure A.1.2: The effective potential corresponding to the circular orbits in the equatorial plane of a black hole is given as a function of the angular momentum of the test particle. This digram was originally derived by Ruffini and Wheeler (right picture, reproduced with permission of the Joseph Henry Laboratories). For details see Landau and Lifshitz (1980) and Rees et al. (1974).

in the Solar System. This discovery luckily occurred when the theoretical understanding of gravitationally collapsed objects, as well as the quantum electrodynamics of the vacuum polarization process, had already reached full maturity.

Three of the most important works in the field of general relativity have certainly been the discovery of the Kerr solution (Kerr, 1963), its generalization to the charged case (Newman et al., 1965) and the formulation by Brandon Carter (1968) of the Hamilton-Jacobi equations for a charged test particle in the metric and electromagnetic field of a Kerr-Newman solution (see e.g. Landau and Lifshitz, 1980). The equations of motion, which are generally second order differential equations, were reduced by Carter to a set of first order differential equations which were then integrated by using an effective potential technique by Ruffini and Wheeler for the Kerr metric (see e.g. Landau and Lifshitz, 1980) and by Ruffini for the Reissner-Nordstrøm geometry (Ruffini, 1973, , see Fig. A.1.2).

All the above mathematical results were essential for understanding the new physics of gravitationally collapsed objects and allowed the publication of a very popular article: "Introducing the black hole" (Ruffini and Wheeler, 1971). In that paper, it was advanced the ansatz that the most general black hole is a solution of the Einstein-Maxwell equations, asymptotically flat and with a regular horizon: the Kerr-Newman solution. Such a solution is characterized only by three parameters: the mass M, the charge Q and the angular momentum L. This ansatz of the "black hole uniqueness theorem" still today after thirty years presents challenges to the mathematical aspects of its complete proof (see e.g. Carter, in press; Bini et al., 2002). In addition to the challenges due to the above mathematical difficulties, in the field of physics this ansatz contains most profound consequences. The fact that, among all the possible highly nonlinear terms characterizing the gravitationally collapsed objects, only the ones corresponding solely to the Einstein-Maxwell equations survive the formation of the horizon has, indeed, extremely profound physical implications. Any departure from such a minimal configuration either collapses on the horizon or is radiated away during the collapse process. This ansatz is crucial in identifying precisely a standard process of gravitational collapse leading to the formation of the black hole and the emission of GRBs. Indeed, in this specific case, the Born-like nonlinear (Born, 1934) terms of the Heisenberg-Euler-Schwinger (Heisenberg and Euler, 1936; Schwinger, 1951) Lagrangian are radiated away prior to the formation of the horizon of the black hole (see e.g. Ruffini et al., in preparation). Only the nonlinearity corresponding solely to the classical Einstein-Maxwell theory is left as the outcome of the gravitational collapse process.

The same effective potential technique (see Landau and Lifshitz, 1980), which allowed the analysis of circular orbits around the black hole, was crucial in reaching the equally interesting discovery of the reversible and irreversible transformations of black holes by Christodoulou and Ruffini (1971), which in turn led to the mass-energy formula of the black hole:

$$E_{BH}^2 = M^2c^4 = \left(M_{\rm ir}c^2 + \frac{Q^2}{2\rho_+}\right)^2 + \frac{L^2c^2}{\rho_+^2}\,, \tag{A.1.2.1}$$

with

$$\frac{1}{\rho_+^4}\left(\frac{G^2}{c^8}\right)\left(Q^4 + 4L^2c^2\right) \leq 1\,, \tag{A.1.2.2}$$

where

$$S = 4\pi\rho_+^2 = 4\pi(r_+^2 + \frac{L^2}{c^2M^2}) = 16\pi\left(\frac{G^2}{c^4}\right)M_{\rm ir}^2\,, \tag{A.1.2.3}$$

is the horizon surface area, $M_{\rm ir}$ is the irreducible mass, r_+ is the horizon radius and ρ_+ is the quasi-spheroidal cylindrical coordinate of the horizon evaluated at the equatorial plane. Extreme black holes satisfy the equality in Eq.(A.1.2.2).

From Eq.(A.1.2.1) follows that the total energy of the black hole E_{BH} can be split into three different parts: rest mass, Coulomb energy and rotational energy. In principle both Coulomb energy and rotational energy can be extracted from the black hole (Christodoulou and Ruffini, 1971). The maximum extractable rotational energy is 29% and the maximum extractable Coulomb energy is 50% of the total energy, as clearly follows from the upper limit for the existence of a black hole, given by Eq.(A.1.2.2). We refer in the following to both these extractable energies as the blackholic energy.

The existence of the black hole and the basic correctness of the circular orbit binding energies has been proven by the observations of Cygnus-X1 (see e.g. Giacconi et al., 1978). However, as already mentioned in binary X-ray sources, the black hole uniquely acts passively by generating the deep potential well in which the accretion process occurs. It has become tantalizing to look for astrophysical objects in order to verify the other fundamental prediction of general relativity that the blackholic energy is the largest energy extractable from any physical object.

We also recall that the feasibility of the blackholic energy extraction has been made possible by the quantum processes of creating, out of classical fields, a plasma of electron-positron pairs in the field of black holes. Heisenberg and Euler (1936) clearly evidenced that a static electromagnetic field stronger than the critical value:

$$E_c = \frac{m_e^2 c^3}{\hbar e} \tag{A.1.2.4}$$

can polarize the vacuum and create electron-positron pairs. The major effort in verifying the correctness of this theoretical prediction has been directed in the analysis of heavy ion collisions (see Ruffini et al., in preparation, and references therein). From an order-of-magnitude estimate, it would appear that around a nucleus with a charge:

$$Z_c \simeq \frac{\hbar c}{e^2} \simeq 137 \tag{A.1.2.5}$$

the electric field can be as strong as the electric field polarizing the vacuum. A more accurate detailed analysis taking into account the bound states levels around a nucleus brings to a value of

$$Z_c \simeq 173 \tag{A.1.2.6}$$

for the nuclear charge leading to the existence of a critical field. From the Heisenberg uncertainty principle it follows that, in order to create a pair, the existence of the critical field should last a time

$$\Delta t \sim \frac{\hbar}{m_e c^2} \simeq 10^{-18}\,\mathrm{s}\,, \tag{A.1.2.7}$$

which is much longer then the typical confinement time in heavy ion collisions which is

$$\Delta t \sim \frac{\hbar}{m_p c^2} \simeq 10^{-21}\,\mathrm{s}\,. \tag{A.1.2.8}$$

This is certainly a reason why no evidence for pair creation in heavy ion collisions has been obtained although remarkable effort has been spent in various accelerators worldwide. Similar experiments involving laser beams meet with analogous difficulties (see e.g. Ruffini et al., in preparation).

Damour and Ruffini (1975) advanced the alternative idea that the critical field condition given in Eq.(A.1.2.4) could be easily reached, and for a time much larger than the one given by Eq.(A.1.2.7), in the field of a Kerr-Newman black hole in a range of masses $3.2M_\odot \leq M_{BH} \leq 7.2 \times 10^6 M_\odot$. In that paper there was generalized to the curved Kerr-Newman geometry the fundamental theoretical framework developed in Minkowski space by Heisenberg and Euler (1936) and Schwinger (1951). This result was made possible by the work on the structure of the Kerr-Newman spacetime previously done by Carter (1968) and by the remarkable mathematical craftsmanship of Thibault Damour then working with one of us (RR) as a post-doc in Princeton. We give on this topic some additional details in the next sections.

The maximum energy extractable in such a process of creating a vast amount of electron-positron pairs around a black hole is given by:

$$E_{max} = 1.8 \times 10^{54} \, (M_{BH}/M_\odot) \text{ erg} \,. \qquad \text{(A.1.2.9)}$$

We concluded in that paper that such a process "naturally leads to a most simple model for the explanation of the recently discovered γ-rays bursts".

At that time, GRBs had not yet been optically identified and nothing was known about their distance and consequently about their energetics. Literally thousands of theories existed in order to explain them and it was impossible to establish a rational dialogue with such an enormous number of alternative theories (see Ruffini, 2001). As we will see, this situation was drastically modified by the observations of BeppoSAX.

A.1.3 CGRO, BeppoSAX and the further theoretical developments

The mystery of GRBs became deeper as the observations of the BATSE instrument on board of the Compton Gamma-Ray Observatory (CGRO) satellite[2] over 9 years proved the isotropy of these sources in the sky (See Fig. A.1.3). In addition to these data, the CGRO satellite gave an unprecedented number of details on the GRB structure, on their spectral properties and time variabilities which have been collected in the fourth BATSE catalog (Paciesas et al., 1999, , see e.g. Fig. A.1.4). Analyzing these BATSE sources the existence of two distinct families of sources became clear (see e.g. Kouveliotou et al., 1993; Tavani, 1998): the long bursts, lasting more then one second and softer

[2]see http://cossc.gsfc.nasa.gov/batse/

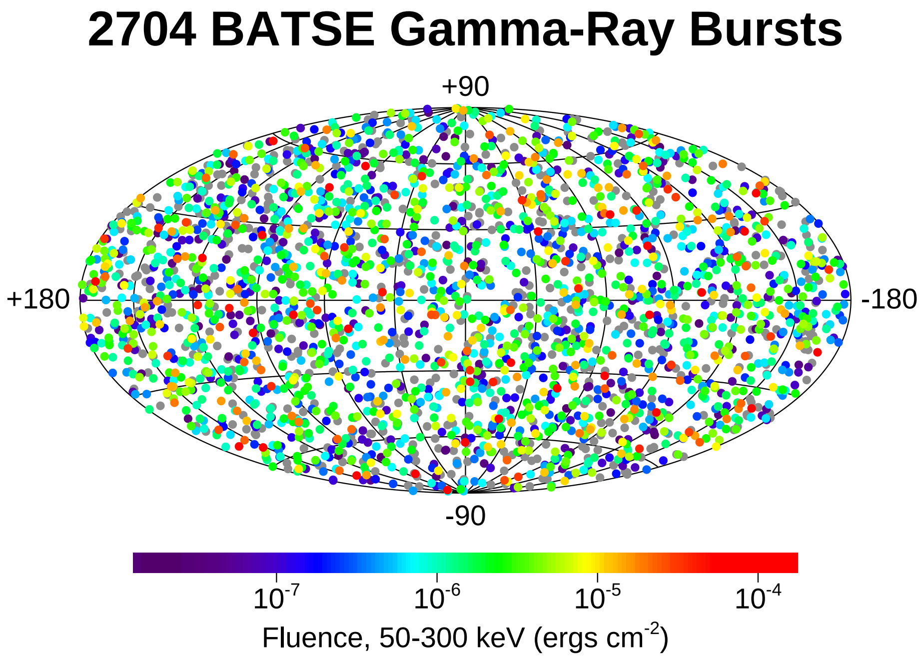

Figure A.1.3: Position in the sky, in galactic coordinates, of 2000 GRB events seen by the CGRO satellite. Their isotropy is evident. Reproduced from BATSE web site by their courtesy.

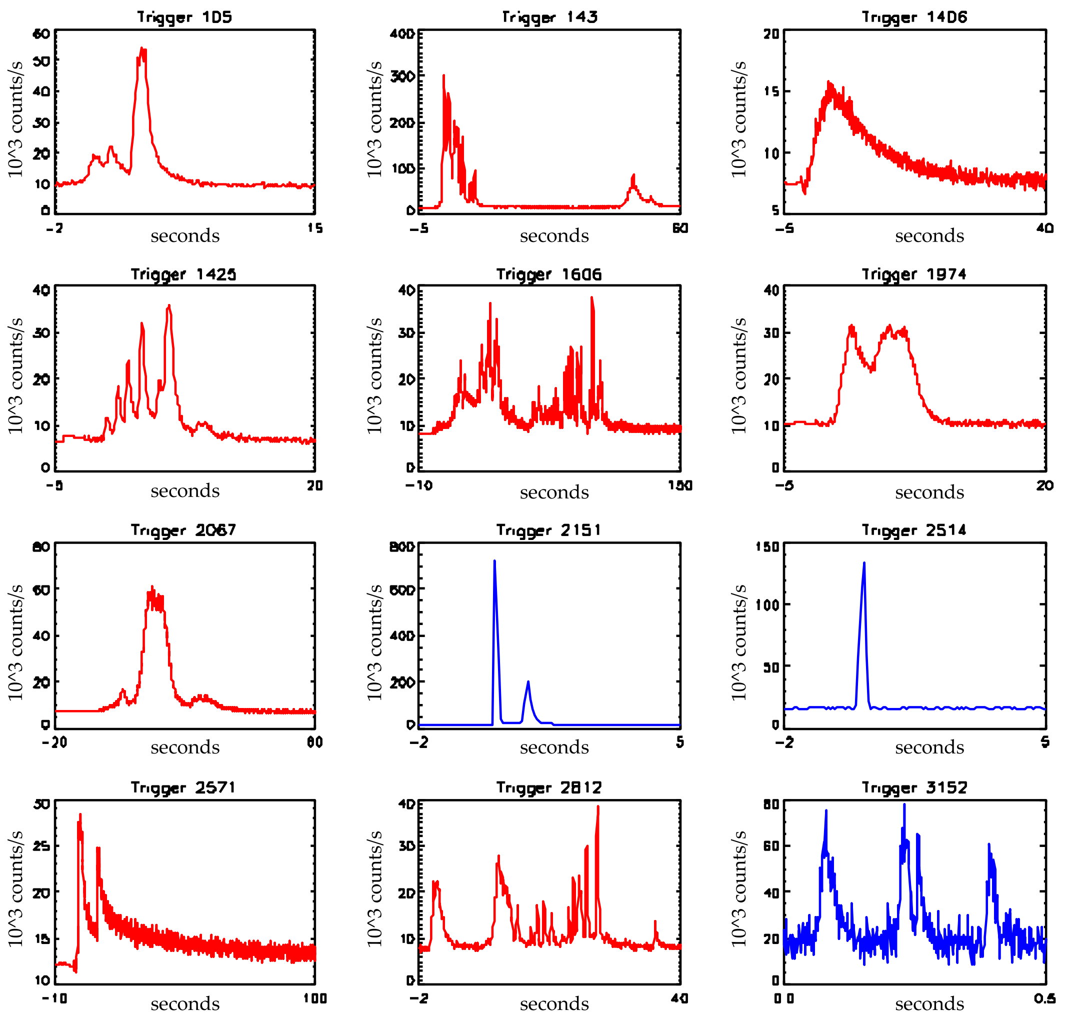

Figure A.1.4: Some GRB light curves observed by the BATSE instrument on board of the CGRO satellite.

in spectra, and the short bursts (see Fig. A.1.6), harder in spectra (see Fig. A.1.5). We shall return shortly on this topic.

The situation drastically changed with the discovery of the afterglow by the Italian-Dutch satellite BeppoSAX (Costa et al., 1997). Such a discovery led to the optical identification of the GRBs by the largest telescopes in the world, including the Hubble Space Telescope, the Keck Telescope in Hawaii and the VLT in Chile, and allowed as well the identification in the radio band of these sources. The outcome of this collaboration between complementary observational technique made possible in 1997 the identification of the distance of these sources from the Earth and of their tremendous energy of the order up to 10^{54} erg/second during the burst, which indeed coincides with the theoretical prediction made by Damour and Ruffini (1975) given in Eq.(A.1.2.9).

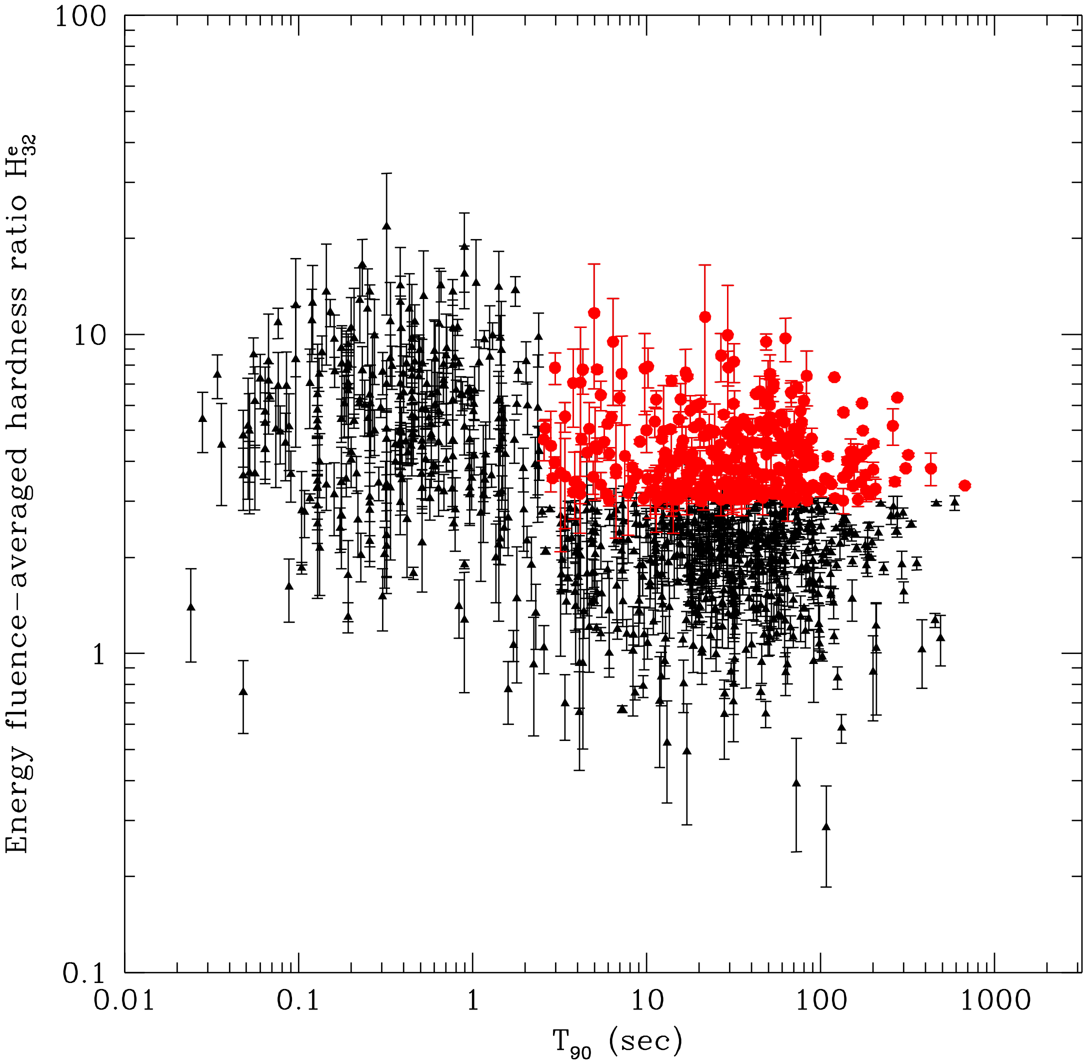

Figure A.1.5: The energy fluence-averaged hardness ratio for short ($T < 1$ s) and long ($T > 1$ s) GRBs are represented. Reproduced, by his kind permission, from Tavani (1998) where the details are given.

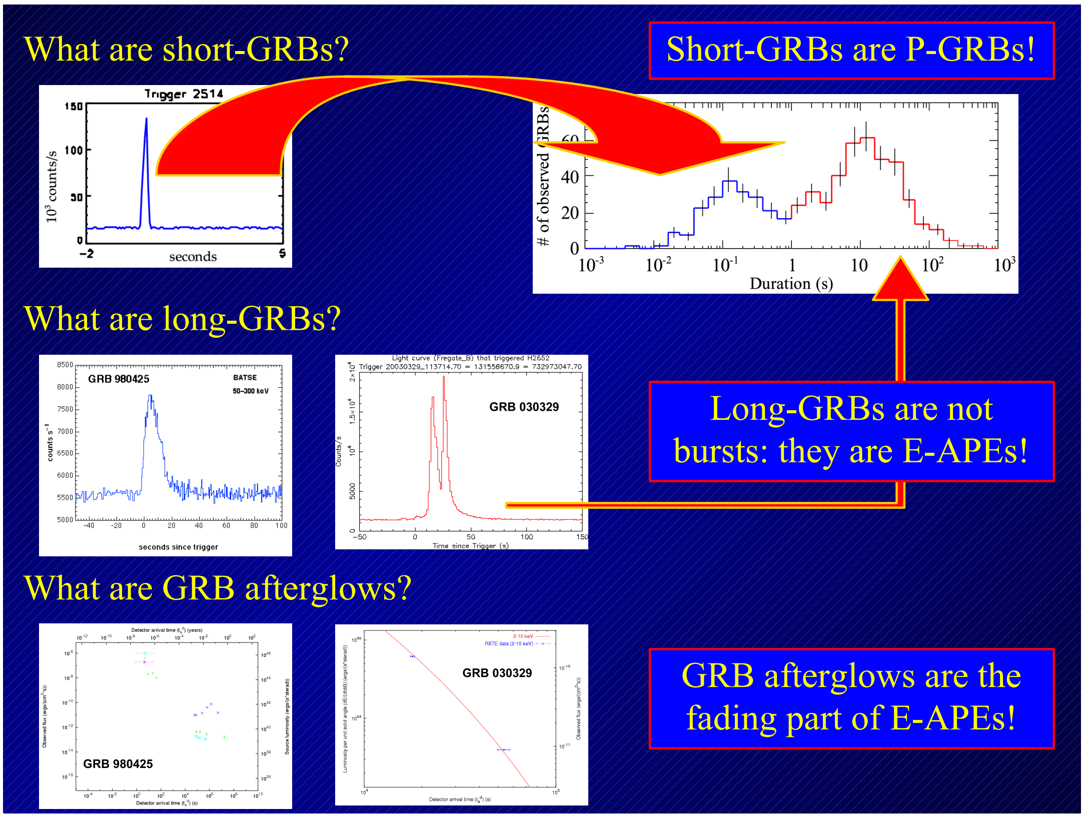

Figure A.1.6: Status of GRB observations following the BATSE and BeppoSAX observations: On the upper right part of the figure are plotted the number of the observed GRBs as a function of their duration. The bimodal distribution corresponding respectively to the short bursts, upper left figure, and the long bursts, middle figure, is quite evident. The afterglow component is represented in the lowest figures. The theoretical goal is to find a coherent astrophysical explanation for all these different phenomena.

The resonance between the X- and gamma ray astronomy from the satellites and the optical and radio astronomy from the ground, had already marked the great success and development of the astrophysics of binary X-ray sources in the seventies (see e.g. Giacconi et al., 1978). This resonance is re-proposed here for GRBs on a much larger scale. The use of much larger satellites, like Chandra and XMM-Newton, and specific space missions, like HETE-II and *Swift*, together with the very lucky circumstance of the development of optical technologies for the telescopes, such as Keck in Hawaii and VLT in Chile, offers today opportunities without precedence in the history of mankind.

Turning now to the theoretical progresses, it is interesting that the idea of using an electron-positron plasma as a basis of a GRB model, introduced in Damour and Ruffini (1975), was independently considered years later in a set of papers by Cavallo and Rees (1978), Cavallo and Horstman (1981) and Horstman and Cavallo (1983). However, these authors did not address the issue of the physical origin of their energy source. They reach their conclusions considering the pair creation and annihilation process occurring in the confinement of a large amount of energy in a region of dimension ~ 10 km typical of a neutron star. No relation to the physics of black holes nor to the energy extraction process from a black hole was envisaged in their interesting considerations, mainly directed to the study of the creation and consequent evolution of such an electron-positron plasma.

After the discovery of the afterglows and the optical identification of GRBs at cosmological distances, implying exactly the energetics predicted in Eq. (A.1.2.9), we returned to the analysis of the vacuum polarization process around a black hole and precisely identified the region around the black hole in which the vacuum polarization process and the consequent creation of electron-positron pairs occur. We defined this region, using the Greek name for pairs (δυάς, δυάδος), to be the "dyadosphere" of the black hole, bounded by the black hole horizon and the dyadosphere radius r_{ds} given by (see Ruffini, 1998; Preparata et al., 1998):

$$r_{ds} = \left(\frac{\hbar}{mc}\right)^{\frac{1}{2}} \left(\frac{GM}{c^2}\right)^{\frac{1}{2}} \left(\frac{m_{\rm p}}{m}\right)^{\frac{1}{2}} \left(\frac{e}{q_{\rm p}}\right)^{\frac{1}{2}} \left(\frac{Q}{\sqrt{G}M}\right)^{\frac{1}{2}} = 1.12 \cdot 10^8 \sqrt{\mu\xi}\,\text{cm}, \tag{A.1.3.1}$$

where we have introduced the dimensionless mass and charge parameters $\mu = M_{BH}/M_{\odot}$, $\xi = Q/(M_{BH}\sqrt{G}) \leq 1$. The total energy of the electron positron pairs, $E^{tot}_{e^{\pm}}$ is equal to the dyadosphere energy E_{dya}.

Our GRB model, like all prevailing models in the existing literature (see e.g. Piran, 2005; Mészáros, 2002; Meszaros, 2006, and references therein), is based on the acceleration of an optically thick electron-positron plasma. The mechanism responsible for the origin and the energetics of such a plasma, either in relation to black hole physics or to other physical processes, has often been discussed qualitatively in the GRB scientific literature but never quantitatively with explicit equations. The concept of the dyadosphere (Ruffini, 1998; Preparata et al., 1998) is the only attempt, as far as we know, to do this. It relates such an electron-positron plasma to black hole physics and to the features of the GRB progenitor star, using explicit equations that satisfy the existing physical laws (see e.g. Christodoulou and Ruffini (1971); Ruffini et al. (2005a) and references therein, see also Misner et al. (1973)). This step is essential if one wishes to identify the physical origin and energetics of GRBs. All the successive evolution of the electron-positron plasma are independent on this step and are indeed common to all prevailing GRB models in the literature. Of course, great differences still exist between the actual treatments of this evolution in the current literature, as we show in the next sections.

Analogies exist between the concept of dyadosphere and the work of Cavallo and Rees (1978), as well as marked conceptual differences. In the dyadosphere the created electron-positron pairs are assumed to reach thermal equilibrium and have an essential role in the dynamical acceleration process of GRBs. In Cavallo and Rees (1978) it is assumed that the created electron-positron pairs do annihilate in a cascade process in a very short bremsstrahlung time scale: they cannot participate in any way to the dynamical phases of the GRB process. It is interesting that these differences can be checked both theoretically and observationally. It should be possible, in the near future, to evaluate all the cross sections involved by the above annihilation processes and assess by a direct explicit analysis which one of the two above approaches is the correct one. On the other side, such two approaches certainly lead to very different predictions for the GRB structure, especially for the short ones. These predictions will certainly be compared to observations in the near future.

We have already emphasized that the study of GRBs is very likely "the" most extensive computational and theoretical investigation ever done in phy- -sics and astrophysics. There are at least three different fields of research which underlie the foundation of the theoretical understanding of GRBs. All three, for different reasons, are very difficult.

The first field of research is special relativity. As one of us (RR) always mention to his students in the course of theoretical physics, this field is paradoxically very difficult since it is extremely simple. In approaching special relativistic phenomena the extremely simple and clear procedures expressed by Einstein in his 1905 classic paper (Einstein, 1905) are often ignored. Einstein makes use in his work of very few physical assumptions, an almost elementary mathematical framework and gives constant attention to a proper operational definition of all observable quantities.

The second field of research essential for understanding the energetics of GRBs deals with quantum electrodynamics and the relativistic process of pair creation in overcritical electromagnetic fields as well as in very high density photon gas. This topic is also very difficult but for a quite different conceptual reason: the process of pair creation, expressed in the classic works of

Heisenberg-Euler-Schwinger (Heisenberg and Euler, 1936; Schwinger, 1951) later developed by many others, is based on a very powerful theoretical framework but has not yet been verified by experimental data. Similarly, the creation of electron-positron pairs from high density and high energy photons lacks still today the needed theoretical description. As we will show in the next sections, there is the tantalizing possibility of observing these phenomena, for the first time, in the astrophysical setting of GRBs on a more grandiose scale.

There is a third field which is essential for the understanding of the GRB phenomenon: general relativity. In this case, contrary to the case of special relativity, the field is indeed very difficult, since it is very difficult both from a conceptual, technical and mathematical point of view. The physical assumptions are indeed complex. The entire concept of geometrization of physics needs a new conceptual approach to the field. The mathematical complexity of the pseudo-Riemannian geometry contrasts now with the simple structure of the pseudo-Euclidean Minkowski space. The operational definition of the observable quantities has to take into account the intrinsic geometrical properties and also the cosmological settings of the source. With GRBs we have the possibility to follow, from a safe position in an asymptotically flat space at large distance, the formation of a black hole horizon with all the associated relativistic phenomena of light bending and time dilatation.

For these reasons GRBs offer an authentic new frontier in the field of physics and astrophysics. We recall that in the special relativity field, for the first time, we observe phenomena occurring at Lorentz gamma factors of approximately 400. In the field of relativistic quantum electro-dynamics we see for the first time the interchange between classical fields and high density photon fields with the created quantum matter-antimatter pairs. In the field of general relativity also for the first time we can test the blackholic energy which is the basic energetic physical variable underlying the entire GRB phenomenon.

The most appealing aspect of this work is that, if indeed these three different fields are treated and approached with the necessary technical and scientific maturity, the model which results has a very large redundancy built-in. The approach requires an unprecedented level of self-consistency. Any departures from the correct theoretical treatment in this very complex system lead to exponential departures from the correct solution and from the correct fit of the observations.

It is so that, as the model is being properly developed and verified, its solution will have existence and uniqueness. In order to build a theoretical GRB model, we have found necessary to establish clear guidelines by introducing three basic paradigms for the interpretation of GRBs.

A.2 The three paradigms identifying the "canonical GRBs"

A.2.1 The Relative Space-Time Transformation (RSTT) paradigm

The ongoing dialogue between our work and the one of the workers on GRBs rests still on some elementary considerations presented by Einstein in his classic article of 1905 (Einstein, 1905). These considerations are quite general and even precede Einstein's derivation, out of first principles, of the Lorentz transformations. We recall here Einstein's words: "We might, of course, content ourselves with time values determined by an observer stationed together with the watch at the origin of the co-ordinates, and co-ordinating the corresponding positions of the hands with light signals, given out by every event to be timed, and reaching him through empty space. But this co-ordination has the disadvantage that it is not independent of the standpoint of the observer with the watch or clock, as we know from experience".

The message by Einstein is simply illustrated in Fig. A.2.1. If we consider in an inertial frame a source (solid green line) moving with high speed and emitting light signals (dashed red lines) along the direction of its motion, a far away observer will measure a delay Δt_a between the arrival time of two signals respectively emitted at the origin and after a time interval Δt in the laboratory frame, which in our case is the frame where the black hole is at rest. The real velocity of the source is given by:

$$v = \frac{\Delta r}{\Delta t} \tag{A.2.1.1}$$

and the apparent velocity is given by:

$$v_{app} = \frac{\Delta r}{\Delta t_a}\,, \tag{A.2.1.2}$$

As pointed out by Einstein the adoption of coordinating light signals simply by their arrival time as in Eq.(A.2.1.2), without an adequate definition of synchronization, is incorrect and leads to unsurmountable difficulties as well as

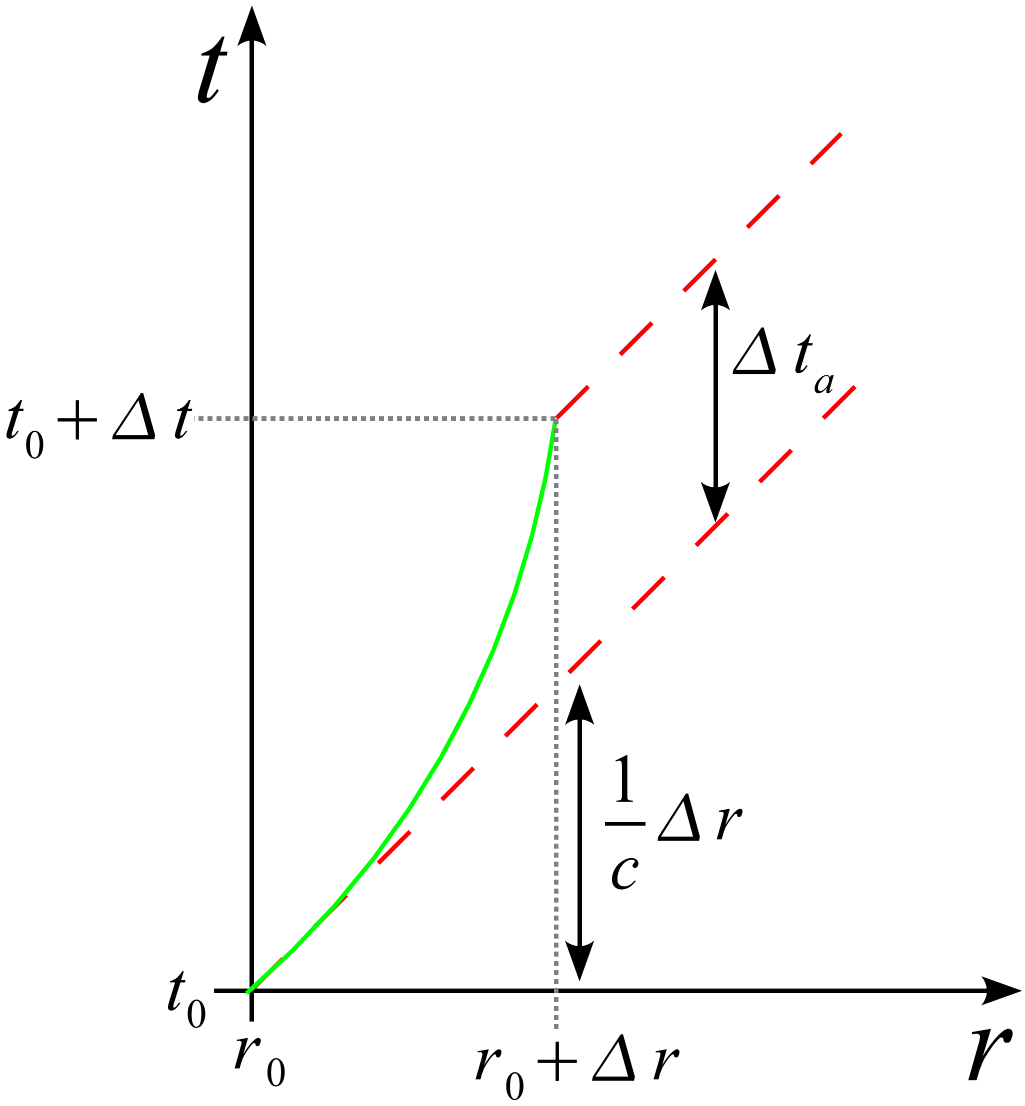

Figure A.2.1: Relation between the arrival time t_a and the laboratory time t. Details in Ruffini et al. (2001c, 2003).

to apparently "superluminal" velocities as soon as motions close to the speed of light are considered.

The use of Δt_a as a time coordinate should be done with proper care. The relation between Δt_a and the correct time parameterization in the laboratory frame has to be taken into account:

$$\Delta t_a = \Delta t - \frac{\Delta r}{c} = \Delta t - \frac{1}{c}\int_{t_\circ}^{t_\circ+\Delta t} v\left(t'\right) dt' . \tag{A.2.1.3}$$

In other words, the relation between the arrival time and the laboratory time cannot be done without a knowledge of the speed along the *entire* world-line of the source. In the case of GRBs, such a worldline starts at the moment of gravitational collapse. It is of course clear that the parameterization in the laboratory frame has to take into account the cosmological redshift z of the source. We then have, at the detector:

$$\Delta t_a^d = (1+z)\,\Delta t_a . \tag{A.2.1.4}$$

In the current GRB literature, Eq.(A.2.1.3) has been systematically neglected by addressing only the afterglow description. Often the integral equation has been approximated by a clearly incorrect instantaneous value:

$$\Delta t_a \simeq \frac{\Delta t}{2\gamma^2} . \tag{A.2.1.5}$$

The attitude has been adopted to consider separately the afterglow part of the GRB phenomenon, without the knowledge of the entire equation of motion of the source.

This point of view has reached its most extreme expression in the works reviewed by Piran (1999, 2000), where the so-called "prompt radiation", lasting on the order of 10^2 s, is considered as a burst emitted by the prolonged activity of an "inner engine". In these models, generally referred to as the "internal shock model", the emission of the afterglow is assumed to follow the "prompt radiation" phase (Rees and Meszaros, 1994; Paczynski and Xu, 1994; Sari and Piran, 1997; Fenimore, 1999; Fenimore et al., 1999).

As we outline in the following sections, this point of view originates from the inability of obtaining the time scale of the "prompt radiation" from a burst structure. These authors consequently appeal to the existence of an "ad hoc" inner engine in the GRB source to solve this problem.

We show in the following sections how this difficulty has been overcome in our approach by interpreting the "prompt radiation" as an integral part of the afterglow and *not* as a burst. This explanation can be reached only through a relativistically correct theoretical description of the entire afterglow (see section A.4) for which is essential the knowledge of the entire past worldline of the source. We show that at 10^2 seconds the emission occurs from a region of dimensions of approximately 10^{16} cm, well within the region of activity of the afterglow.

We can now turn to the first paradigm, the relative space-time transformation (RSTT) paradigm (Ruffini et al., 2001c) which emphasizes the importance of a global analysis of the GRB phenomenon encompassing both the optically thick and the afterglow phases. Since all the data are received in the detector arrival time, it is essential to know the equations of motion of all relativistic phases with $\gamma > 1$ of the GRB sources in order to reconstruct the time coordinate in the laboratory frame, see Eq.(A.2.1.3). Contrary to other phenomena in nonrelativistic physics or astrophysics, where every phase can be examined separately from the others, in the case of GRBs all the phases are inter-related by their signals received in arrival time t_a^d. It is necessary, in order to describe the physics of the source, to derive the laboratory time t as a function of the arrival time t_a^d along the entire past worldline of the source using Eq.(A.2.1.4).

An additional difference, also linked to special relativity, between our treatment and the ones in the current literature relates to the assumption of the existence of scaling laws in the afterglow phase: the power law dependence of the Lorentz gamma factor on the radial coordinate is usually systematically assumed. From the proper use of the relativistic transformations and by the direct numerical and analytic integration of the special relativistic equations of motion we demonstrate (see the following report about "Relativistic effects in Physics and Astrophysics") that no simple power-law relation can be derived for the equations of motion of the system. This situation is not new for workers in relativistic theories: scaling laws exist in the extreme ultrarelativistic regimes and in the Newtonian ones but not in the intermediate fully relativistic regimes (see e.g. Ruffini, 1973).

A.2.2 The Interpretation of the Burst Structure (IBS) paradigm

We turn now to the second paradigm, which is more complex since it deals with all the different phases of the GRB phenomenon. We first address the dynamical phases following the dyadosphere formation.

After the vacuum polarization process around a black hole, one of the topics of the greatest scientific interest is the analysis of the dynamics of the electron-positron plasma formed in the dyadosphere. This issue was addressed by us in a collaboration with Jim Wilson at Livermore. The numerical simulations of this problem were developed at Livermore, while the semi-analytic approach was developed in Rome (see Ruffini et al., 1999, 2000, and section A.3).

The corresponding treatment in the framework of the Cavallo, Rees et al.

analysis was performed by Piran et al. (1993) also using a numerical approach, by Bisnovatyi-Kogan and Murzina (1995) using an analytic approach and by Meszaros et al. (1993) using a numerical and semi-analytic approach.

Although some analogies exists between these treatments, they are significantly different in the theoretical details and in the final results (see Bianco et al., 2006b, and section the following report about "Relativistic effects in Physics and Astrophysics"). Since the final result of the GRB model is extremely sensitive to any departure from the correct treatment, it is indeed very important to detect at every step the appearance of possible errors.

A.2.2.1 The optically thick phase of the fireshell

There are some common conclusion to all these treatments: the electron-positron plasma is initially optically thick and expands reaching very high values of the Lorentz gamma factor until the transparency; the plasma shell expands but the Lorentz contraction is such that its width in the laboratory frame appears to be constant. This self acceleration of the thin shell is the distinguishing factor of GRBs, conceptually very different from the physics of a fireball developed by the inner pressure of an atomic bomb explosion in the Earth's atmosphere. In the case of GRBs the region interior to the shell is inert and with pressure totally negligible: the entire dynamics occurs on the shell itself. For this reason, we refer in the following to the self accelerating shell as the "fireshell".

There is a major difference between our approach and the ones of Piran, Mészáros and Rees. In our approach the dyadosphere is assumed to be initially filled uniquely with an electron-positron plasma, without any baryonic contamination. Such an electron-positron plasma expands in substantial agreement with the results presented in the work of Bisnovatyi-Kogan and Murzina (1995). In our model the fireshell of electron-positron pairs and photons (PEM pulse, see Ruffini et al., 1999) evolves and then meets the remnant of the star progenitor of the newly formed black hole. The fireshell is then loaded with baryons. A new fireshell is formed of electron-positron-photons and baryons (PEMB pulse, see Ruffini et al., 2000) which expands all the way until transparency is reached. At transparency the emitted photons give origin to the P-GRB (see Ruffini et al., 2001b, and Fig. A.2.2).

In our approach, the baryon loading is measured by a dimensionless quantity

$$B = \frac{M_B c^2}{E_{dya}}, \tag{A.2.2.1}$$

which gives direct information about the mass $M_B = N_B m_p$ of the remnant, where m_p is the proton mass. The corresponding treatment done by Piran and collaborators (Shemi and Piran, 1990; Piran et al., 1993) and by Meszaros et al. (1993) differs in one important respect: the baryonic loading is assumed

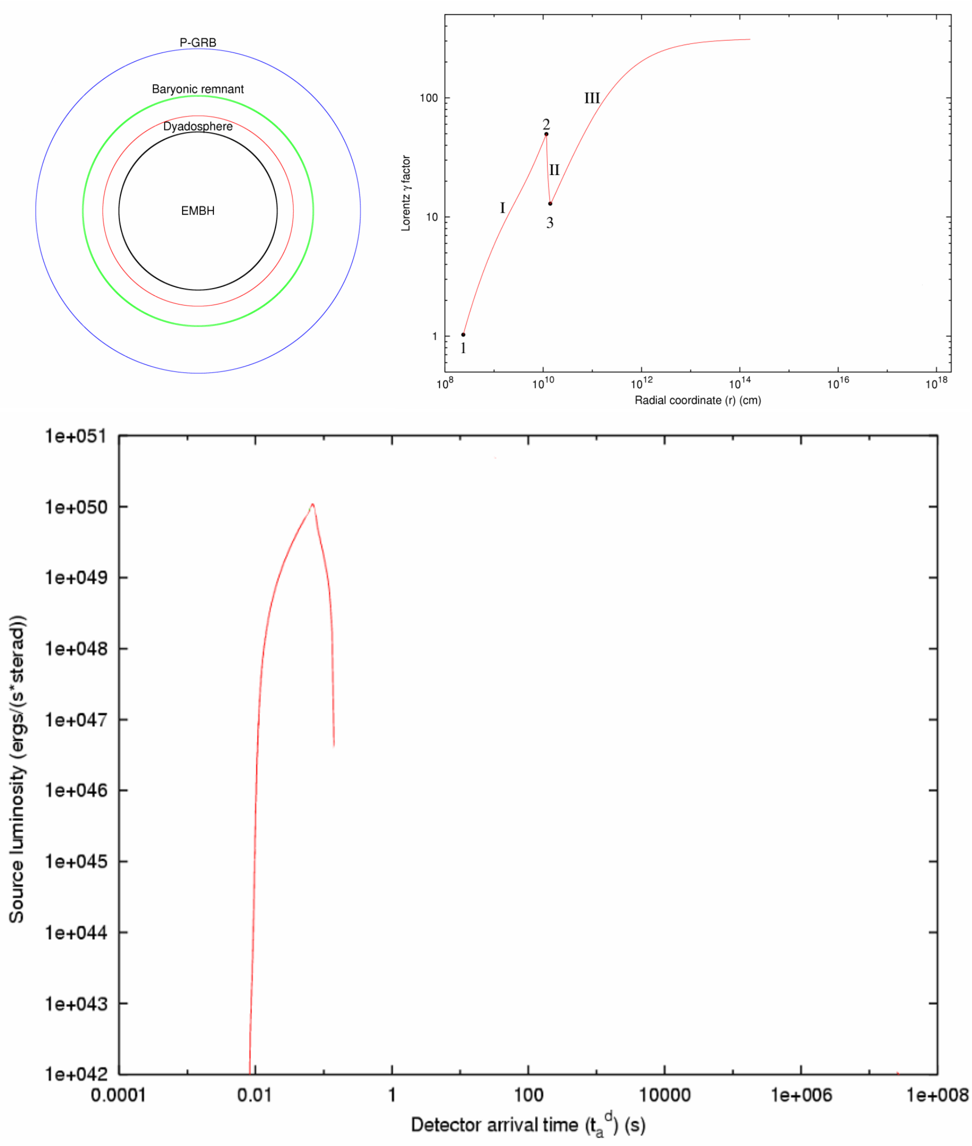

Figure A.2.2: Above: The optically thick phase of the fireshell evolution are qualitatively represented in this diagram. There are clearly recognizable 1) the PEM pulse phase, 2) the impact on the baryonic remnant, 3) the PEMB pulse phase and the final approach to transparency with the emission of the P-GRB. Details in Ruffini et al. (2003). Below: The P-GRB emitted at the transparency point at a time of arrival t_a^d which has been computed following the prescriptions of Eq.(A.2.1.3). Details in Ruffini et al. (2001b, 2003).

to occur from the beginning of the electron-positron pair formation and no relation to the mass of the remnant of the collapsed progenitor star is attributed to it. While our results are comparable with the ones obtained by Piran under the same initial conditions, the set of approximations adopted by Meszaros et al. (1993) appears to be too radical and leads to different results violating energy and momentum conservation (see section the following report about "Relativistic effects in Physics and Astrophysics"and Bianco et al., 2006b).

From our analysis (Ruffini et al., 2000) it also becomes clear that such expanding dynamical evolution can only occur for values of $B \leq 10^{-2}$. This prediction, as we will show shortly in the many GRB sources considered, is very satisfactorily confirmed by observations.

From the value of the B parameter, related to the mass of the remnant, it therefore follows that the collapse to a black hole leading to a GRB is drastically different from the collapse to a neutron star. While in the case of a neutron star collapse a very large amount of matter is expelled, in many instances well above the mass of the neutron star itself, in the case of black holes leading to a GRB only a very small fraction of the initial mass ($\sim 10^{-2}$ or less) is ejected. The collapse to a black hole giving rise to a GRB appears to be much smoother than any collapse process considered until today: almost 99.9% of the star has to be collapsing simultaneously!

We summarize in Fig. A.2.2 the optically thick phase of the fireshell evolution: we start from a given total electron-positron pairs energy $E^{tot}_{e^\pm}$; the fireshell self-accelerates outward; an abrupt decrease in the value of the Lorentz gamma factor occurs by the engulfment of the baryonic loading followed by a further self-acceleration until the fireshell becomes transparent.

The photon emission at this transparency point is the P-GRB. An accelerated beam of baryons with an initial Lorentz gamma factor $\gamma_\circ$ starts to interact with the interstellar medium at typical distances from the black hole of $r_\circ \sim 10^{14}$ cm and at a photon arrival time at the detector on the Earth surface of $t_a^d \sim 0.1$ s. These values determine the initial conditions of the afterglow.

A.2.2.2 The afterglow

After reaching transparency and the emission of the P-GRB, the ABM pulse interacts with the CBM and gives rise to the afterglow (see Fig. A.2.3).

We first look to the initial value problem. The initial conditions of the afterglow era are determined at the end of the optically thick era when the P-GRB is emitted. As recalled in the section A.5, the transparency condition is determined by a time of arrival t_a^d, a value of the Lorentz gamma factor $\gamma_\circ$, a value of the radial coordinate $r_\circ$, an amount of baryonic matter M_B which are only functions of the two parameters $E^{tot}_{e^\pm}$ and B (see Eq.(A.2.2.1)).

This connection to the optically thick era is missing in the current approach in the literature (see Piran, 1999, and references therein). The initial condi-

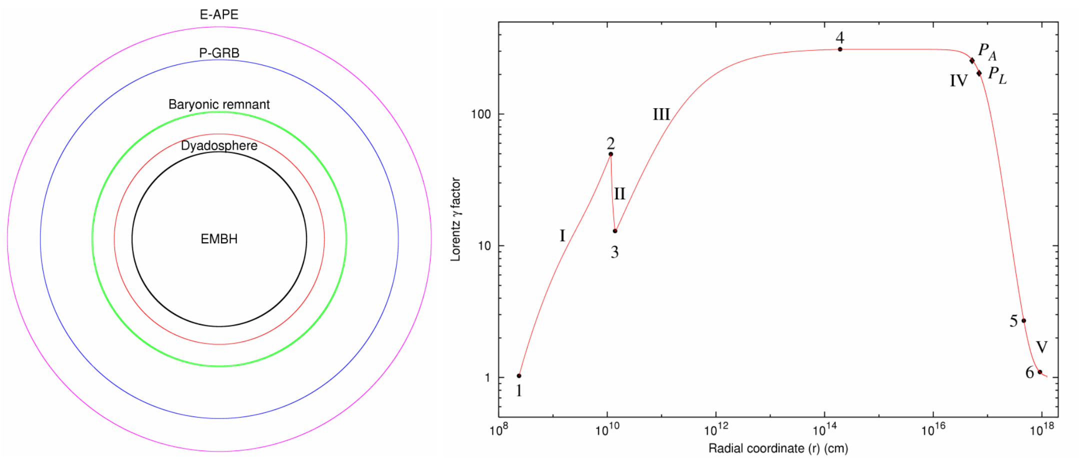

Figure A.2.3: The GRB afterglow phase is here represented together with the optically thick phase (see Fig. A.2.2). The value of the Lorentz gamma factor is here given from the transparency point all the way to the ultrarelativisitc, relativistic and non relativistic regimes. Details in Ruffini et al. (2003).

tions at the beginning of the afterglow are obtained by a best fit of the later parts of the afterglow. The order of magnitude estimate usually quoted for the characteristic time scale to be expected for a burst emitted by a GRB at the moment of transparency at the end of the optically thick expansion phase is given by $\tau \sim GM/c^3$. For a $10M_\odot$ black hole this will give $\sim 10^{-3}$ s. There are reasons today not to take seriously such an order of magnitude estimate (see e.g. Ruffini et al., 2005d). In any case this time is much shorter than the ones typically observed in "prompt radiation" of the long bursts, from a few seconds all the way to 10^2 s. In the current literature, in order to explain the "prompt radiation" and overcome the above difficulty it has been generally assumed that its origin should be related to a prolonged "inner engine" activity preceding the afterglow which is not well identified.

The way out of this dichotomy in our model is drastically different: **1)** indeed the optically thick phase exists, is crucial to the GRB phenomenon and terminates with a burst: the P-GRB; **2)** the "prompt radiation" follows the P-GRB; **3)** the "prompt radiation" is not a burst: it is actually the temporally extended peak emission of the afterglow (E-APE). The observed structures of the prompt radiation can all be traced back to inhomogeneities in the CBM (see Fig. A.2.4 and Ruffini et al., 2002a).

This approach was first tested on GRB 991216. Both the relative intensity and time separation of the P-GRB and the afterglow were duly explained (see Fig. A.2.4) choosing a total electron-positron pairs energy $E^{tot}_{e^\pm} = 4.83 \times 10^{53}$ erg and a baryon loading $B = 3.0 \times 10^{-3}$ (see Ruffini et al., 2001b, 2002a, 2003, 2005a). Similarly, the temporal substructure in the prompt emission was explicitly shown to be related to the CBM inhomogeneities (see section A.5.1).

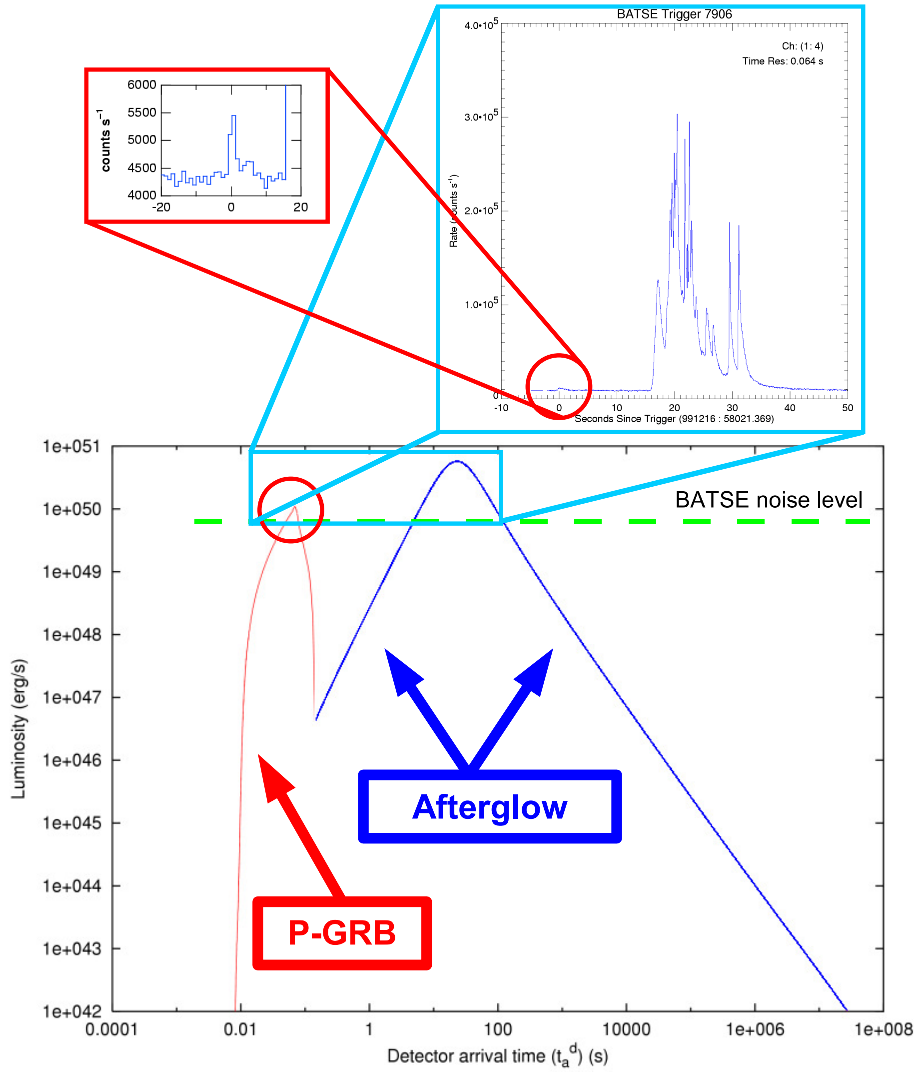

Figure A.2.4: The detailed features of GRB 991216 evidenced by our theoretical models are here reproduced. The P-GRB, the "prompt radiation" and what is generally called the afterglow. The prompt emission observed by BATSE coincides with the extended afterglow peak emission (E-APE) and has been considered as a burst only as a consequence of the high noise threshold in the observations. The small precursor is identified with the P-GRB. For this source we have $B \simeq 3.0 \times 10^{-3}$ and $\langle n_{cbm} \rangle \sim 1.0$ particles/cm^3. Details in Ruffini et al. (2001b, 2002a, 2003, 2005a).

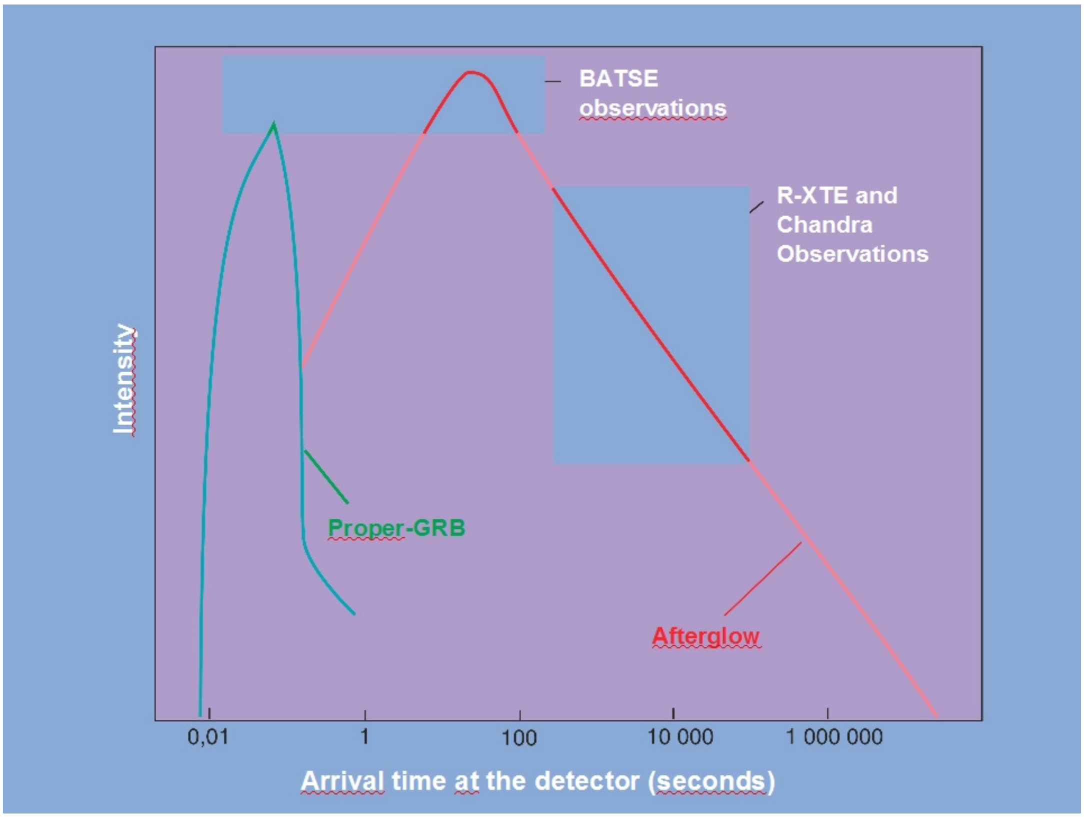

Figure A.2.5: Bolometric luminosity of P-GRB and afterglow as a function of the arrival time. Details in Ruffini et al. (2003). Reproduced and adapted from Ruffini et al. (2002b) with the kind permission of the publisher.

Following this early analysis, and the subsequent ones on additional sources, it became clear that the CBM structure evidenced by our analysis is quite different from the traditional description in the current literature. Far from considering analogies with shock wave processes developed within fluidodynamic approach, it appears to us that the correct CBM description is a discrete one, composed of uncorrelated overdense “blobs” of typical size $\Delta R \sim 10^{14}$ cm widely spaced in underdense and inert regions.

We can then formulate the second paradigm, the interpretation of the burst structure (IBS) paradigm (Ruffini et al., 2001b), which covers three fundamental issues leading to the unequivocal identification of the canonical GRB structure:
a) the existence of two different components: the P-GRB and the afterglow related by precise equations determining their relative amplitude and temporal sequence (see Fig. A.2.5, Ruffini et al., 2003, and section A.5);
b) what in the literature has been addressed as the “prompt emission” and considered as a burst, in our model is not a burst at all — instead it is just the emission from the peak of the afterglow (see the clear confirmation of this

result by the *Swift* data of e.g. GRB 050315 in section A.9 and in Ruffini et al., 2006a,b);
c) the crucial role of the parameter B in determining the relative amplitude of the P-GRB to the afterglow and discriminating between the short and the long bursts (see Fig. A.2.6). Both short and long bursts arise from the same physical phenomena: the gravitational collapse to a black hole endowed with electromagnetic structure and the formation of its dyadosphere.

The fundamental diagram determining the relative intensity of the P-GRB and the afterglow as a function of the dimensionless parameter B is shown in Fig. A.2.6. The main difference relates to the amount of baryonic matter engulfed by the electron-positron plasma in their optically thick phase prior to transparency. For $B < 10^{-5}$ the intensity of the P-GRB is larger and dominates the afterglow. This corresponds to the "genuine" short bursts (see section A.5.2 and Bernardini et al., 2007). For $10^{-5} < B \leq 10^{-2}$ the afterglow dominates the GRB. For $B > 10^{-2}$ we may observe a third class of "bursts", eventually related to a turbulent process occurring prior to transparency (Ruffini et al., 2000). This third family should be characterized by smaller values of the Lorentz gamma factors than in the case of the short or long bursts.

Particularly enlightening for the gradual transition to the short bursts as a function of the B parameter is the diagram showing how GRB 991216 bolometric light curve would scale changing the only B value (see Fig. A.2.7).

Moving from these two paradigms, and the prototypical case of GRB 991216, we have extended our analysis to a larger number of sources, such as GRB 970228 (Bernardini et al., 2007), GRB 980425 (Ruffini et al., 2004a, 2007b), GRB 030329 (Bernardini et al., 2004), GRB 031203 (Bernardini et al., 2005a), GRB 050315 (Ruffini et al., 2006b), which have led to a confirmation of the validity of our canonical GRB structure (see Fig. A.2.8). In addition, progresses have been made in our theoretical comprehension, which will be presented in the section A.5.2.

A.2.3 The GRB-Supernova Time Sequence (GSTS) paradigm

Following the result of Galama et al. (1998) who discovered the temporal coincidence of GRB 980425 and SN 1998bw, the association of other nearby GRBs with Type Ib/c SNe has been spectroscopically confirmed (see Tab. A.2.1). The approaches in the current literature have attempted to explain both the SN and the GRB as two aspects of the same astrophysical phenomenon. Hence, GRBs have been assumed to originate from a specially strong SN process, a hypernova or a collapsar (see e.g. Paczynski, 1998; Kulkarni et al., 1998; Iwamoto et al., 1998; Woosley and Bloom, 2006, and references

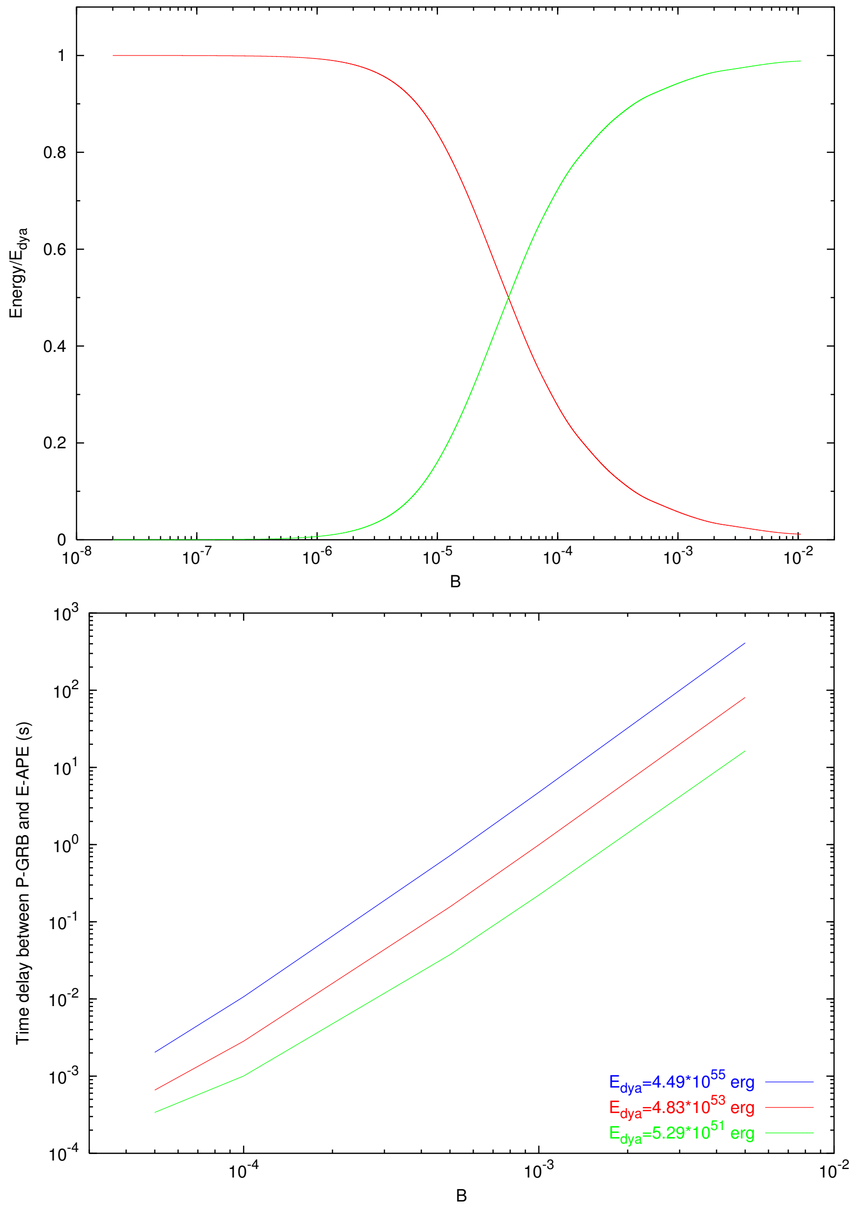

Figure A.2.6: Above: The energy radiated in the P-GRB (the red line) and in the afterglow (the green line), in units of the total electron-positron pairs energy ($E^{tot}_{e^{\pm}} = E_{dya}$), are plotted as functions of the B parameter. **Below:** The arrival time delay between the P-GRB and the peak of the afterglow is plotted as a function of the B parameter for three selected values of E_{dya}.

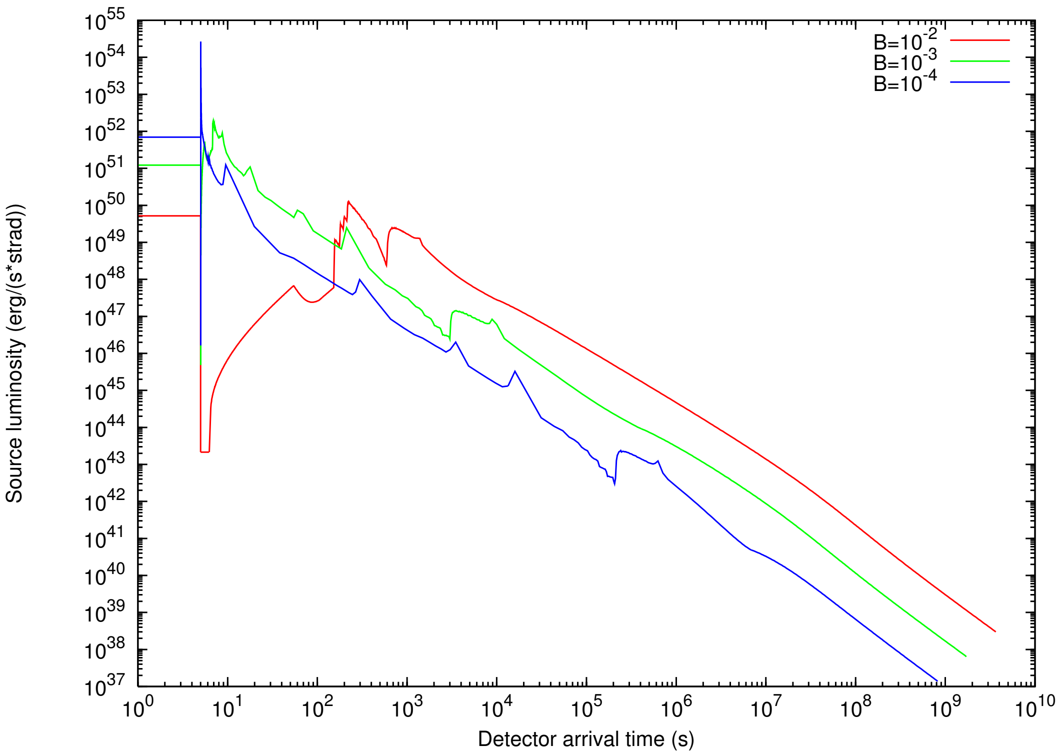

Figure A.2.7: The bolometric luminosity of a source with the same total energy and CBM distribution of GRB991216 is here represented for selected values of the B parameter, ranging from $B = 10^{-2}$ to $B = 10^{-4}$. The actual value for GRB991216 is $B = 3.0 \times 10^{-3}$. As expected, for smaller values of the B parameter the intensity of the P-GRB increases and the total energy of the afterglow decreases. What is most remarkable is that the luminosity in the early part of the afterglow becomes very spiky and the peak luminosity actually increases.

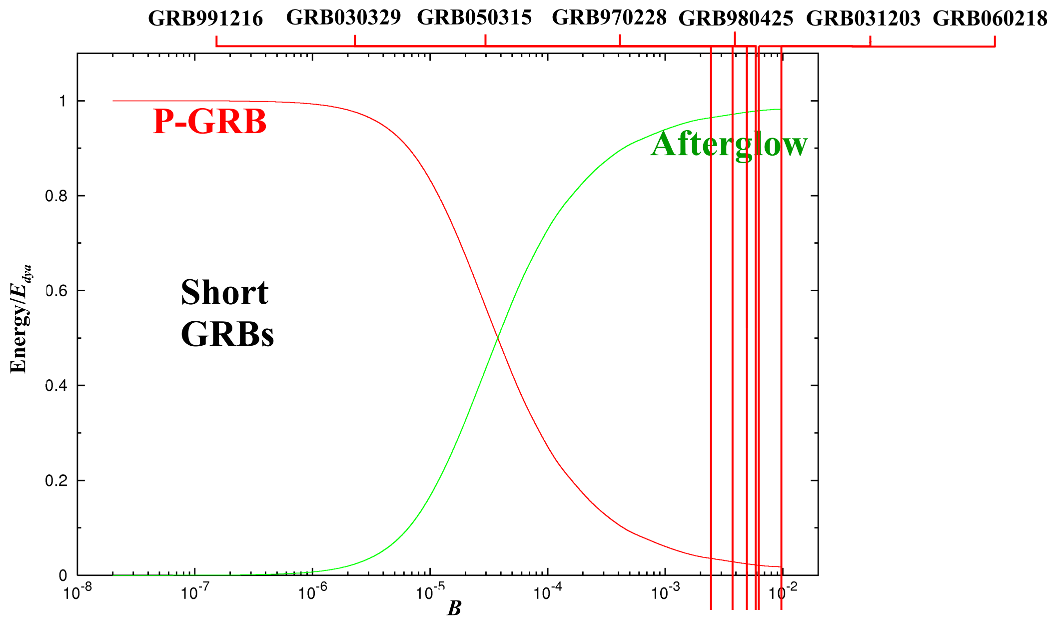

Figure A.2.8: Same as Fig. A.2.6 with the values determined for GRB 991216, GRB 030329, GRB 980425, GRB 970228, GRB 050315, GRB 031203, GRB 060218. Remarkably, they are consistently smaller than, or equal to in the special case of GRB 060218, the absolute upper limit $B \lesssim 10^{-2}$ established in Ruffini et al. (2000). In order to determine the value of the B parameter and the total energy we have performed the complete fit of each source. In particular, we have fitted for each source the observed luminosities in selected energy bands of the entire afterglow including the prompt emission. We have verified that in each source the hard-to-soft spectral evolution is correctly fitted and we have compared the theoretically computed spectral lag with the observations. Where applicable, we have also computed the relative intensity and temporal separation between the P-GRB and the peak of the afterglow and compared these values with the observed ones. The absence of spectral lag in the P-GRB is automatically verified by our model.

Table A.2.1: see: a) Ruffini et al. (2007b); b) Bernardini et al. (2005a); c) Bernardini et al. (2004); d) Ruffini et al. (2006b); e) Bernardini et al. (2007); f) Ruffini et al. (2005a); g) see Kaneko et al. (2007); h) Mazzali, P., private communication at MG11 meeting in Berlin, July 2006; i) evaluated fitting the URCAs with a power law followed by an exponentially decaying part; j) respectively Mirabal et al. (2006), Galama et al. (1998), Prochaska et al. (2004), Greiner et al. (2003), Kelson and Berger (2005), Infante et al. (2001), Bloom et al. (2001), Piro (2001); k) respectively Kennea et al. (2006), Sakamoto et al. (2006a), XRR is considered in Kennea et al. (2006), while XRF as suggested by Watson et al. (2004), Kennea et al. (2006), Vaughan et al. (2006), Bloom et al. (2001).

GRB/SN	$E_{e^\pm}^{tot}$	$E_{SN}^{bolom\,g}$	$E_{SN}^{kin\,h}$	E_{URCA}^{i}	B	$\gamma_\circ$	z^j	S_X/S_γ^k	$\langle n_{ism}\rangle$ (#/cm^3)
060218/2006aj	1.8×10^{50}	9.2×10^{48}	2.0×10^{51}	?	1.0×10^{-2}	99	0.033	3.54(XRF)	1.0
980425/1998bw[a]	1.2×10^{48}	2.3×10^{49}	1.0×10^{52}	3×10^{48}	7.7×10^{-3}	124	0.0085	0.58 (XRR)	2.5×10^{-2}
031203/2003lw[b]	1.8×10^{50}	3.1×10^{49}	1.5×10^{52}	2×10^{49}	7.4×10^{-3}	133	0.105	0.49(XRR/XRF)	0.3
030329/2003dh[c]	2.1×10^{52}	1.8×10^{49}	8.0×10^{51}	3×10^{48}	4.8×10^{-3}	206	0.168	0.56(XRR)	1.0
050315[d]	1.5×10^{53}				4.5×10^{-3}	217	1.949	1.58(XRF)	0.8
970228/?[e]	1.4×10^{54}				5.0×10^{-3}	326	0.695	GRB	1.0×10^{-3}
991216[f]	4.8×10^{53}				2.7×10^{-3}	340	1.0	GRB	3.0

therein). Both these possibilities imply very dense and strongly wind-like CBM structure.

In our model we assumed that the GRB consistently originates from the gravitational collapse to a black hole. The SN follows instead the very complex pattern of the final evolution of a massive star, possibly leading to a neutron star or to a complete explosion but never to a black hole. The temporal coincidence of the two phenomena, the SN explosion and the GRB, have then to be explained by the novel concept of "induced gravitational collapse", introduced in Ruffini et al. (2001a). We have to recognize that still today we do not have a precise description of how this process of "induced gravitational collapse" occurs. At this stage, it is more a framework to be implemented by additional theoretical work and observations. Two different possible scenarios have been outlined. In the first version (Ruffini et al., 2001a) we have considered the possibility that the GRBs may have caused the trigger of the SN event. For the occurrence of this scenario, the companion star had to be in a very special phase of its thermonuclear evolution and three different possibilities were considered:

1. A white dwarf, close to its critical mass. In this case, the GRB may implode the star enough to ignite thermonuclear burning.

2. The GRB enhances in an iron-silicon core the capture of the electrons on the iron nuclei and consequently decreases the Fermi energy of the core, leading to the onset of gravitational instability.

3. The pressure waves of the GRB may trigger a massive and instantaneous nuclear burning process leading to the collapse.

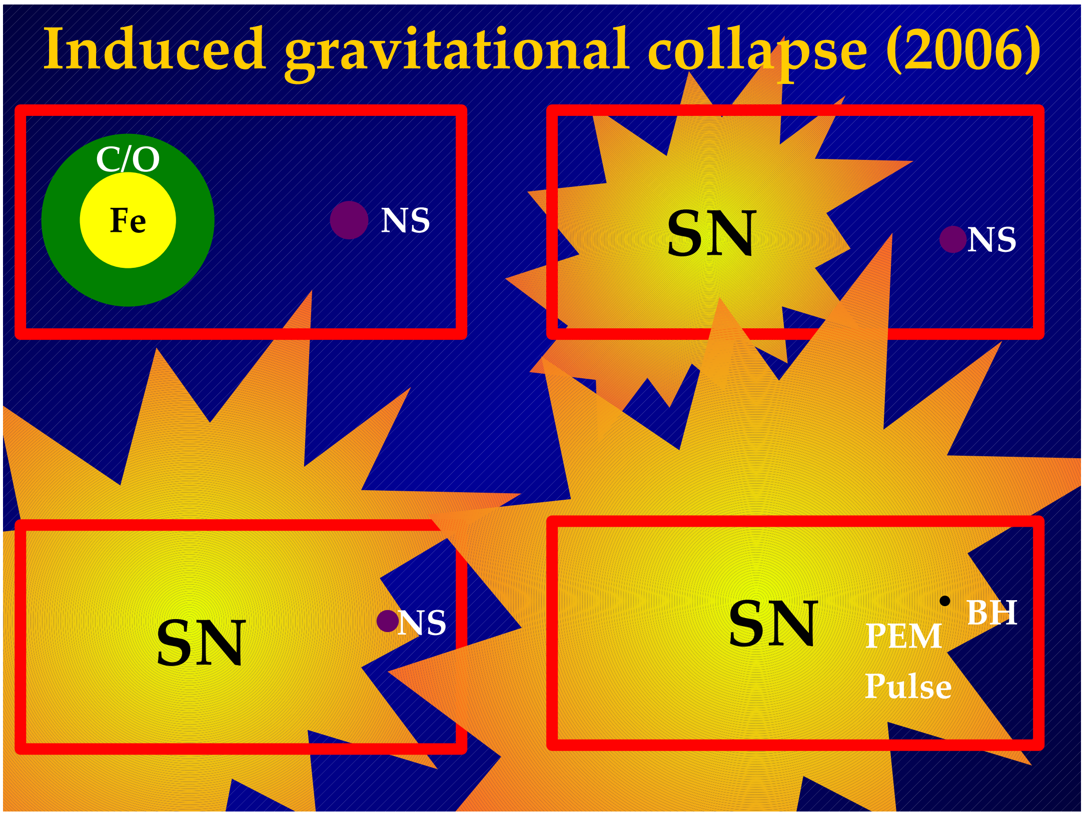

Figure A.2.9: A possible process of gravitational collapse to a black hole "induced" by the Ib/c SN on a companion neutron star in a close binary system. Details in Ruffini (2006).

More recently (see Ruffini, in pressa; Ruffini et al., 2007b), a quite different possibility has been envisaged: the SN, originating from a very evolved core, undergoes explosion in presence of a companion neutron star with a mass close to its critical one. The SN blast wave may then trigger the collapse of the companion neutron star to a black hole and the emission of the GRB (see Fig. A.2.9). It is clear that, in both scenarios, the GRB and the SN occur in a binary system.

There are many reasons to propose this concept of "induced gravitational collapse":

1. The fact that GRBs occur from the gravitational collapse to a black hole.

2. The fact that CBM density for the occurrence of GRBs is inferred from the analysis of the afterglow to be on the order of 1 particle/cm^3 (see Tab. A.2.1) except for few cases (see e.g. sections A.7 and A.12). This implies that the process of collapse has occurred in a region of space filled with a very little amount of baryonic matter. The only significant contribution to the baryonic matter component in this process is

the one represented by the fireshell baryon loading, which is anyway constrained by the inequality $B \leq 10^{-2}$.

3. The fact that the energetics of the GRBs associated with SNe appears to be particularly weak is consistent with the energy originating from the gravitational collapse to the smallest possible black hole: the one with mass M just over the neutron star critical mass.

There are also at work very clearly selection effects among the association between SNe and GRBs:

1. Many type Ib/c SNe exists without an associated GRB (Guetta and Della Valle, 2007).

2. Some GRBs do not show the presence of a SN associated, although they are close enough for the SN to be observed (see e.g. Della Valle et al., 2006).

3. The presence in all observed GRB-SN systems of an URCA source, a peculiar late time X-ray emission. These URCA sources have been identified and presented for the first time at the Tenth Marcel Grossmann meeting held in Rio de Janeiro (Brazil) in the Village of Urca, and named consequently. They appear to be one of the most novel issues still to be understood on GRBs. We will return on these aspects in the section A.7.5.

The issue of triggering the gravitational collapse instability induced by the GRB on the progenitor star of the supernova or, vice versa, by the supernova on the progenitor star of the GRB needs accurate timing. The occurrence of new nuclear physics and/or relativistic phenomena is very likely. The general relativistic instability induced on a nearby star by the formation of a black hole needs some very basic new developments.

Only a very preliminary work exists on this subject, by Jim Wilson and his collaborators (see e.g. the paper by Mathews and Wilson, 2005). The reason for the complexity in answering such a question is simply stated: unlike the majority of theoretical work on black holes and binary X-ray sources, which deals mainly with one-body black hole solutions in the Newtonian field of a companion star, we now have to address a many-body problem in general relativity. We are starting in these days to reconsider, in this framework, some classic works by Fermi (1921); Hanni and Ruffini (1973); Majumdar (1947); Papapetrou (1945); Parker et al. (1973); Bini et al. (2007a,b) which may lead to a new understanding of general relativistic effects in these many-body systems. This is a welcome effect of GRBs on the conceptual development of general relativity.

A.3 The optically thick “fireshell”

After this excursus on historical background let’s start with the description of equations characterizing the e^+e^- plasma.

A.3.1 The fireshell in the Livermore code

A.3.1.1 The hydrodynamics and the rate equation for the plasma of e^+e^--pairs

The evolution of the e^+e^--pair plasma generated in the dyadosphere has been treated in Ruffini et al. (1999, 2000). We recall here the basic governing equations in the most general case in which the plasma fluid is composed of e^+e^--pairs, photons and baryonic matter. The plasma is described by the stress-energy tensor

$$T^{\mu\nu} = pg^{\mu\nu} + (p+\rho)U^\mu U^\nu\,, \tag{A.3.1.1}$$

where ρ and p are respectively the total proper energy density and pressure in the comoving frame of the plasma fluid and U^μ is its four-velocity, satisfying

$$g_{tt}(U^t)^2 + g_{rr}(U^r)^2 = -1\,, \tag{A.3.1.2}$$

where U^r and U^t are the radial and temporal contravariant components of the 4-velocity and

$$ds^2 = g_{tt}(r)dt^2 + g_{rr}(r)dr^2 + r^2 d\theta^2 + r^2\sin^2\theta d\phi^2\,, \tag{A.3.1.3}$$

where $g_{tt}(r) \equiv -\alpha^2(r)$, $g_{rr}(r) = \alpha^{-2}(r)$, $\alpha^2 = \alpha^2\,(r) = 1 - 2M/r + Q^2/r^2$ (M and Q are the total energy and charge of the core as measured at infinity).

The conservation law for baryon number can be expressed in terms of the proper baryon number density n_B

$$\begin{aligned}(n_B U^\mu)_{;\mu} &= g^{-\frac{1}{2}}(g^{-\frac{1}{2}} n_B U^\nu)_{,\nu} \\ &= (n_B U^t)_{,t} + \frac{1}{r^2}(r^2 n_B U^r)_{,r} = 0\,. \end{aligned} \tag{A.3.1.4}$$

The radial component of the energy-momentum conservation law of the plasma fluid reduces to

$$\frac{\partial p}{\partial r} + \frac{\partial}{\partial t}\left((p+\rho)U^t U_r\right) + \frac{1}{r^2}\frac{\partial}{\partial r}\left(r^2(p+\rho)U^r U_r\right) - \frac{1}{2}(p+\rho)\left[\frac{\partial g_{tt}}{\partial r}(U^t)^2 + \frac{\partial g_{rr}}{\partial r}(U^r)^2\right] = 0\,. \tag{A.3.1.5}$$

The component of the energy-momentum conservation law of the plasma fluid equation along a flow line is

$$\begin{aligned} U_\mu (T^{\mu\nu})_{;\nu} &= -(\rho U^\nu)_{;\nu} - p(U^\nu)_{;\nu}, \\ &= -g^{-\frac{1}{2}}(g^{\frac{1}{2}}\rho U^\nu)_{,\nu} - p g^{-\frac{1}{2}}(g^{\frac{1}{2}}U^\nu)_{,\nu} \\ &= (\rho U^t)_{,t} + \frac{1}{r^2}(r^2\rho U^r)_{,r} \\ &+ p\left[(U^t)_{,t} + \frac{1}{r^2}(r^2 U^r)_{,r}\right] = 0\,. \end{aligned} \tag{A.3.1.6}$$

We define also the total proper internal energy density ϵ and the baryonic mass density ρ_B in the comoving frame of the plasma fluid,

$$\epsilon \equiv \rho - \rho_B, \quad \rho_B \equiv n_B m c^2\,. \tag{A.3.1.7}$$

A.3.1.2 The numerical integration

A computer code (Wilson et al., 1998a,b) has been used to evolve the spherically symmetric general relativistic hydrodynamic equations starting from the dyadosphere.

We define the generalized gamma factor γ and the radial 3-velocity in the laboratory frame V^r

$$\gamma \equiv \sqrt{1 + U^r U_r}, \quad V^r \equiv \frac{U^r}{U^t}. \tag{A.3.1.8}$$

From Eqs.(A.3.1.3, A.3.1.2), we then have

$$(U^t)^2 = -\frac{1}{g_{tt}}(1 + g_{rr}(U^r)^2) = \frac{1}{\alpha^2}\gamma^2. \tag{A.3.1.9}$$

Following Eq.(A.3.1.7), we also define

$$E \equiv \epsilon\gamma, \quad D \equiv \rho_B\gamma, \quad \text{and} \quad \tilde{\rho} \equiv \rho\gamma \tag{A.3.1.10}$$

so that the conservation law of baryon number (A.3.1.4) can then be written as

$$\frac{\partial D}{\partial t} = -\frac{\alpha}{r^2}\frac{\partial}{\partial r}\left(\frac{r^2}{\alpha}D V^r\right). \tag{A.3.1.11}$$

Eq.(A.3.1.6) then takes the form,

$$\frac{\partial E}{\partial t} = -\frac{\alpha}{r^2}\frac{\partial}{\partial r}(\frac{r^2}{\alpha}EV^r) - p\left[\frac{\partial \gamma}{\partial t} + \frac{\alpha}{r^2}\frac{\partial}{\partial r}(\frac{r^2}{\alpha}\gamma V^r)\right]. \tag{A.3.1.12}$$

Defining the radial momentum density in the laboratory frame

$$S_r \equiv \alpha(p+\rho)U^t U_r = (D + \Gamma E)U_r, \tag{A.3.1.13}$$

we can express the radial component of the energy-momentum conservation law given in Eq.(A.3.1.5) by

$$\begin{aligned}
\frac{\partial S_r}{\partial t} &= -\frac{\alpha}{r^2}\frac{\partial}{\partial r}(\frac{r^2}{\alpha}S_r V^r) - \alpha\frac{\partial p}{\partial r} \\
&- \frac{\alpha}{2}(p+\rho)\left[\frac{\partial g_{tt}}{\partial r}(U^t)^2 + \frac{\partial g_{rr}}{\partial r}(U^r)^2\right] \\
&= -\frac{\alpha}{r^2}\frac{\partial}{\partial r}(\frac{r^2}{\alpha}S_r V^r) - \alpha\frac{\partial p}{\partial r} \\
&- \alpha\left(\frac{M}{r^2} - \frac{Q^2}{r^3}\right)\left(\frac{D+\Gamma E}{\gamma}\right)\left[\left(\frac{\gamma}{\alpha}\right)^2 + \frac{(U^r)^2}{\alpha^4}\right].
\end{aligned} \tag{A.3.1.14}$$

In order to determine the number-density of e^+e^- pairs, we use the pair rate equation. We define the e^+e^--pair density in the laboratory frame $N_{e^\pm} \equiv \gamma n_{e^\pm}$ and $N_{e^\pm}(T) \equiv \gamma n_{e^\pm}(T)$, where $n_{e^\pm}(T)$ is the total proper number density of pairs in comoving frame at thermodynamic equilibrium with temperature T in the process $e^+ + e^- \to \gamma + \gamma$ ($n_{e^-}(m, T) = n_\gamma(T)$), $n_{e^\pm}$ is the total proper number density of pairs in comoving frame at a generic time before reaching the equilibrium. We write the rate equation in the form

$$\frac{\partial N_{e^\pm}}{\partial t} = -\frac{\alpha}{r^2}\frac{\partial}{\partial r}(\frac{r^2}{\alpha}N_{e^\pm}V^r) + \overline{\sigma v}(N^2_{e^\pm}(T) - N^2_{e^\pm})/\gamma^2\,, \tag{A.3.1.15}$$

These partial differential equations have been integrated in Livermore starting from the dyadosphere distributions given in Fig. 17 (Right) in Ruffini et al. (2003) and assuming as usual ingoing boundary conditions on the horizon of the black hole. A simplified set of ordinary differential equations has been integrated in Rome and the results have been validated by comparison with the ones obtained in Livermore.

A.3.2 The fireshell in the Rome code

A.3.2.1 Era I: expansion of PEM-pulse

After the explosion from the dyadosphere a thermal plasma of e^+e^- pairs and photons optically thick with respect to scattering processes begins to expand at ultrarelativistic velocity. In this era the expansion takes place in a region of very low baryonic contamination. Details on the e^+e^- pairs creation are given in the previous report about "Electron-positron pairs in physics and astrophysics".

Recalling that the local number density of electron and positron pairs created as a function of radius is given by (Preparata et al., 1998):

$$n_{e^+e^-}(r) = \frac{Q}{4\pi r^2 \left(\frac{\hbar}{mc}\right) e}\left[1 - \left(\frac{r}{r_{ds}}\right)^2\right], \qquad \text{(A.3.2.1)}$$

where r_{ds} is the dyadosphere radius (see section A.1.3 and the previous report about "Electron-positron pairs in physics and astrophysics")the limit on such baryonic contamination, where ρ_{B_c} is the mass-energy density of baryons, is given by

$$\rho_{B_c} \ll m_p n_{e^+e^-}(r) = 3.2 \cdot 10^8 \left(\frac{r_{ds}}{r}\right)^2 \left[1 - \left(\frac{r}{r_{ds}}\right)^2\right] (g/cm^3). \qquad \text{(A.3.2.2)}$$

Near the horizon $r \simeq r_+$, this gives

$$\rho_{B_c} \ll m_p n_{e^+e^-}(r) = 1.86 \cdot 10^{14} \left(\frac{\xi}{\mu}\right) (g/cm^3), \qquad \text{(A.3.2.3)}$$

and near the radius of the dyadosphere r_{ds}:

$$\rho_{B_c} \ll m_p n_{e^+e^-}(r) = 3.2 \cdot 10^8 \left[1 - \left(\frac{r}{r_{ds}}\right)^2\right]_{r \to r_{ds}} (g/cm^3). \qquad \text{(A.3.2.4)}$$

Such conditions can be easily satisfied in the collapse to a black hole, but not necessarily in a collapse to a neutron star.

Consequently we have solved the equations governing a plasma composed solely of e^+e^--pairs and electromagnetic radiation, starting at time zero from the dyadosphere configurations corresponding to constant density in Fig. A.3.1.

The plasma of e^+e^- pairs and photons is described by the covariant energy-momentum tensor $T^{\mu\nu}$ given in Eq.(A.3.1.1).

It is assumed that the gravitational interaction with central black hole is

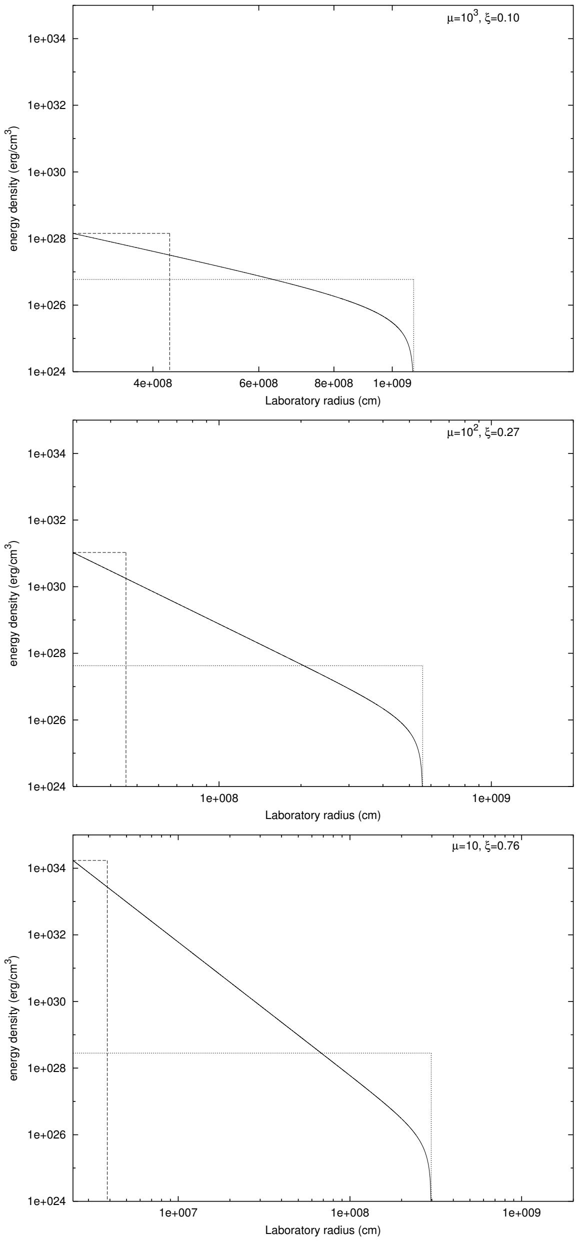

Figure A.3.1: Three different dyadospheres corresponding to the same value of E_{dya} and to different values of the two parameters μ and ξ are given. The three different configurations are markedly different in their spatial extent as well as in their energy-density distribution (see text).

negligible with respect to the total energy of PEM-pulse such that a fluid expansion with special relativistic equations can be considered.

Moreover it is assumed that photons remain trapped inside fireball until complete transparency, i.e. the emission of electromagnetic radiation is negligible during the first phases of expansion, being therefore adiabatic (Ruffini et al., 1999). This assumption is valid until the photon mean free path is negligible with respect to the thickness of pulse.

The thermodynamic quantities used to describe the process are the total proper internal energy density of pulse ϵ, given by $\epsilon = \epsilon_{e^+} + \epsilon_{e^-} + \epsilon_\gamma$, where ϵ_{e^+} (ϵ_{e^-}) is total proper internal energy density of electrons (positrons) and ϵ_γ of photons. The proper number density of pairs $n_{e^\pm}$, if the system is in thermodynamic equilibrium initially at temperature T of order $T \sim MeV$, enough for e^+e^- pair creation, equals the proper number density of photons n_γ. This is not valid at lower temperature (Bianco et al., 2001). The pressure is $p = p_{e^+} + p_{e^-} + p_\gamma$, where $p_{e^\pm}$ are electrons and positrons pressures and p_γ is photons pressure. The system is highly relativistic, so the equation of state $p = \epsilon/3$ can be considered valid. This equation of state is represented with thermal index Γ:

$$\Gamma = 1 + \frac{p}{\epsilon} \,. \tag{A.3.2.5}$$

Fermi integrals

Thermodynamical quantities introduced above are expressed in terms of integrals over Bose distribution for photons and Fermi distribution for e^+e^- pairs with zero chemical potentials μ_γ and $\mu_{e^\pm}$. We begin from the reaction $e^+ + e^- \to \gamma + \gamma$. From statistical mechanics it is known that given a thermodynamic system at temperature T kept inside a volume V and made of a number of particle variable N, the thermodynamic equilibrium is expressed by the condition that the potential free energy of Helmholtz $F(T, V, N)$ is stationary with respect to N variations:

$$\left(\frac{\partial F}{\partial N}\right)_{T,V} = 0; \tag{A.3.2.6}$$

by definition chemical potential μ is given by

$$\mu = \left(\frac{\partial F}{\partial N}\right)_{T,V}; \tag{A.3.2.7}$$

so that for a system made by a photon gas at equilibrium with matter with respect to creation and adsorption processes, we have $\mu_\gamma = 0$ (Landau and Lifshitz, 1980). We assume the chemical potential of electrons and positrons to be equal to zero: $\mu_{e^-} = \mu_{e^+} = 0$. In the following the expressions of thermodynamical quantities as Fermi integrals are listed. The proper number density of electrons (Weinberg, 1972) is given by

$$\begin{aligned} n_{e^-}(m, T, \mu_{e^-}) &= \frac{2}{h^3}\int \frac{d^3p}{e^{\frac{\sqrt{(pc)^2+(mc^2)^2}}{kT}}+1} = \\ &= \frac{8\pi}{h^3}\int_0^{+\infty} \frac{p^2}{e^{\frac{\sqrt{(pc)^2+(mc^2)^2}}{kT}}+1}dp = \\ &= \frac{aT^3}{k}\frac{7}{8}\frac{1}{A}\int_0^{+\infty}\frac{z^2}{e^{\sqrt{z^2+(mc^2/kT)^2}}+1}dz, \end{aligned} \quad (A.3.2.8)$$

where $z = pc/kT$, m is the electron mass, T is the temperature of fireshell in comoving frame, $a = 8\pi^5k^4/15h^3c^3 = 1.37 \times 10^{26}$ erg/(cm^3 MeV^4, k is the Boltzmann constant and $A = (7/4)(\pi^4/15)$ is a numerical constant introduced for convenience.
Since the thermodynamic equilibrium is assumed and in all cases analyzed the initial temperature is larger than e^+e^- pairs creation threshold ($T > 1$ MeV), the proper number density of electrons is roughly equal to that one of photons:

$$n_{e^\pm} \sim n_{e^-}(T) \sim n_\gamma(T); \quad (A.3.2.9)$$

in these conditions the number of particles is conserved:

$$(n_{e^\pm}U^\mu)_{;\mu} = 0. \quad (A.3.2.10)$$

Later on, for $T \ll 1$MeV (see Fig. A.3.2), e^+e^- pairs go on in annihilation but can not be created anymore, therefore

$$n_\gamma(T) > n_{e^\pm} > n_{e^\pm}(T) \quad (A.3.2.11)$$

as shown in Fig. A.3.3.

The total proper internal energy density for photons is given by

$$\epsilon_\gamma = \frac{2}{h^3}\int \frac{h\nu}{e^{\frac{h\nu}{kT}}-1}d^3p = aT^4 \quad (A.3.2.12)$$

where $p = h\nu/c$. The total proper internal energy density for electrons is

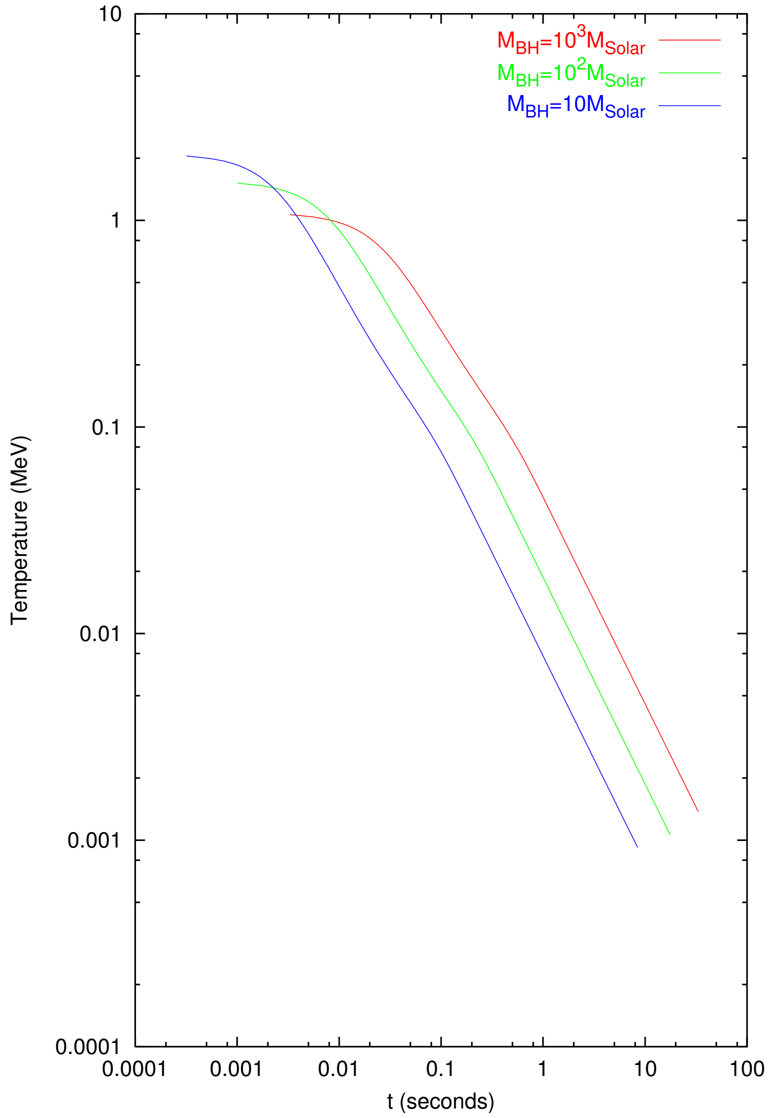

Figure A.3.2: Temperature in comoving system as a function of emission time for different values of black hole mass μ.

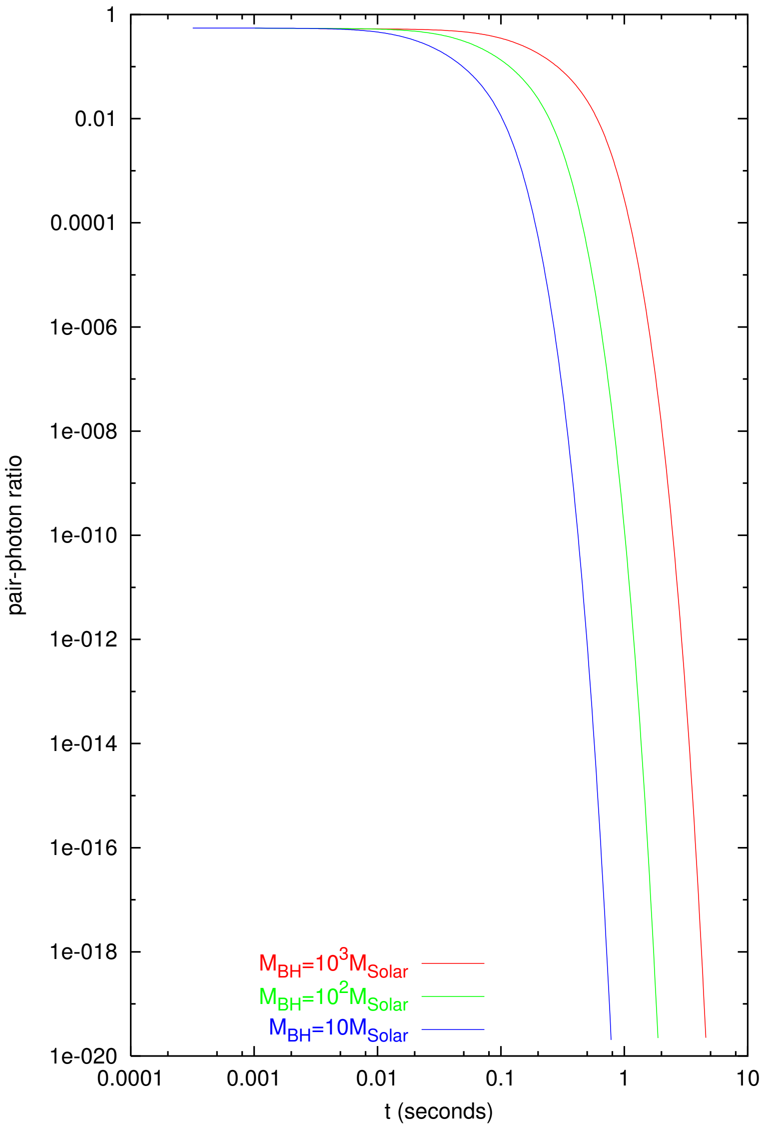

Figure A.3.3: Ratio between number density of pairs e^+e^- $n_{e^\pm}$ and number density of photons $n_\gamma\,(T)$ as a function of emission time for different values of black hole mass μ.

given by:

$$\begin{aligned}
\epsilon_{e^-} &= \frac{2}{h^3}\int \frac{\sqrt{(pc)^2+(mc^2)^2}}{e^{\frac{\sqrt{(pc)^2+(mc^2)^2}}{kT}}+1} d^3p = \\
&= \frac{8\pi}{h^3}\int_0^{+\infty} \frac{p^2\sqrt{(pc)^2+(mc^2)^2}}{e^{\frac{\sqrt{(pc)^2+(mc^2)^2}}{kT}}+1} dp = \\
&= aT^4\frac{7}{4}\frac{1}{A}\int_0^{+\infty} \frac{z^2\sqrt{z^2+(mc^2/kT)^2}}{e^{\sqrt{z^2+(mc^2/kT)^2}}+1} dz
\end{aligned} \tag{A.3.2.13}$$

Therefore the total proper internal energy density of the PEM-pulse, summing up all the contributions of photons and e^+e^- pairs, is given by

$$\epsilon_{tot} = aT^4\left[1+\frac{7}{4}\frac{2}{A}\int_0^{+\infty} \frac{z^2\sqrt{z^2+(mc^2/kT)^2}}{e^{\sqrt{z^2+(mc^2/kT)^2}}+1} dz\right] \tag{A.3.2.14}$$

where the factor 2 in front of the integral takes into account of electrons and positrons.
About the pressure of the photons it holds

$$p_\gamma = \frac{\epsilon_\gamma}{3} = \frac{aT^4}{3}; \tag{A.3.2.15}$$

and about the pressure of electrons

$$\begin{aligned}
p_{e^-} &= \frac{2}{3h^3}\int \frac{1}{e^{\frac{\sqrt{(pc)^2+(mc^2)^2}}{kT}}+1}\cdot\frac{(pc)^2}{\sqrt{(pc)^2+(mc^2)^2}} d^3p = \\
&= \frac{8\pi}{3h^3}\int_0^{+\infty} \frac{p^2}{e^{\frac{\sqrt{(pc)^2+(mc^2)^2}}{kT}}+1}\cdot\frac{(pc)^2}{\sqrt{(pc)^2+(mc^2)^2}} dp = \\
&= \frac{aT^4}{3}\frac{7}{4}\frac{1}{A}\int_0^{+\infty} \frac{z^4}{e^{\sqrt{z^2+(mc^2/kT)^2}}+1}\cdot\frac{1}{\sqrt{z^2+(mc^2/kT)^2}} dz
\end{aligned} \tag{A.3.2.16}$$

Therefore the total pressure of PEM-pulse is given by

$$p_{tot} = \frac{aT^4}{3}\left[1+\frac{7}{4}\frac{2}{A}\int_0^{+\infty} \frac{z^4}{e^{\sqrt{z^2+(mc^2/kT)^2}}+1}\cdot\frac{1}{\sqrt{z^2+(mc^2/kT)^2}} dz\right]. \tag{A.3.2.17}$$

Numerical code

In the following we recall a zeroth order approximation of the fully relativistic equations of the previous section (Ruffini et al., 1999):
(i) Since we are mainly interested in the expansion of the e^+e^- plasma away from the black hole, we neglect the gravitational interaction.
(ii) We describe the expanding plasma by a special relativistic set of equations.

In the PEM-pulse phase the expansion in vacuum is described by a set of equation expressing:

- entropy conservation, because of the assumption that emission of electromagnetic radiation is negligible up to transparency;
- energy conservation, because the increase of kinetic energy is compensated by a decrease of total internal energy.

For the expansion of a single shell, the adiabaticity is given by

$$d\left(V\epsilon\right) + pdV = dE + pdV = 0\,, \tag{A.3.2.18}$$

where V is the volume of the shell in the comoving frame and $E = V\epsilon$ is the total proper internal energy of plasma (the subscript "$\circ$" refers to the initial values). By using the equation of state Eq.(A.3.2.5) we find

$$dln\epsilon + \Gamma dlnV = 0 \tag{A.3.2.19}$$

and, by integrating, we find

$$\frac{\epsilon_\circ}{\epsilon} = \left(\frac{V}{V_\circ}\right)^\Gamma ; \tag{A.3.2.20}$$

recalling that $V = \mathcal{V}\gamma$, where $\mathcal{V}$ is the volume in the laboratory frame, we find

$$\frac{\epsilon_\circ}{\epsilon} = \left(\frac{V}{V_\circ}\right)^\Gamma = \left(\frac{\mathcal{V}}{\mathcal{V}_\circ}\right)^\Gamma \left(\frac{\gamma}{\gamma_\circ}\right)^\Gamma . \tag{A.3.2.21}$$

The total energy conservation of the shell implies (Ruffini et al., 1999):

$$(\Gamma\epsilon)\mathcal{V}\gamma^2 = (\Gamma\epsilon_\circ)\mathcal{V}_\circ\gamma_\circ^2; \tag{A.3.2.22}$$

and this gives the evolution for γ:

$$\gamma = \gamma_\circ\sqrt{\frac{\epsilon_\circ\mathcal{V}_\circ}{\epsilon\mathcal{V}}} \tag{A.3.2.23}$$

Substituting this expression for γ in (A.3.2.21) the final equation for proper internal energy density is found

$$\epsilon = \epsilon_\circ \left(\frac{\mathcal{V}_\circ}{\mathcal{V}}\right)^{\frac{\Gamma}{2-\Gamma}} \tag{A.3.2.24}$$

The evolution of a plasma of e^+e^- pairs and photons should be treated by relativistic hydrodynamics equations describing the variation of the number of particles in the process. The 4-vector number density of pairs is defined $(n_{e^\pm}U^\mu)$, which in the comoving frame reduces to the 4-vector $(n_{e^\pm}, 0, 0, 0)$. The law of number conservation for pairs is

$$\begin{aligned} (n_{e^\pm}U^\mu)_{;\mu} &= \frac{1}{\sqrt{-g}}\left(\sqrt{-g}n_{e^\pm}U^\mu\right)_{,\mu} = \\ &= \left(n_{e^\pm}U^t\right)_{,t} + \frac{1}{r^2}\left(r^2 n_{e^\pm}U^r\right)_{,r} = 0 \end{aligned} \tag{A.3.2.25}$$

where $g = \| g^{\mu\nu} \| = -r^4 sin^2\theta$ is the determinant of Reissner-Nordstrøm metric. In the system processes of creation and annihilation of particles occur due to collisions between particles. If the number of particles is conserved, it holds $(n_{e^\pm}U^\mu)_{;\mu} = 0$; if not, in the assumptions that only binary collisions between particles occur and in the hypothesis of molecular caos, the Eq.(A.3.2.25) becomes

$$(n_{e^\pm}U^\mu)_{;\mu} = \overline{\sigma v}\left[n_{e^-}(T)n_{e^+}(T) - n_{e^-}n_{e^+}\right] \tag{A.3.2.26}$$

where σ is the cross section for the process of creation and annihilation of pairs, given by

$$\sigma = \frac{\pi r_e^2}{\alpha_\circ + 1}\left[\frac{\alpha_\circ^2 + 4\alpha_\circ + 1}{\alpha_\circ^2 - 1}\ln\left(\alpha_\circ + \sqrt{\alpha_\circ^2 - 1}\right) - \frac{\alpha_\circ + 3}{\sqrt{\alpha_\circ^2 - 1}}\right], \tag{A.3.2.27}$$

with $\alpha_\circ = \frac{E}{mc^2}$ and E total energy of positrons in the laboratory frame, and $r_e = \frac{e^2}{mc^2}$ the classical radius of electron, v is the sound velocity in the fireball:

$$v = c\sqrt{\frac{p_{tot}}{\epsilon_{tot}}}, \tag{A.3.2.28}$$

and $\overline{\sigma v}$ is the mean value of σv; for σ we use as a first approximation the Thomson cross section, $\sigma_T = 0.665 \cdot 10^{-24} cm^2$; $n_{e^\pm}(T)$ is the total proper number density of electrons and positrons in comoving frame at thermodynamic equilibrium in the process $e^+ + e^- \rightarrow \gamma + \gamma$ $(n_{e^-}(m,T) = n_\gamma(T))$, $n_{e^\pm}$ is the total proper number density of electrons and positrons in comoving frame at

a generic time before reaching the equilibrium.
Using the approximation of special relativity, the 4-velocity is written $U^{\mu} = (\gamma, \gamma\frac{v}{c})$; Eq.(A.3.2.26) in hybrid form becomes

$$\frac{\partial\left(n_{e^{\pm}}\gamma\right)}{\partial t} = -\frac{1}{r^2}\frac{\partial}{\partial r}\left(r^2 n_{e^{\pm}}\gamma V^r\right) + \overline{\sigma v}\left(n^2_{e^{\pm}}(T) - n^2_{e^{\pm}}\right), \qquad \text{(A.3.2.29)}$$

valid for electrons and positrons.
Now we have a complete set of equations for numerical integration: (A.3.2.24), (A.3.2.23) and (A.3.2.29).

If we now turn from a single shell to a finite distribution of shells, we can introduce the average values of the proper internal energy and pair number densities $(\epsilon, n_{e^{\pm}})$ for the PEM-pulse, where the average γ-factor is defined by

$$\gamma = \frac{1}{\mathcal{V}}\int_{\mathcal{V}}\gamma(r)d\mathcal{V}, \qquad \text{(A.3.2.30)}$$

and $\mathcal{V}$ is the total volume of the shell in the laboratory frame (Ruffini et al., 1999).

In principle we could have an infinite number of possible schemes to define geometry of the expanding shell. Three different possible schemes have been proposed (Ruffini et al., 1999):

- Sphere. An expansion with radial component of 4-velocity proportional to the distance from the black hole $U_r(r) = U\frac{r}{\mathcal{R}(t)}$, where U is the radial component of 4-velocity on the external surface of PEM-pulse (having radius $\mathcal{R}(t)$), the factor γ from (A.3.2.30) is

  $$\gamma = \frac{3}{8U^3}\left[2U\left(1+U^2\right)^{\frac{3}{2}} - U\left(1+U^2\right)^{\frac{1}{2}} - ln\left(U + \sqrt{1+U^2}\right)\right]; \qquad \text{(A.3.2.31)}$$

  this distribution corresponds to a uniform and time decreasing density, like in Friedmann model for the universe;

- Slab 1. An expansion with thickness of fireball constant $\mathcal{D} = r_{ds} - r_+$ in laboratory frame, with $U_r(r) = U_r = cost$ and $\gamma = \sqrt{1 + {U_r}^2}$; this distribution does not require an average;

- Slab 2. An expansion with thickness of fireball constant in comoving frame of PEM-pulse.

The result has been compared with the one of hydrodynamic equation in general relativity (Ruffini et al., 1999, see Fig. A.3.4). Excellent agreement has been found with the scheme in which the thickness of fireball is constant in laboratory frame: what happens is that the thickness in comoving frame increases, but due to the Lorentz contraction, it is kept constant in laboratory

frame and equal to $\mathcal{D}$. In this case $U_r = \sqrt{\gamma^2 - 1}$, where γ is computed by conservation equations.
A similar situation occurs for the temperature of PEM-pulse. In the comoving frame the temperature decreases as $T' \sim R^{-1}$, in accordance with results in literature (Piran, 1999). Since γ monotonically increases as $\gamma \sim R$ (Ruffini et al., 2001c), in laboratory frame $T = \gamma T' \sim constant$ (Ruffini et al., 2000); photons are blue-shifted in laboratory frame in such a way that, at least in the first phase, the temperature measured by an observer at infinity is constant. The numerical value of the temperature of equilibrium at each instant is found by imposing the equivalence, within a certain precision, of Eq. (A.3.2.14) numerically computed and Eq. (A.3.2.24).

Even if the PEM-pulse is optically thick in the expansion before transparency, photons located at a distance from the external surface less their mean free path can escape and reach the observer at infinity. The mean free path in the comoving frame is given by

$$L_\gamma = \frac{1}{\sigma n_{e^+e^-}} \sim 10^{-6} cm \qquad \text{(A.3.2.32)}$$

while in laboratory frame is given by $\lambda = L_\gamma/\gamma \sim 10^{-8}$cm. However the luminosity emitted at this stage is negligible, since the ratio between λ and the thickness of the fireball $\mathcal{D}$ in the laboratory frame (with $\mathcal{D} \sim 10^9$cm) is of the order of $\lambda/\mathcal{D} \simeq 10^{-17}$.

A.3.2.2 Era II: interaction of the PEM pulse with remnant

The PEM pulse expands initially in a region of very low baryonic contamination created by the process of gravitational collapse. As it moves outside the baryonic remnant of the progenitor star is swept up. The existence of such a remnant is necessary in order to guarantee the overall charge neutrality of the system: the collapsing core has the opposite charge of the remnant and the system as a whole is clearly neutral. The number of extra charges in the baryonic remnant negligibly affects the overall charge neutrality of the PEM pulse.

The baryonic matter remnant is assumed to be distributed well outside the dyadosphere in a shell of thickness Δ between an inner radius $r_{\rm in}$ and an outer radius $r_{\rm out} = r_{\rm in} + \Delta$ at a distance from the black hole not so big that the PEM pulse expanding in vacuum has reached yet transparency and not so small that the system will reach enough high value of Lorentz γ in order to not be stopped in the collision (see Fig. A.2.2). For example we choose

$$r_{\rm in} = 100 r_{\rm ds}, \quad \Delta = 10 r_{\rm ds}. \qquad \text{(A.3.2.33)}$$

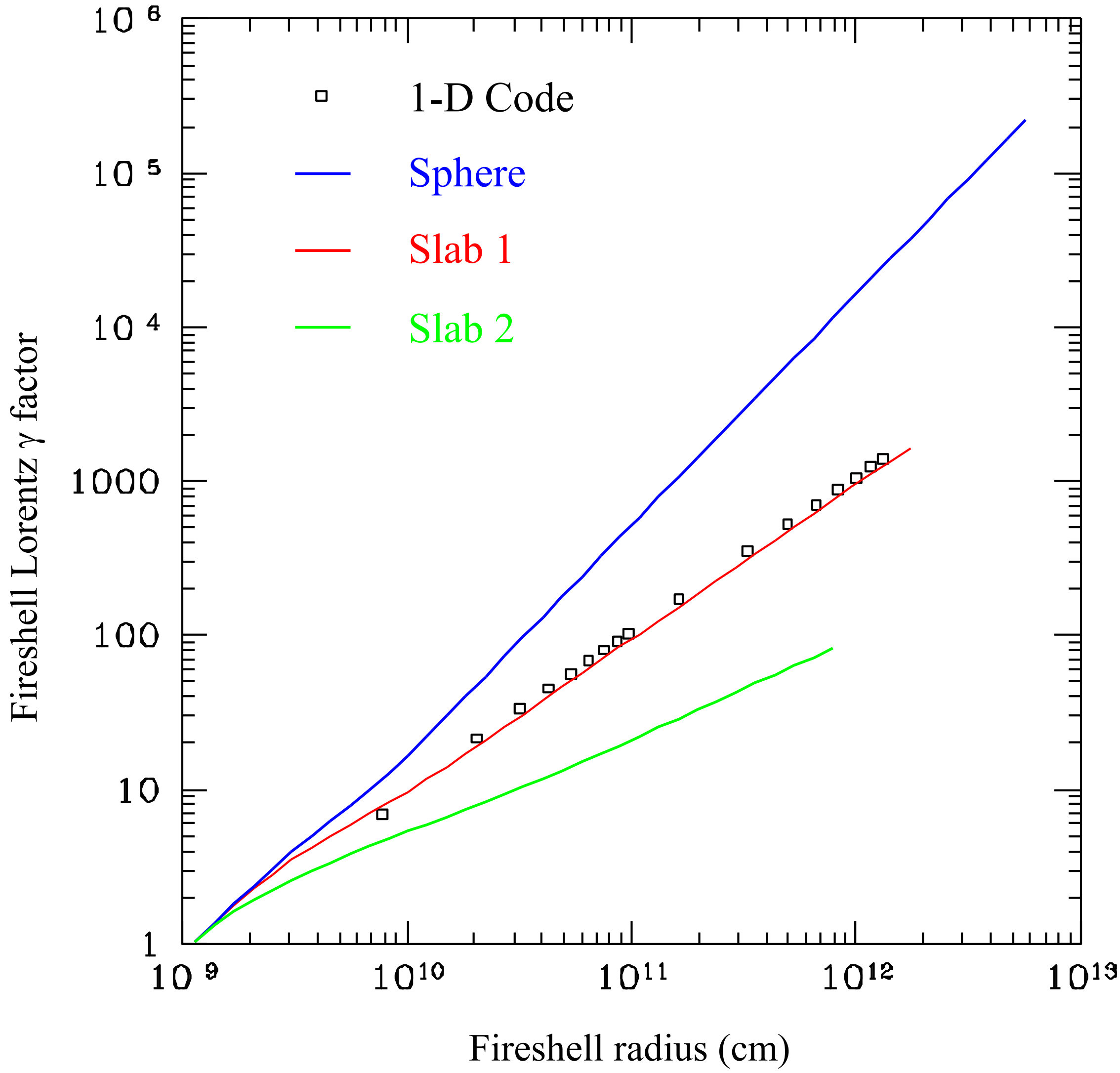

Figure A.3.4: Lorentz γ factor as a function of radial coordinate. Three schemes of expansion of PEM-pulse (see text) are compared with solution of hydrodynamics relativistic equations numerically integrated for a black hole with $\mu = 10^3$ and $\xi = 0.1$. The result is in accordance with the scheme of a fireball with constant thickness in laboratory frame.

The total baryonic mass $M_B = N_B m_p$ is assumed to be a fraction of the dyadosphere initial total energy $(E_{\rm dya})$. The total baryon-number N_B is then expressed as a function of the dimensionless parameter B given by Eq.(A.2.2.1). We shall see below the role of B in the determination of the features of the GRBs. We already saw the sense in which B and $E^{tot}_{e^\pm} = E_{\rm dya}$ can be considered to be the only two free parameters of the black hole theory for the entire GRB family, the so called "long bursts" (see section A.2.2.2). For the so called "genuine short bursts" the black hole theory depends on the two other parameters μ, ξ, since in that case $B = 0$ since most of the energy, unless the whole energy, in the pulse is emitted at transparency. The baryon number density n_B is assumed to be a constant

$$n_B = \frac{N_B}{V_B}, \quad \bar{\rho}_B = m_p n_B c^2. \tag{A.3.2.34}$$

As the PEM pulse reaches the region $r_{\rm in} < r < r_{\rm out}$, it interacts with the baryonic matter which is assumed to be at rest. In our model we make the following assumptions to describe this interaction:

- the PEM pulse does not change its geometry during the interaction;
- the collision between the PEM pulse and the baryonic matter is assumed to be inelastic;
- the baryonic matter reaches thermal equilibrium with the photons and pairs of the PEM pulse.

These assumptions are valid if: (i) the total energy of the PEM pulse is much larger than the total mass-energy of baryonic matter M_B, $10^{-8} < B \leq 10^{-2}$ (see Fig. A.3.5); (ii) the ratio of the comoving number density of pairs and baryons at the moment of collision $n_{e^+e^-}/n_B$ is very high (e.g., $10^6 < n_{e^+e^-}/n_B < 10^{12}$); (iii) the PEM pulse has a large value of the gamma factor ($\gamma > 100$).

In the collision between the PEM pulse and the baryonic matter at $r_{\rm out} > r > r_{\rm in}$, we impose total conservation of energy and momentum. We consider the collision process between two radii r_2, r_1 satisfying $r_{\rm out} > r_2 > r_1 > r_{\rm in}$ and $r_2 - r_1 \ll \Delta$. The amount of baryonic mass acquired by the PEM pulse is

$$\Delta M = \frac{M_B}{V_B}\frac{4\pi}{3}(r_2^3 - r_1^3), \tag{A.3.2.35}$$

where M_B/V_B is the mean-density of baryonic matter at rest in the laboratory frame.

As for energy density of dyadosphere, here we also choose a simplification for the energy density: in fact during the passage of the shell a deposition of material on the external surface of the fireball creates; however we neglected this effect and assumed that this material after collision diffuses

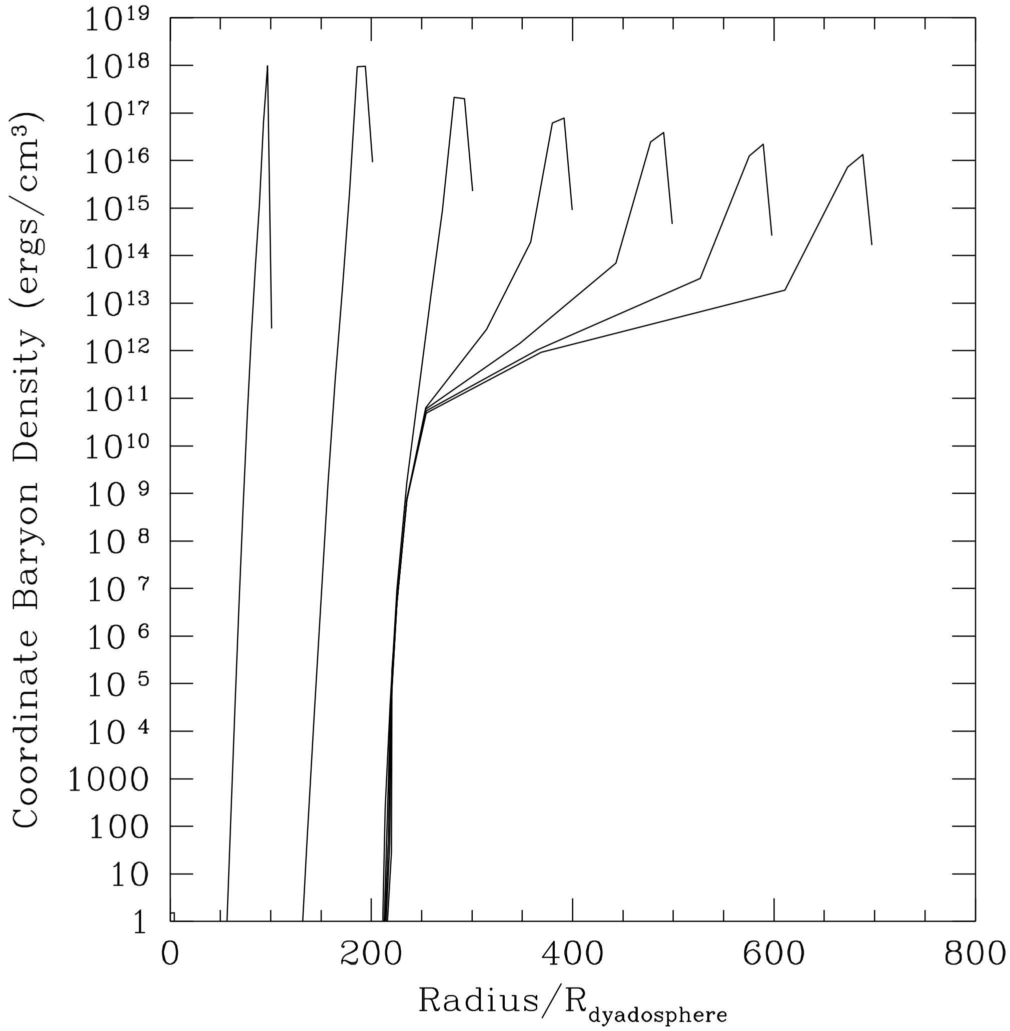

Figure A.3.5: A sequence of snapshots of coordinate baryon energy density is shown from the one dimensional hydrodynamic calculations of the Livermore code. The radial coordinate is given in units of dyadosphere radii (r_{ds}). At $r \simeq 100 r_{ds}$ there is located a baryonic matter shell corresponding to a baryon loading $B = 1.3 \times 10^{-2}$. For this baryon shell mass we see a significant departure from the constant thickness solution for the fireshell dynamics and a clear instability occurs. Details in Ruffini et al. (2000). As we will see, this result, peculiar of our treatment, will play a major role in the theoretical interpretation of GRBs.

instantaneously in the pulse with a constant density:

$$n'_B = \frac{N'_B}{V}, \tag{A.3.2.36}$$

where N'_B is the number of particle of the remnant shell swept up by the pulse.

The conservation of total energy leads to the estimate of the corresponding quantities before (with "$\circ$") and after such a collision

$$(\Gamma\epsilon_\circ + \bar{\rho}_B^\circ)\gamma_\circ^2 \mathcal{V}_\circ + \Delta M = (\Gamma\epsilon + \bar{\rho}_B + \frac{\Delta M}{V} + \Gamma\Delta\epsilon)\gamma^2\mathcal{V}, \tag{A.3.2.37}$$

where $\Delta\epsilon$ is the corresponding increase of internal energy due to the collision. Similarly the momentum-conservation gives

$$(\Gamma\epsilon_\circ + \bar{\rho}_B^\circ)\gamma_\circ U_r^\circ \mathcal{V}_\circ = (\Gamma\epsilon + \bar{\rho}_B + \frac{\Delta M}{V} + \Gamma\Delta\epsilon)\gamma U_r \mathcal{V}, \tag{A.3.2.38}$$

where the radial component of the four-velocity of the PEM pulse is $U_r^\circ = \sqrt{\gamma_\circ^2 - 1}$ and Γ is the thermal index. We then find

$$\Delta\epsilon = \frac{1}{\Gamma}\left[(\Gamma\epsilon_\circ + \bar{\rho}_B^\circ)\frac{\gamma_\circ U_r^\circ \mathcal{V}_\circ}{\gamma U_r \mathcal{V}} - (\Gamma\epsilon + \bar{\rho}_B + \frac{\Delta M}{V})\right], \tag{A.3.2.39}$$

$$\gamma = \frac{a}{\sqrt{a^2-1}}, \quad a \equiv \frac{\gamma_\circ}{U_r^\circ} + \frac{\Delta M}{(\Gamma\epsilon_\circ + \bar{\rho}_B^\circ)\gamma_\circ U_r^\circ \mathcal{V}_\circ}. \tag{A.3.2.40}$$

These equations determine the gamma factor γ and the internal energy density $\epsilon = \epsilon_\circ + \Delta\epsilon$ in the capture process of baryonic matter by the PEM pulse.

The effect of the collision of the PEM pulse with the remnant leads to the following consequences:

- a reheating of the plasma in the comoving frame but not in the laboratory frame; an increase of the number of e^+e^- pairs and of free electrons originated from the ionization of those atoms remained in the baryonic remnant; correspondingly this gives an overall increase of the opacity of the pulse;

- the more the amount of baryonic matter swept up, the more internal energy of the PEMB pulse is converted in kinetic energy of baryons.

By describing the interaction of PEM pulse with remnant as completely inelastic collision of two particles, one can compute by the energy-momentum conservation equation the decrease of the Lorentz gamma factor and the increase of internal energy as function of B parameter and also the ultrarelativistic approximation ($\gamma_\circ \to \infty$):

1. an abrupt decrease of the gamma factor given by

$$\gamma_{coll} = \gamma_\circ \frac{1+B}{\sqrt{\gamma_\circ{}^2\left(2B+B^2\right)+1}} \overset{\gamma_\circ\to\infty}{\to} \frac{B+1}{\sqrt{B^2+2B}},$$

2. an increase of the internal energy in the comoving frame E_{coll} developed in the collision given by

$$\frac{E_{coll}}{E_{dya}} = \frac{\sqrt{\gamma_\circ{}^2\left(2B+B^2\right)+1}}{\gamma_\circ} - \left(\frac{1}{\gamma_\circ}+B\right) \overset{\gamma_\circ\to\infty}{\to} -B+\sqrt{B^2+2B},$$

This approximation applies when the final gamma factor at the end of the PEM pulse era is larger than γ_{coll}, right panel in Fig. A.2.2.

In this phase of expansion, another thermodynamic quantity has not been considered: the chemical potential μ of the electrons from ionization of baryonic remnant. We remind that the total proper number density of electrons of ionization is given by

$$n^b_{e^-}(m,T,\mu) = \frac{aT^3}{k}\frac{7}{8}\frac{1}{A}\int_0^{+\infty}\frac{z^2}{e^{\sqrt{z^2+(mc^2/kT)^2}+\frac{\mu}{kT}}+1}dz \tag{A.3.2.41}$$

four equations are imposed to find a formula useful for numerical computation: the first one is the thermodynamical equilibrium of fireball, or

$$n_{e^\pm}(T_\circ) = n_\gamma(T_\circ); \tag{A.3.2.42}$$

the second one is

$$n^b_{e^-} = \bar{Z} n_B \tag{A.3.2.43}$$

where $1/2 < \bar{Z} < 1$, with $\bar{Z} = 1$ for hydrogen atoms and $\bar{Z} = 1/2$ for baryonic matter in general; the third one derives from the definition of B A.2.2.1, and states a relation between the two densities n_B and $n_{e^\pm}$: from definition of B, we have

$$\frac{N_B}{N_{e^\pm}(T_\circ)} = B\frac{E_{dya}}{m_p c^2}\frac{1}{N_{e^\pm}(T_\circ)} = 10^b \tag{A.3.2.44}$$

where $T_\circ$ is the initial temperature of fireshell and b is a parameter ($b < 0$) defined by (A.3.2.44); so if $V_\circ$ is the initial volume of dyadosphere and w the initial volume of the baryonic shell

$$n^\circ_B = 10^b n_{e^\pm}(T_\circ)\frac{V_\circ}{w}; \tag{A.3.2.45}$$

finally the fourth one is the conservation law of baryonic matter

$$(n^b_{e^-}U^\mu)_{;\mu} = 0. \tag{A.3.2.46}$$

Therefore the chemical potential μ is numerically determined at a certain time of expansion if the initial temperature $T_\circ$ of fireshell and the initial volume of baryonic shell w are known and, at that time, the volume V, the temperature T and the Lorentz factor γ of the fireball, the volume of the baryonic shell swept up vb and the ratio $\frac{n^b_{e^-}(T)}{n^b_{e^-}}$:

$$2\zeta(3)\bar{Z}10^b \frac{n^b_{e^-}(T)}{n^b_{e^-}} \frac{T_0{}^3 w}{T^3 V\gamma} \left(\frac{vb}{w}\right) = \int_0^{+\infty} \frac{z^2}{e^{\sqrt{z^2+(mc^2/kT)^2}+\frac{\mu}{kT}}+1} dz \quad \text{(A.3.2.47)}$$

where the factor in brackets $\left(\frac{vb}{w}\right)$ must be considered only for $r > r_{\text{out}}$, while the proportionality factor is the function zeta of Riemann $\zeta(x)$ for computation of n_γ, with $\zeta(3) = 1.202$.
Therefore the equations for this phase are (A.3.2.29), (A.3.2.36), (A.3.2.39), (A.3.2.40), and (A.3.2.47).

A.3.2.3 Era III: expansion of PEMB pulse

After the engulfment of the baryonic matter of the remnant the plasma formed of e^+e^--pairs, electromagnetic radiation and baryonic matter expands again as a sharp pulse, namely the PEMB pulse. The calculation is continued as the plasma fluid expands, cools and the e^+e^- pairs recombine until it becomes optically thin:

$$\int_R dr(n_{e^\pm} + \bar{Z}n_B)\sigma_T \simeq O(1), \quad \text{(A.3.2.48)}$$

where $\sigma_T = 0.665 \cdot 10^{-24}\text{cm}^2$ is the Thomson cross-section and the integration is over the radial interval of the PEMB pulse in the comoving frame. In order to study the PEMB pulse expansion the validity of the slab approximation adopted for the PEM pulse phase has to be verified; otherwise the full hydrodynamics relativistic equations should be integrated. The PEMB pulse evolution firstly has been simulated by integrating the general relativistic hydrodynamical equations with the Livermore codes, for a total energy in the dyadosphere of 3.1×10^{54} erg and a baryonic shell of thickness $\Delta = 10r_{\text{ds}}$ at rest at a radius of $100r_{\text{ds}}$ and $B \simeq 1.3 \cdot 10^{-4}$.

In analogy with the special relativistic treatment for the PEM pulse, presented above (see also Ruffini et al., 1999), for the adiabatic expansion of the PEMB pulse in the constant-slab approximation described by the Rome codes

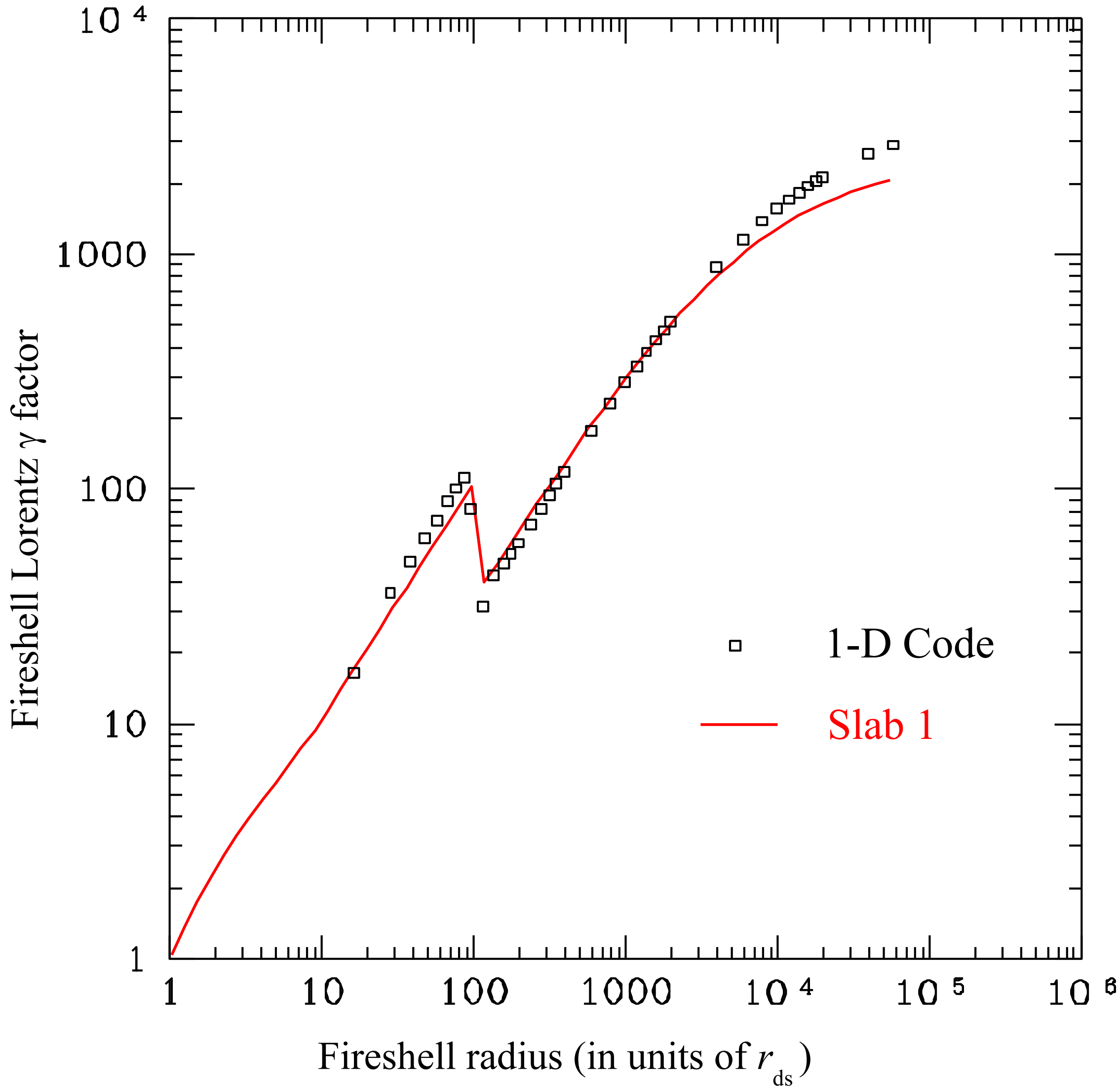

Figure A.3.6: Lorentz γ factor as a function of radial coordinate from the PEMB-pulse simulation is compared with the γ factor as solution of hydrodynamics relativistic equations numerically integrated (open squares) for $E_{dya} = 3.1 \times 10^{54}$erg and $B = 1.3 \times 10^{-4}$, $r_{\rm in} = 100 r_{\rm ds}$ and $\Delta = 10 r_{\rm ds}$. The result is in accordance with the scheme of a fireshell with constant thickness in laboratory frame which is valid up to $B = 10^{-2}$.

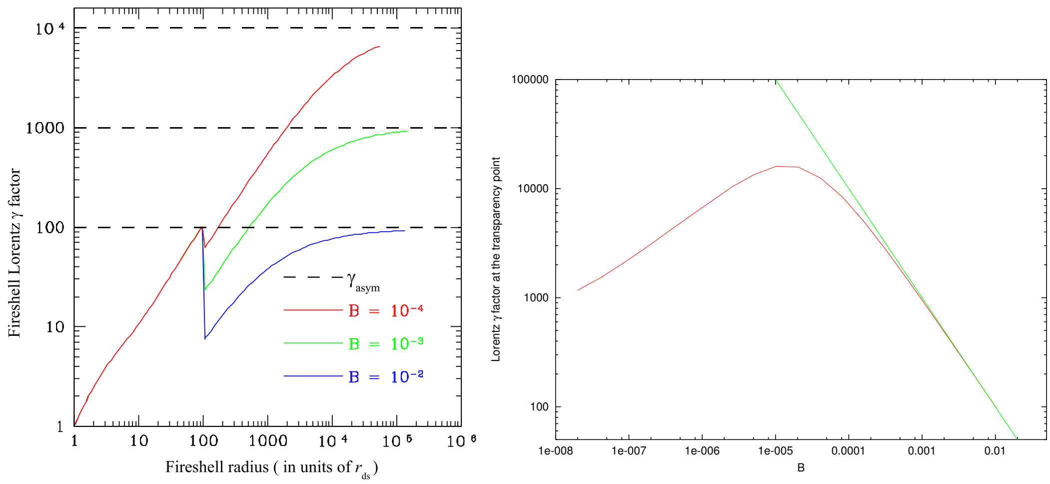

Figure A.3.7: Left: The gamma factors are given as functions of the radius in units of the dyadosphere radius for selected values of B for the typical case $E_{dya} = 3.1 \times 10^{54}$ erg. The asymptotic values $\gamma_{\rm asym} = E_{\rm dya}/(M_B c^2) = 10^4, 10^3, 10^2$ are also plotted. The collision of the PEM pulse with the baryonic remnant occurs at $r/r_{ds} = 100$ where the jump occurs. **Right:** The γ factor (red line) at the transparency point is plotted as a function of the B parameter. The asymptotic value (green line) $E_{\rm dya}/(M_B c^2)$ is also plotted.

the following hydrodynamical equations with $\bar{\rho}_B \neq 0$ has been found

$$\frac{n_B^\circ}{n_B} = \frac{V}{V_\circ} = \frac{\mathcal{V}\gamma}{\mathcal{V}_\circ\gamma_\circ}, \tag{A.3.2.49}$$

$$\frac{\epsilon_\circ}{\epsilon} = \left(\frac{V}{V_\circ}\right)^\Gamma = \left(\frac{\mathcal{V}}{\mathcal{V}_\circ}\right)^\Gamma \left(\frac{\gamma}{\gamma_\circ}\right)^\Gamma, \tag{A.3.2.50}$$

$$\gamma = \gamma_\circ \sqrt{\frac{(\Gamma\epsilon_\circ + \bar{\rho}_B^\circ)\mathcal{V}_\circ}{(\Gamma\epsilon + \bar{\rho}_B)\mathcal{V}}}, \tag{A.3.2.51}$$

$$\frac{\partial}{\partial t}(N_{e^\pm}) = -N_{e^\pm}\frac{1}{\mathcal{V}}\partial\mathcal{V}\partial t + \overline{\sigma v}\frac{1}{\gamma^2}(N_{e^\pm}^2(T) - N_{e^\pm}^2). \tag{A.3.2.52}$$

In these equations ($r > r_{\rm out}$) the comoving baryonic mass and number densities are $\bar{\rho}_B = M_B/V$ and $n_B = N_B/V$, where V is the comoving volume of the PEMB pulse.

The result is shown in Fig. A.3.6 (Ruffini et al., 2000) where the bulk gamma factor as computed from the Rome and Livermore codes are compared and very good agreement has been found. This validates the constant-thickness approximation in the case of the PEMB pulse as well. On this basis we easily estimate a variety of physical quantities for an entire range of values of B.

For the same black hole different cases have been considered (Ruffini et al., 2000). The results of the integration show that for the first parameter range the PEMB pulse propagates as a sharp pulse of constant thickness in the laboratory frame, but already for $B \simeq 1.3 \cdot 10^{-2}$ the expansion of the PEMB pulse becomes much more complex, turbulence phenomena can not be neglected any more and the constant-thickness approximation ceases to be valid.

It is also interesting to evaluate the final value of the gamma factor of the PEMB pulse when the transparency condition given by Eq.(A.3.2.48) is reached as a function of B (see Fig. A.3.7). For a given black hole, there is a *maximum* value of the gamma factor at transparency. By further increasing the value of B the entire E_{dya} is transferred into the kinetic energy of the baryons (see also Ruffini et al., 2000).

In Fig. A.3.7-Left we plot the gamma factor of the PEMB pulse as a function of radial distance for different amounts of baryonic matter. The diagram extends to values of the radial coordinate at which the transparency condition given by Eq.(A.3.2.48) is reached. The "asymptotic" gamma factor

$$\gamma_{\rm asym} \equiv \frac{E_{\rm dya}}{M_B c^2} \tag{A.3.2.53}$$

is also shown for each curve. The closer the gamma value approaches the "asymptotic" value (A.3.2.53) at transparency, the smaller the intensity of the radiation emitted in the burst and the larger the amount of kinetic energy left in the baryonic matter (see Fig. A.3.7-Right).

A.3.2.4 The approach to transparency: the thermodynamical quantities

As the condition of transparency expressed by Eq.(A.3.2.48) is reached the *injector phase* terminates. The electromagnetic energy of the PEMB pulse is released in the form of free-streaming photons — the P-GRB. The remaining energy of the PEMB pulse is released as an ABM pulse.

We now proceed to the analysis of the approach to the transparency condition. It is then necessary to turn from the pure dynamical description of the PEMB pulse described in the previous sections to the relevant thermodynamic parameters. Also such a description at the time of transparency needs the knowledge of the thermodynamical parameters in all previous eras of the GRB.

As above we shall consider as a typical case a black hole of $E_{dya} = 3.1 \times 10^{54}$ erg and $B = 10^{-2}$. One of the key thermodynamical parameters is represented by the temperature of the PEM and PEMB pulses. It is given as a function of the radius both in the comoving and in the laboratory frames in Fig. A.3.8. Before the collision the PEM pulse expands keeping its temperature in the laboratory frame constant while its temperature in the comoving frame falls (see Ruffini et al., 1999). In fact we have:

$$\frac{d(\epsilon\gamma^2\mathcal{V})}{dt} = 0, \tag{A.3.2.54}$$

where the baryon mass-density is $\rho_B = 0$ and the thermal energy-density of photons and e^+e^--pairs is $\epsilon = \sigma_B T^4(1 + f_{e^+e^-})$, σ_B is the Boltzmann constant and $f_{e^+e^-}$ is the Fermi-integral for e^+ and e^-. This leads to

$$\epsilon\gamma^2\mathcal{V} = E_{\rm dya}, \quad T^4\gamma^2\mathcal{V} = \text{const.} \tag{A.3.2.55}$$

Since e^+ and e^- in the PEM pulse are extremely relativistic, we have the equation of state $p \simeq \epsilon/3$ and the thermal index defined in Eq. (A.3.2.5) $\Gamma \simeq 4/3$ in the evolution of PEM pulse. Eq.(A.3.2.55) is thus equivalent to

$$T^3\gamma\mathcal{V} \simeq \text{const.} \tag{A.3.2.56}$$

These two equations (A.3.2.54) and (A.3.2.56) result in the constancy of the laboratory temperature $T\gamma$ in the evolution of the PEM pulse.

It is interesting to note that Eqs.(A.3.2.55) and (A.3.2.56) hold as well in the cross-over region where $T \sim m_e c^2$ and e^+e^- annihilation takes place. In fact from the conservation of entropy it follows that asymptotically we have

$$\frac{(VT^3)_{T<m_e c^2}}{(VT^3)_{T>m_e c^2}} = \frac{11}{4}, \tag{A.3.2.57}$$

exactly for the same reasons and physics scenario discussed in the cosmological framework by Weinberg (see e.g. Eq. (15.6.37) of Weinberg, 1972). The same considerations when repeated for the conservation of the total energy $\epsilon\gamma V = \epsilon\gamma^2\mathcal{V}$ following from Eq. (A.3.2.54) then lead to

$$\frac{(VT^4\gamma)_{T<m_e c^2}}{(VT^4\gamma)_{T>m_e c^2}} = \frac{11}{4}. \tag{A.3.2.58}$$

The ratio of these last two quantities gives asymptotically

$$T_\circ = (T\gamma)_{T>m_e c^2} = (T\gamma)_{T<m_e c^2}, \tag{A.3.2.59}$$

where $T_\circ$ is the initial average temperature of the dyadosphere at rest.

During the collision of the PEM pulse with the remnant we have an increase in the number density of e^+e^- pairs (see Fig. A.3.8). This transition corresponds to an *increase* of the temperature in the comoving frame and a *decrease* of the temperature in the laboratory frame as a direct effect of the dropping of the gamma factor (see Fig. A.3.7).

After the collision we have the further acceleration of the PEMB pulse (see

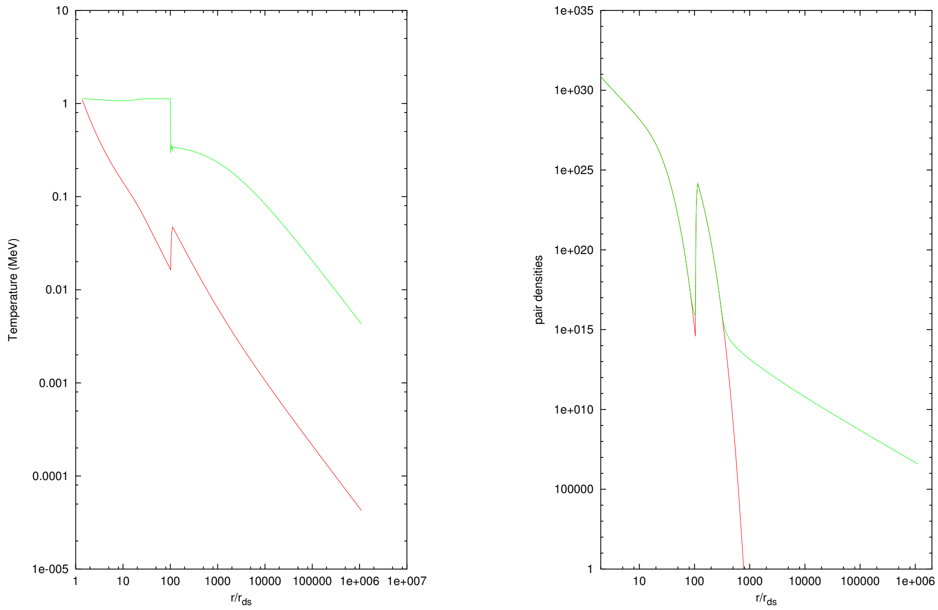

Figure A.3.8: Left: The temperature of the plasma in the comoving frame T'(MeV) (the red line) and in the laboratory frame $\gamma T'$ (the green line) are plotted as functions of the radius in the unit of the dyadosphere radius $r_{\rm ds}$. **Right:** The number densities $n_{e^+e^-}(T)$ (the red line) computed by the Fermi integral and $n_{e^+e^-}$ (the green line) computed by the rate equation (see section A.3.1.1) are plotted as functions of the radius. $T' \ll m_e c^2$, two curves strongly divergent due to e^+e^--pairs frozen out of the thermal equilibrium. The peak at $r \simeq 100 r_{\rm ds}$ is due to the internal energy developed in the collision.

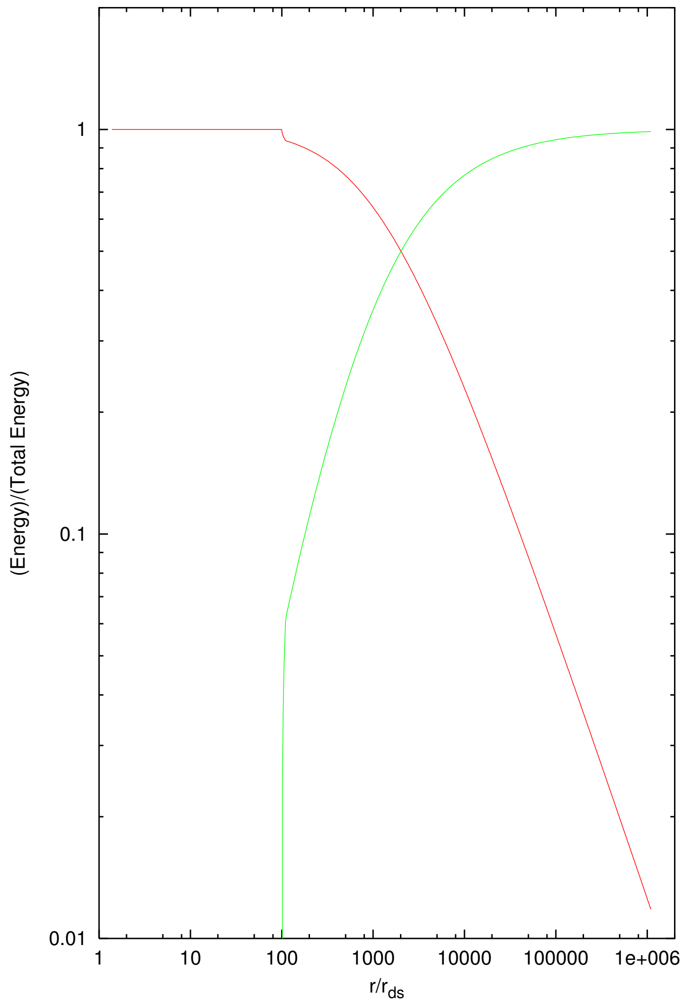

Figure A.3.9: The energy of the non baryonic components of the PEMB pulse (the red line) and the kinetic energy of the baryonic matter (the green line) in unit of the total energy are plotted as functions of the radius in the unit of the dyadosphere radius $r_{\rm ds}$.

Fig. A.3.7). The temperature now decreases both in the laboratory and the comoving frame (see Fig. A.3.8). Before the collision the total energy of the e^+e^- pairs and the photons is constant and equal to $E_{\rm dya}$. After the collision

$$E_{\rm dya} = E_{\rm Baryons} + E_{e^+e^-} + E_{\rm photons}, \tag{A.3.2.60}$$

which includes both the total energy $E_{e^+e^-} + E_{\rm photons}$ of the nonbaryonic components and the kinetic energy $E_{\rm Baryons}$ of the baryonic matter

$$E_{\rm Baryons} = \bar{\rho}_B V(\gamma - 1). \tag{A.3.2.61}$$

In Fig. A.3.9 we plot both the total energy $E_{e^+e^-} + E_{\rm photons}$ of the nonbaryonic components and the kinetic energy $E_{\rm Baryons}$ of the baryonic matter as functions of the radius for the typical case $E_{\rm dya} = 3.1 \times 10^{54}$ erg and $B = 10^{-2}$. Further details are given in Ruffini et al. (2000).

A.4 The optically thin "fireshell": the afterglow

The consensus has been reached that the afterglow emission originates from a relativistic thin shell of baryonic matter propagating in the CBM and that its description can be obtained from the relativistic conservation laws of energy and momentum. In both our approach and in the other ones in the current literature (see e.g. Piran, 1999; Chiang and Dermer, 1999; Ruffini et al., 2003; Bianco and Ruffini, 2005a) such conservations laws are used. The main difference is that in the current literature an ultra-relativistic approximation, following the Blandford and McKee (1976) self-similar solution, is widely adopted while we use the exact solution of the equations of motion. We express such equations in a finite difference formulation. For the differential formulation, which will be most useful in comparing and contrasting our exact solutions with the ones in the current literature, see the following report about "Relativistic effects in Physics and Astrophysics".

In analogy and by extension of the results obtained for the PEM and PEMB pulse cases, we also assume that the expansion of the ABM pulse through the CBM occurs keeping its width constant in the laboratory frame, although the results are quite insensitive to this assumption. Then we assume that this interaction can be represented by a sequence of inelastic collisions of the expanding ABM pulse with a large number of thin and cold CBM spherical shells at rest in the laboratory frame. Each of these swept up shells of thickness Δr has a mass $\Delta M_{\rm cbm}$ and is assumed to be located between two radial distances r_1 and r_2 (where $r_2 - r_1 = \Delta r \ll r_1$) in the laboratory frame. These collisions create an internal energy $\Delta E_{\rm int}$.

We indicate by $\Delta\epsilon$ the increase in the proper internal energy density due to the collision with a single shell and by ρ_B the proper energy density of the swept up baryonic matter. This includes the baryonic matter composing the remnant, already swept up in the PEMB pulse formation, and the baryonic matter from the CBM swept up by the ABM pulse:

$$\rho_B = \frac{(M_B + M_{\rm cbm})\, c^2}{V}. \tag{A.4.0.1}$$

Here V is the ABM pulse volume in the comoving frame, M_B is the mass of the baryonic remnant and $M_{\rm cbm}$ is the CBM mass swept up from the transparency point through the r in the laboratory frame:

$$M_{\rm cbm} = m_p n_{\rm cbm} \frac{4\pi}{3} \left(r^3 - r_\circ{}^3 \right) , \qquad \text{(A.4.0.2)}$$

where m_p the proton mass and $n_{\rm cbm}$ the number density of the CBM in the laboratory frame.

The energy conservation law in the laboratory frame at a generic step of the collision process is given by

$$\rho_{B_1} {\gamma_1}^2 \mathcal{V}_1 + \Delta M_{\rm cbm} c^2 = \left(\rho_{B_1} \frac{V_1}{V_2} + \frac{\Delta M_{\rm cbm} c^2}{V_2} + \Delta\epsilon \right) {\gamma_2}^2 \mathcal{V}_2, \qquad \text{(A.4.0.3)}$$

where the quantities with the index "1" are calculated before the collision of the ABM pulse with an elementary shell of thickness Δr and the quantities with "2" after the collision, γ is the gamma factor and $\mathcal{V}$ the volume of the ABM pulse in the laboratory frame so that $V = \gamma\mathcal{V}$. The momentum conservation law in the laboratory frame is given by

$$\rho_{B_1} \gamma_1 U_{r_1} \mathcal{V}_1 = \left(\rho_{B_1} \frac{V_1}{V_2} + \frac{\Delta M_{\rm cbm} c^2}{V_2} + \Delta\epsilon \right) \gamma_2 U_{r_2} \mathcal{V}_2, \qquad \text{(A.4.0.4)}$$

where $U_r = \sqrt{\gamma^2 - 1}$ is the radial covariant component of the four-velocity vector (see Ruffini et al., 1999, 2000). We thus obtain

$$\begin{aligned} \Delta\epsilon &= \rho_{B_1} \frac{\gamma_1 U_{r_1} \mathcal{V}_1}{\gamma_2 U_{r_2} \mathcal{V}_2} - \left(\rho_{B_1} \frac{V_1}{V_2} + \frac{\Delta M_{\rm cbm} c^2}{V_2} \right) , && \text{(A.4.0.5)} \\ \gamma_2 &= \frac{a}{\sqrt{a^2-1}}, \quad a \equiv \frac{\gamma_1}{U_{r_1}} + \frac{\Delta M_{\rm cbm} c^2}{\rho_{B_1} \gamma_1 U_{r_1} \mathcal{V}_1}. && \text{(A.4.0.6)} \end{aligned}$$

We can use for $\Delta\varepsilon$ the following expression

$$\Delta\varepsilon = \frac{E_{{\rm int}_2}}{V_2} - \frac{E_{{\rm int}_1}}{V_1} = \frac{E_{{\rm int}_1} + \Delta E_{\rm int}}{V_2} - \frac{E_{{\rm int}_1}}{V_1} = \frac{\Delta E_{\rm int}}{V_2} \qquad \text{(A.4.0.7)}$$

because we have assumed a "fully radiative regime" and so $E_{{\rm int}_1} = 0$. Substituting Eq.(A.4.0.6) in Eq.(A.4.0.5) and applying Eq.(A.4.0.7), we obtain:

$$\Delta E_{\rm int} = \rho_{B_1} V_1 \sqrt{1 + 2\gamma_1 \frac{\Delta M_{\rm cbm} c^2}{\rho_{B_1} V_1} + \left(\frac{\Delta M_{\rm cbm} c^2}{\rho_{B_1} V_1} \right)^2} - \rho_{B_1} V_1 \left(1 + \frac{\Delta M_{\rm cbm} c^2}{\rho_{B_1} V_1} \right) , \qquad \text{(A.4.0.8)}$$

$$\gamma_2 = \frac{\gamma_1 + \frac{\Delta M_{\rm cbm} c^2}{\rho_{B_1} V_1}}{\sqrt{1 + 2\gamma_1 \frac{\Delta M_{\rm cbm} c^2}{\rho_{B_1} V_1} + \left(\frac{\Delta M_{\rm cbm} c^2}{\rho_{B_1} V_1} \right)^2}} . \qquad \text{(A.4.0.9)}$$

A.5 The “canonical GRB” bolometric light curve

We assume that the internal energy due to kinetic collision is instantly radiated away and that the corresponding emission is isotropic. Let $\Delta\varepsilon$ be the internal energy density developed in the collision. In the comoving frame the energy per unit of volume and per solid angle is simply

$$\left(\frac{dE}{dVd\Omega}\right)_\circ = \frac{\Delta\varepsilon}{4\pi} \tag{A.5.0.1}$$

due to the fact that the emission is isotropic in this frame. The total number of photons emitted is an invariant quantity independent of the frame used. Thus we can compute this quantity as seen by an observer in the comoving frame (which we denote with the subscript “$\circ$”) and by an observer in the laboratory frame (which we denote with no subscripts). Doing this we find:

$$\frac{dN_\gamma}{dtd\Omega d\Sigma} = \left(\frac{dN_\gamma}{dtd\Omega d\Sigma}\right)_\circ \Lambda^{-3}\cos\vartheta\,, \tag{A.5.0.2}$$

where ϑ is the angle between the radial expansion velocity of a point on the fireshell surface and the line of sight, $\cos\vartheta$ comes from the projection of the elementary surface of the shell on the direction of propagation and $\Lambda = \gamma(1-\beta\cos\vartheta)$ is the Doppler factor introduced in the two following differential transformation

$$d\Omega_\circ = d\Omega \times \Lambda^{-2} \tag{A.5.0.3}$$

for the solid angle transformation and

$$dt_\circ = dt \times \Lambda^{-1} \tag{A.5.0.4}$$

for the time transformation. An extra Λ factor comes from the energy transformation:

$$E_\circ = E \times \Lambda \tag{A.5.0.5}$$

(see also Chiang and Dermer, 1999). Thus finally we obtain:

$$\frac{dE}{dtd\Omega d\Sigma} = \left(\frac{dE}{dtd\Omega d\Sigma}\right)_\circ \Lambda^{-4}\cos\vartheta\,. \tag{A.5.0.6}$$

Doing this we clearly identify $\left(\frac{dE}{dtd\Omega d\Sigma}\right)_\circ$ as the energy density in the comoving frame up to a factor $\frac{v}{4\pi}$ (see Eq.(A.5.0.1)). Then we have:

$$\frac{dE}{dtd\Omega} = \int_{shell} \frac{\Delta\varepsilon}{4\pi}\, v\ \cos\vartheta\ \Lambda^{-4}\ d\Sigma\,, \tag{A.5.0.7}$$

where the integration in $d\Sigma$ is performed over the visible area of the ABM pulse at laboratory time t, namely with $0 \le \vartheta \le \vartheta_{max}$ and ϑ_{max} is the boundary of the visible region defined by (see also the following report about "Relativistic effects in Physics and Astrophysics"):

$$\cos\vartheta_{max} = \frac{v}{c}\,. \tag{A.5.0.8}$$

Eq.(A.5.0.7) gives us the energy emitted toward the observer per unit solid angle and per unit laboratory time t in the laboratory frame.

What we really need is the energy emitted per unit solid angle and per unit detector arrival time t_a^d, so we must use the complete relation between t_a^d and t given by (see also the following report about "Relativistic effects in Physics and Astrophysics"):

$$t_a^d = (1+z)\left[t - \frac{r}{c}\,(t)\cos\vartheta + \frac{r^\star}{c}\right]\,, \tag{A.5.0.9}$$

where $r^\star$ is the initial size of the fireshell. First we have to multiply the integrand in Eq.(A.5.0.7) by the factor $\left(dt/dt_a^d\right)$ to transform the energy density generated per unit of laboratory time t into the energy density generated per unit arrival time t_a^d. Then we have to integrate with respect to $d\Sigma$ over the EQTS corresponding to arrival time t_a^d instead of the ABM pulse visible area at laboratory time t. The analog of Eq.(A.5.0.7) for the source luminosity in detector arrival time is then:

$$\frac{dE_\gamma}{dt_a^d d\Omega} = \int_{EQTS} \frac{\Delta\varepsilon}{4\pi}\, v\ \cos\vartheta\ \Lambda^{-4}\ \frac{dt}{dt_a^d} d\Sigma\,. \tag{A.5.0.10}$$

It is important to note that, in the present case of GRB 991216, the Doppler factor Λ^{-4} in Eq.(A.5.0.10) enhances the apparent luminosity of the burst, as compared to the intrinsic luminosity, by a factor which at the peak of the afterglow is in the range between 10^{10} and 10^{12}!

We are now able to reproduce in Fig. A.2.5 the general behavior of the luminosity starting from the P-GRB to the latest phases of the afterglow as a function of the arrival time. It is generally agreed that the GRB afterglow originates from an ultrarelativistic shell of baryons with an initial Lorentz factor $\gamma_\circ \sim 200$–300 with respect to the CBM (see e.g. Ruffini et al., 2003; Bianco and Ruffini, 2004, and references therein). Using GRB 991216 as a prototype, in

Table A.5.1: For each CBM density peak represented in Fig. A.5.1 we give the initial radius r, the corresponding comoving time τ, laboratory time t, arrival time at the detector t_a^d, diameter of the ABM pulse visible area d_v, Lorentz factor γ and observed duration Δt_a^d of the afterglow luminosity peaks generated by each density peak. In the last column, the apparent motion in the radial coordinate, evaluated in the arrival time at the detector, leads to an enormous "superluminal" behavior, up to $9.5 \times 10^4\,c$.

Peak	$r(cm)$	$\tau(s)$	$t(s)$	$t_a^d(s)$	$d_v(cm)$	$\Delta t_a^d(s)$	γ	"Superluminal" $v \equiv \frac{r}{t_a^d}$
A	4.50×10^{16}	4.88×10^3	1.50×10^6	15.8	2.95×10^{14}	0.400	303.8	$9.5 \times 10^4 c$
B	5.20×10^{16}	5.74×10^3	1.73×10^6	19.0	3.89×10^{14}	0.622	265.4	$9.1 \times 10^4 c$
C	5.70×10^{16}	6.54×10^3	1.90×10^6	22.9	5.83×10^{14}	1.13	200.5	$8.3 \times 10^4 c$
D	6.20×10^{16}	7.64×10^3	2.07×10^6	30.1	9.03×10^{14}	5.16	139.9	$6.9 \times 10^4 c$
E	6.50×10^{16}	9.22×10^3	2.17×10^6	55.9	2.27×10^{15}	10.2	57.23	$3.9 \times 10^4 c$
F	6.80×10^{16}	1.10×10^4	2.27×10^6	87.4	2.42×10^{15}	10.6	56.24	$2.6 \times 10^4 c$

Ruffini et al. (2001c,b) we have shown how from the time varying bolometric intensity of the afterglow it is possible to infer the average density $\langle n_{cbm} \rangle = 1$ particle/cm^3 of the CBM in a region of approximately 10^{17} cm surrounding the black hole giving rise to the GRB phenomenon.

The summary of these general results are shown in Fig. A.2.4, where the P-GRB, the emission at the peak of the afterglow in relation to the "prompt emission" and the latest part of the afterglow are clearly identified for the source GRB 991216. Details in Ruffini et al. (2003).

A.5.1 On the structures in the afterglow peak emission

We are now ready to reconsider the problem of the CBM inhomogeneity generating the temporal substructures in the E-APE by integrating on the EQTS surfaces and improving on the considerations based on the purely radial approximation. It was shown in Ruffini et al. (2002a) that the theoretical interpretation of the intensity variations in the prompt phase in the afterglow implies the presence in the CBM of inhomogeneities of typical scale 10^{15} cm. Such inhomogeneities were there represented for simplicity as spherically symmetric over-dense regions with $\langle n_{cbm}^{od} \rangle \simeq 10^2 \langle n_{cbm} \rangle$ separated by under-dense regions with $\langle n_{cbm}^{ud} \rangle \simeq 10^{-2} \langle n_{cbm} \rangle$ also of typical scale $\sim 10^{15}$ cm in order to keep $\langle n_{cbm} \rangle$ constant (see Fig. A.5.1 and Tab. A.5.1).

The results are given in Fig. A.5.2. We obtain, in perfect agreement with the observations:

1. the theoretically computed intensity of the A, B, C peaks as a function of the CBM inhomogneities;

2. the fast rise and exponential decay shape for each peak;

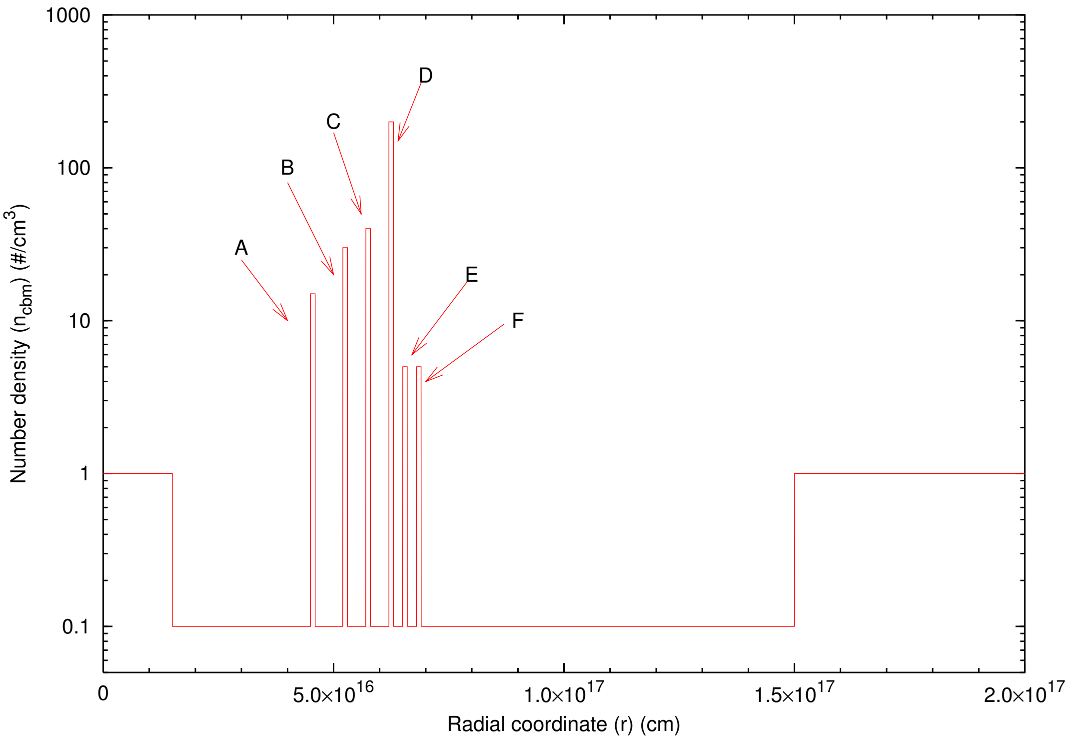

Figure A.5.1: The density profile ("mask") of an CBM cloud used to reproduce the GRB 991216 temporal structure. As before, the radial coordinate is measured from the black hole. In this cloud we have six "spikes" with overdensity separated by low density regions. Each spike has the same spatial extension of 10^{15} cm. The cloud average density is $< n_{cbm} >= 1$ particle/cm^3.

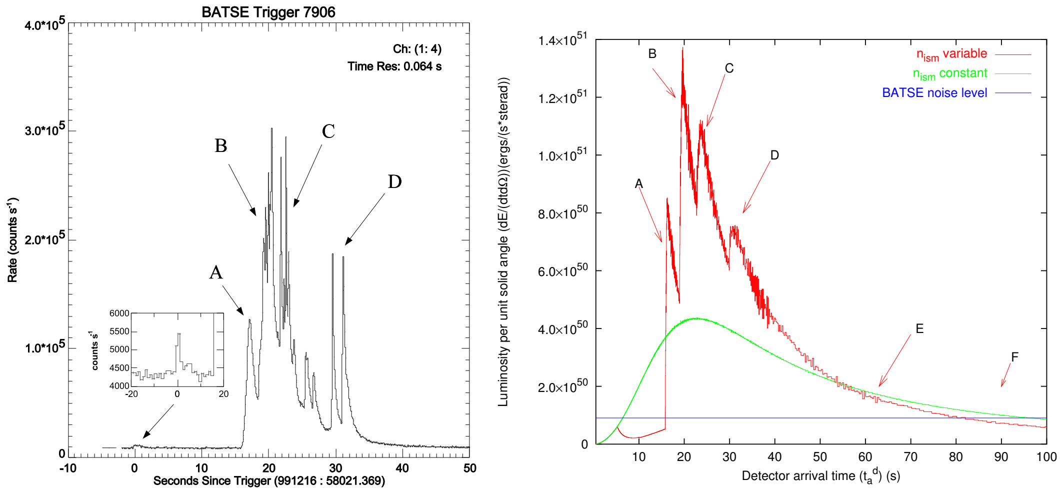

Figure A.5.2: Left: The BATSE data on the E-APE of GRB 991216 (source: Curves (1999)) together with an enlargement of the P-GRB data (source: Response (1999)). For convenience each E-APE peak has been labeled by a different uppercase Latin letter. **Right:** The source luminosity connected to the mask in Fig. A.5.1 is given as a function of the detector arrival time (red "spiky" line) with the corresponding curve for the case of constant $n_{cbm} = 1\,\text{particle}/\text{cm}^3$ (green smooth line) and the BATSE noise level (blue horizontal line). The "noise" observed in the theoretical curves is due to the discretization process adopted, described in Ruffini et al. (2002a), for the description of the angular spreading of the scattered radiation. For each fixed value of the laboratory time we have summed 500 different contributions from different angles. The integration of the equation of motion of this system is performed in $22, 314, 500$ contributions to be considered. An increase in the number of steps and in the precision of the numerical computation would lead to a smoother curve.

3. a continuous and smooth emission between the peaks.

Interestingly, the signals from shells E and F, which have a density inhomogeneity comparable to A, are undetectable. The reason is due to a variety of relativistic effects and partly to the spreading in the arrival time, which for A, corresponding to $\gamma = 303.8$ is $0.4s$ while for E (F) corresponding to $\gamma = 57.23$ (56.24) is of $10.2\,\text{s}$ $(10.6\,\text{s})$ (see Tab. A.5.1 and Ruffini et al., 2002a).

In the case of D, the agreement with the arrival time is reached, but we do not obtain the double peaked structure. The ABM pulse visible area diameter at the moment of interaction with the D shell is $\sim 1.0 \times 10^{15}$ cm, equal to the extension of the CBM shell (see Tab. A.5.1 and Ruffini et al., 2002a). Under these conditions, the concentric shell approximation does not hold anymore: the disagreement with the observations simply makes manifest the need for a more detailed description of the three dimensional nature of the CBM cloud.

The physical reasons for these results can be simply summarized: we can distinguish two different regimes corresponding in the afterglow of GRB 991216 respectively to $\gamma > 150$ and to $\gamma < 150$. For different sources this value may be slightly different. In the E-APE region ($\gamma > 150$) the GRB substructure intensities indeed correlate with the CBM inhomogeneities. In this limited region (see peaks A, B, C) the Lorentz gamma factor of the ABM pulse ranges from $\gamma \sim 304$ to $\gamma \sim 200$. The boundary of the visible region is smaller than the thickness ΔR of the inhomogeneities (see Tab. A.5.1). Under this condition the adopted spherical approximation is not only mathematically simpler but also fully justified. The angular spreading is not strong enough to wipe out the signal from the inhomogeneity spike.

As we descend in the afterglow ($\gamma < 150$), the Lorentz gamma factor decreases markedly and in the border line case of peak D $\gamma \sim 140$. For the peaks E and F we have $\gamma \sim 50$ and, under these circumstances, the boundary of the visible region becomes much larger than the thickness ΔR of the inhomogeneities (see Tab. A.5.1). A three dimensional description would be necessary, breaking the spherical symmetry and making the computation more difficult. However we do not need to perform this more complex analysis for peaks E and F: any three dimensional description would *a fortiori* augment the smoothing of the observed flux. The spherically symmetric description of the inhomogeneities is already enough to prove the overwhelming effect of the angular spreading (Ruffini et al., 2002a).

From our analysis we show that the Dermer and Mitman (1999) conclusions are correct for $\gamma \sim 300$ and do indeed hold for $\gamma > 150$. However, as the gamma factor drops from $\gamma \sim 150$ to $\gamma \sim 1$ (see Fig A.2.3), the intensity due to the inhomogeneities markedly decreases also due to the angular spreading (events E and F). The initial Lorentz factor of the ABM pulse $\gamma \sim 310$ decreases very rapidly to $\gamma \sim 150$ as soon as a fraction of a typical CBM cloud is engulfed (see Tab. A.5.1). We conclude that the "tomography" is indeed effective, but uniquely in the first CBM region close to the source and for GRBs with $\gamma > 150$.

One of the most striking feature in our analysis is clearly represented by the fact that the inhomogeneities of a mask of radial dimension of the order of 10^{17} cm give rise to arrival time signals of the order of 20 s. This outstanding result implies an apparent "superluminal velocity" of $\sim 10^5 c$ (see Tab. A.5.1). The "superluminal velocity" here considered, first introduced in Ruffini et al. (2001c), refers to the motion along the line of sight. This effect is proportional to γ^2. It is much larger than the one usually considered in the literature, within the context of radio sources and microquasars (see e.g. Mirabel and Rodriguez, 1994), referring to the component of the velocity at right angles to the line of sight (see details in Ruffini et al., 2002a). This second effect is in fact proportional to γ (see Rees, 1966). We recall that this "superluminal velocity" was the starting point for the enunciation of the RSTT paradigm (Ruffini et al., 2001c), emphasizing the need of the knowledge of the *entire* past worldlines of the source. This need has been further clarified here in the determination of the EQTS surfaces which indeed depend on an integral of the Lorentz gamma factor extended over the *entire* past worldlines of the source. In turn, therefore, the agreement between the observed structures and the theoretical predicted ones (see Figs. A.2.4–A.5.2) is also an extremely stringent additional test on the values of the Lorentz gamma factor determined as a function of the radial coordinate within the fireshell model (see Fig. A.2.3).

A.5.2 The "canonical" GRB scenario: "genuine" and "fake" short GRBs

Summarizing, unlike treatments in the current literature (see e.g. Piran, 2005; Meszaros, 2006, and references therein), we define a "canonical GRB" light curve with two sharply different components (see Fig. A.2.4 and Ruffini et al., 2001b, 2007a; Bernardini et al., 2007):

1. **The P-GRB:** it has the imprint of the black hole formation, an harder spectrum and no spectral lag (Bianco et al., 2001; Ruffini et al., 2005d).

2. **The afterglow:** it presents a clear hard-to-soft behavior (Bernardini et al., 2005a; Ruffini et al., 2004b, 2006b); the peak of the afterglow contributes to what is usually called the "prompt emission" (see e.g. Ruffini et al., 2001b, 2006b; Dainotti et al., 2007).

The ratio between the total time-integrated luminosity of the P-GRB (namely, its total energy) and the corresponding one of the afterglow is the crucial quantity for the identification of GRBs' nature. Such a ratio, as well as the temporal separation between the corresponding peaks, is a function of the B parameter (Ruffini et al., 2001b).

When the P-GRB is the leading contribution to the emission and the afterglow is negligible we have a "genuine" short GRB (Ruffini et al., 2001b). This is the case where $B \lesssim 10^{-5}$ (see Fig. A.2.8): in the limit $B \to 0$ the afterglow vanishes (see Fig. A.2.8). In the other GRBs, with $10^{-4} \lesssim B \lesssim 10^{-2}$, the afterglow contribution is generally predominant (see Fig. A.2.8; for the existence of the upper limit $B \lesssim 10^{-2}$ see Ruffini et al., 2000; Dainotti et al., 2007). Still, this case presents two distinct possibilities:

- The afterglow peak luminosity is **larger** than the P-GRB one. A clear example of this situation is GRB 991216, represented in Fig. A.2.4.

- The afterglow peak luminosity is **smaller** than the P-GRB one. A clear example of this situation is GRB 970228, represented in Fig. A.12.1.

The simultaneous occurrence of an afterglow with total time-integrated luminosity larger than the P-GRB one, but with a smaller peak luminosity, is indeed explainable in terms of a peculiarly small average value of the CBM density, compatible with a galactic halo environment, and not due to the intrinsic nature of the source (see Fig. A.12.1 and Bernardini et al., 2007). Such a small average CBM density deflates the afterglow peak luminosity. Of course, such a deflated afterglow lasts much longer, since the total time-integrated luminosity in the afterglow is fixed by the value of the B parameter (see above and Fig. A.12.3). In this sense, GRBs belonging to this class are only "fake" short GRBs. This is GRB class identified by Norris and Bonnell (2006), which also GRB 060614 belongs to, and which has GRB 970228 as a prototype (Bernardini et al., 2007).

Our "canonical GRB" scenario, therefore, especially points out the need to distinguish between "genuine" and "fake" short GRBs:

- The **"genuine" short GRBs** inherit their features from an intrinsic property of their sources. The very small fireshell baryon loading, in fact, implies that the afterglow time-integrated luminosity is negligible with respect to the P-GRB one.

- The **"fake" short GRBs**, instead, inherit their features from the environment. The very small CBM density, in fact, implies that the afterglow peak luminosity is lower than the P-GRB one, even if the afterglow total time-integrated luminosity is higher. This deflated afterglow peak can be observed as a "soft bump" following the P-GRB spike, as in GRB 970228 (Bernardini et al., 2007), GRB 060614 (Caito et al., in preparation), and the sources analyzed by Norris and Bonnell (2006).

A sketch of the different possibilities depending on the fireshell baryon loading B and the average CBM density $\langle n_{cbm} \rangle$ is given in Fig. A.5.3.

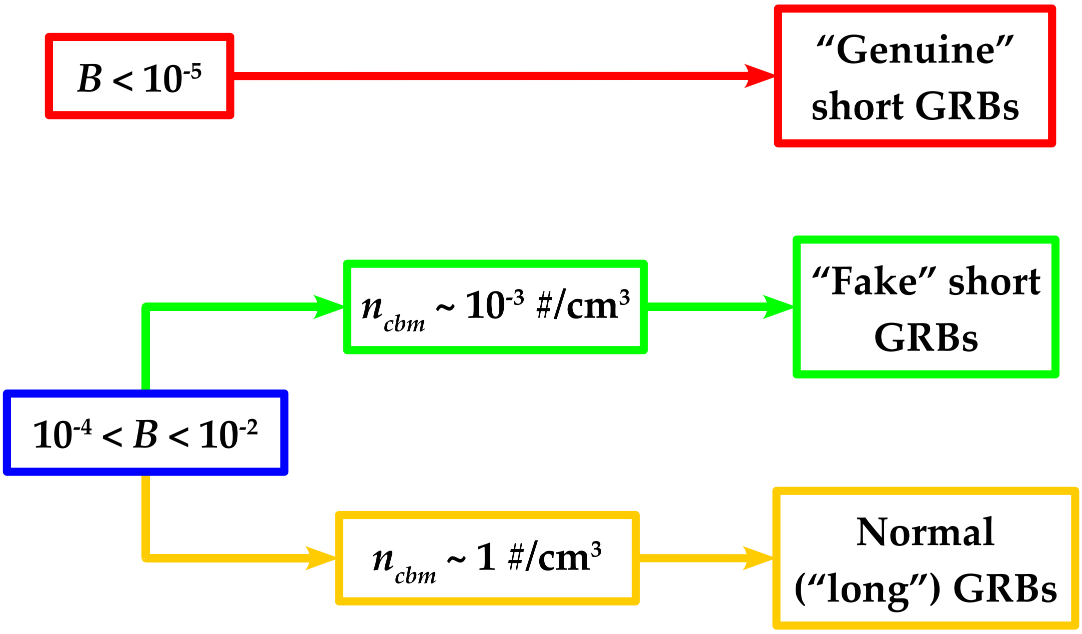

Figure A.5.3: A sketch summarizing the different possibilities predicted by the "canonical GRB" scenario depending on the fireshell baryon loading B and the average CBM density $\langle n_{cbm} \rangle$.

A.6 The spectra of the afterglow

In our approach we focus uniquely on the X and gamma ray radiation, which appears to be conceptually much simpler than the optical and radio emission. It is perfectly predictable by a set of constitutive equations (see section A.6.1), which leads to directly verifiable and very stable features in the spectral distribution of the observed GRB afterglows. In line with the observations of GRB 991216 and other GRB sources, we assume in the following that the X and gamma ray luminosity represents approximately 90% of the energy flux of the afterglow, while the optical and radio emission represents only the remaining 10%.

This approach differs significantly from the other ones in the current literature, where attempts are made to explain at once all the multi-wavelength emission in the radio, optical, X and gamma ray as coming from a common origin which is linked to boosted synchrotron emission. Such an approach has been shown to have a variety of difficulties (Ghirlanda et al., 2002; Preece et al., 1998) and cannot anyway have the instantaneous variability needed to explain the structure in the "prompt radiation" in an external shock scenario, which is indeed confirmed by our model.

A.6.1 The luminosity in fixed energy bands

Here the fundamental new assumption is adopted (see also Ruffini et al., 2004b) that the X and gamma ray radiation during the entire afterglow phase has a thermal spectrum in the comoving frame. The temperature is then given by:

$$T_s = \left[\Delta E_{\rm int} / \left(4\pi r^2 \Delta\tau \sigma \mathcal{R}\right)\right]^{1/4} , \tag{A.6.1.1}$$

where $\Delta E_{\rm int}$ is the internal energy developed in the collision with the CBM in a time interval $\Delta\tau$ in the co-moving frame, σ is the Stefan-Boltzmann constant and

$$\mathcal{R} = A_{eff} / A_{vis} , \tag{A.6.1.2}$$

is the ratio between the "effective emitting area" of the ABM pulse of radius r and its total visible area, which accounts for the CBM filamentary structure (Ruffini et al., 2005c). Due to the CBM inhomogeneities the ABM emitting region is in fact far from being homogeneous. In GRB 991216 such a factor is observed to be decreasing during the afterglow between: $3.01 \times 10^{-8} \geq \mathcal{R} \geq$

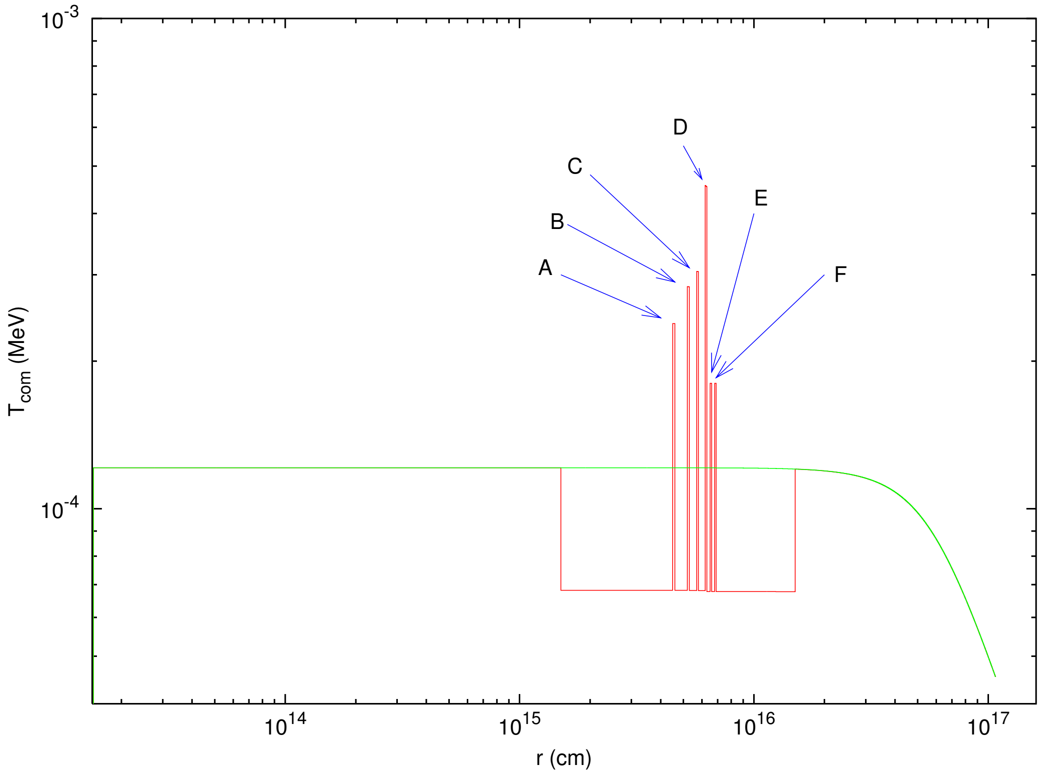

Figure A.6.1: The temperature in the comoving frame of the shock front corresponding to the density distribution with the six spikes A,B,C,D,E,F presented in Fig. A.5.1. The green line corresponds to an homogeneous distribution with $n_{cbm} = 1$. Details in Ruffini et al. (2005c).

5.01×10^{-12} (Ruffini et al., 2004b).

The temperature in the comoving frame corresponding to the density distribution described in Ruffini et al. (2002a) is shown in Fig. A.6.1.

We are now ready to evaluate the source luminosity in a given energy band. The source luminosity at a detector arrival time t_a^d, per unit solid angle $d\Omega$ and in the energy band $[\nu_1, \nu_2]$ is given by (see Ruffini et al., 2003, 2004b):

$$\frac{dE_\gamma^{[\nu_1,\nu_2]}}{dt_a^d d\Omega} = \int_{EQTS} \frac{\Delta\varepsilon}{4\pi}\, v\, \cos\vartheta\, \Lambda^{-4}\, \frac{dt}{dt_a^d} W(\nu_1, \nu_2, T_{arr})\, d\Sigma\,, \tag{A.6.1.3}$$

where $\Delta\varepsilon = \Delta E_{int}/V$ is the energy density released in the interaction of the ABM pulse with the CBM inhomogeneities measured in the comoving frame, $\Lambda = \gamma(1-(v/c)\cos\vartheta)$ is the Doppler factor, $W(\nu_1, \nu_2, T_{arr})$ is an "effective weight" required to evaluate only the contributions in the energy band $[\nu_1, \nu_2]$, $d\Sigma$ is the surface element of the EQTS at detector arrival time t_a^d on which the integration is performed (see also Ruffini et al., 2005c) and T_{arr} is the observed temperature of the radiation emitted from $d\Sigma$:

$$T_{arr} = T_s / \left[\gamma \left(1 - (v/c) \cos\vartheta\right) (1+z)\right] \ . \qquad (A.6.1.4)$$

The "effective weight" $W(\nu_1, \nu_2, T_{arr})$ is given by the ratio of the integral over the given energy band of a Planckian distribution at a temperature T_{arr} to the total integral aT_{arr}^4:

$$W(\nu_1, \nu_2, T_{arr}) = \frac{1}{aT_{arr}^4} \int_{\nu_1}^{\nu_2} \rho(T_{arr}, \nu)\, d\left(\frac{h\nu}{c}\right)^3 \ , \qquad (A.6.1.5)$$

where $\rho(T_{arr}, \nu)$ is the Planckian distribution at temperature T_{arr}:

$$\rho(T_{arr}, \nu) = \left(2/h^3\right) h\nu / \left(e^{h\nu/(kT_{arr})} - 1\right) \qquad (A.6.1.6)$$

A.6.2 The time integrated spectra and the hard-to-soft transition

We turn now to the much debated issue of the origin of the observed hard-to-soft spectral transition during the GRB observations (see e.g. Frontera et al., 2000; Ghirlanda et al., 2002; Piran, 1999; Piro et al., 1999). We consider the instantaneous spectral distribution of the observed radiation for three different EQTSs:

- $t_a^d = 10$ s, in the early radiation phase near the peak of the luminosity,
- $t_a^d = 1.45 \times 10^5$ s, in the last observation of the afterglow by the Chandra satellite, and
- $t_a^d = 10^4$ s, chosen in between the other two (see Fig. A.6.2).

The observed hard-to-soft spectral transition is then explained and traced back to:

1. a time decreasing temperature of the thermal spectrum measured in the comoving frame,
2. the GRB equations of motion,
3. the corresponding infinite set of relativistic transformations.

A clear signature of our model is the existence of a common low-energy behavior of the instantaneous spectrum represented by a power-law with index $\alpha = 0.9$. This prediction will be possibly verified in future observations.

Starting from these instantaneous values, we integrate the spectra in arrival time obtaining what is usually fit in the literature by the "Band relation"

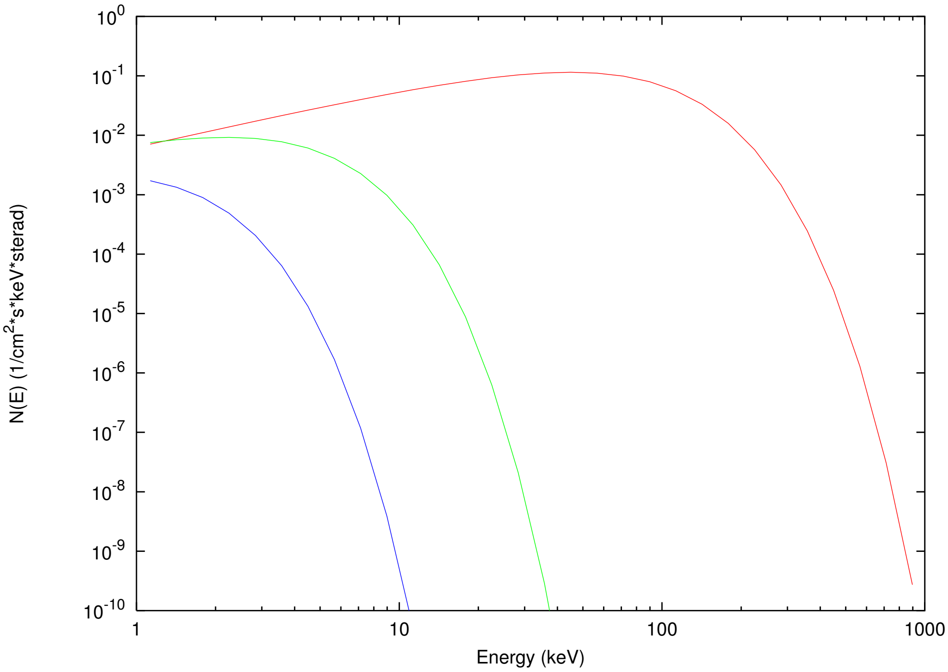

Figure A.6.2: The instantaneous spectra of the radiation observed in GRB 991216 at three different EQTS respectively, from top to bottom, for $t_a^d = 10$ s, $t_a^d = 10^4$ s and $t_a^d = 1.45 \times 10^5$ s. These diagrams have been computed assuming a constant $\langle n_{cbm} \rangle \simeq 1$ particle/cm^3 and clearly explains the often quoted hard-to-soft spectral evolution in GRBs. Details in Ruffini et al. (2004b).

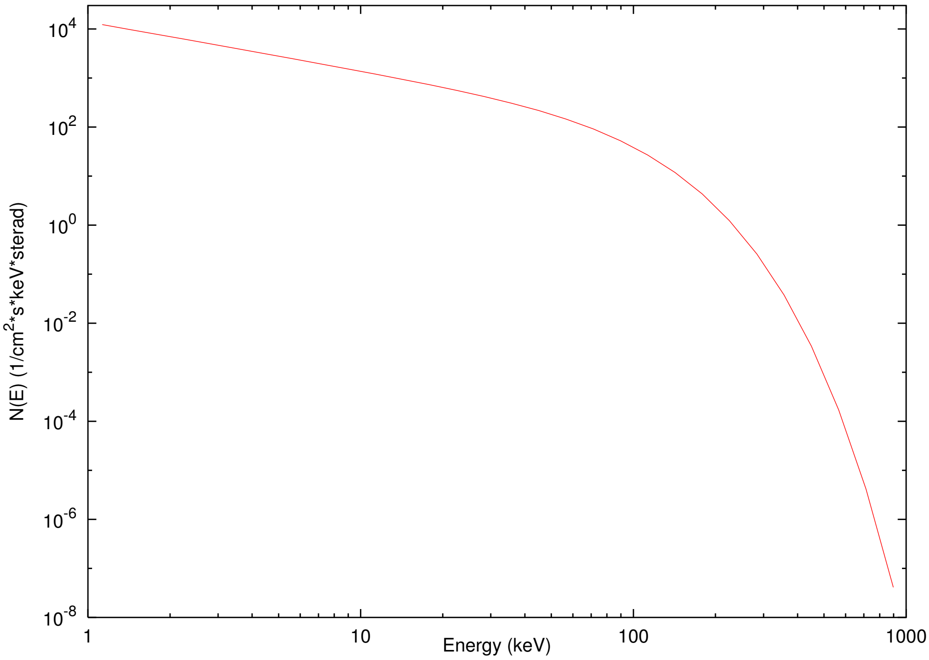

Figure A.6.3: The time-integrated spectrum of the radiation observed in GRB 991216. The low energy part of the curve below 10 keV is fit by a power-law with index $\alpha = -1.05$ and the high energy part above 500 keV is fit by a power-law with an index $\beta < -16$. Details in Ruffini et al. (2004b).

(Band et al., 1993). Indeed we find for our integrated spectra a low energy spectral index $\alpha = -1.05$ and an high energy spectral index $\beta < -16$ when interpreted within the framework of a Band relation (see Fig. A.6.3). This theoretical result can be submitted to a direct confrontation with the observations of GRB 991216 and, most importantly, the entire theoretical framework which we have developed can now be applied to any GRB, as we will se in section A.8. The theoretical predictions on the luminosity in fixed energy bands so obtained can be then straightforwardly confronted with the observational data.

A.6.3 Evidence for isotropic emission in GRB991216

We give in Fig. A.6.4 the results of the fit of the GRB 991216 light curves in the two energy bands 50–300 keV (observed by BATSE) and 2–10 keV (observed by R-XTE and Chandra). We already pointed out in the previous section the agreement with the data of the "prompt" radiation obtained by BATSE in the energy range 50–300 keV (see blue line in Fig. A.6.4). We here show the fit of the data obtained by the R-XTE and Chandra satellites (Halpern et al., 2000)

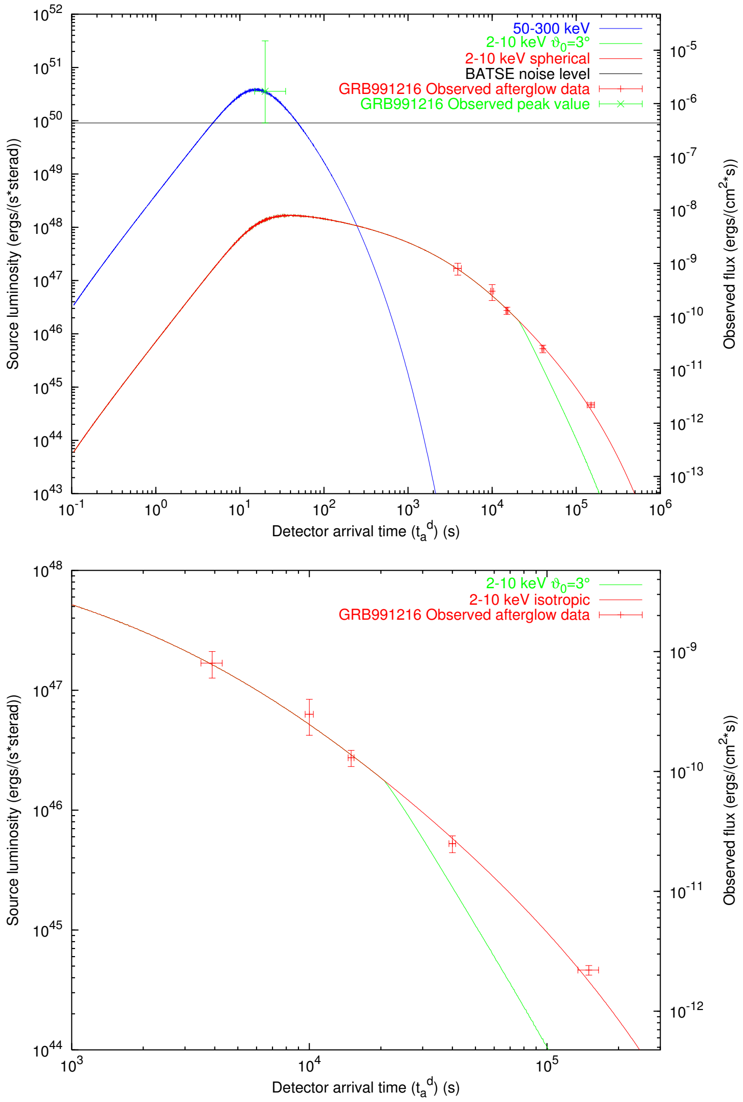

Figure A.6.4: Above: Best fit of the afterglow data of GRB 991216. The blue line is the luminosity in the 50–300 keV energy band. The red line is the luminosity in the 2–10 keV band computed assuming spherical symmetry. The observational data from R-XTE and Chandra (see Halpern et al., 2000) are perfectly consistent with such an assumption. The presence of a $\vartheta_\circ = 3^\circ$ half-opening beaming angle (green line) is ruled out. **Below:** Enlargement of the plot in the region of the afterglow observational data from R-XTE and Chandra.

in the energy range 2–10 keV (see red line in Fig. A.6.4). These data refer to the decaying part of the afterglow and cover a time span of $\sim 10^6$ s.

We have also computed, within our global self-consistent approach which fits both the "prompt" radiation and the decaying part of the afterglow, the flux in the 2–10 keV range which would be expected for a beamed emission with half opening angle $\vartheta_\circ = 3^\circ$, which is the value claimed in the current literature for GRB 991216 (see Halpern et al., 2000, and Fig. A.6.4). The presence of beaming is manifest, as expected, in the decaying part of the afterglow and is incompatible with the data. In fact, the actual afterglow luminosity in fixed energy bands, in spherical symmetry, does not have a simple power law dependence on arrival time (see Fig. A.6.4). This circumstance has been erroneously interpreted, in the usual presentation in the literature, as a broken power-law supporting the existence of jet-like structures in GRBs. Moreover, the slope of the beamed emission and the arrival time at which the break occurs have been there computed using the approximate equations (see the following report about "Relativistic effects in Physics and Astrophysics"and Bianco and Ruffini, 2004, 2005b,a, 2006). If one assumes the presence of jets in a consistent afterglow theory, one finds that the break corresponding to the purported beaming appears at an arrival time incompatible with the observations (see Fig. A.6.4 and Ruffini et al., 2006c).

A.7 On the GRB-SN association

Models of GRBs based on a single source (the "collapsar") generating both the SN and the GRB abounds in the literature (see e.g. Woosley and Bloom, 2006). Since the two phenomena are qualitatively very different, in our approach we have emphasized the concept of induced gravitational collapse, which occurs strictly in a binary system. The SN originates from a star evolved out of the main sequence and the GRB from the collapse to a black hole. The concept of induced collapse implies at least two alternative scenarios. In the first, the GRB triggers a SN explosion in the very last phase of the thermonuclear evolution of a companion star (Ruffini et al., 2001a). In the second, the early phases of the SN induce gravitational collapse of a companion neutron star to a black hole (Ruffini, 2006). Of course, in absence of SN, there is also the possibility that the collapse to a black hole, generating the GRB, occurs in a single star system or in the final collapse of a binary neutron star system. Still, in such a case there is also the possibility that the black hole progenitor is represented by a binary system composed by a white dwarf and/or a neutron star and/or a black hole in various combinations. What is most remarkable is that, following the "uniqueness of the black hole" (see Ruffini, in pressb), all these collapses lead to a common GRB independently of the nature of their progenitors.

Having obtained success in the fit of GRB 991216, as well as of GRB 031203 and GRB 050315 (see sections A.8 and A.9), we turn to the application of our theoretical analysis to the GRBs associated with SNe. We start with GRB 980425 / SN 1998bw. We have however to caution about the validity of this fit. From the available data of BeppoSAX, BATSE, XMM and Chandra, only the data of the prompt emission ($t_a^d < 10^2$ s) and of the latest afterglow phases ($t_a^d > 10^5$ s all the way to more than 10^8 s!) were available. Our fit refers only to the prompt emission, as usually interpreted as the peak of the afterglow. The fit, therefore, represents an underestimate of the GRB 980425 total energy and in this sense it is not surprising that it does not fit the Amati et al. (2002) relation. The latest afterglow emission, the URCA-1 emission, presents a different problematic which we will shortly address (see below).

A.7.1 GRB 980425 / SN 1998bw / URCA-1

The best fit of the observational data of GRB 980425 (Pian et al., 2000; Frontera et al., 2000) leads to $E_{e^\pm}^{tot} = 1.2 \times 10^{48}$ erg and $B = 7.7 \times 10^{-3}$. This implies

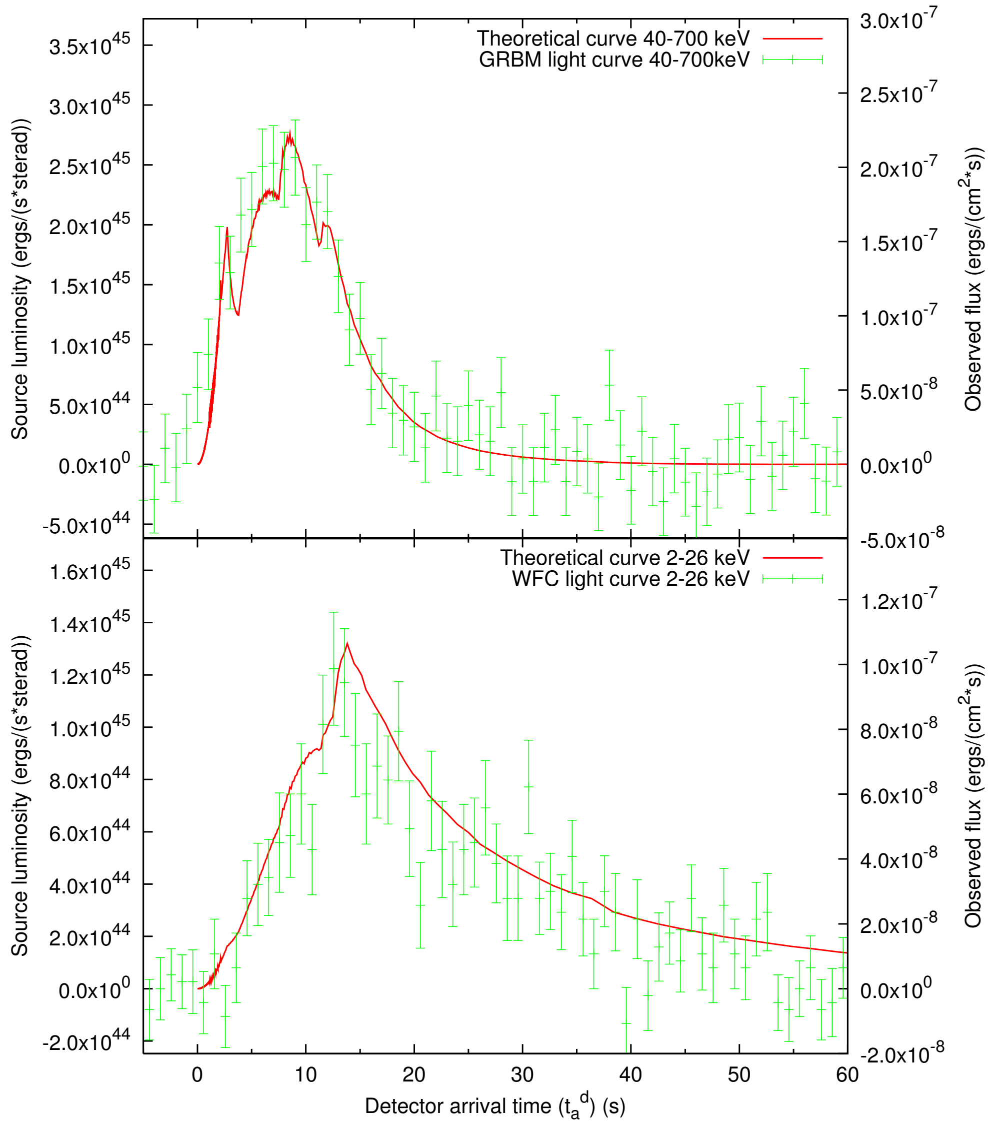

Figure A.7.1: Theoretical light curves of GRB 980425 prompt emission in the 40–700 keV and 2–26 keV energy bands (red line), compared with the observed data respectively from Beppo-SAX GRBM and WFC (see Pian et al., 2000; Frontera et al., 2000).

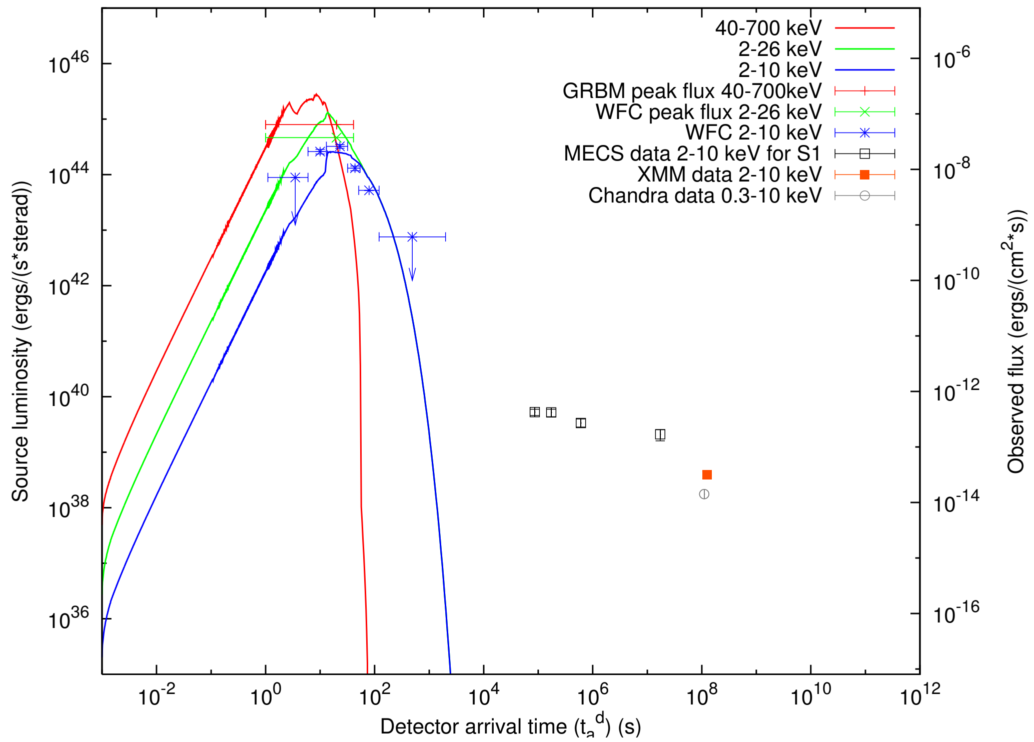

Figure A.7.2: Theoretical light curves of GRB 980425 in the 40–700 keV (red line), 2–26 keV (green line), 2–10 keV (blue line) energy bands, represented together with URCA-1 observational data. All observations are by BeppoSAX (Pian et al., 2000), with the exception of the last two URCA-1 points, which is observed by XMM and Chandra (Pian et al., 2004; Kouveliotou et al., 2004).

an initial $e^{\pm}$ plasma with $N_{e^+e^-} = 3.6 \times 10^{53}$ and with an initial temperature $T = 1.2$ MeV. After the transparency point, the initial Lorentz gamma factor of the accelerated baryons is $\gamma_\circ = 124$. The variability of the luminosity, due to the inhomogeneities of the CBM, is characterized by a density contrast $\delta n/n \sim 10^{-1}$ on a length scale of $\Delta \sim 10^{14}$ cm. We determine the effective CBM parameters to be: $\langle n_{cbm} \rangle = 2.5 \times 10^{-2}$ particle$/cm^3$ and $\langle \mathcal{R} \rangle = 1.2 \times 10^{-8}$.

In Fig. A.7.1 we test our specific theoretical assumptions comparing our theoretically computed light curves in the 40–700 and 2–26 keV energy bands with the observations by the BeppoSAX GRBM and WFC during the first 60 s of data (see Pian et al., 2000; Frontera et al., 2000). The agreement between observations and theoretical predictions in Fig. A.7.1 is very satisfactory.

In Fig. A.7.2 we summarize some of the problematic implicit in the old pre-*Swift* era: data are missing in the crucial time interval between 60 s and 10^5 s, when the BeppoSAX NFI starts to point the GRB 980425 location. In this region we have assumed, for the effective CBM parameters, constant values inferred by the last observational data. Currently we are relaxing this condition, also in view of the interesting paper by Ghisellini et al. (2006).

The follow-up of GRB980425 with BeppoSAX NFI 10 hours, one week and 6 months after the event revealed the presence of an X-ray source consistent with SN1998bw (Pian et al., 2000), confirmed also by observations by XMM (Pian et al., 2004) and Chandra (Kouveliotou et al., 2004). The S1 X-ray light curve shows a decay much slower than usual X-ray GRB afterglows (Pian et al., 2000). We then address to this peculiar X-ray emission as "URCA-1" (see section A.2.3 and the following sections). In Fig. A.7.3A we represent the URCA-1 observations (Pian et al., 2000, 2004; Kouveliotou et al., 2004). The separation between the light curves of GRB 980425 in the 2–700 keV energy band, of SN 1998bw in the optical band (Nomoto et al., 2007; Pian et al., 2006), and of the above mentioned URCA-1 observations is evident.

A.7.2 GRB 030329 / SN 2003dh / URCA-2

For GRB 030329 we have obtained (see Bernardini et al., 2004, 2005b; Ruffini et al., 2007b) a total energy $E^{tot}_{e^{\pm}} = 2.12 \times 10^{52}$ erg and a baryon loading $B = 4.8 \times 10^{-3}$. This implies an initial $e^{\pm}$ plasma with $N_{e^+e^-} = 1.1 \times 10^{57}$ and with an initial temperature $T = 2.1$ MeV. After the transparency point, the initial Lorentz gamma factor of the accelerated baryons is $\gamma_\circ = 206$. The effective CBM parameters are $\langle n_{cbm} \rangle = 2.0$ particle$/cm^3$ and $\langle \mathcal{R} \rangle = 2.8 \times 10^{-9}$, with a density contrast $\delta n/n \sim 10$ on a length scale of $\Delta \sim 10^{14}$ cm. The resulting fit of the observations, both of the prompt phase and of the afterglow have been presented in Bernardini et al. (2004, 2005b). We compare in Fig. A.7.3B the light curves of GRB 030329 in the 2–400 keV energy band, of SN 2003dh in the optical band (Nomoto et al., 2007; Pian et al., 2006) and of the possible

Table A.7.1: a) see Kaneko et al. (2007); b) Mazzali, P., private communication at MG11 meeting in Berlin, July 2006; c) evaluated fitting the URCAs with a power law followed by an exponentially decaying part; d) evaluated assuming a mass of the neutron star $M = 1.5M_\odot$ and $T \sim 5$–7 keV in the source rest frame; e) see Galama et al. (1998); Greiner et al. (2003); Prochaska et al. (2004); Mirabal et al. (2006).

GRB	$E^{tot}_{e^\pm}$ (erg)	B	γ_0	E^{bolom}_{SN} (erg)[a]	E^{kin}_{SN} (erg)[b]	E_{URCA} (erg)[c]	$\frac{E^{tot}_{e^\pm}}{E_{URCA}}$	$\frac{E^{kin}_{SN}}{E_{URCA}}$	R_{NS} (km)[d]	z^e
980425	1.2×10^{48}	7.7×10^{-3}	124	2.3×10^{49}	1.0×10^{52}	3×10^{48}	0.4	1.7×10^{4}	8	0.0085
030329	2.1×10^{52}	4.8×10^{-3}	206	1.8×10^{49}	8.0×10^{51}	3×10^{49}	6×10^{2}	1.2×10^{3}	14	0.1685
031203	1.8×10^{50}	7.4×10^{-3}	133	3.1×10^{49}	1.5×10^{52}	2×10^{49}	8.2	3.0×10^{3}	20	0.105
060218	1.8×10^{50}	1.0×10^{-2}	99	9.2×10^{48}	2.0×10^{51}	?	?	?	?	0.033

URCA-2 emission observed by XMM-EPIC in 2–10 keV energy band (Tiengo et al., 2003, 2004).

A.7.3 GRB 031203 / SN 2003lw / URCA-3

We will show in section A.8 the detailed analysis of GRB 031203 which leads to a total energy $E^{tot}_{e^\pm} = 1.85 \times 10^{50}$ erg and to a baryon loading $B = 7.4 \times 10^{-3}$. This implies an initial $e^\pm$ plasma with $N_{e^+e^-} = 3.0 \times 10^{55}$ and with an initial temperature $T = 1.5$ MeV. After the transparency point, the initial Lorentz gamma factor of the accelerated baryons is $\gamma_\circ = 132$. The effective CBM parameters are $\langle n_{cbm} \rangle = 1.6 \times 10^{-1}$ particle$/cm^3$ and $\langle \mathcal{R} \rangle = 3.7 \times 10^{-9}$, with a density contrast $\delta n/n \sim 10$ on a length scale of $\Delta \sim 10^{15}$ cm. In Fig. A.7.3C we compare the light curves of GRB 031203 in the 2–200 keV energy band, of SN 2003lw in the optical band (Nomoto et al., 2007; Pian et al., 2006) and of the possible URCA-3 emission observed by XMM-EPIC in the 0.2–10 keV energy band (Watson et al., 2004) and by Chandra in the 2–10 keV energy band (Soderberg et al., 2004).

A.7.4 The GRB / SN / URCA connection

In Tab. A.7.1 we summarize the representative parameters of the above three GRB-SN systems together with GRB 060218-SN 2006aj which will be presented in section A.11, including the very large kinetic energy observed in all SNe (Mazzali, 2006). Some general conclusions on these weak GRBs at low redshift, associated to SN Ib/c, can be established on the ground of our analysis:

1) From the detailed fit of their light curves, as well as their accurate spectral analysis, it follows that all the above GRB sources originate consistently from the formation of a black hole. This result extends to this low-energy GRB class at small cosmological redshift the applicability of our model, which now

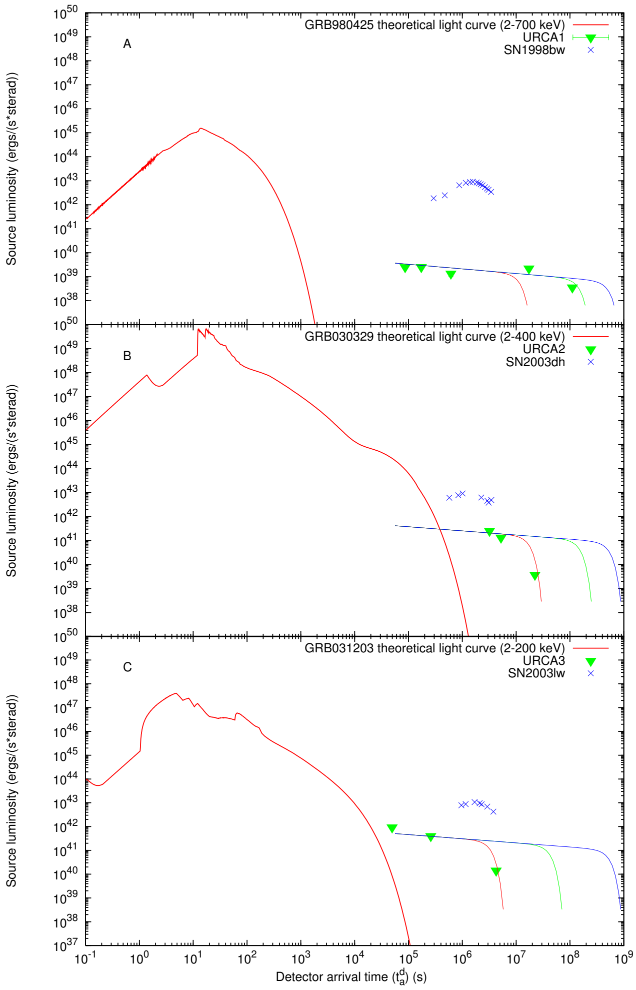

Figure A.7.3: Theoretically computed light curves of GRB 980425 in the 2–700 keV band (A), of GRB 030329 in the 2–400 keV band (B) and of GRB 031203 in the 2–200 keV band (C) are represented, together with the URCA observational data and qualitative representative curves for their emission, fitted with a power law followed by an exponentially decaying part. The luminosity of the SNe in the $3000 - 24000$ Å are also represented (Nomoto et al., 2007; Pian et al., 2006).

spans over a range of energy of six orders of magnitude from 10^{48} to 10^{54} ergs (Ruffini et al., 2003, 2004a, 2007b; Bernardini et al., 2004, 2005b,a; Ruffini et al., 2006b). Distinctive of this class is the very high value of the baryon loading which in one case (GRB 060218, see section A.11 and Dainotti et al., 2007) is very close to the maximum limit compatible with the dynamical stability of the adiabatic optically thick acceleration phase of the GRBs (Ruffini et al., 2000). Correspondingly, the maximum Lorentz gamma factors are systematically smaller than the ones of the more energetic GRBs at large cosmological distances. This in turn implies the smoothness of the observed light curves in the so-called "prompt phase". The only exception to this is the case of GRB 030329.

2) The accurate fits of the GRBs allow us to infer also some general properties of the CBM. While the size of the clumps of the inhomogeneities is $\Delta \approx 10^{14}$ cm, the effective CBM average density is consistently smaller than in the case of more energetic GRBs: we have in fact $\langle n_{cbm} \rangle$ in the range between $\sim 10^{-6}$ particle/cm^3 (GRB 060218) and $\sim 10^{-1}$ particle/cm^3 (GRB 031203), while only in the case of GRB 030329 it is ~ 2 particle/cm^3. We are also currently studying a characteristic trend in the variability of $\mathcal{R}$ during some specific bursts as well as the physical origin of the consistently smaller effective CBM density $\langle n_{cbm} \rangle$ values observed in these sources (see Dainotti et al., 2007).

3) Still within their weakness these four GRB sources present a large variability in their total energy: a factor 10^4 between GRB 980425 and GRB 030329. Remarkably, the SNe emission both in their very high kinetic energy and in their bolometric energy appear to be almost constant respectively 10^{52} erg and 10^{49} erg. The URCAs present also a remarkably steady behavior around a "standard luminosity" and a typical temporal evolution. The weakness in the energetics of GRB 980425 and GRB 031203, and the sizes of their dyadospheres, suggest that they originate from the formation of the smallest possible black hole, just over the critical mass of the neutron star (see Fig. A.2.9 and Ruffini, 2006).

A.7.5 URCA-1, URCA-2 and URCA-3

We turn to the search for the nature of URCA-1, URCA-2 and URCA-3. These systems are not yet understood and may have an important role in the comprehension of the astrophysical scenario of GRB sources. It is important to perform additional observations in order to verify if the URCA sources are related to the black hole originating the GRB phenomenon or to the SN. Even a single observation of an URCA source with a GRB in absence of a SN would prove their relation with the black hole formation. Such a result is today theoretically unexpected and would open new problematics in relativistic astrophysics and in the physics of black holes. Alternatively, even a single observation of an URCA source during the early expansion phase of a Type Ib/c

SN in absence of a GRB would prove the early expansion phases of the SN remnants. In the case that none of such two conditions are fulfilled, then the URCA sources must be related to the GRBs occurring in presence of a SN. In such a case, one of the possibilities would be that for the first time we are observing a newly born neutron star out of the supernova phenomenon unveiled by the GRB. This last possibility would offer new fundamental information about the outcome of the gravitational collapse, and especially about the equations of state at supranuclear densities and about a variety of fundamental issues of relativistic astrophysics of neutron stars.

The names of "URCA-1" and "URCA-2" for the peculiar late X-ray emission of GRB 980425 and GRB 030329 were given in the occasion of the Tenth Marcel Grossmann meeting held in Rio de Janeiro (Brazil) in the Village of Urca (see Ruffini et al., 2005b). Their identification was made at that time and presented at that meeting. However, there are additional reasons for the choice of these names. Another important physical phenomenon was indeed introduced in 1941 in the same Village of Urca by George Gamow and Mario Schoenberg (see Gamow and Schoenberg, 1941). The need for a rapid cooling process due to neutrino anti-neutrino emission in the process of gravitational collapse leading to the formation of a neutron star was there considered for the first time. It was Gamow who named this cooling as "Urca process" (see Gamow, 1970). Since then, a systematic analysis of the theory of neutron star cooling was advanced by Tsuruta (1964, 1979); Tsuruta and Cameron (1966); Tsuruta et al. (2002); Canuto (1978). The coming of age of X-ray observatories such as Einstein (1978-1981), EXOSAT (1983-1986), ROSAT (1990-1998), and the contemporary missions of Chandra and XMM-Newton since 1999 dramatically presented an observational situation establishing very embarrassing and stringent upper limits to the surface temperature of neutron stars in well known historical supernova remnants (see e.g. Romani, 1987). It was so that, for some remnants, notably SN 1006 and the Tycho supernova, the upper limits to the surface temperatures were significantly lower than the temperatures given by standard cooling times (see e.g. Romani, 1987). Much of the theoretical works has been mainly directed, therefore, to find theoretical arguments in order to explain such low surface temperature $T_s \sim 0.5$–1.0×10^6 K — embarrassingly low, when compared to the initial hot ($\sim 10^{11}$ K) birth of a neutron star in a supernova explosion (see e.g. Romani, 1987). Some important contributions in this researches have been presented by van Riper (1988, 1991); Burrows and Lattimer (1986); Lattimer et al. (1994); Yakovlev and Pethick (2004). The youngest neutron star to be searched for thermal emission has been the pulsar PSR J0205+6449 in 3C 58 (see e.g. Yakovlev and Pethick, 2004), which is 820 years old! Trümper (2005) reported evidence for the detection of thermal emission from the crab nebula pulsar which is, again, 951 years old.

URCA-1, URCA-2 and URCA-3 may explore a totally different regime: the X-ray emission possibly from a recently born neutron star in the first days –

months of its existence. The thermal emission from the young neutron star surface would in principle give information on the equations of state in the core at supranuclear densities and on the detailed mechanism of the formation of the neutron star itself with the related neutrino emission. It is also possible that the neutron star is initially fast rotating and its early emission could be dominated by the magnetospheric emission or by accretion processes from the remnant which would overshadow the thermal emission. A periodic signal related to the neutron star rotational period should in principle be observable in a close enough GRB-SN system. In order to attract attention to this problematic, we have given in Tab. A.7.1 an estimate of the corresponding neutron star radius for URCA-1, URCA-2 and URCA-3. It has been pointed out (see e.g. Pian et al., 2000) the different spectral properties between the GRBs and the URCAs. It would be also interesting to compare and contrast the spectra of all URCAs in order to evidence any analogy among them. Observations of a powerful URCA source on time scales of 0.1–10 seconds would be highly desirable.

A.8 Application to GRB 031203

GRB 031203 was observed by IBIS, on board of the INTEGRAL satellite (see Mereghetti and Gotz, 2003), as well as by XMM (Watson et al., 2004) and Chandra (Soderberg et al., 2004) in the $2-10$ keV band, and by VLT (Soderberg et al., 2004) in the radio band. It appears as a typical long burst (Sazonov et al., 2004a), with a simple profile and a duration of ≈ 40 s. The burst fluence in the $20-200$ keV band is $(2.0 \pm 0.4) \times 10^{-6}$ erg/cm^2 (Sazonov et al., 2004a), and the measured redshift is $z = 0.106$ (Prochaska et al., 2004). We analyze in the following the gamma-ray signal received by INTEGRAL. The observations in other wavelengths, in analogy with the case of GRB 980425 (Pian et al., 2000; Ruffini et al., 2004a, 2007b), could be related to the supernova event, as also suggested by Soderberg et al. (2004), and they will be examined elsewhere.

The INTEGRAL observations find a direct explanation in our theoretical model. We reproduce correctly the observed time variability of the prompt emission (see Fig. A.8.1 and Bernardini et al., 2005a). The radiation produced by the interaction of the optically thin fireshell with the CBM agrees with observations both for intensity and time structure.

The progress in reproducing the X and $\gamma-$ray emission as originating from a thermal spectrum in the comoving frame of the burst (Ruffini et al., 2004b) leads to the characterization of the instantaneous spectral properties which are shown to drift from hard to soft during the evolution of the system (see section A.6.2). The convolution of these instantaneous spectra over the observational time scale is in very good agreement with the observed power-law spectral shape.

A.8.1 The initial conditions

The best fit of the observational data leads to a total energy of the electron-positron plasma $E_{e^\pm}^{tot} = 1.85 \times 10^{50}$ erg. Assuming a black hole mass $M = 10M_\odot$, we then have a black hole charge to mass ratio $\xi = 6.8 \times 10^{-3}$; the plasma is created between the radii $r_1 = 2.95 \times 10^6$ cm and $r_2 = 2.81 \times 10^7$ cm with an initial temperature $T = 1.52$ MeV and a total number of pairs $N_{e^\pm} = 2.98 \times 10^{55}$. The amount of baryonic matter in the remnant is $B = 7.4 \times 10^{-3}$.

After the transparency point and the P-GRB emission, the initial Lorentz gamma factor of the accelerated baryons is $\gamma_\circ = 132.8$ at an arrival time at the detector $t_a^d = 8.14 \times 10^{-3}$ s and a distance from the Black Hole $r_\circ = 6.02 \times 10^{12}$ cm. The CBM parameters are: $< n_{cbm} >= 0.3$ particle/cm^3 and $< \mathcal{R} >= 7.81 \times 10^{-9}$.

A.8.2 The GRB luminosity in fixed energy bands

The aim of our model is to derive from first principles both the luminosity in selected energy bands and the time resolved/integrated spectra. We recall that the luminosity in selected energy bands is evaluated integrating over the EQTSs (see Ruffini et al., 2004b, and section A.6.1) the energy density released in the interaction of the accelerated baryons with the CBM measured in the co-moving frame, duly boosted in the observer frame. The radiation viewed in the comoving frame of the accelerated baryonic matter is assumed to have a thermal spectrum and to be produced by the interaction of the CBM with the front of the expanding baryonic shell.

In order to evaluate the contributions in the band $[\nu_1, \nu_2]$ we have to multiply the bolometric luminosity with an "effective weight" $W(\nu_1, \nu_2, T_{arr})$, where T_{arr} is the observed temperature. $W(\nu_1, \nu_2, T_{arr})$ is given by the ratio of the integral over the given energy band of a Planckian distribution at temperature T_{arr} to the total integral aT_{arr}^4 (Ruffini et al., 2004b). The resulting expression for the emitted luminosity is Eq.(A.6.1.3).

A.8.3 The "prompt emission"

In order to compare our theoretical prediction with the observations, it is important to notice that there is a shift between the initial time of the GRB event and the moment in which the satellite instrument has been triggered. In fact, in our model the GRB emission starts at the transparency point when the P-GRB is emitted. If the P-GRB is under the threshold of the instrument, the trigger starts a few seconds later with respect to the real beginning of the event. Therefore it is crucial, in the theoretical analysis, to estimate and take into due account this time delay. In the present case it results in $\Delta t_a^d = 3.5$ s (see the bold red line in Fig. A.8.1). In what follows, the detector arrival time is referred to the onset of the instrument.

The structure of the prompt emission of GRB 031203, which is a single peak with a slow decay, is reproduced assuming an CBM which has not a constant density but presents several density spikes with $< n_{cbm} >= 0.16$ particle/cm^3. Such density spikes corresponding to the main peak are modeled as three spherical shells with width Δ and density contrast $\Delta n/n$: we adopted for the first peak $\Delta = 3.0 \times 10^{15}$ cm and $\Delta n/n = 8$, for the second peak $\Delta = 1.0 \times 10^{15}$ cm and $\Delta n/n = 1.5$ and for the third one $\Delta = 7.0 \times 10^{14}$ cm and $\Delta n/n = 1$. To describe the details of the CBM filamentary structure

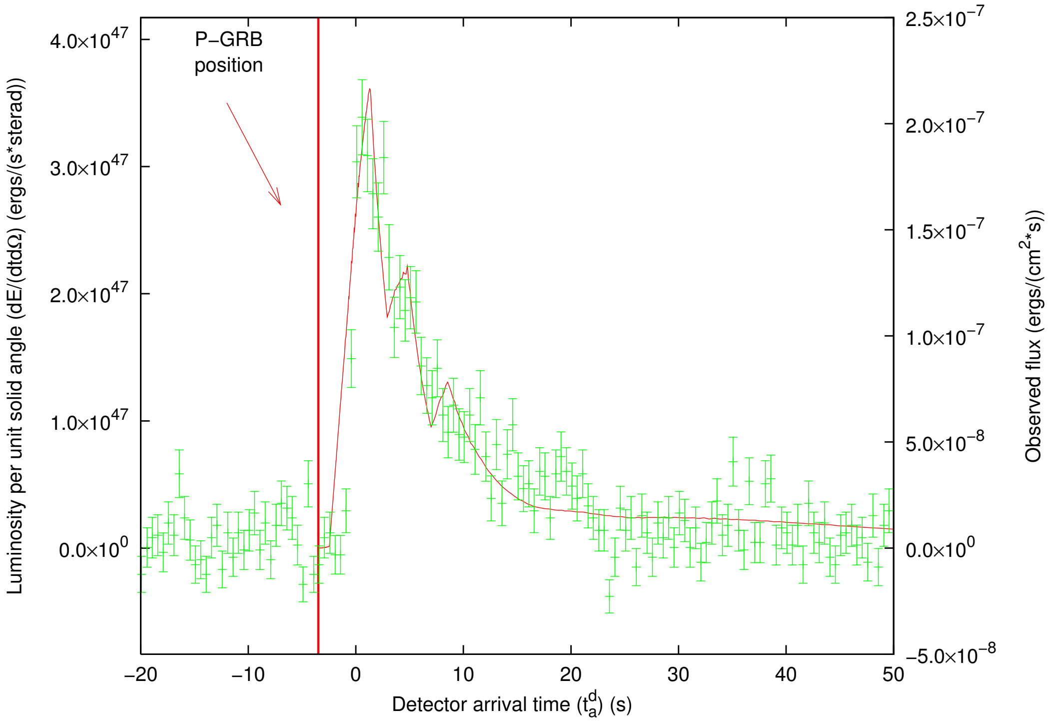

Figure A.8.1: Theoretically simulated light curve of the GRB 031203 prompt emission in the 20 − 200 keV energy band (solid red line) is compared with the observed data (green points) from Sazonov et al. (2004a). The vertical bold red line indicates the time position of P-GRB.

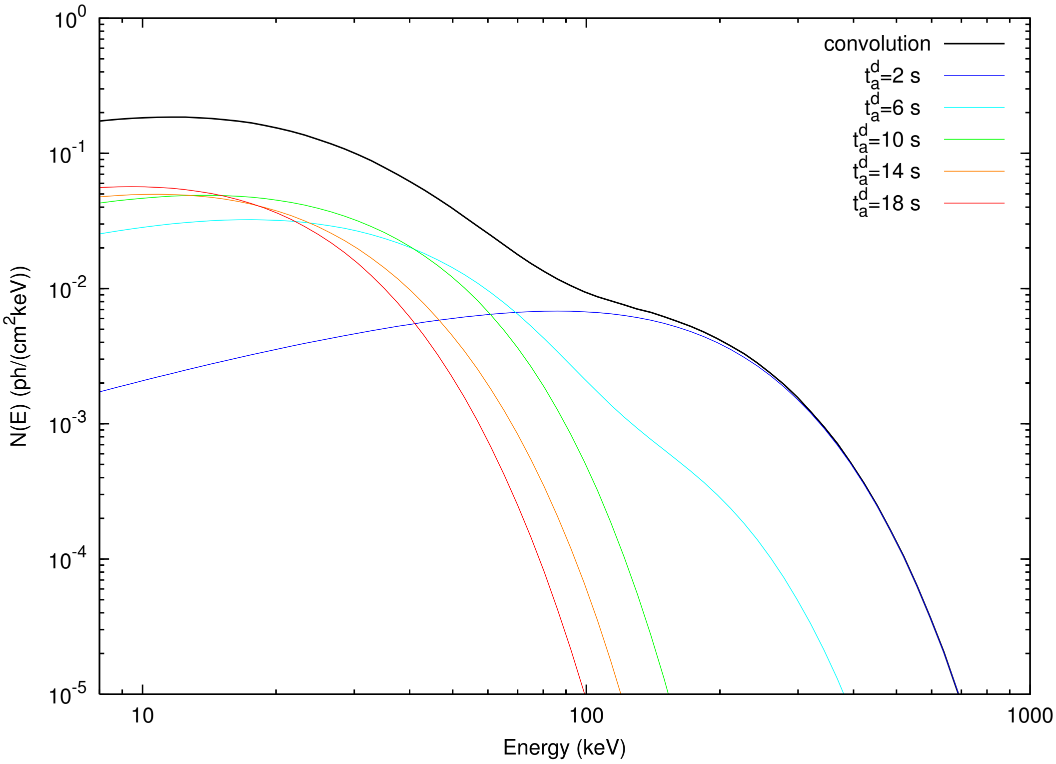

Figure A.8.2: Five different theoretically predicted instantaneous photon number spectrum $N(E)$ for $t_a^d = 2, 6, 10, 14, 18$ s are here represented (colored curves) together with their own temporal convolution (black bold curve). The shapes of the instantaneous spectra are not blackbodies due to the spatial convolution over the EQTS (see text).

we would require an intensity vs. time information with an arbitrarily high resolving power. With the finite resolution of the INTEGRAL instrument, we can only describe the average density distribution compatible with the given accuracy. Only structures at scales of 10^{15} cm can be identified. Smaller structures would need a stronger signal and/or a smaller time resolution of the detector. The three clouds here considered are necessary and sufficient to reproduce the observed light curve: a smaller number would not fit the data, while a larger number is unnecessary and would be indeterminable.

The result (see Fig. A.8.1) shows a good agreement with the light curve reported by Sazonov et al. (2004a), and it provides a further evidence for the possibility of reproducing light curves with a complex time variability through CBM inhomogeneities (Ruffini et al., 2002a, 2003, 2005a).

A.8.4 The instantaneous spectrum

As outlined in sectionA.6.2, in addition to the the luminosity in fixed energy bands we can derive also the instantaneous photon number spectrum $N(E)$. In Fig. A.8.2 are shown samples of time-resolved spectra for five different values of the arrival time which cover the whole duration of the event.

It is manifest from this picture that, although the spectrum in the comoving frame of the expanding pulse is thermal, the shape of the final spectrum in the laboratory frame is clearly non thermal. In fact, as explained in Ruffini et al. (2004b) and in section A.6.2, each single instantaneous spectrum is the result of an integration of hundreds of thermal spectra over the corresponding EQTS. This calculation produces a non thermal instantaneous spectrum in the observer frame (see Fig. A.8.2).

Another distinguishing feature of the GRBs spectra which is also present in these instantaneous spectra, as shown in Fig. A.8.2, is the hard to soft transition during the evolution of the event (Crider et al., 1997; Piran, 1999; Frontera et al., 2000; Ghirlanda et al., 2002). In fact the peak of the energy distributions E_p drift monotonically to softer frequencies with time (see Fig. A.8.3). This feature explains the change in the power-law low energy spectral index α (Band et al., 1993) which at the beginning of the prompt emission of the burst ($t_a^d = 2$ s) is $\alpha = 0.75$, and progressively decreases for later times (see Fig. A.8.2). In this way the link between E_p and α identified by Crider et al. (1997) is explicitly shown. This theoretically predicted evolution of the spectral index during the event unfortunately cannot be detected in this particular burst by INTEGRAL because of the not sufficient quality of the data (poor photon statistics, see Sazonov et al., 2004a).

A.8.5 The time-integrated spectrum: comparison with the observed data

The time-integrated observed GRB spectra show a clear power-law behavior. Within a different framework Shakura, Sunyaev and Zel'dovich (see e.g. Pozdniakov et al., 1983, and references therein) argued that it is possible to obtain such power-law spectra from a convolution of many non power-law instantaneous spectra evolving in time. This result was recalled and applied to GRBs by Blinnikov et al. (1999) assuming for the instantaneous spectra a thermal shape with a temperature changing with time. They showed that the integration of such energy distributions over the observation time gives a typical power-law shape possibly consistent with GRB spectra.

Our specific quantitative model is more complicated than the one considered by Blinnikov et al. (1999): as pointed out in section A.6.2, the instantaneous spectrum here is not a black body. Each instantaneous spectrum is

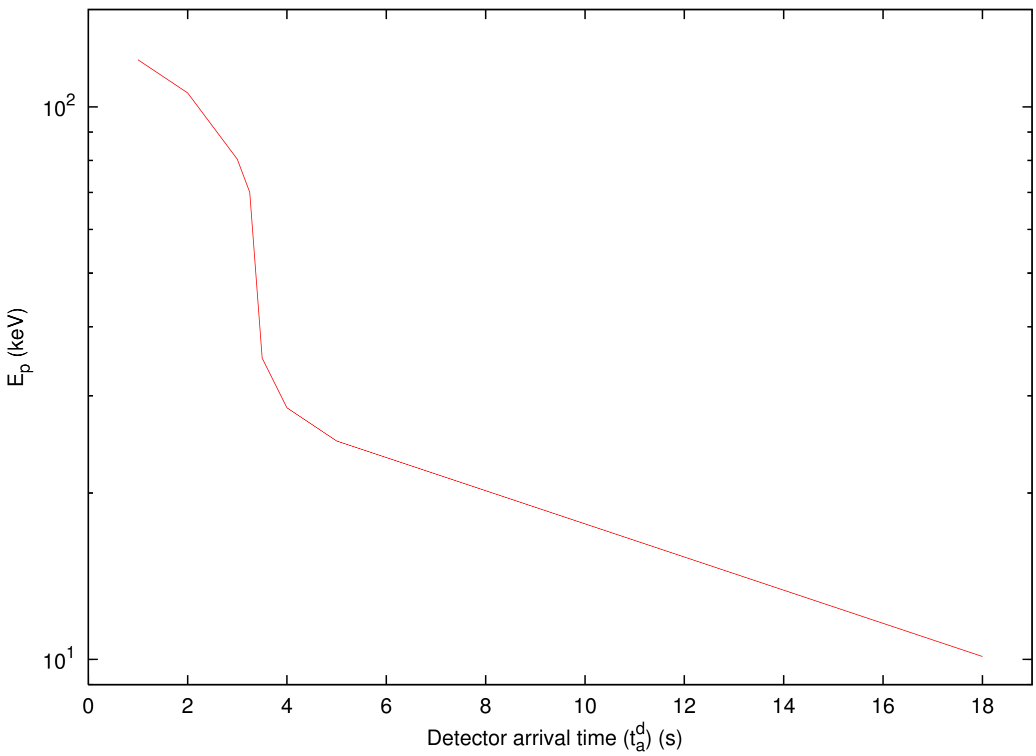

Figure A.8.3: The energy of the peak of the instantaneous photon number spectrum $N(E)$ is here represented as a function of the arrival time during the "prompt emission" phase. The clear hard to soft behavior is shown.

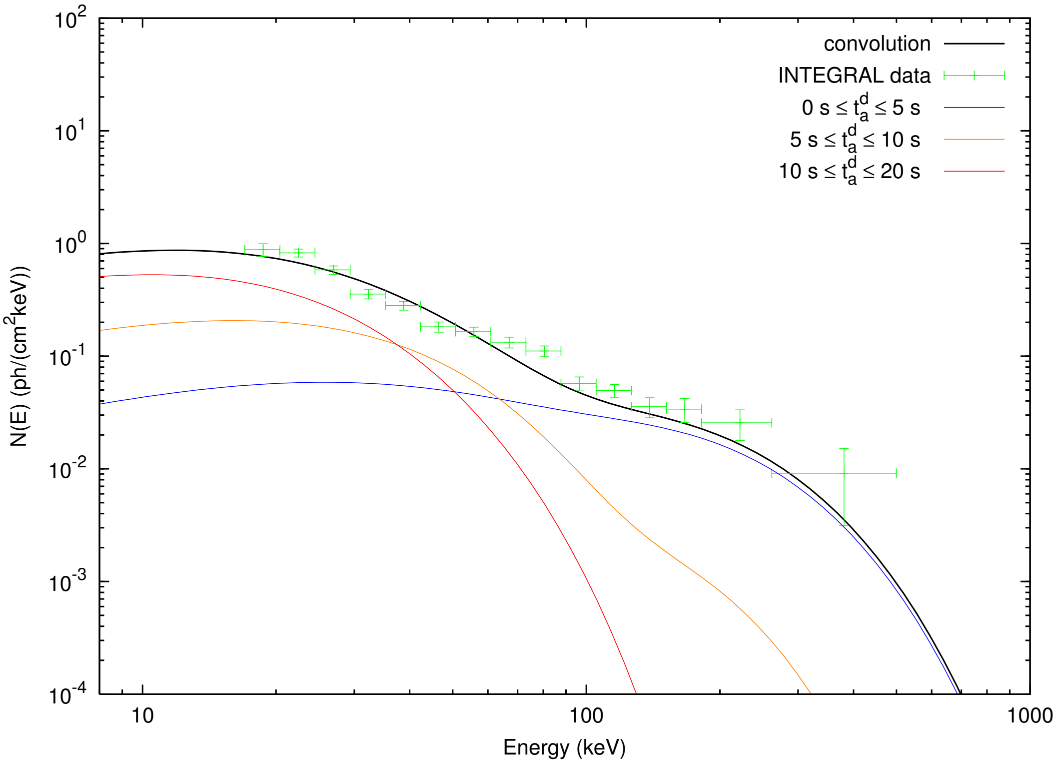

Figure A.8.4: Three theoretically predicted time-integrated photon number spectra $N(E)$ are here represented for $0 \leq t_a^d \leq 5$ s, $5 \leq t_a^d \leq 10$ s and $10 \leq t_a^d \leq 20$ s (colored curves). The hard to soft behavior presented in Fig. A.8.3 is confirmed. Moreover, the theoretically predicted time-integrated photon number spectrum $N(E)$ corresponding to the first 20 s of the "prompt emission" (black bold curve) is compared with the data observed by INTEGRAL (green points, see Sazonov et al., 2004a,b). This curve is obtained as a convolution of 108 instantaneous spectra, which are enough to get a good agreement with the observed data.

obtained by an integration over the corresponding EQTS: it is itself a convolution, weighted by appropriate Lorentz and Doppler factors, of $\sim 10^6$ thermal spectra with variable temperature. Therefore, the time-integrated spectra are not plain convolutions of thermal spectra: they are convolutions of convolutions of thermal spectra (see Fig. A.8.2).

The simple power-law shape of the integrated spectrum is more evident if we sum tens of instantaneous spectra, as in Fig. A.8.4. In this case we divided the prompt emission in three different time interval, and for each one we integrated on time the energy distribution. The resulting three time-integrated spectra have a clear non-thermal behavior, and still present the characteristic hard to soft transition.

Finally, we integrated the photon number spectrum $N(E)$ over the whole duration of the prompt event (see again Fig. A.8.4): in this way we obtain a typical non-thermal power-law spectrum which results to be in good agreement with the INTEGRAL data (see Sazonov et al., 2004a,b) and gives a clear evidence of the possibility that the observed GRBs spectra are originated from a thermal emission.

The precise knowledge we have here acquired on GRB 031203 helps in clarifying the overall astrophysical system GRB 031203 - SN 2003lw - the $2-10$ keV XMM and Chandra data (see sections A.7.3 and A.7.5, where the late $2-10$ keV XMM and Chandra data are also discussed).

A.9 Application to GRB 050315

GRB 050315 (Vaughan et al., 2006) has been triggered and located by the BAT instrument (Barthelmy, 2004; Barthelmy et al., 2005a) on board of the *Swift* satellite (Gehrels et al., 2004) at 2005-March-15 20:59:42 UT (Parsons et al., 2005). The narrow field instrument XRT (Burrows et al., 2004, 2005a) began observations ~ 80 s after the BAT trigger, one of the earliest XRT observations yet made, and continued to detect the source for ~ 10 days (Vaughan et al., 2006). The spectroscopic redshift has been found to be $z = 1.949$ (Kelson and Berger, 2005).

We present here the results of the fit of the *Swift* data of this source in 5 energy bands in the framework of our theoretical model, pointing out a new step toward the uniqueness of the explanation of the overall GRB structure. We first recall the essential features of our theoretical model; then we fit the GRB 050315 observations by both the BAT and XRT instruments; we also present the instantaneous spectra for selected values of the detector arrival time ranging from 60 s (i.e. during the so called "prompt emission") all the way to 3.0×10^4 s (i.e. the latest afterglow phases).

A.9.1 The fit of the observations

The best fit of the observational data leads to a total energy of the black hole dyadosphere, generating the $e^\pm$ plasma, $E_{e^\pm}^{tot} = 1.46 \times 10^{53}$ erg (the observational *Swift* E_{iso} is $> 2.62 \times 10^{52}$ erg, see Vaughan et al., 2006), so that the plasma is created between the radii $r_1 = 5.88 \times 10^6$ cm and $r_2 = 1.74 \times 10^8$ cm with an initial temperature $T = 2.05 MeV$ and a total number of pairs $N_{e^+e^-} = 7.93 \times 10^{57}$. The second parameter of the theory, the amount M_B of baryonic matter in the plasma, is found to be such that $B \equiv M_B c^2 / E_{dya} = 4.55 \times 10^{-3}$. The transparency point and the P-GRB emission occurs then with an initial Lorentz gamma factor of the accelerated baryons $\gamma_\circ = 217.81$ at a distance $r = 1.32 \times 10^{14}$ cm from the black hole.

A.9.1.1 The BAT data

In Fig. A.9.1 we represent our theoretical fit of the BAT observations in the three energy channels 15–25 keV, 25–50 keV and 50–100 keV and in the whole 15–350 keV energy band.

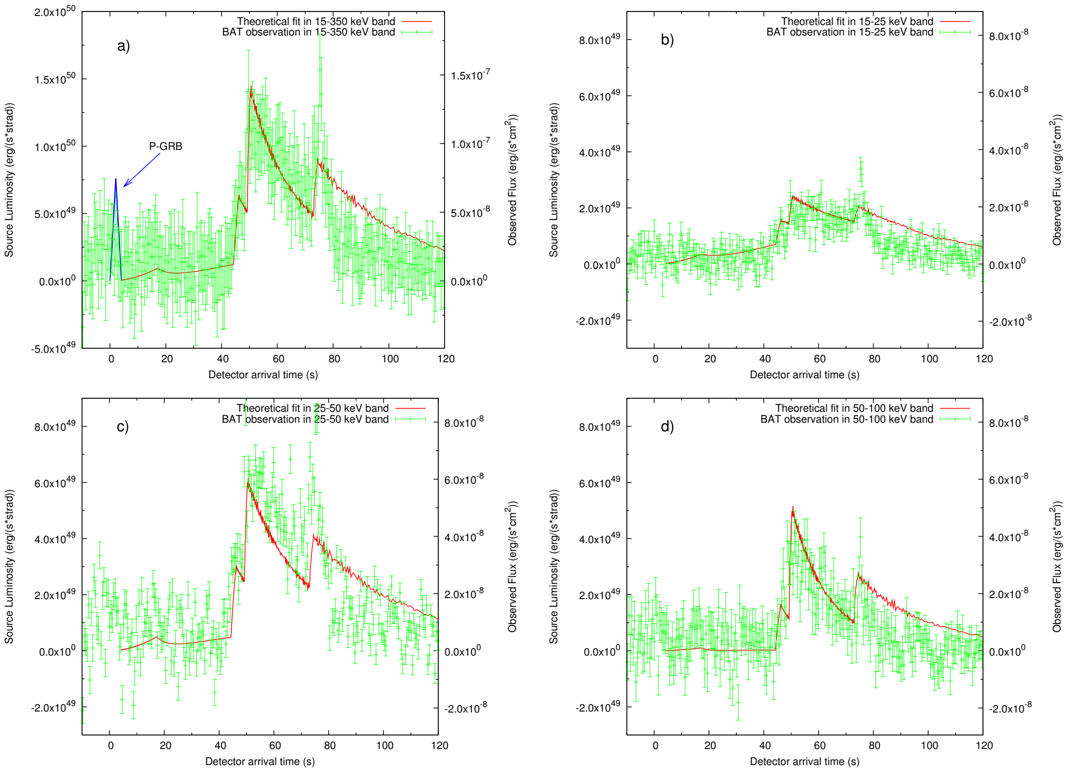

Figure A.9.1: Our theoretical fit (red line) of the BAT observations (green points) of GRB 050315 in the 15–350 keV (a), 15–25 keV (b), 25–50 keV (c), 50–100 keV (d) energy bands (Vaughan et al., 2006). The blue line in panel (a) represents our theoretical prediction for the intensity and temporal position of the P-GRB.

In our model the GRB emission starts at the transparency point when the P-GRB is emitted; this instant of time is often different from the moment in which the satellite instrument triggers, due to the fact that sometimes the P-GRB is under the instrumental noise threshold or comparable with it. In order to compare our theoretical predictions with the observations, it is important to estimate and take into account this time shift. In the present case of GRB 050315 it has been observed (see Vaughan et al., 2006) a possible precursor before the trigger. Such a precursor is indeed in agreement with our theoretically predicted P-GRB, both in its isotropic energy emitted (which we theoretically predict to be $E_{P-GRB} = 1.98 \times 10^{51}$ erg) and its temporal separation from the peak of the afterglow (which we theoretically predicted to be $\Delta t_a^d = 51$ s). In Fig. A.9.1a the blue line shows our theoretical prediction for the P-GRB in agreement with the observations.

After the P-GRB emission, all the observed radiation is produced by the interaction of the expanding baryonic shell with the interstellar medium. In order to reproduce the complex time variability of the light curve of the prompt emission as well as of the afterglow, we describe the CBM filamentary structure, for simplicity, as a sequence of overdense spherical regions separated by much less dense regions. Such overdense regions are nonhomogeneously filled, leading to an effective emitting area A_{eff} determined by the dimensionless parameter $\mathcal{R}$ (see previous sections and Ruffini et al., 2004b, 2005c, for details). Clearly, in order to describe any detailed structure of the time variability an authentic three dimensional representation of the CBM structure would be needed. However, this finer description would not change the substantial agreement of the model with the observational data. Anyway, in the "prompt emission" phase, the small angular size of the source visible area due to the relativistic beaming makes such a spherical approximation an excellent one (see also for details Ruffini et al., 2002a).

The structure of the "prompt emission" has been reproduced assuming three overdense spherical CBM regions with width Δ and density contrast $\Delta n/\langle n\rangle$: we chose for the first region, at $r = 4.15 \times 10^{16}$ cm, $\Delta = 1.5 \times 10^{15}$ cm and $\Delta n/\langle n\rangle = 5.17$, for the second region, at $r = 4.53 \times 10^{16}$ cm, $\Delta = 7.0 \times 10^{14}$ cm and $\Delta n/\langle n\rangle = 36.0$ and for the third region, at $r = 5.62 \times 10^{16}$ cm, $\Delta = 5.0 \times 10^{14}$ cm and $\Delta n/\langle n\rangle = 85.4$. The CBM mean density during this phase is $\langle n_{cbm}\rangle = 0.81$ particles/cm^3 and $\langle\mathcal{R}\rangle = 1.4 \times 10^{-7}$. With this choice of the density mask we obtain agreement with the observed light curve, as shown in Fig. A.9.1. A small discrepancy occurs in coincidence with the last peak: this is due to the fact that at this stage the source visible area due to the relativistic beaming is comparable with the size of the clouds, therefore the spherical shell approximation should be duly modified by a detailed analysis of a full three-dimensional treatment of the CBM filamentary structure. Such a topic is currently under investigation (see also for details Ruffini et al., 2002a). Fig. A.9.1 shows also the theoretical fit of the light curves in the three BAT energy channels in which the GRB has been detected (15–25 keV in Fig.

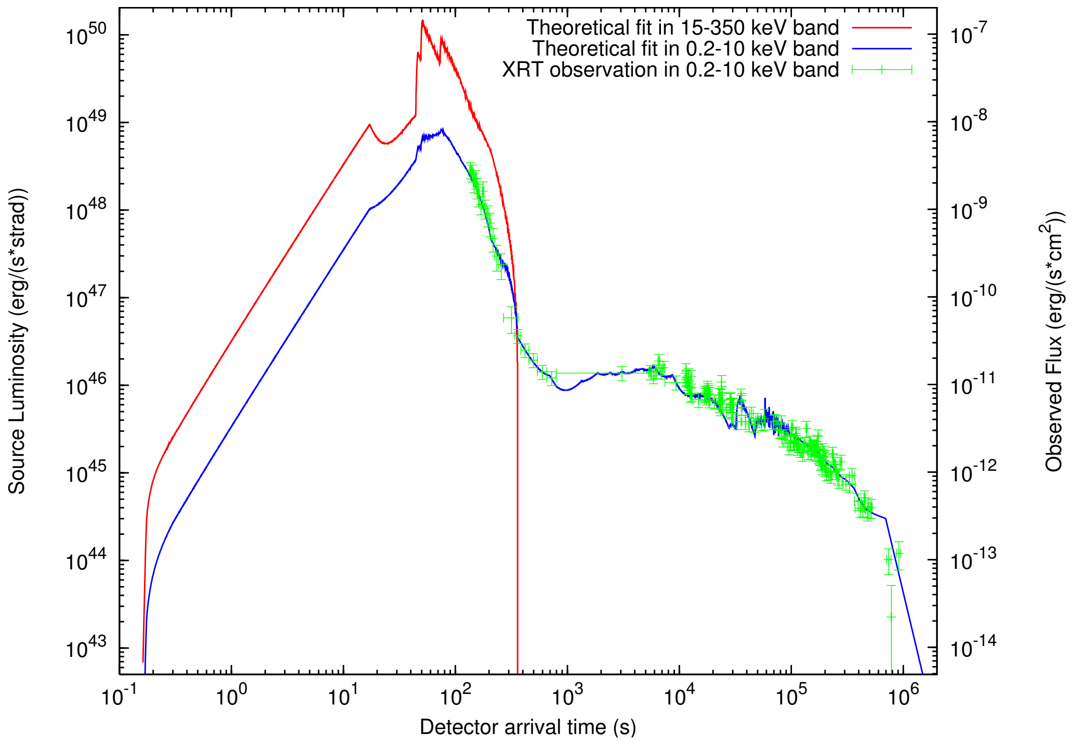

Figure A.9.2: Our theoretical fit (blue line) of the XRT observations (green points) of GRB 050315 in the 0.2–10 keV energy band (Vaughan et al., 2006). The theoretical fit of the BAT observations (see Fig. A.9.1a) in the 15–350 keV energy band is also represented (red line).

A.9.1b, 25–50 keV in Fig. A.9.1c, 50–100 keV in Fig. A.9.1d).

A.9.1.2 The XRT data

The same analysis can be applied to explain the features of the XRT light curve in the afterglow phase. It has been recently pointed out (Nousek et al., 2006) that almost all the GRBs observed by *Swift* show a "canonical behavior": an initial very steep decay followed by a shallow decay and finally a steeper decay. In order to explain these features many different approaches have been proposed (Meszaros, 2006; Nousek et al., 2006; Panaitescu et al., 2006; Zhang et al., 2006a). In our treatment these behaviors are automatically described by the same mechanism responsible for the prompt emission described above: the baryonic shell expands in an CBM region, between $r = 9.00 \times 10^{16}$ cm and $r = 5.50 \times 10^{18}$ cm, which is significantly at lower density ($\langle n_{cbm} \rangle = 4.76 \times 10^{-4}$ particles/cm^3, $\langle \mathcal{R} \rangle = 7.0 \times 10^{-6}$) then the one corresponding to the prompt emission, and this produces a slower decrease of the velocity of the baryons with a consequent longer duration of the afterglow emission. The initial steep decay of the observed flux is due to the

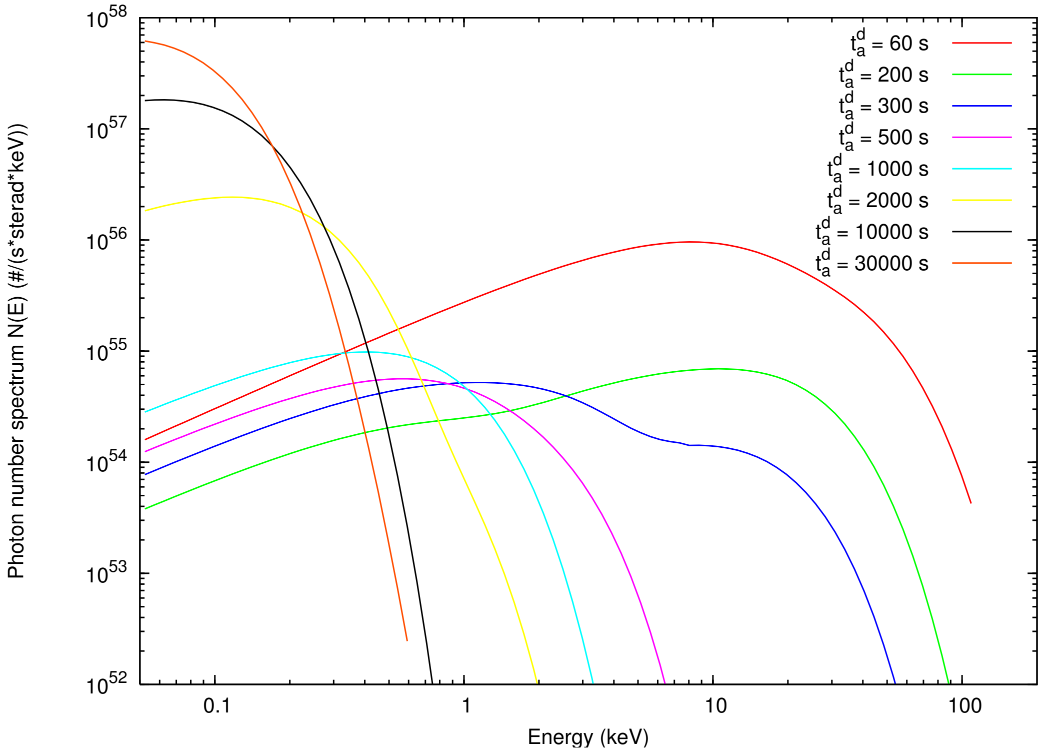

Figure A.9.3: Eight theoretically predicted instantaneous photon number spectra $N(E)$ are here represented for different values of the arrival time (colored curves). The hard to soft behavior is confirmed.

smaller number of collisions with the CBM. In Fig. A.9.2 is represented our theoretical fit of the XRT data, together with the theoretically computed 15–350 keV light curve of Fig. A.9.1a (without the BAT observational data to not overwhelm the picture too much).

What is impressive is that no different scenarios need to be advocated in order to explain the features of the light curves: both the prompt and the afterglow emission are just due to the thermal radiation in the comoving frame produced by inelastic collisions with the CBM duly boosted by the relativistic transformations over the EQTSs.

A.9.2 The instantaneous spectrum

In addition to the the luminosity in fixed energy bands we can derive also the instantaneous photon number spectrum $N(E)$ starting from the same assumptions. In Fig. A.9.3 are shown samples of time-resolved spectra for eight different values of the arrival time which cover the whole duration of the event. It is manifest from this picture that, although the spectrum in the comoving frame of the expanding pulse is thermal, the shape of the final spectrum in the laboratory frame is clearly non thermal. In fact, as explained in Ruffini et al. (2004b), each single instantaneous spectrum is the result of an integration of thousands of thermal spectra over the corresponding EQTS. This calculation produces a non thermal instantaneous spectrum in the observer frame (see Fig. A.9.3).

A distinguishing feature of the GRBs spectra which is also present in these instantaneous spectra is the hard to soft transition during the evolution of the event (Crider et al., 1997; Piran, 1999; Frontera et al., 2000; Ghirlanda et al., 2002). In fact the peak of the energy distribution E_p drifts monotonically to softer frequencies with time. This feature is linked to the change in the power-law low energy spectral index α (Band et al., 1993), so the correlation between α and E_p (Crider et al., 1997) is explicitly shown.

It is important to stress that there is no difference in the nature of the spectrum during the prompt and the afterglow phases: the observed energy distribution changes from hard to soft, with continuity, from the "prompt emission" all the way to the latest phases of the afterglow.

A.9.3 Problems with the definition of "long" GRBs

The confirmation by *Swift* of our prediction of the overall afterglow structure, and especially the coincidence of the "prompt emission" with the peak of the afterglow, opens a new problematic in the definition of the long GRBs. It is clear, in fact, that the identification of the "prompt emission" in the current GRB literature is not at all intrinsic to the phenomenon but is merely due to the threshold of the instruments used in the observations (e.g. BATSE in the 50–300 keV energy range, or BeppoSAX GRBM in 40–700 keV, or *Swift* BAT in 15–350 keV). As it is clear from Fig. A.9.4, there is no natural way to identify in the source a special extension of the peak of the afterglow that is not the one purely defined by the experimental threshold. It is clear, therefore, that long GRBs, as defined till today, are just the peak of the afterglow and there is no way, as explained above, to define their "prompt emission" duration as a characteristic signature of the source. As the *Swift* observations show, the duration of the long GRBs has to coincide with the duration of the entire afterglow. A Kouveliotou - Tavani plot of the long GRBs, done following our interpretation which is clearly supported by the recent *Swift* data (see Fig. A.9.4), will present enormous dispersion on the temporal axis.

We recall that in our theory both "short" and "long" GRBs originate from the same process of black hole formation. The major difference between the two is the value of the baryon loading parameter B (see Fig. A.2.6). In the limit of small baryon loading, all the plasma energy is emitted at the transparency in the P-GRB, with negligible afterglow observed flux. For higher values of the baryon loading, the relative energy content of the P-GRB with respect to the afterglow diminishes (see Ruffini et al., 2005a, and references

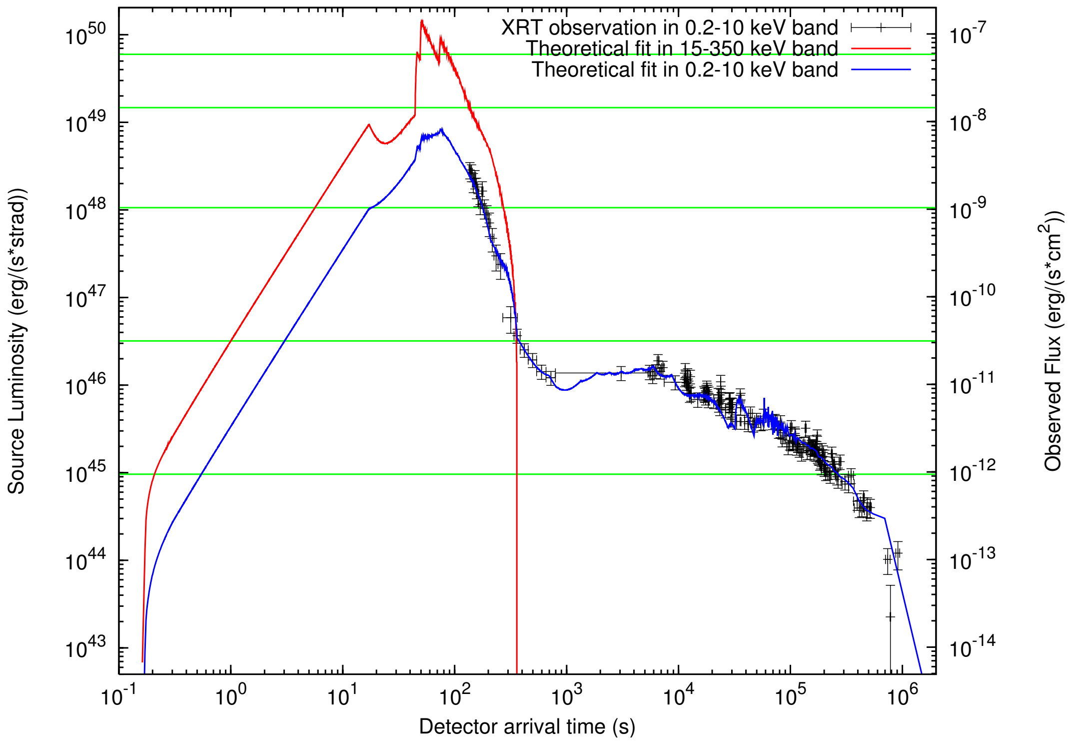

Figure A.9.4: Same as Fig. A.9.2. The horizontal green lines corresponds to different possible instrumental thresholds. It is clear that long GRB durations are just functions of the observational threshold.

therein).

A.10 Application to GRB 011121

A.10.1 A widely debated issue: the interpretation of flares

A flare is a large scale activity in excess on the underlying light curve that manifests as a bump in luminosity rather intense and sharp in the decaying phase of the X-Ray afterglow.

When the first flare was detected by BeppoSAX, on the X-Ray light curve of GRB 011121, it was assumed as an extremely peculiar phenomenon. However, by the advent of the Swift Mission, many flares have been discovered in the light curves of about the 50% of the total amount of X-Ray afterglows observed: it was clear that flares are a very typical feature of GRBs phenomenon. The many observations collected until today show that flares are random events that manifest in different shapes and in all sizes, in each kind of burst (both long and short) and at each measure of redshift. X-Ray flares have been observed in all phases of the X-Ray light curve, the peak time ranges between 95 s and 75 ks. There are light curves with more than one flare, although the more frequent case exhibits one single pulse on the Gamma-Ray peak followed by one or two flares. They are often characterized by large flux variations, can be strongly energetics and in some cases flares have surpassed the original GRB (ex. GRB 060526). This extreme variability and, in particular, the smallness of the time interval in which these big variation of flux happens, makes hard to give reason of such a phenomenon.

As discussed in the previous sections, in our theory the multiwavelength emission is entirely due to the fully inelastic collisions of the baryonic remnants of the fireshell with the CBM. Flares also, as characteristic parts of the afterglow, can be naturally explained in this context. The most relevant results of recent data analysis made on big samples (Chincarini et al., 2007; Falcone et al., 2007) are consistent with our hypothesis of inelastic collisions as the origin of flares. In fact, first of all, flares manifest until very late times and follow the typical hard to soft evolution; then, bumps become broader as the time increases, consistently with a general trend of GRB light curves. Moreover, the distribution of intensity ratios between successive Gamma-Ray pulses and that between successive X-Ray flares is the same, while there is no correlation between the number of pulses of the Gamma-Ray emission and the number of X-Ray flares. These last features seem to establish a common origin of Gamma-Ray bumps and X-Ray flares, and this is consistent with our hypothesis concerning to which the entire emission (from the Gamma 'Prompt emission' to the late Afterglow phase) is generated by the same inelastic collisions process.

On the other hand, it is difficult to conciliate all these aspects within the standard model or any other model founded on an internal shock process (eventually followed by an external shock phase). In particular, is hardly explained the presence of flares at very late times and their strong, rapid variation of flux. As already said, this is one of the most debated peculiarity of the appearing flares. It has been found that $\langle dt/t \rangle = 0.13 \pm 0.10$, corresponding to variations of flux of one or also two orders of magnitude. It's a shared opinion that an external shock scenario can't reproduce a similar range of variability, but we are able to show that this is consistent with our fully inelastic collision hypothesis. This assumption implies just the consideration of the three-dimensional structure of the CBM, until now neglected for the radial approximation modeling for the CBM profile. We realized a first attempt to check this idea by its application on the burst with the first flare observed, GRB 011121.

A.10.2 The first step on the first flare: analysis of GRB 011121

GRB 011121 is a near, long burst with $T_{90} = 28$ s and redshift $z = 0.36$ (Infante et al., 2001). Its fluence (Price et al., 2002) is 2.4×10^{-5} erg/cm^2 that corresponds, in the hypothesis of isotropic emission at the observed redshift, to an energy in the band $2 - 700$ keV of 2.8×10^{52} erg. This is the second brightest source detected by BeppoSAX in γ-rays and X-rays. At the time $t = 240$ s, in the X-ray $2 - 26$ keV energy band, there is a big flare(Piro et al., 2005; Greiner et al., 2003). It lasts about seventy seconds ($dt/t \sim 0.29$) and corresponds to a bump of an order of magnitude in luminosity. It is however very soft, since its energy is about 3% of the total amount of the prompt emission (Piro et al., 2005).

In figure A.10.1 we present the observed GRB 011121 light curves in the three different energy bands we analyzed, together with their theoretical fit in the framework of our model: $40 - 700$ keV, $2 - 26$ keV, $2 - 10$ keV. Looking at the observational data we can see that the $40 - 700$ keV energy band light curve presents a temporal profile particularly regular, smooth and homogeneous, while the $2 - 26$ keV light curve has a remarkably irregular profile. This is quite anomalous, in fact generally the light curves in these energy bands presents just the opposite trend.

In figure A.10.1 there is also an enlargement of the flare of this source that shows in detail the comparison between the theoretical light curve and the observational data.

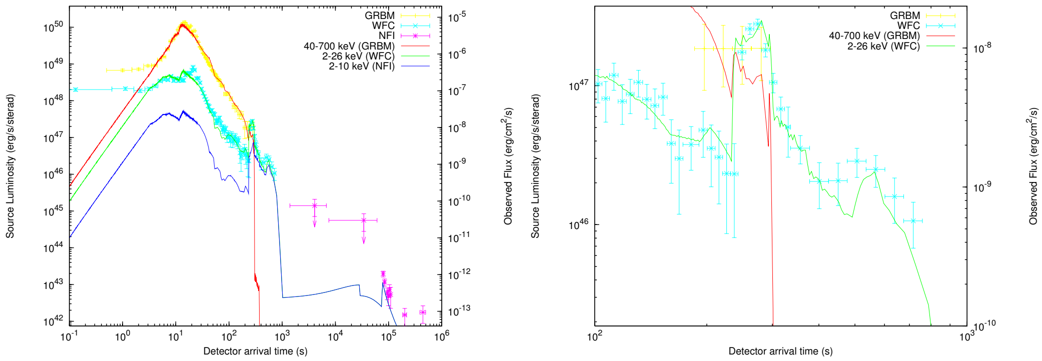

Figure A.10.1: Left: Theoretical fit of the GRB 011121 light curves in the 40 − 700 keV (BeppoSAX GRBM), 2 − 26 keV (BeppoSAX WFC), 2/10 keV (BeppoSAX NFI). **Right:** Enlargement of the Flare.

In the computation of the theoretical light curve for the flare we reproduce it as due to a spherical cloud of CBM along the line of sight introducing, in this way, a three-dimensional structure for the Circum Burst Medium. In fact, in the first approximation, we assume a modeling of thin spherical shells for the distribution of the CBM. This allows us to consider a purely radial profile in the expansion (Ruffini et al., 2002a, 2003) . This radial approximation is valid until the visible area of emission of photons is sufficiently small with respect to the characteristic size of the CBM shell. The visiblre area of emission is defined by the maximum value of the viewing angle; it varies with time and is inversely proportional to the Lorentz Gamma Factor(see the previous). So it happens that, at the beginning of the expansion, when the Gamma Factor is big (about 10^2), the effective distribution of the CBM doesn't matter for the narrowness of the viewing angle but, at the end of the expansion, the remarkable lessening of the Gamma Factor produces a strong increase of the viewing angle and a correct estimation of the CBM by the introduction of the angular coordinate distribution becomes necessary.

We can see that our results are in very good agreement with the observational data, also in the late tail of the flare. In particular, the short time variability has been successfully reproduced.

Here we performed just a first attempt of application of our interpretation of flares and we found an encouraging result. Now we plan to verify our hypothesis by its application to other sources and to produce a detailed cinematic and dynamic theory concerning this fundamental features of Gamma-Ray Burst.

A.11 Application to GRB 060218

GRB 060218 triggered the BAT instrument of *Swift* on 18 February 2006 at 03:36:02 UT and has a $T_{90} = (2100 \pm 100)$ s (Cusumano et al., 2006). The XRT instrument (Kennea et al., 2006; Cusumano et al., 2006) began observations ~ 153 s after the BAT trigger and continued for ~ 12.3 days (Sakamoto et al., 2006a). The source is characterized by a flat γ-ray light curve and a soft spectrum (Barbier et al., 2006). It has an X-ray light curve with a long, slow rise and gradual decline and it is considered an X-Ray Flash (XRF) since its peak energy occurs at $E_p = 4.9^{+0.4}_{-0.3}$ keV (Campana et al., 2006a). It has been observed by the *Chandra* satellite on February 26.78 and March 7.55 UT ($t \simeq 8.8$ and 17.4 days) for 20 and 30 ks respectively (Soderberg et al., 2006b). The spectroscopic redshift has been found to be $z = 0.033$ (Sollerman et al., 2006; Mirabal et al., 2006). The corresponding isotropic equivalent energy is $E_{iso} = (1.9 \pm 0.1) \times 10^{49}$ erg (Sakamoto et al., 2006a) which sets this GRB as a low luminous one, consistent with most of the GRBs associated with SNe (Liang et al., 2007; Cobb et al., 2006; Guetta and Della Valle, 2007).

GRB 060218 is associated with SN2006aj whose expansion velocity is $v \sim 0.1c$ (Pian et al., 2006; Fatkhullin et al., 2006; Soderberg et al., 2006a; Cobb et al., 2006). The host galaxy of SN2006aj is a low luminosity, metal poor star forming dwarf galaxy (Ferrero et al., 2007) with an irregular morphology (Wiersema et al., 2007), similar to the ones of other GRBs associated with SNe (Modjaz et al., 2006; Sollerman et al., 2006).

A.11.1 The fit of the observed data

In this section we present the fit of our fireshell model to the observed data (see Figs. A.11.1, A.11.4). The fit leads to a total energy of the $e^{\pm}$ plasma $E_{e^{\pm}}^{tot} = 2.32 \times 10^{50}$ erg, with an initial temperature $T = 1.86$ MeV and a total number of pairs $N_{e^{\pm}} = 1.79 \times 10^{55}$. The second parameter of the theory, $B = 1.0 \times 10^{-2}$, is the highest value ever observed and is close to the limit for the stability of the adiabatic optically thick acceleration phase of the fireshell (for further details see Ruffini et al., 2000). The Lorentz gamma factor obtained solving the fireshell equations of motion (Bianco and Ruffini, 2005b,a) is $\gamma_{\circ} = 99.2$ at the beginning of the afterglow phase at a distance from the progenitor $r_{\circ} = 7.82 \times 10^{12}$ cm. It is much larger than $\gamma \sim 5$ estimated by Kaneko et al. (2007) and Toma et al. (2007).

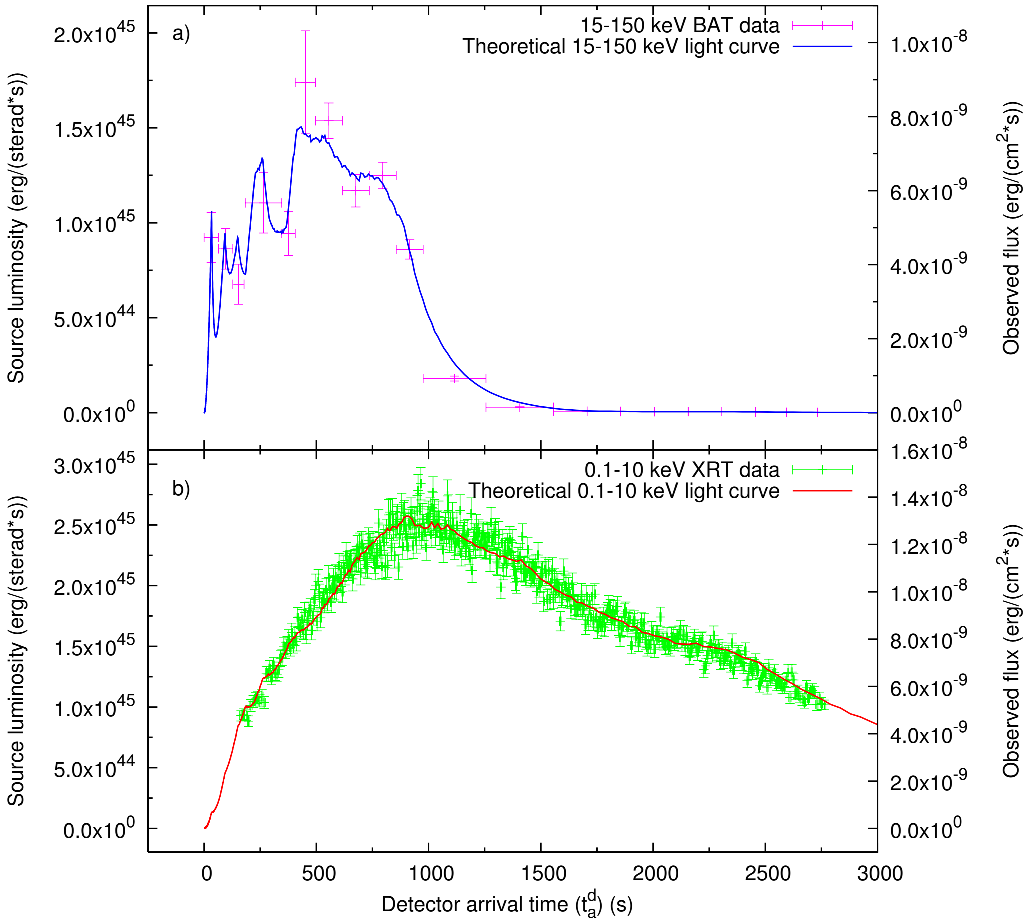

Figure A.11.1: GRB 060218 prompt emission: a) our theoretical fit (blue line) of the BAT observations in the 15–150 keV energy band (pink points); b) our theoretical fit (red line) of the XRT observations in the 0.3–10 keV energy band (green points) (Data from: Campana et al., 2006a).

In Fig. A.11.1 we show the afterglow light curves fitting the prompt emission both in the BAT (15–150 keV) and in the XRT (0.3–10 keV) energy ranges, as expected in our "canonical GRB" scenario (Dainotti et al., 2007). Initially the two luminosities are comparable to each other, but for a detector arrival time $t_a^d > 1000$ s the XRT curves becomes dominant. The displacement between the peaks of these two light curves leads to a theoretically estimated spectral lag greater than 500 s in perfect agreement with the observations (see Liang et al., 2006). We obtain that the bolometric luminosity in this early part coincides with the sum of the BAT and XRT light curves (see Fig. A.11.4) and the luminosity in the other energy ranges is negligible.

We recall that at $t_a^d \sim 10^4$ s there is a sudden enhancement in the radio luminosity and there is an optical luminosity dominated by the SN2006aj emission (see Campana et al., 2006a; Soderberg et al., 2006b; Fan et al., 2006). Although our analysis addresses only the BAT and XRT observations, for $r > 10^{18}$ cm corresponding to $t_a^d > 10^4$ s the fit of the XRT data implies two new features: **1)** a sudden increase of the $\mathcal{R}$ factor from $\mathcal{R} = 1.0 \times 10^{-11}$ to $\mathcal{R} = 1.6 \times 10^{-6}$, corresponding to a significantly more homogeneous effective CBM distribution (see Fig.A.11.5b); **2)** an XRT luminosity much smaller than the bolometric one (see Fig. A.11.4). These theoretical predictions may account for the energetics of the enhancement of the radio and possibly optical and UV luminosities. Therefore, we identify two different regimes in the afterglow, one for $t_a^d < 10^4$ s and the other for $t_a^d > 10^4$ s. Nevertheless, there is a unifying feature: the determined effective CBM density decreases with the distance r monotonically and continuously through both these two regimes from $n_{cbm} = 1$ particle/cm^3 at $r = r_\circ$ to $n_{cbm} = 10^{-6}$ particle/cm^3 at $r = 6.0 \times 10^{18}$ cm: $n_{cbm} \propto r^{-\alpha}$, with $1.0 \lesssim \alpha \lesssim 1.7$ (see Fig. A.11.5a).

Our assumption of spherical symmetry is supported by the observations which set for GRB 060218 an opening beaming angle larger than $\sim 37^\circ$ (Liang et al., 2007; Campana et al., 2006a; Soderberg et al., 2006b; Guetta and Della Valle, 2007).

A.11.2 The procedure of the fit

The arrival time of each photon at the detector depends on the entire previous history of the fireshell (Ruffini et al., 2001c). Moreover, all the observables depends on the EQTS (Bianco and Ruffini, 2004, 2005b) which, in turn, depend crucially on the equations of motion of the fireshell. The CBM engulfment has to be computed self-consistently through the entire dynamical evolution of the fireshell and not separately at each point. Any change in the CBM distribution strongly influences the entire dynamical evolution of the fireshell and, due to the EQTS structure, produces observable effects up to a much later time. For example if we change the density mask at a certain distance from the black hole we modify the shape of the lightcurve and consequently the evolution changes at larger radii corresponding to later times. Anyway the change of the density is not the only problem to face in the fitting of the source, in fact first of all we have to choose the energy in order to have Lorentz gamma factor sufficiently high to fit the entire GRB. In order to show the sensitivity of the fitting procedure I also present two examples of fits with the same value of B and different value of $E^{tot}_{e^{\pm}}$.

The first example has an $E^{tot}_{e^{\pm}} = 1.36 \times 10^{50}$ erg . This fit resulted unsuccessfully as we see from the Fig.A.11.2, because the bolometric lightcurve is under the XRT peak of the afterglow. This means that the value of the energy chosen is too small to fit any data points after the peak of the afterglow. So we have to increase the value of the Energy to a have a better fit. In fact the parameters values have been found with various attempt in order to obtain the best fit.

The second example is characterized by $E^{tot}_{e^{\pm}} = 1.61 \times 10^{50}$ erg and the all the data are fitted except for the last point from 2.0×10^2s to the end (see Fig. A.11.3). I attempt to fit these last points trying to diminuishes the R values in order to enhance the energy emission, but again the low value of the Lorentz gamma factor, that in this case is 3 prevent the fireshell to expand. So again in this case the value of the Energy chosen is too small, but it is better than the previous attempt. In this case we increased the energy value of the 24%, but it is not enough so we decide to increase 16%.

So the final fit is characterized by the $B = 1.0 \times 10^{-2}$ and by the $E^{tot}_{e^{\pm}} = 2.32 \times 10^{50}$ erg. With this value of the energy we are able to fit all the experimental points.

A.11.3 The fireshell fragmentation

GRB 060218 presents different peculiarities: the extremely long T_{90}, the very low effective CBM density decreasing with the distance and the largest possible value of $B = 10^{-2}$. These peculiarities appear to be correlated. Following Ruffini et al. (2007b), we propose that in the present case the fireshell is fragmented. This implies that the surface of the fireshell does not increase any longer as r^2 but as r^{β} with $\beta < 2$. Consequently, the effective CBM density n_{cbm} is linked to the actual one n^{act}_{cbm} by:

$$n_{cbm} = \mathcal{R}_{shell} n^{act}_{cbm}\,, \quad \text{with} \quad \mathcal{R}_{shell} \equiv (r^{\star}/r)^{\alpha}\,, \tag{A.11.3.1}$$

where $r^{\star}$ is the starting radius at which the fragmentation occurs and $\alpha = 2 - \beta$ (see Fig. A.11.5a). For $r^{\star} = r_{\circ}$ we have $n^{act}_{cbm} = 1$ particles/cm^3, as expected for a "canonical GRB" (Ruffini et al., 2007a) and in agreement with the apparent absence of a massive stellar wind in the CBM (Soderberg et al., 2006b; Fan et al., 2006; Li, 2007).

The $\mathcal{R}$ parameter defined in Eq.(A.11.3.2) has to take into account both the

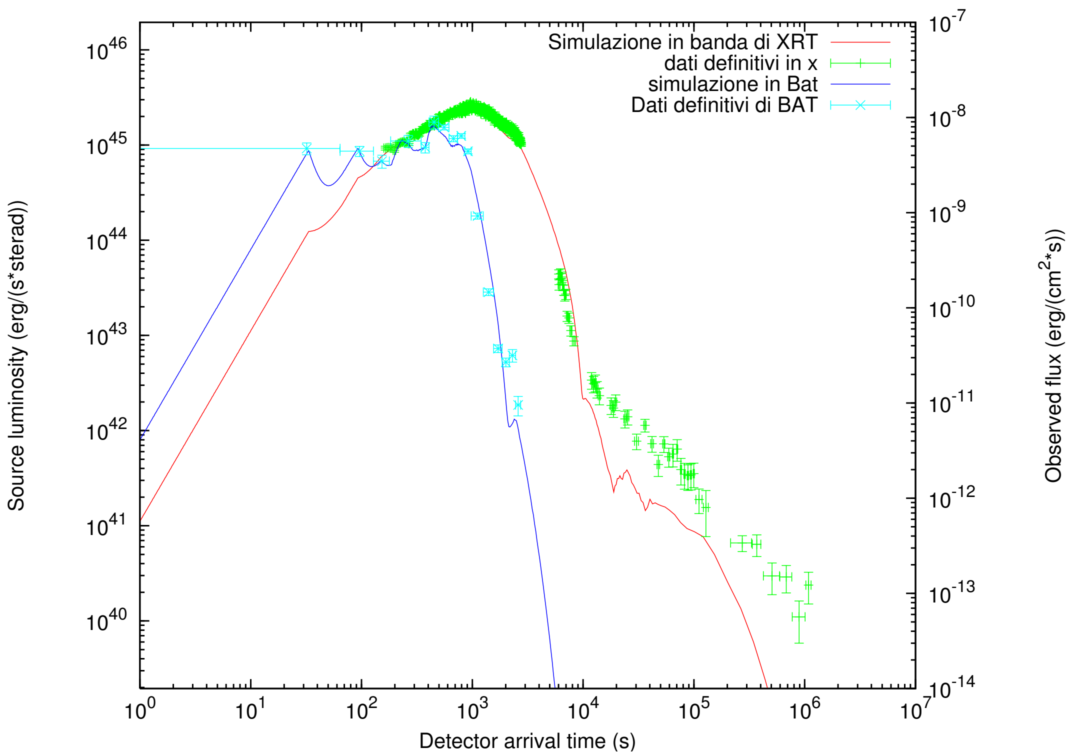

Figure A.11.2: GRB 060218 light curves with $E_{e^\pm}^{tot} = 1.36 \times 10^{50}$ erg: our theoretical fit (blue line) of the 15–150 keV BAT observations (pink points), our theoretical fit (red line) of the 0.3–10 keV XRT observations (green points) and the 0.3–10 keV *Chandra* observations (black points) are represented together with our theoretically computed bolometric luminosity (black line) (Data from: Campana et al. (2006a); Soderberg et al. (2006b)).

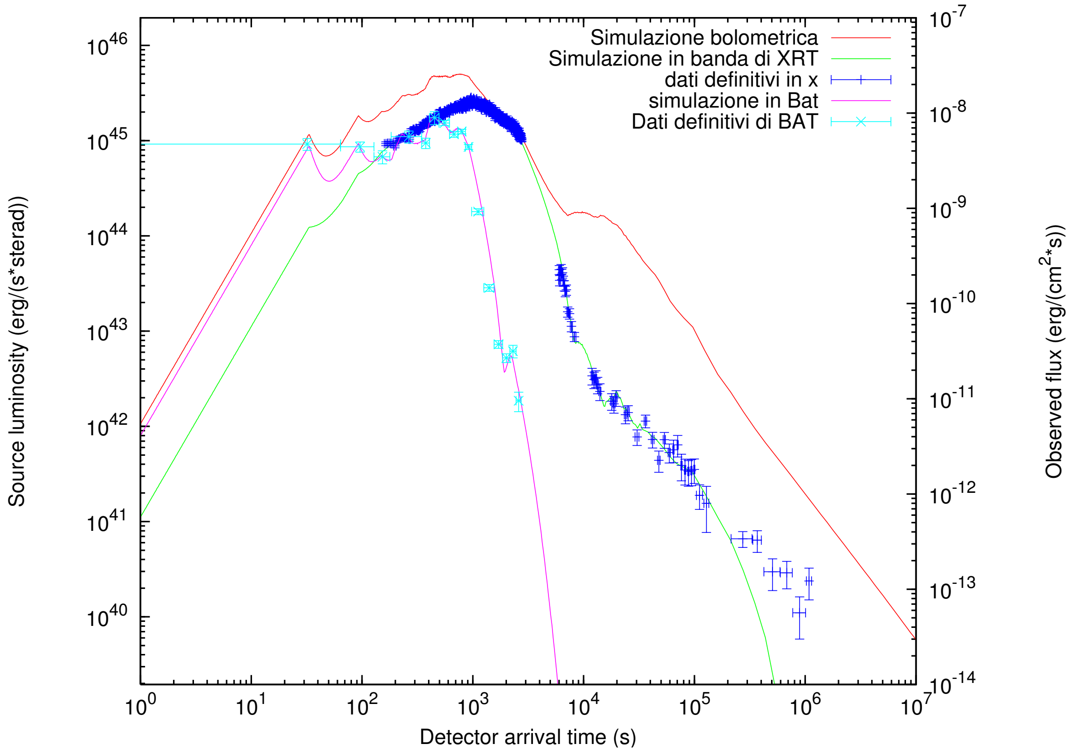

Figure A.11.3: GRB 060218 light curves with $E_{e^\pm}^{tot} = 1.61 \times 10^{50}$ erg: our theoretical fit (blue line) of the 15–150 keV BAT observations (pink points), our theoretical fit (red line) of the 0.3–10 keV XRT observations (green points) and the 0.3–10 keV *Chandra* observations (black points) are represented together with our theoretically computed bolometric luminosity (black line). Data from: Campana et al. (2006a); Soderberg et al. (2006b).

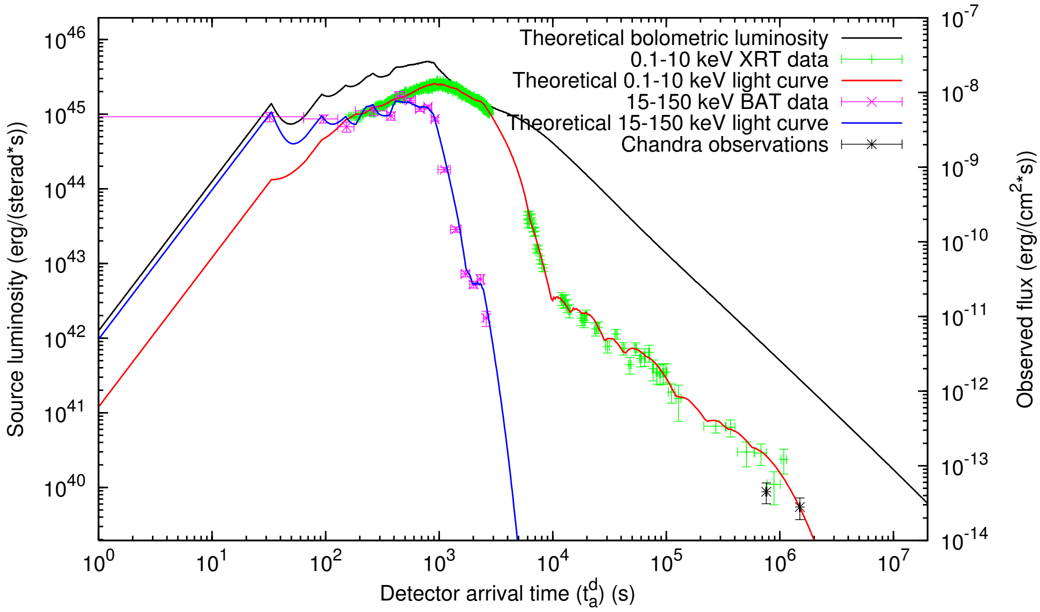

Figure A.11.4: GRB 060218 complete light curves: our theoretical fit (blue line) of the 15–150 keV BAT observations (pink points), our theoretical fit (red line) of the 0.3–10 keV XRT observations (green points) and the 0.3–10 keV *Chandra* observations (black points) are represented together with our theoretically computed bolometric luminosity (black line) (Data from: Campana et al., 2006a; Soderberg et al., 2006b).

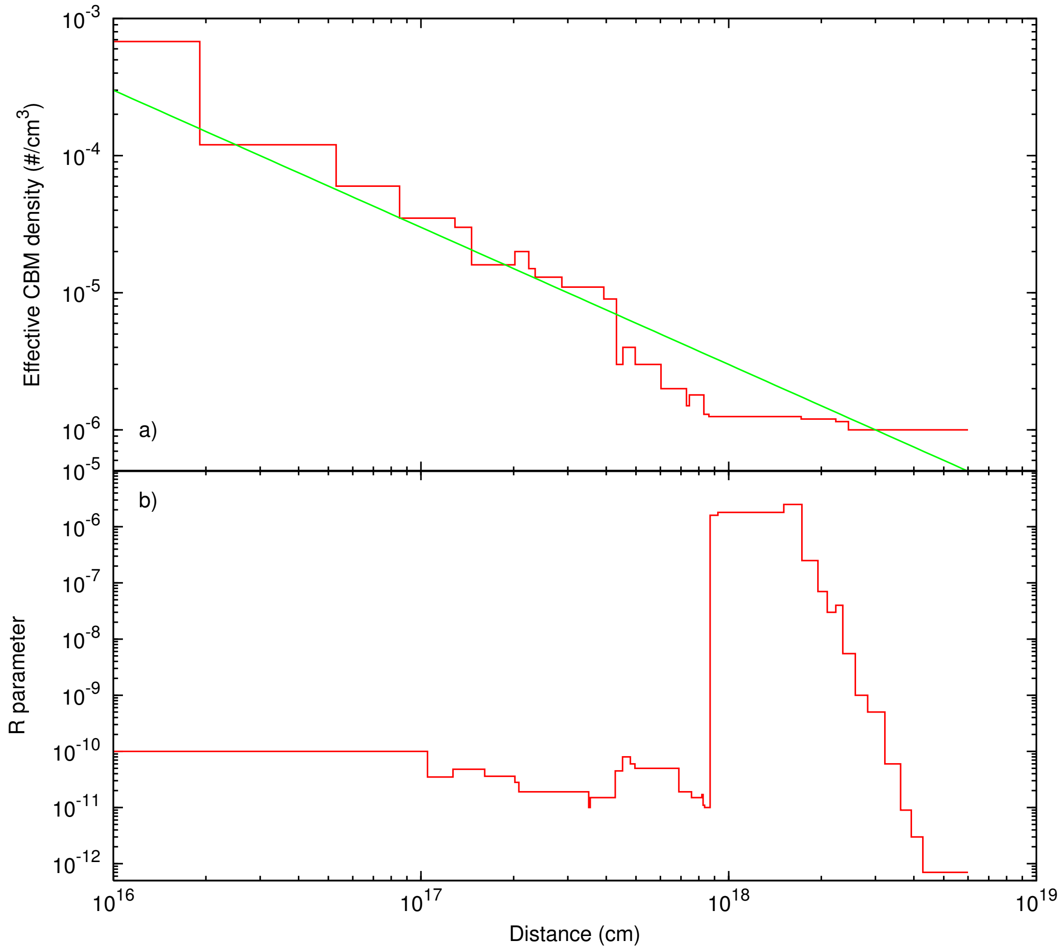

Figure A.11.5: The CBM distribution parameters: a) the effective CBM number density (red line) monotonically decreases with the distance r following Eq.(A.11.3.1) (green line); b) the $\mathcal{R}$ parameter vs. distance.

effect of the fireshell fragmentation ($\mathcal{R}_{shell}$) and of the effective CBM porosity ($\mathcal{R}_{cbm}$):

$$\mathcal{R} \equiv \mathcal{R}_{shell} \times \mathcal{R}_{cbm} \,. \tag{A.11.3.2}$$

The phenomenon of the clumpiness of the ejecta, whose measure is the filling factor, is an aspect well known in astrophysics. For example, in the case of Novae the filling factor has been measured to be in the range 10^{-2}–10^{-5} (Ederoclite et al., 2006). Such a filling factor coincides, in our case, with $\mathcal{R}_{shell}$.

A.11.4 Binaries as progenitors of GRB-SN systems

The majority of the existing models in the literature appeal to a single astrophysical phenomenon to explain both the GRB and the SN ("collapsar", see e.g. Woosley and Bloom, 2006). On the contrary, a distinguishing feature of our theoretical approach is to differentiate between the SN and the GRB process. The GRB is assumed to occur during the formation process of a black hole. The SN is assumed to lead to the formation of a neutron star (NS) or to a complete disruptive explosion without remnants and, in no way, to the formation of a black hole. In the case of SN2006aj the formation of such a NS has been actually inferred by Maeda et al. (2007) because of the large amount of ^{58}Ni ($0.05M_\odot$). Moreover the significantly small initial mass of the SN progenitor star $M \approx 20M_\odot$ is expected to form a NS rather than a black hole when its core collapses (Maeda et al., 2007; Ferrero et al., 2007; Mazzali et al., 2006; Nomoto et al., 2007). In order to fulfill both the above requirement, we assume that the progenitor of the GRB and the SN consists of a binary system formed by a NS close to its critical mass collapsing to a black hole, and a companion star evolved out of the main sequence originating the SN. The temporal coincidence between the GRB and the SN phenomenon is explained in term of the concept of "induced" gravitational collapse (Ruffini et al., 2001a, 2007b). There is also the distinct possibility of observing the young born NS out of the SN (see e.g. Ruffini et al., 2007b, and references therein).

It has been often proposed that GRBs associated with SNe Ib/c, at smaller redshift $0.0085 < z < 0.168$ (see e.g. Della Valle, 2006, and references therein), form a different class, less luminous and possibly much more numerous than the high luminosity GRBs at higher redshift (Pian et al., 2006; Soderberg et al., 2004; Maeda et al., 2007; Della Valle, 2006). Therefore they have been proposed to originate from a separate class of progenitors (Liang et al., 2007; Cobb et al., 2006). In our model this is explained by the nature of the progenitor system leading to the formation of the black hole with the smallest possible mass: the one formed by the collapse of a just overcritical NS (Ruffini, in pressa; Ruffini et al., 2007b).

The recent observation of GRB 060614 at $z = 0.125$ without an associated

SN (Della Valle et al., 2006; Mangano et al., 2007) gives strong support to our scenario, alternative to the collapsar model. Also in this case the progenitor of the GRB appears to be a binary system composed of two NSs or a NS and a white dwarf.

A.11.5 Conclusions

GRB 060218 presents a variety of peculiarities, including its extremely large T_{90} and its classification as an XRF. Nevertheless, a crucial point of our analysis is that we have successfully applied to this source our "canonical GRB" scenario.

Within our model there is no need for inserting GRB 060218 in a new class of GRBs, such as the XRFs, alternative to the "canonical" ones. This same point recently received strong observational support in the case of GRB 060218 (Liang et al., 2006) and a consensus by other models in the literature (Kaneko et al., 2007).

The anomalously long T_{90} led us to infer a monotonic decrease in the CBM effective density giving the first clear evidence for a fragmentation in the fireshell. This phenomenon appears to be essential in understanding the features of also other GRBs (see e.g. GRB 050315 in Ruffini et al., 2007b; Bernardini et al., 2007).

Our "canonical GRB" scenario originates from the gravitational collapse to a black hole and is now confirmed over a 10^6 range in energy (see e.g. Ruffini et al., 2007a, and references therein). It is clear that, although the process of gravitational collapse is unique, there is a large variety of progenitors which may lead to the formation of black holes, each one with precise signatures in the energetics. The low energetics of the class of GRBs associated with SNe, and the necessity of the occurrence of the SN, naturally leads in our model to identify their progenitors with the formation of the smallest possible black hole originating from a NS overcoming his critical mass in a binary system. For GRB 060218 there is no need within our model for a new or unidentified source such as a magnetar or a collapsar.

GRB 060218 is the first GRB associated with SN with complete coverage of data from the onset all the way up to $\sim 10^6$ s. This fact offers an unprecedented opportunity to verify theoretical models on such a GRB class. For example, GRB 060218 fulfills the Amati et al. (2002) relation unlike other sources in its same class. **This is particularly significant, since GRB 060218 is the only source in such a class to have an excellent data coverage without gaps. We are currently examining if the missing data in the other sources of such a class may have a prominent role in their non-fulfillment of the Amati et al. (2002) relation (Dainotti et al., in preparation; see also Ghisellini et al., 2006).**

A.12 Application to GRB 970228

GRB 970228 was detected by the Gamma-Ray Burst Monitor (GRBM, 40–700 keV) and Wide Field Cameras (WFC, 2–26 keV) on board BeppoSAX on February 28.123620 UT (Frontera et al., 1998). The burst prompt emission is characterized by an initial 5 s strong pulse followed, after 30 s, by a set of three additional pulses of decreasing intensity (Frontera et al., 1998). Eight hours after the initial detection, the NFIs on board BeppoSAX were pointed at the burst location for a first target of opportunity observation and a new X-ray source was detected in the GRB error box: this is the first "afterglow" ever detected (Costa et al., 1997). A fading optical transient has been identified in a position consistent with the X-ray transient (van Paradijs et al., 1997), coincident with a faint galaxy with redshift $z = 0.695$ (Bloom et al., 2001). Further observations by the Hubble Space Telescope clearly showed that the optical counterpart was located in the outskirts of a late-type galaxy with an irregular morphology (Sahu et al., 1997).

The BeppoSAX observations of GRB 970228 prompt emission revealed a discontinuity in the spectral index between the end of the first pulse and the beginning of the three additional ones (Costa et al., 1997; Frontera et al., 1998, 2000). The spectrum during the first 3 s of the second pulse is significantly harder than during the last part of the first pulse (Frontera et al., 1998, 2000), while the spectrum of the last three pulses appear to be consistent with the late X-ray afterglow (Frontera et al., 1998, 2000). This was soon recognized by Frontera et al. (1998, 2000) as pointing to an emission mechanism producing the X-ray afterglow already taking place after the first pulse.

As shown in sec. A.5.2, the simultaneous occurrence of an afterglow with total time-integrated luminosity larger than the P-GRB one, but with a smaller peak luminosity, is indeed explainable in terms of a peculiarly small average value of the CBM density and not due to the intrinsic nature of the source. In this sense, GRBs belonging to this class are only "fake" short GRBs. We show that GRB 970228 is a very clear example of this situation. We identify the initial spikelike emission with the P-GRB, and the late soft bump with the peak of the afterglow. GRB 970228 shares the same morphology and observational features with the sources analyzed by Norris and Bonnell (2006) as well as with e.g. GRB 050709 (Villasenor et al., 2005), GRB 050724 (Campana et al., 2006b) and GRB 060614 (see appendix H.2 and Gehrels et al., 2006). Therefore, we propose GRB 970228 as a prototype for this new GRB class.

A.12.1 The analysis of GRB 970228 prompt emission

In Fig. A.12.1 we present the theoretical fit of BeppoSAX GRBM (40–700 keV) and WFC (2–26 keV) light curves of GRB 970228 prompt emission (Frontera et al., 1998). Within our "canonical GRB" scenario we identify the first main pulse with the P-GRB and the three additional pulses with the afterglow peak emission, consistently with the above mentioned observations by Costa et al. (1997) and Frontera et al. (1998). Such last three pulses have been reproduced assuming three overdense spherical CBM regions (see Fig. A.12.2) with a very good agreement (see Fig. A.12.1).

We therefore obtain for the two parameters characterizing the source in our model $E_{e^\pm}^{tot} = 1.45 \times 10^{54}$ erg and $B = 5.0 \times 10^{-3}$. This implies an initial $e^\pm$ plasma created between the radii $r_1 = 3.52 \times 10^7$ cm and $r_2 = 4.87 \times 10^8$ cm with a total number of $e^\pm$ pairs $N_{e^\pm} = 1.6 \times 10^{59}$ and an initial temperature $T = 1.7$ MeV. The theoretically estimated total isotropic energy emitted in the P-GRB is $E_{P-GRB} = 1.1\% E_{e^\pm}^{tot} = 1.54 \times 10^{52}$ erg, in excellent agreement with the one observed in the first main pulse ($E_{P-GRB}^{obs} \sim 1.5 \times 10^{52}$ erg in $2-700$ keV energy band, see Fig. A.12.1), as expected due to their identification. After the transparency point at $r_0 = 4.37 \times 10^{14}$ cm from the progenitor, the initial Lorentz gamma factor of the fireshell is $\gamma_0 = 199$. On average, during the afterglow peak emission phase we have for the CBM $\langle \mathcal{R} \rangle = 1.5 \times 10^{-7}$ and $\langle n_{cbm} \rangle = 9.5 \times 10^{-4}$ particles/cm^3. This very low average value for the CBM density is compatible with the observed occurrence of GRB 970228 in its host galaxy's halo (Sahu et al., 1997; van Paradijs et al., 1997; Panaitescu, 2006) and it is crucial in explaining the light curve behavior.

The values of $E_{e^\pm}^{tot}$ and B we determined are univocally fixed by two tight constraints. The first one is the total energy emitted by the source all the way up to the latest afterglow phases (i.e. up to $\sim 10^6$ s). The second one is the ratio between the total time-integrated luminosity of the P-GRB and the corresponding one of the whole afterglow (i.e. up to $\sim 10^6$ s). In particular, in GRB 970228 such a ratio results to be $\sim 1.1\%$ (see Fig. A.2.8). However, the P-GRB peak luminosity actually results to be much more intense than the afterglow one (see Fig. A.12.1). This is due to the very low average value of the CBM density $\langle n_{cbm} \rangle = 9.5 \times 10^{-4}$ particles/cm^3, which produces a less intense afterglow emission. Since the afterglow total time-integrated luminosity is fixed, such a less intense emission lasts longer than what we would expect for an average density $\langle n_{cbm} \rangle \sim 1$ particles/cm^3.

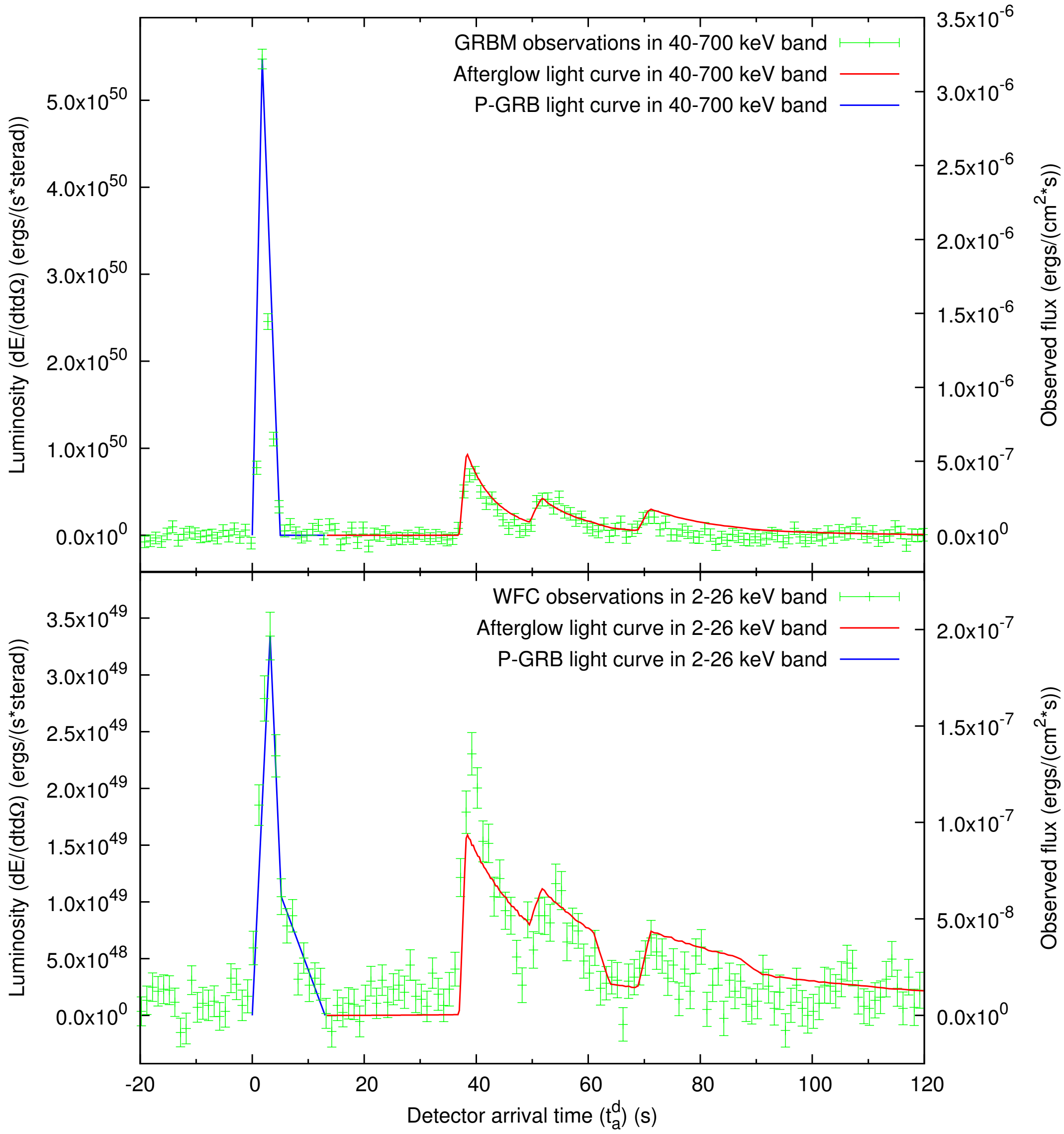

Figure A.12.1: The "canonical GRB" light curve theoretically computed for the prompt emission of GRB 970228. BeppoSAX GRBM (40–700 keV, above) and WFC (2–26 keV, below) light curves (data points) are compared with the afterglow peak theoretical ones (solid lines). The onset of the afterglow coincides with the end of the P-GRB (represented qualitatively by the dotted lines). For this source we have $B \simeq 5.0 \times 10^{-3}$ and $\langle n_{cbm} \rangle \sim 10^{-3}$ particles/cm^3.

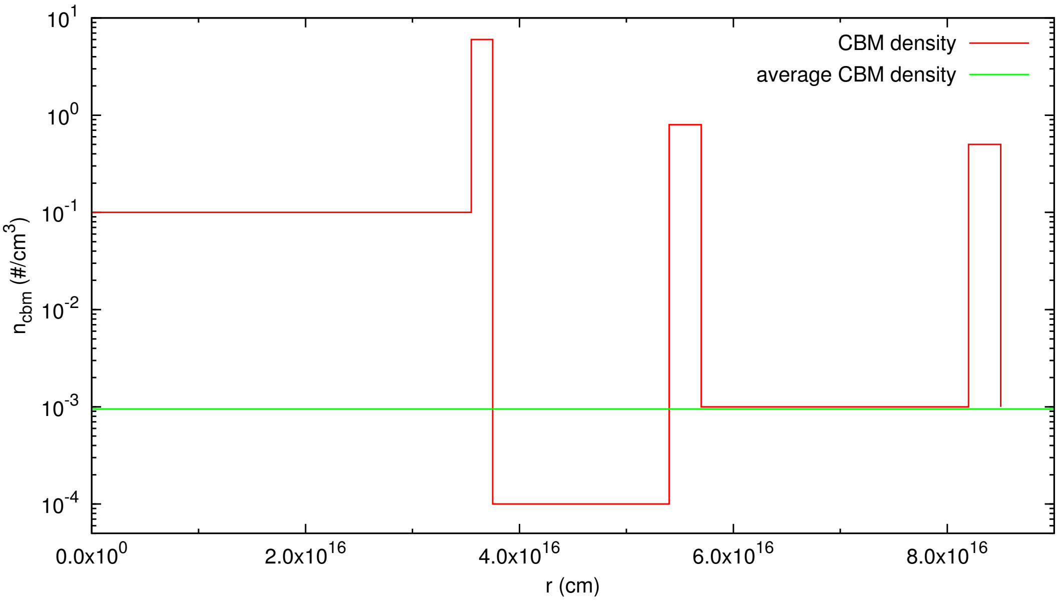

Figure A.12.2: The CBM density profile we assumed to reproduce the last three pulses of the GRB 970228 prompt emission (red line), together with its average value $\langle n_{cbm} \rangle = 9.5 \times 10^{-4}$ particles/cm^3 (green line).

A.12.2 Rescaling the CBM density

We present now an explicit example in order to probe the crucial role of the average CBM density in explaining the relative intensities of the P-GRB and of the afterglow peak in GRB 970228. We keep fixed the basic parameters of the source, namely the total energy $E_{e^\pm}^{tot}$ and the baryon loading B, therefore keeping fixed the P-GRB and the afterglow total time-integrated luminosities. Then we rescale the CBM density profile given in Fig. A.12.2 by a constant numerical factor in order to raise its average value to the standard one $\langle n_{ism} \rangle = 1$ particle/cm^3. We then compute the corresponding light curve, shown in Fig. A.12.3.

We notice a clear enhancement of the afterglow peak luminosity with respect to the P-GRB one in comparison with the fit of the observational data presented in Fig. A.12.1. The two light curves actually crosses at $t_a^d \simeq 1.8 \times 10^4$ s since their total time-integrated luminosities must be the same. The GRB "rescaled" to $\langle n_{ism} \rangle = 1$ particle/cm^3 appears to be totally similar to, e.g., GRB 050315 (Ruffini et al., 2006b) and GRB 991216 (Ruffini et al., 2003, 2004b, 2005a).

It is appropriate to emphasize that, although the two underlying CBM density profiles differ by a constant numerical factor, the two afterglow light curves in Fig. A.12.3 do not. This is because the absolute value of the CBM density at each point affects in a non-linear way all the following evolution of the fireshell due to the feedback on its dynamics (Bianco and Ruffini, 2005a).

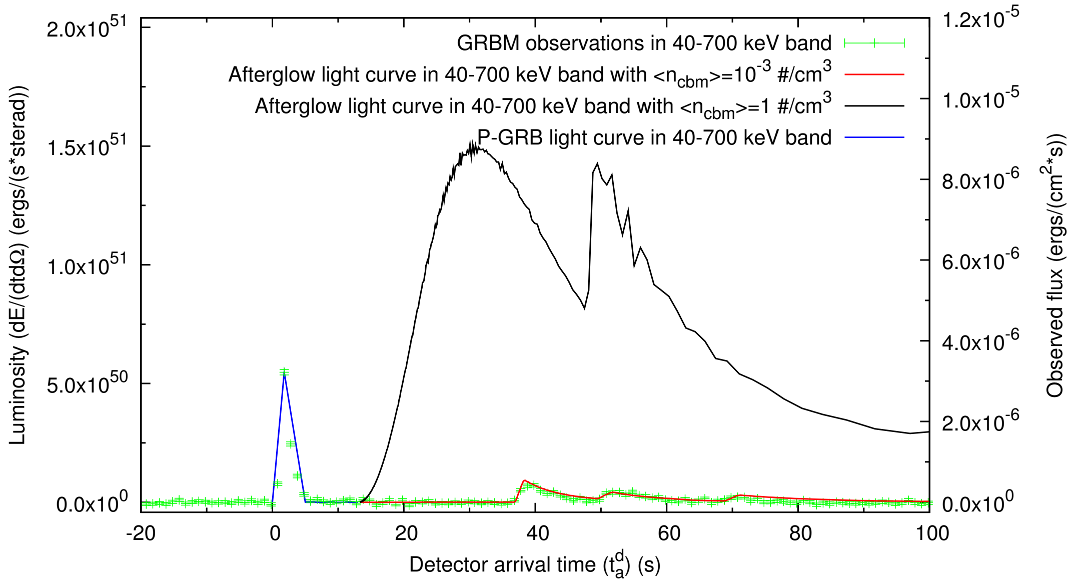

Figure A.12.3: The theoretical fit of the BeppoSAX GRBM observations (red line, see Fig. A.12.1) is compared with the afterglow light curve in the 40–700 keV energy band obtained rescaling the CBM density to $\langle n_{cbm} \rangle = 1$ particle/cm^3 keeping constant its shape and the values of the fundamental parameters of the theory $E^{tot}_{e^\pm}$ and B (black line). The P-GRB duration and luminosity (blue line), depending only on $E^{tot}_{e^\pm}$ and B, are not affected by this process of rescaling the CBM density.

Moreover, the shape of the surfaces of equal arrival time of the photons at the detector (EQTS) is strongly elongated along the line of sight (Bianco and Ruffini, 2005b). Therefore photons coming from the same CBM density region are observed over a very long arrival time interval.

A.12.3 GRB 970228 and the Amati relation

We turn now to the "Amati relation" (Amati et al., 2002; Amati, 2006) between the isotropic equivalent energy emitted in the prompt emission E_{iso} and the peak energy of the corresponding time-integrated spectrum $E_{p,i}$ in the source rest frame. It has been shown by Amati et al. (2002); Amati (2006) that this correlation holds for almost all the "long" GRBs which have a redshift and an $E_{p,i}$ measured, but not for the ones classified as "short" (Amati, 2006). If we focus on the "fake" short GRBs, namely the GRBs belonging to this new class, at least in one case (GRB 050724 Campana et al., 2006b) it has been shown that the correlation is recovered if also the extended emission is considered (Amati, 2007).

It clearly follows from our treatment that for the "canonical GRBs" with large values of the baryon loading and high $\langle n_{cbm} \rangle$, which presumably are most of the GRBs for which the correlation holds, the leading contribution to the prompt emission is the afterglow peak emission. The case of the "fake" short GRBs is completely different: it is crucial to consider separately the two components since the P-GRB contribution to the prompt emission in this case is significant.

To test this scenario, we evaluated from our fit of GRB 970228 E_{iso} and $E_{p,i}$ only for the afterglow peak emission component, i.e. from $t_a^d = 37$ s to $t_a^d = 81.6$ s. We found an isotropic energy emitted in the 2–400 keV energy band $E_{iso} = 1.5 \times 10^{52}$ erg, and $E_{p,i} = 90.3$ keV. As it is clearly shown in Fig. A.12.4, the sole afterglow component of GRB 970228 prompt emission is in perfect agreement with the Amati relation. If this behavior is confirmed for other GRBs belonging to this new class, this will enforce our identification of the "fake" short GRBs. This result will also provide a theoretical explanation for the the apparent absence of such correlation for the initial spikelike component in the different nature of the P-GRB.

A.12.4 Conclusions

We conclude that GRB 970228 is a "canonical GRB" with a large value of the baryon loading quite near to the maximum $B \sim 10^{-2}$ (see Fig. A.2.8). The difference with e.g. GRB 050315 (Ruffini et al., 2006b) or GRB 991216 (Ruffini et al., 2003, 2004b, 2005a) is the low average value of the CBM density $\langle n_{cbm} \rangle \sim 10^{-3}$ particles/cm^3 which deflates the afterglow peak lumi-

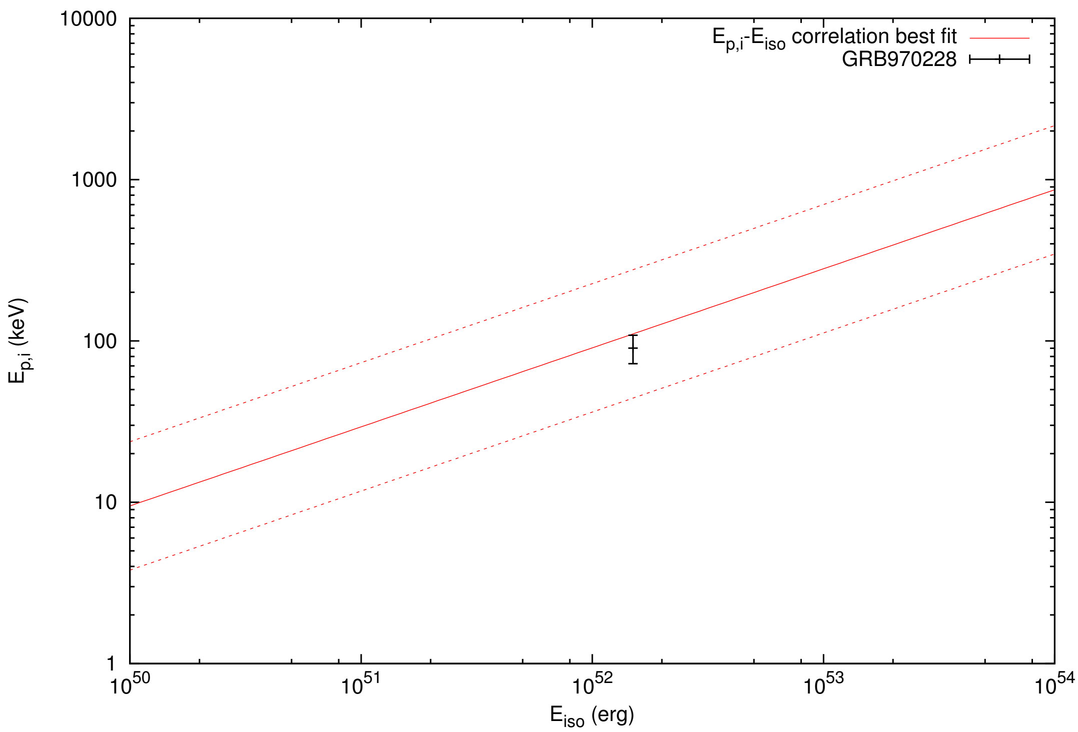

Figure A.12.4: The estimated values for $E_{p,i}$ and E_{iso} obtained by our analysis (black dot) compared with the "Amati relation" (Amati et al., 2002): the solid line is the best fitting power law (Amati, 2006) and the dashed lines delimit the region corresponding to a vertical logarithmic deviation of 0.4 (Amati, 2006). The uncertainty in the theoretical estimated value for $E_{p,i}$ has been assumed conservatively as 20%.

nosity. Hence, the predominance of the P-GRB, coincident with the initial spikelike emission, over the afterglow is just apparent: 98.9% of the total time-integrated luminosity is indeed in the afterglow component. Such a low average CBM density is consistent with the occurrence of GRB 970228 in the galactic halo of its host galaxy (Sahu et al., 1997; van Paradijs et al., 1997), where lower CBM densities have to be expected (Panaitescu, 2006).

We propose GRB 970228 as the prototype for the new class of GRBs comprising GRB 060614 and the GRBs analyzed by Norris and Bonnell (2006). We naturally explain the hardness and the absence of spectral lag in the initial spikelike emission with the physics of the P-GRB originating from the gravitational collapse leading to the black hole formation. The hard-to-soft behavior in the afterglow is also naturally explained by the physics of the relativistic fireshell interacting with the CBM, clearly evidenced in GRB 031203 (Bernardini et al., 2005a) and in GRB 050315 (Ruffini et al., 2006b). Also justified is the applicability of the Amati relation to the sole afterglow component (see Amati, 2006, 2007).

This class of GRBs with $z \sim 0.4$ appears to be nearer than the other GRBs detected by *Swift* ($z \sim 2.3$, see Guetta, 2006). This may be explained by the afterglow peak luminosity deflation. The absence of a jet break in those afterglows has been pointed out (Campana et al., 2006b; Watson et al., 2006a), consistently with our spherically symmetric approach. Their association with non-star-forming host galaxies appears to be consistent with the merging of a compact object binary (Barthelmy et al., 2005b; Fox et al., 2005). It is here appropriate, however, to caution on this conclusion, since the association of GRB 060614 and GRB 970228 with the explosion of massive stars is not excluded (Della Valle et al., 2006; Galama et al., 2000).

Most of the sources of this class appear indeed not to be related to bright "Hypernovae", to be in the outskirts of their host galaxies (Fox et al., 2005, see above) and a consistent fraction of them are in galaxy clusters with CBM densities $\langle n_{cbm} \rangle \sim 10^{-3}$ particles/cm^3 (see e.g. Lewis et al., 2003; Berger et al., 2007). This suggests a spiraling out binary nature of their progenitor systems (Kramer, in press) made of neutron stars and/or white dwarfs leading to a black hole formation.

Moreover, we verified the applicability of the Amati relation to the sole afterglow component in GRB 970228 prompt emission, in analogy with what happens for some of the GRBs belonging to this new class. In fact it has been shown by Amati (2006, 2007) that the "fake" short GRBs do not fulfill the $E_{p,i}$–E_{iso} correlation when the sole spiklike emission is considered, while they do if the long soft bump is included. Since the spikelike emission and the soft bump contributions are comparable, it is natural to expect that the soft bump alone will fulfill the correlation as well.

Within our "canonical GRB" scenario the sharp distinction between the P-GRB and the afterglow provide a natural explanation for the observational features of the two contributions. We naturally explain the hardness and the absence of spectral lag in the initial spikelike emission with the physics of the P-GRB originating from the gravitational collapse leading to the black hole formation. The hard-to-soft behavior in the afterglow is also naturally explained by the physics of the relativistic fireshell interacting with the CBM, clearly evidenced in GRB 031203 (Bernardini et al., 2005a) and in GRB 050315 (Ruffini et al., 2006b). Therefore, we expect naturally that the $E_{p,i}$–E_{iso} correlation holds only for the afterglow component and not for the P-GRB. Actually we find that the correlation is recovered for the afterglow peak emission of GRB 970228.

In the original work by Amati et al. (2002); Amati (2006) only the prompt emission is considered and not the late afterglow one. In our theoretical approach the afterglow peak emission contributes to the prompt emission and continues up to the latest GRB emission. Hence, the meaningful procedure within our model to recover the Amati relation is to look at a correlation between the total isotropic energy and the peak of the time-integrated spectrum of the whole afterglow. A first attempt to obtain such a correlation has already been performed using GRB 050315 as a template, giving very satisfactory results (see section H.5).

Bibliography

AKSENOV, A., RUFFINI, R. AND VERESHCHAGIN, G.
≪Thermalization of nonequilibrium electron-positron-photon plasmas≫.
Phys. Rev. Lett., **99(12)**, p. 125003 (2007).

AKSENOV, A., RUFFINI, R. AND VERESHCHAGIN, G.
submitted to Phys. Rev. D (2008).

AKSENOV, A., RUFFINI, R. AND VERESHCHAGIN, G.
Phys. Rev. D (submitted to).

AMATI, L.
≪The $e_{p,i}$-e_{iso} correlation in gamma-ray bursts: updated observational status, re-analysis and main implications≫.
MNRAS, **372**, pp. 233–245 (2006).

AMATI, L.
talk presented at the congress "10^{th} Italian-Korean Meeting", Pescara, Italy, June 25-29 (2007).

AMATI, L., DELLA VALLE, M., FRONTERA, F., MALESANI, D., GUIDORZI, C., MONTANARI, E. AND PIAN, E.
≪On the consistency of peculiar grbs 060218 and 060614 with the $e_{p,i}$ - e_{iso} correlation≫.
A&A, **463**, pp. 913–919 (2007).

AMATI, L., FRONTERA, F., TAVANI, M., IN'T ZAND, J.J.M., ANTONELLI, A., COSTA, E., FEROCI, M., GUIDORZI, C., HEISE, J., MASETTI, N. ET AL.
≪Intrinsic spectra and energetics of bepposax gamma-ray bursts with known redshifts≫.
A&A, **390**, pp. 81–89 (2002).

AMATI, L., GUIDORZI, C., FRONTERA, F., DELLA VALLE, M., FINELLI, F., LANDI, R. AND MONTANARI, E.
≪Measuring the cosmological parameters with the ep,i-eiso correlation of gamma-ray bursts≫.
ArXiv:0805.0377 (2008).

ATKINSON, R.D. AND HOUTERMANS, F.G.
≪Zur quantenmechanik der α-strahlung≫.
Zeitschrift fur Physik, **58**, pp. 478–496 (1929a).

ATKINSON, R.D.E. AND HOUTERMANS, F.G.
≪Zur frage der aufbaumöglichkeit der elemente in sternen≫.
Zeitschrift fur Physik, **54**, pp. 656–665 (1929b).

BAND, D., MATTESON, J., FORD, L., SCHAEFER, B., PALMER, D., TEEGARDEN, B., CLINE, T., BRIGGS, M., PACIESAS, W., PENDLETON, G. ET AL.
≪Batse observations of gamma-ray burst spectra. i - spectral diversity≫.
ApJ, **413**, pp. 281–292 (1993).

BARBIER, L., BARTHELMY, S., CUMMINGS, J., CUSUMANO, G., FENIMORE, E., GEHRELS, N., HULLINGER, D., KRIMM, H., MARKWARDT, C., PALMER, D. ET AL.
≪Preliminary refined analysis of the swift-bat trigger 191157.≫
GCN, **4780** (2006).

BARTHELMY, S.D.
≪Burst alert telescope (bat) on the swift midex mission≫.
In K.A. Flanagan and O.H.W. Siegmund (eds.), *X-Ray and Gamma-Ray Instrumentation for Astronomy XIII.*, volume 5165 of *Society of Photo-Optical Instrumentation Engineers (SPIE) Conference Proceedings*, pp. 175–189 (2004).

BARTHELMY, S.D., BARBIER, L.M., CUMMINGS, J.R., FENIMORE, E.E., GEHRELS, N., HULLINGER, D., KRIMM, H.A., MARKWARDT, C.B., PALMER, D.M., PARSONS, A. ET AL.
≪The burst alert telescope (bat) on the swift midex mission≫.
Space Science Reviews, **120**, pp. 143–164 (2005a).

BARTHELMY, S.D., CHINCARINI, G., BURROWS, D.N., GEHRELS, N., COVINO, S., MORETTI, A., ROMANO, P., O'BRIEN, P.T., SARAZIN, C.L., KOUVELIOTOU, C. ET AL.
≪An origin for short γ-ray bursts unassociated with current star formation≫.
Nature, **438**, pp. 994–996 (2005b).

BELL, S.J. AND HEWISH, A.
≪Angular size and flux density of the small source in the crab nebula at 81.5 mc/s≫.
Nature, **213**, p. 1214 (1967).

BERGER, E., SHIN, M.S., MULCHAEY, J.S. AND JELTEMA, T.E.
≪Galaxy clusters associated with short grbs. i. the fields of grbs 050709, 050724, 050911, and 051221a≫.
ApJ, **660**, pp. 496–503 (2007).

BERNARDINI, M.G., BIANCO, C.L., CAITO, L., DAINOTTI, M.G., GUIDA, R. AND RUFFINI, R.

≪Grb 970228 and a class of grbs with an initial spikelike emission≫.
A&A, **474**, pp. L13–L16 (2007).

BERNARDINI, M.G., BIANCO, C.L., CAITO, L., DAINOTTI, M.G., GUIDA, R. AND RUFFINI, R.
≪Grb970228 and the class of grbs with an initial spikelike emission: do they follow the amati relation?≫
In C.L. Bianco and S.S. Xue (eds.), *Relativistic Astrophysics*, volume 966 of *American Institute of Physics Conference Series*, pp. 7–11 (2008).

BERNARDINI, M.G., BIANCO, C.L., CHARDONNET, P., FRASCHETTI, F., RUFFINI, R. AND XUE, S.S.
≪A new astrophysical "triptych": Grb030329/sn2003dh/urca-2≫.
In E. Fenimore and M. Galassi (eds.), *Gamma-Ray Bursts: 30 Years of Discovery*, volume 727 of *American Institute of Physics Conference Series*, pp. 312–315 (2004).

BERNARDINI, M.G., BIANCO, C.L., CHARDONNET, P., FRASCHETTI, F., RUFFINI, R. AND XUE, S.S.
≪Theoretical interpretation of the luminosity and spectral properties of grb 031203≫.
ApJ, **634**, pp. L29–L32 (2005a).

BERNARDINI, M.G., BIANCO, C.L., RUFFINI, R., XUE, S.S., CHARDONNET, P. AND FRASCHETTI, F.
≪General features of grb 030329 in the embh model≫.
In M. Novello, S. Perez Bergliaffa and R. Ruffini (eds.), *The Tenth Marcel Grossmann Meeting. On recent developments in theoretical and experimental general relativity, gravitation and relativistic field theories*, p. 2459 (Singapore: World Scientific, 2005b).

BETHE, H.A.
≪Energy production in stars≫.
Physical Review, **55**, pp. 103–103 (1939).

BIANCO, C.L., BERNARDINI, M.G., CAITO, L., DAINOTTI, M.G., GUIDA, R. AND RUFFINI, R.
≪The "fireshell" model and the "canonical" grb scenario.≫
In C.L. Bianco and S.S. Xue (eds.), *Relativistic Astrophysics*, volume 966 of *American Institute of Physics Conference Series*, pp. 12–15 (2008a).

BIANCO, C.L., BERNARDINI, M.G., CAITO, L., DAINOTTI, M.G., GUIDA, R. AND RUFFINI, R.
≪Short and canonical grbs≫.
In M. Galassi, D. Palmer and E. Fenimore (eds.), *GAMMA-RAY BURSTS 2007: Proceedings of the Santa Fe Conference*, volume 1000 of *American Institute of Physics Conference Series*, pp. 305–308 (2008b).

BIANCO, C.L., CAITO, L. AND RUFFINI, R.
≪Theoretical interpretation of grb 011121≫.
Il Nuovo Cimento B, **121**, p. 1441 (2006a).

BIANCO, C.L. AND RUFFINI, R.
≪Exact versus approximate equitemporal surfaces in gamma-ray burst afterglows≫.
ApJ, **605**, pp. L1–L4 (2004).

BIANCO, C.L. AND RUFFINI, R.
≪Exact versus approximate solutions in gamma-ray burst afterglows≫.
ApJ, **633**, pp. L13–L16 (2005a).

BIANCO, C.L. AND RUFFINI, R.
≪On the exact analytic expressions for the equitemporal surfaces in gamma-ray burst afterglows≫.
ApJ, **620**, pp. L23–L26 (2005b).

BIANCO, C.L. AND RUFFINI, R.
≪Exact versus approximate beaming formulae in gamma-ray burst afterglows≫.
ApJ, **644**, pp. L105–L108 (2006).

BIANCO, C.L., RUFFINI, R., VERESHCHAGIN, G. AND XUE, S.S.
≪Equations of motion and initial and boundary conditions for gamma-ray burst≫.
Journal of the Korean Physical Society, **49**, p. 722 (2006b).

BIANCO, C.L., RUFFINI, R. AND XUE, S.S.
≪The elementary spike produced by a pure e^+e^- pair-electromagnetic pulse from a black hole: The pem pulse≫.
A&A, **368**, pp. 377–390 (2001).

BINI, D., CHERUBINI, C., JANTZEN, R.T. AND RUFFINI, R.
≪Teukolsky master equation —de rham wave equation for the gravitational and electromagnetic fields in vacuum—≫.
Progress of Theoretical Physics, **107**, pp. 967–992 (2002).

BINI, D., GERALICO, A. AND RUFFINI, R.
≪Charged massive particle at rest in the field of a reissner-nordström black hole≫.
Phys. Rev. D, **75(4)**, p. 044012 (2007a).

BINI, D., GERALICO, A. AND RUFFINI, R.
≪On the equilibrium of a charged massive particle in the field of a reissner nordström black hole≫.
Physics Letters A, **360**, pp. 515–517 (2007b).

BISNOVATYI-KOGAN, G.S. AND MURZINA, M.V.A.
≪Early stages of relativistic fireball expansion≫.
Phys. Rev. D, **52**, pp. 4380–4392 (1995).

BLANDFORD, R.D. AND MCKEE, C.F.
≪Fluid dynamics of relativistic blast waves≫.
Physics of Fluids, **19**, pp. 1130–1138 (1976).

BLATTNIG, S.R., SWAMINATHAN, S.R., KRUGER, A.T., NGOM, M. AND NORBURY, J.W.
≪Parametrizations of inclusive cross sections for pion production in proton-proton collisions≫.
Phys. Rev. D, **62(9)**, p. 094030 (2000).

BLINNIKOV, S.I., KOZYREVA, A.V. AND PANCHENKO, I.E.
≪Gamma-ray bursts: When does a blackbody spectrum look non-thermal?≫
Astronomy Reports, **43**, pp. 739–747 (1999).

BLINNIKOV, S.I., NOVIKOV, I.D., PEREVODCHIKOVA, T.V. AND POLNAREV, A.G.
≪Exploding neutron stars in close binaries≫.
Soviet Astronomy Letters, **10**, p. 177 (1984).

BLOOM, J.S., DJORGOVSKI, S.G. AND KULKARNI, S.R.
≪The redshift and the ordinary host galaxy of grb 970228≫.
ApJ, **554**, pp. 678–683 (2001).

BORN, M.
≪On the quantum theory of the electromagnetic field≫.
Royal Society of London Proceedings Series A, **143**, pp. 410–437 (1934).

BURBIDGE, E.M., BURBIDGE, G.R., FOWLER, W.A. AND HOYLE, F.
≪Synthesis of the elements in stars≫.
Reviews of Modern Physics, **29**, pp. 547–650 (1957).

BURLON, D., GHIRLANDA, G., GHISELLINI, G., LAZZATI, D., NAVA, L., NARDINI, M. AND CELOTTI, A.
≪Precursors in swift gamma ray bursts with redshift≫.
ApJ (in press).

BURROWS, A. AND LATTIMER, J.M.
≪The birth of neutron stars≫.
ApJ, **307**, pp. 178–196 (1986).

BURROWS, D.N., HILL, J.E., NOUSEK, J.A., KENNEA, J.A., WELLS, A., OSBORNE, J.P., ABBEY, A.F., BEARDMORE, A., MUKERJEE, K., SHORT, A.D.T. ET AL.
≪The swift x-ray telescope≫.
Space Science Reviews, **120**, pp. 165–195 (2005a).

BURROWS, D.N., HILL, J.E., NOUSEK, J.A., WELLS, A.A., CHINCARINI, G., ABBEY, A.F., BEARDMORE, A.P., BOSWORTH, J., BRÄUNINGER, H.W., BURKERT, W. ET AL.
≪The swift x-ray telescope≫.
In K.A. Flanagan and O.H.W. Siegmund (eds.), *X-Ray and Gamma-Ray Instrumentation for Astronomy XIII*, volume 5165 of *Society of Photo-Optical Instrumentation Engineers (SPIE) Conference Proceedings*, pp. 201–216 (2004).

BURROWS, D.N., ROMANO, P., FALCONE, A., KOBAYASHI, S., ZHANG, B., MORETTI, A., O'BRIEN, P.T., GOAD, M.R., CAMPANA, S., PAGE, K.L. ET AL.
≪Bright x-ray flares in gamma-ray burst afterglows≫.
Science, **309**, pp. 1833–1835 (2005b).

CAITO, L., BERNARDINI, M.G., BIANCO, C.L., DAINOTTI, M.G., GUIDA, R. AND RUFFINI, R.
≪Grb 060614: a progress report≫.
In C.L. Bianco and S.S. Xue (eds.), *Relativistic Astrophysics*, volume 966 of *American Institute of Physics Conference Series*, pp. 16–20 (2008).

CAITO, L., BERNARDINI, M.G., BIANCO, C.L., DAINOTTI, M.G., GUIDA, R. AND RUFFINI, R.
In R.T. Jantzen, H. Kleinert and R. Ruffini (eds.), *The Eleventh Marcel Grossmann Meeting.* (Singapore: World Scientific, in press).

CAMPANA, S., MANGANO, V., BLUSTIN, A.J., BROWN, P., BURROWS, D.N., CHINCARINI, G., CUMMINGS, J.R., CUSUMANO, G., DELLA VALLE, M., MALESANI, D. ET AL.
≪The association of grb 060218 with a supernova and the evolution of the shock wave≫.
Nature, **442**, pp. 1008–1010 (2006a).

CAMPANA, S., TAGLIAFERRI, G., LAZZATI, D., CHINCARINI, G., COVINO, S., PAGE, K., ROMANO, P., MORETTI, A., CUSUMANO, G., MANGANO, V. ET AL.
≪The x-ray afterglow of the short gamma ray burst 050724≫.
A&A, **454**, pp. 113–117 (2006b).

CANUTO, V.
≪Neutron stars≫.

In R. Giacconi and R. Ruffini (eds.), *Physics and Astrophysics of Neutron Stars and Black Holes*, pp. 448–527 (1978).

CARTER, B.
≪Global structure of the kerr family of gravitational fields≫.
Physical Review, **174**, pp. 1559–1571 (1968).

CARTER, B.
In D.L. Wiltshire, M. Visser and S. Scott (eds.), *The Kerr Spacetime* (Cambridge University Press, in press, in press).

CAVALLO, G. AND HORSTMAN, H.M.
≪Spectrum of cosmic fireballs≫.
Astrophysics and Space Science, **75**, pp. 117–123 (1981).

CAVALLO, G. AND REES, M.J.
≪A qualitative study of cosmic fireballs and gamma-ray bursts≫.
MNRAS, **183**, pp. 359–365 (1978).

CHIANG, J. AND DERMER, C.D.
≪Synchrotron and synchrotron self-compton emission and the blast-wave model of gamma-ray bursts≫.
ApJ, **512**, pp. 699–710 (1999).

CHINCARINI, G., MORETTI, A., ROMANO, P., FALCONE, A.D., MORRIS, D., RACUSIN, J., CAMPANA, S., GUIDORZI, C., TAGLIAFERRI, G., BURROWS, D.N. ET AL.
≪The first survey of x-ray flares from gamma ray bursts observed by swift: Temporal properties and morphology≫.
ArXiv:astro-ph/0702371 (2007).

CHRISTODOULOU, D. AND RUFFINI, R.
≪Reversible transformations of a charged black hole.≫
Phys. Rev. D, **4**, pp. 3552–3555 (1971).

COBB, B.E., BAILYN, C.D., VAN DOKKUM, P.G. AND NATARAJAN, P.
≪Sn 2006aj and the nature of low-luminosity gamma-ray bursts≫.
ApJ, **645**, pp. L113–L116 (2006).

COSTA, E., FRONTERA, F., HEISE, J., FEROCI, M., IN'T ZAND, J., FIORE, F., CINTI, M.N., DAL FIUME, D., NICASTRO, L., ORLANDINI, M. ET AL.
≪Discovery of an x-ray afterglow associated with the γ-ray burst of 28 february 1997≫.
Nature, **387**, pp. 783–785 (1997).

COVINO, S., VERGANI, S.D., MALESANI, D., MOLINARI, E., D'AVANZO, P., CHINCARINI, G., ZERBI, F.M., ANTONELLI, L.A., CONCONI, P., TESTA, V. ET AL.
≪The afterglow onset for GRB060418 and GRB060607A≫.
ArXiv:0710.0727 (2007).

CRIDER, A., LIANG, E.P., SMITH, I.A., PREECE, R.D., BRIGGS, M.S., PENDLETON, G.N., PACIESAS, W.S., BAND, D.L. AND MATTESON, J.L.
≪Evolution of the low-energy photon spectral in gamma-ray bursts≫.
ApJ, **479**, p. L39 (1997).

CURVES, B.G.L.
http://gammaray. msfc. nasa. gov/batse/grb/lightcurve/ (1999).

CUSUMANO, G., BARTHELMY, S., GEHRELS, N., HUNSBERGER, S., IMMLER, S., MARSHALL, F., PALMER, D. AND SAKAMOTO, T.
≪Grb 060218: Swift-bat detection of a possible burst.≫
GCN, **4775** (2006).

DAINOTTI, M.G., BERNARDINI, M.G., BIANCO, C.L., CAITO, L., GUIDA, R. AND RUFFINI, R.
≪Grb 060218 and grbs associated with supernovae ib/c≫.
A&A, **471**, pp. L29–L32 (2007).

DAMOUR, T. AND RUFFINI, R.
≪Quantum electrodynamical effects in kerr-newman geometries.≫
Physical Review Letters, **35**, pp. 463–466 (1975).

DAVIES, M.B., LEVAN, A.J., LARSSON, J., KING, A.R. AND FRUCHTER, A.S.
≪Progenitors of long gamma-ray bursts≫.
In M. Axelsson and F. Ryde (eds.), *Gamma-Ray Bursts: Prospects for GLAST*, volume 906 of *American Institute of Physics Conference Series*, pp. 69–78 (2007).

DELLA VALLE, M.
≪Supernova and grb connection: Observations and questions≫.
In S.S. Holt, N. Gehrels and J.A. Nousek (eds.), *Gamma-Ray Bursts in the Swift Era*, volume 836 of *American Institute of Physics Conference Series*, pp. 367–379 (2006).

DELLA VALLE, M., CHINCARINI, G., PANAGIA, N., TAGLIAFERRI, G., MALESANI, D., TESTA, V., FUGAZZA, D., CAMPANA, S., COVINO, S., MANGANO, V. ET AL.
≪An enigmatic long-lasting γ-ray burst not accompanied by a bright supernova≫.
Nature, **444**, pp. 1050–1052 (2006).

DERMER, C.D.
≪On spectral and temporal variability in blazars and gamma-ray bursts≫.
ApJ, **501**, p. L157 (1998).

DERMER, C.D., BÖTTCHER, M. AND CHIANG, J.
≪The external shock model of gamma-ray bursts: Three predictions and a paradox resolved≫.
ApJ, **515**, pp. L49–L52 (1999).

DERMER, C.D. AND MITMAN, K.E.
≪Short-timescale variability in the external shock model of gamma-ray bursts≫.
ApJ, **513**, pp. L5–L8 (1999).

DEZALAY, J.P., BARAT, C., TALON, R., SYUNYAEV, R., TEREKHOV, O. AND KUZNETSOV, A.
≪Short cosmic events - a subset of classical grbs?≫
In W.S. Paciesas and G.J. Fishman (eds.), *American Institute of Physics Conference Series*, volume 265 of *American Institute of Physics Conference Series*, pp. 304–309 (1992).

EDDINGTON, A.S.
Brit. Assoc. Repts., **45** (1920).

EDEROCLITE, A., MASON, E., DELLA VALLE, M., GILMOZZI, R., WILLIAMS, R.E., GERMANY, L., SAVIANE, I., MATTEUCCI, F., SCHAEFER, B.E., WALTER, F. ET AL.
≪Early spectral evolution of nova sagittarii 2004 (v5114 sagittarii)≫.
A&A, **459**, pp. 875–883 (2006).

EICHLER, D., LIVIO, M., PIRAN, T. AND SCHRAMM, D.N.
≪Nucleosynthesis, neutrino bursts and gamma-rays from coalescing neutron stars≫.
Nature, **340**, pp. 126–128 (1989).

EINSTEIN, A.
≪Zur elektrodynamik bewegter körper≫.
Annalen der Physik, **322**, pp. 891–921 (1905).

FALCONE, A.D., MORRIS, D., RACUSIN, J., CHINCARINI, G., MORETTI, A., ROMANO, P., BURROWS, D.N., PAGANI, C., STROH, M., GRUPE, D. ET AL.
≪The first survey of x-ray flares from gamma ray bursts observed by swift: Spectral properties and energetics≫.
ArXiv:0706.1564 (2007).

FAN, Y.Z., PIRAN, T. AND XU, D.
≪The interpretation and implication of the afterglow of grb 060218≫.

Journal of Cosmology and Astro-Particle Physics, **9**, p. 13 (2006).

FATKHULLIN, T.A., SOKOLOV, V.V., MOISEEV, A.V., GUZIY, S. AND CASTRO-TIRADO, A.J.
≪Grb 060218: emergence of the underlying sn spectrum.≫
GCN, **4809** (2006).

FENIMORE, E.E.
≪The average temporal and spectral evolution of gamma-ray bursts≫.
ApJ, **518**, pp. 375–379 (1999).

FENIMORE, E.E., COOPER, C., RAMIREZ-RUIZ, E., SUMNER, M.C., YOSHIDA, A. AND NAMIKI, M.
≪Gamma-ray bursts and relativistic shells: The surface filling factor≫.
ApJ, **512**, pp. 683–692 (1999).

FENIMORE, E.E., MADRAS, C.D. AND NAYAKSHIN, S.
≪Expanding relativistic shells and gamma-ray burst temporal structure≫.
ApJ, **473**, p. 998 (1996).

FENIMORE, E.E. AND RAMIREZ-RUIZ, E.
≪Redshifts For 220 BATSE Gamma-Ray Bursts Determined by Variability and the Cosmological Consequences≫.
arXiv:astro-ph/0004176 (2000).

FERMI, E.
≪Sull'elettrostatica di un campo gravitazionale uniforme e sul peso delle masse elettromagnetiche≫.
Nuovo Cimento, **22**, pp. 176–188 (1921).

FERMI, E.
≪High Energy Nuclear Events≫.
Progress of Theoretical Physics, **5**, pp. 570–583 (1950).

FERRERO, P., PALAZZI, E., PIAN, E. AND SAVAGLIO, S.
≪Optical observations of grb 060218/sn 2006aj and its host galaxy≫.
In *American Institute of Physics Conference Series*, volume 924 of *American Institute of Physics Conference Series*, pp. 120–125 (2007).

FINZI, A. AND WOLF, R.A.
≪Early-type magnetic stars≫.
ApJ, **153**, p. 865 (1968).

FIRMANI, C., GHISELLINI, G., AVILA-REESE, V. AND GHIRLANDA, G.
≪Discovery of a tight correlation among the prompt emission properties of long gamma-ray bursts≫.
MNRAS, **370**, pp. 185–197 (2006).

FIRMANI, C., GHISELLINI, G., GHIRLANDA, G. AND AVILA-REESE, V.
≪A new method optimized to use gamma-ray bursts as cosmic rulers≫.
MNRAS, **360**, pp. L1–L5 (2005).

FLETCHER, R.S., GAISSER, T.K., LIPARI, P. AND STANEV, T.
≪sibyll: An event generator for simulation of high energy cosmic ray cascades≫.
Phys. Rev. D, **50**, pp. 5710–5731 (1994).

FOX, D.B., FRAIL, D.A., PRICE, P.A., KULKARNI, S.R., BERGER, E., PIRAN, T., SODERBERG, A.M., CENKO, S.B., CAMERON, P.B., GAL-YAM, A. ET AL.
≪The afterglow of grb 050709 and the nature of the short-hard γ-ray bursts≫.
Nature, **437**, pp. 845–850 (2005).

FRAIL, D.A., KULKARNI, S.R., SARI, R., DJORGOVSKI, S.G., BLOOM, J.S., GALAMA, T.J., REICHART, D.E., BERGER, E., HARRISON, F.A., PRICE, P.A. ET AL.
≪Beaming in gamma-ray bursts: Evidence for a standard energy reservoir≫.
ApJ, **562**, pp. L55–L58 (2001).

FRAIL, D.A., WAXMAN, E. AND KULKARNI, S.R.
≪A 450 day light curve of the radio afterglow of grb 970508: Fireball calorimetry≫.
ApJ, **537**, pp. 191–204 (2000).

FRONTERA, F., AMATI, L., COSTA, E., MULLER, J.M., PIAN, E., PIRO, L., SOFFITTA, P., TAVANI, M., CASTRO-TIRADO, A., DAL FIUME, D. ET AL.
≪Prompt and delayed emission properties of gamma-ray bursts observed with bepposax≫.
ApJSS, **127**, pp. 59–78 (2000).

FRONTERA, F., COSTA, E., PIRO, L., MULLER, J.M., AMATI, L., FEROCI, M., FIORE, F., PIZZICHINI, G., TAVANI, M., CASTRO-TIRADO, A. ET AL.
≪Spectral properties of the prompt x-ray emission and afterglow from the gamma-ray burst of 1997 february 28≫.
ApJ, **493**, p. L67 (1998).

FRYER, C.L., WOOSLEY, S.E., HERANT, M. AND DAVIES, M.B.
≪Merging White Dwarf/Black Hole Binaries and Gamma-Ray Bursts≫.
ApJ, **520**, pp. 650–660 (1999).

FYNBO, J.P.U., WATSON, D., THÖNE, C.C., SOLLERMAN, J., BLOOM, J.S., DAVIS, T.M., HJORTH, J., JAKOBSSON, P., JØRGENSEN, U.G., GRAHAM, J.F. ET AL.

«No supernovae associated with two long-duration γ-ray bursts».
Nature, **444**, pp. 1047–1049 (2006).

GAL-YAM, A., FOX, D.B., PRICE, P.A., OFEK, E.O., DAVIS, M.R., LEONARD, D.C., SODERBERG, A.M., SCHMIDT, B.P., LEWIS, K.M., PETERSON, B.A. ET AL.
«A novel explosive process is required for the γ-ray burst grb 060614».
Nature, **444**, pp. 1053–1055 (2006).

GALAMA, T.J., FRAIL, D.A., SARI, R., BERGER, E., TAYLOR, G.B. AND KULKARNI, S.R.
«Continued Radio Monitoring of the Gamma-Ray Burst 991208».
ApJ, **585**, pp. 899–907 (2003).

GALAMA, T.J., TANVIR, N., VREESWIJK, P.M., WIJERS, R.A.M.J., GROOT, P.J., ROL, E., VAN PARADIJS, J., KOUVELIOTOU, C., FRUCHTER, A.S., MASETTI, N. ET AL.
«Evidence for a supernova in reanalyzed optical and near-infrared images of grb 970228».
ApJ, **536**, pp. 185–194 (2000).

GALAMA, T.J., VREESWIJK, P.M., VAN PARADIJS, J., KOUVELIOTOU, C., AUGUSTEIJN, T., BÖHNHARDT, H., BREWER, J.P., DOUBLIER, V., GONZALEZ, J.F., LEIBUNDGUT, B. ET AL.
«An unusual supernova in the error box of the γ-ray burst of 25 april 1998».
Nature, **395**, pp. 670–672 (1998).

GAMOW, G.
Nuclear Physics (Oxford, 1938, 1938).

GAMOW, G.
My wordlines - an informal autobiography (New York: Viking press, 1970).

GAMOW, G. AND HOUTERMANS, F.G.
«Zur quantenmechanik des radioaktiven kerns».
Zeitschrift fur Physik, **52**, pp. 496–509 (1929).

GAMOW, G. AND SCHOENBERG, M.
«Neutrino theory of stellar collapse».
Physical Review, **59**, pp. 539–547 (1941).

GEHRELS, N., CHINCARINI, G., GIOMMI, P., MASON, K.O., NOUSEK, J.A., WELLS, A.A., WHITE, N.E., BARTHELMY, S.D., BURROWS, D.N., COMINSKY, L.R. ET AL.
«The swift gamma-ray burst mission».
ApJ, **611**, pp. 1005–1020 (2004).

GEHRELS, N., NORRIS, J.P., BARTHELMY, S.D., GRANOT, J., KANEKO, Y., KOUVELIOTOU, C., MARKWARDT, C.B., MÉSZÁROS, P., NAKAR, E., NOUSEK, J.A. ET AL.
≪A new γ-ray burst classification scheme from grb060614≫.
Nature, **444**, pp. 1044–1046 (2006).

GEHRELS, N., SARAZIN, C.L., O'BRIEN, P.T., ZHANG, B., BARBIER, L., BARTHELMY, S.D., BLUSTIN, A., BURROWS, D.N., CANNIZZO, J., CUMMINGS, J.R. ET AL.
≪A short γ-ray burst apparently associated with an elliptical galaxy at redshift z = 0.225≫.
Nature, **437**, pp. 851–854 (2005).

GHIRLANDA, G., CELOTTI, A. AND GHISELLINI, G.
≪Time resolved spectral analysis of bright gamma ray bursts≫.
A&A, **393**, pp. 409–423 (2002).

GHIRLANDA, G., GHISELLINI, G. AND FIRMANI, C.
≪Gamma-ray bursts as standard candles to constrain the cosmological parameters≫.
New Journal of Physics, **8**, p. 123 (2006).

GHIRLANDA, G., GHISELLINI, G. AND LAZZATI, D.
≪The collimation-corrected gamma-ray burst energies correlate with the peak energy of their νf_ν spectrum≫.
ApJ, **616**, pp. 331–338 (2004).

GHISELLINI, G., GHIRLANDA, G., MEREGHETTI, S., BOSNJAK, Z., TAVECCHIO, F. AND FIRMANI, C.
≪Are grb980425 and grb031203 real outliers or twins of grb060218?≫
MNRAS, **372**, pp. 1699–1709 (2006).

GIACCONI, R., RUFFINI, R., GIACCONI, R. AND RUFFINI, R. (eds.).
Physics and astrophysics of neutron stars and black holes (1978).

GOLD, T.
≪Rotating neutron stars as the origin of the pulsating radio sources≫.
Nature, **218**, p. 731 (1968).

GOLD, T.
≪Rotating neutron stars and the nature of pulsars≫.
Nature, **221**, p. 25 (1969).

GOODMAN, J.
≪Are gamma-ray bursts optically thick?≫
ApJ, **308**, pp. L47–L50 (1986).

GRANOT, J. AND LOEB, A.
≪Radio Imaging of Gamma-Ray Burst Jets in Nearby Supernovae≫.
ApJ, **593**, pp. L81–L84 (2003).

GRANOT, J., PIRAN, T. AND SARI, R.
≪Images and spectra from the interior of a relativistic fireball≫.
ApJ, **513**, pp. 679–689 (1999).

GREINER, J., KLOSE, S., SALVATO, M., ZEH, A., SCHWARZ, R., HARTMANN, D.H., MASETTI, N., STECKLUM, B., LAMER, G., LODIEU, N. ET AL.
≪Grb 011121: A collimated outflow into wind-blown surroundings≫.
ApJ, **599**, pp. 1223–1237 (2003).

GREINER, J., KRUEHLER, T., FYNBO, J.P.U., ROSSI, A., SCHWARZ, R., KLOSE, S., SAVAGLIO, S., TANVIR, N.R., MCBREEN, S., TOTANI, T. ET AL.
≪Grb 080913 at redshift 6.7≫.
arXiv:0810.2314 (2008).

GRUZINOV, A. AND WAXMAN, E.
≪Gamma-ray burst afterglow: Polarization and analytic light curves≫.
ApJ, **511**, pp. 852–861 (1999).

GUETTA, D.
≪Short grbs: Rates and luminosity function implications≫.
ArXiv:astro-ph/0610408 (2006).

GUETTA, D. AND DELLA VALLE, M.
≪On the rates of gamma-ray bursts and type ib/c supernovae≫.
ApJ, **657**, pp. L73–L76 (2007).

GUIDA, R., BERNARDINI, M.G., BIANCO, C.L., CAITO, L., DAINOTTI, M.G. AND RUFFINI, R.
≪The amati relation in the "fireshell" model≫.
A&A, **487**, pp. L37–L40 (2008).

GUIDA, R., BERNARDINI, M.G., BIANCO, C.L., CAITO, L., DAINOTTI, M.G. AND RUFFINI, R.
In R.T. Jantzen, H. Kleinert and R. Ruffini (eds.), *The Eleventh Marcel Grossmann Meeting.* (Singapore: World Scientific, in press).

HALPERN, J.P., UGLESICH, R., MIRABAL, N., KASSIN, S., THORSTENSEN, J., KEEL, W.C., DIERCKS, A., BLOOM, J.S., HARRISON, F., MATTOX, J. ET AL.
≪Grb 991216 joins the jet set: Discovery and monitoring of its optical afterglow≫.
ApJ, **543**, pp. 697–703 (2000).

HANNI, R.S. AND RUFFINI, R.
≪Lines of force of a point charge near a schwarzschild black hole.≫
Phys. Rev. D, **8**, pp. 3259–3265 (1973).

HEISENBERG, W.
≪Über die Entstehung von Mesonen in Vielfachprozessen≫.
Zeitschrift fur Physik, **126**, pp. 569–582 (1949).

HEISENBERG, W. AND EULER, H.
≪Folgerungen aus der diracschen theorie des positrons≫.
Zeitschrift fur Physik, **98**, pp. 714–732 (1936).

HORSTMAN, H.M. AND CAVALLO, G.
≪The energy spectrum of cosmic fireballs≫.
A&A, **122**, pp. 119–123 (1983).

HUANG, Y.F., CHENG, K.S. AND GAO, T.T.
≪Modeling the Optical Afterglow of GRB 030329≫.
ApJ, **637**, pp. 873–879 (2006).

HUANG, Y.F., LU, Y., WONG, A.Y.L. AND CHENG, K.S.
≪A Detailed Study on the Equal Arrival Time Surface Effect in Gamma-Ray Burst Afterglows≫.
Chinese Journal of Astronomy and Astrophysics, **7**, pp. 397–404 (2007).

INFANTE, L., GARNAVICH, P.M., STANEK, K.Z. AND WYRZYKOWSKI, L.
≪Grb011121: possible redshift, continued decay.≫
GCN, **1152** (2001).

IWAMOTO, K., MAZZALI, P.A., NOMOTO, K., UMEDA, H., NAKAMURA, T., PATAT, F., DANZIGER, I.J., YOUNG, T.R., SUZUKI, T., SHIGEYAMA, T. ET AL.
≪A hypernova model for the supernova associated with the γ-ray burst of 25 april 1998≫.
Nature, **395**, pp. 672–674 (1998).

JIN, Z.P. AND FAN, Y.Z.
≪GRB 060418 and 060607A: the medium surrounding the progenitor and the weak reverse shock emission≫.
MNRAS, **378**, pp. 1043–1048 (2007).

KANEKO, Y., RAMIREZ-RUIZ, E., GRANOT, J., KOUVELIOTOU, C., WOOSLEY, S.E., PATEL, S.K., ROL, E., ZAND, J.J.M.I., VAN DER HORST, A.J., WIJERS, R.A.M.J. ET AL.
≪Prompt and afterglow emission properties of gamma-ray bursts with spectroscopically identified supernovae≫.
ApJ, **654**, pp. 385–402 (2007).

KANN, D.A., KLOSE, S., ZHANG, B., WILSON, A.C., BUTLER, N.R., MALESANI, D., NAKAR, E., ANTONELLI, L.A., CHINCARINI, G., COBB, B.E. ET AL.
≪The afterglows of swift-era gamma-ray bursts. ii. short/hard (type i) vs. long/soft (type ii) optical afterglows≫.
ArXiv:0804.1959 (2008).

KELNER, S.R., AHARONIAN, F.A. AND BUGAYOV, V.V.
≪Energy spectra of gamma rays, electrons, and neutrinos produced at proton-proton interactions in the very high energy regime≫.
Phys. Rev. D, **74(3)**, p. 034018 (2006).

KELSON, D. AND BERGER, E.
≪Grb 050315: absorption redshift.≫
GCN, **3101** (2005).

KENNEA, J.A., BURROWS, D.N., CUSUMANO, G. AND TAGLIAFERRI, G.
≪Subject: Grb 060218: Swift xrt position.≫
GCN, **4776** (2006).

KERR, R.P.
≪Gravitational field of a spinning mass as an example of algebraically special metrics≫.
Physical Review Letters, **11**, pp. 237–238 (1963).

KLEBESADEL, R.W.
≪The durations of gamma-ray bursts≫.
In C. Ho, R.I. Epstein and E.E. Fenimore (eds.), *Gamma-Ray Bursts - Observations, Analyses and Theories*, pp. 161–168 (Cambridge University Press, 1992).

KOUVELIOTOU, C., MEEGAN, C.A., FISHMAN, G.J., BHAT, N.P., BRIGGS, M.S., KOSHUT, T.M., PACIESAS, W.S. AND PENDLETON, G.N.
≪Identification of two classes of gamma-ray bursts≫.
ApJ, **413**, pp. L101–L104 (1993).

KOUVELIOTOU, C., WOOSLEY, S.E., PATEL, S.K., LEVAN, A., BLANDFORD, R., RAMIREZ-RUIZ, E., WIJERS, R.A.M.J., WEISSKOPF, M.C., TENNANT, A., PIAN, E. ET AL.
≪Chandra observations of the x-ray environs of sn 1998bw/grb 980425≫.
ApJ, **608**, pp. 872–882 (2004).

KRAMER, M.
In R.T. Jantzen, H. Kleinert and R. Ruffini (eds.), *The Eleventh Marcel Grossmann Meeting*. (Singapore: World Scientific, in press).

KULKARNI, S.R., FRAIL, D.A., WIERINGA, M.H., EKERS, R.D., SADLER, E.M., WARK, R.M., HIGDON, J.L., PHINNEY, E.S. AND BLOOM, J.S.
≪Radio emission from the unusual supernova 1998bw and its association with the γ-ray burst of 25 april 1998≫.
Nature, **395**, pp. 663–669 (1998).

LANDAU, L.D. AND LIFSHITZ, E.M.
The classical theory of fields (Course of theoretical physics - Pergamon International Library of Science, Technology, Engineering and Social Studies, Oxford: Pergamon Press, 4th rev.engl.ed., 1975).

LANDAU, L.D. AND LIFSHITZ, E.M.
Statistical physics. Pt.1, Pt.2 (Course of theoretical physics, Pergamon International Library of Science, Technology, Engineering and Social Studies, Oxford: Pergamon Press, 3rd rev.and enlarg. ed., 1980).

LANGER, N.
≪Massive Star Evolution at Low Metallicity – What We Don't Know≫.
In H.J.G.L.M. Lamers, N. Langer, T. Nugis and K. Annuk (eds.), *Stellar Evolution at Low Metallicity: Mass Loss, Explosions, Cosmology*, volume 353 of *Astronomical Society of the Pacific Conference Series*, pp. 15–19 (2006).

LATTIMER, J.M., VAN RIPER, K.A., PRAKASH, M. AND PRAKASH, M.
≪Rapid cooling and the structure of neutron stars≫.
ApJ, **425**, pp. 802–813 (1994).

LEACH, R.W. AND RUFFINI, R.
≪On the masses of x-ray sources≫.
ApJ, **180**, p. L15 (1973).

LEDOUX, C., VREESWIJK, P., SMETTE, A., JAUNSEN, A. AND KAUFER, A.
≪VLT/UVES observations of GRB 060607.≫
GRB Coordinates Network, **5237**, pp. 1–+ (2006).

LEIBUNDGUT, B.
≪Cosmological implications from observations of type ia supernovae≫.
ARAA, **39**, pp. 67–98 (2001).

LEWIS, A.D., BUOTE, D.A. AND STOCKE, J.T.
≪Chandra observations of a2029: The dark matter profile down to below $0.01r_{vir}$ in an unusually relaxed cluster≫.
ApJ, **586**, pp. 135–142 (2003).

LI, L.X.
≪Shock breakout in type ibc supernovae and application to grb 060218/sn 2006aj≫.
MNRAS, **375**, pp. 240–256 (2007).

LIANG, E. AND ZHANG, B.
≪Model-independent multivariable gamma-ray burst luminosity indicator and its possible cosmological implications≫.
ApJ, **633**, pp. 611–623 (2005).

LIANG, E., ZHANG, B., VIRGILI, F. AND DAI, Z.G.
≪Low-luminosity gamma-ray bursts as a unique population: Luminosity function, local rate, and beaming factor≫.
ApJ, **662**, pp. 1111–1118 (2007).

LIANG, E.W., ZHANG, B.B., STAMATIKOS, M., ZHANG, B., NORRIS, J., GEHRELS, N., ZHANG, J. AND DAI, Z.G.
≪Temporal profiles and spectral lags of xrf 060218≫.
ApJ, **653**, pp. L81–L84 (2006).

MACFADYEN, A.I. AND WOOSLEY, S.E.
≪Collapsars: Gamma-Ray Bursts and Explosions in "Failed Supernovae"≫.
ApJ, **524**, pp. 262–289 (1999).

MAEDA, K., KAWABATA, K., TANAKA, M., NOMOTO, K., TOMINAGA, N., HATTORI, T., MINEZAKI, T., KURODA, T., SUZUKI, T., DENG, J. ET AL.
≪Sn 2006aj associated with xrf 060218 at late phases: Nucleosynthesis signature of a neutron star-driven explosion≫.
ApJ, **658**, pp. L5–L8 (2007).

MAJUMDAR, S.D.
≪A class of exact solutions of einstein's field equations≫.
Physical Review, **72**, pp. 390–398 (1947).

MANGANO, V., HOLLAND, S.T., MALESANI, D., TROJA, E., CHINCARINI, G., ZHANG, B., LA PAROLA, V., BROWN, P.J., BURROWS, D.N., CAMPANA, S. ET AL.
≪Swift observations of grb 060614: an anomalous burst with a well behaved afterglow≫.
A&A, **470**, pp. 105–118 (2007).

MATHEWS, G.J. AND WILSON, J.R.
≪Relativistic induced compression of neutron stars and white dwarfs≫.
In M. Novello, S. Perez Bergliaffa and R. Ruffini (eds.), *The Tenth Marcel Grossmann Meeting. On recent developments in theoretical and experimental general relativity, gravitation and relativistic field theories*, p. 1802 (Singapore: World Scientific, 2005).

MAZZALI, P.
talk presented at the congress "Swift and GRBs: unveiling the relativistic universe", Venice, Italy, June 5-9 (2006).

MAZZALI, P.A., DENG, J., NOMOTO, K., SAUER, D.N., PIAN, E., TOMINAGA, N., TANAKA, M., MAEDA, K. AND FILIPPENKO, A.V.
≪A neutron-star-driven x-ray flash associated with supernova sn 2006aj≫.
Nature, **442**, pp. 1018–1020 (2006).

MEREGHETTI, S. AND GOTZ, D.
≪Grb 031203: further analysis of integral data.≫
GCN, **2460** (2003).

MÉSZÁROS, P.
≪Theories of gamma-ray bursts≫.
ARAA, **40**, pp. 137–169 (2002).

MESZAROS, P.
≪Gamma-ray bursts.≫
Reports of Progress in Physics, **69**, pp. 2259–2322 (2006).

MESZAROS, P., LAGUNA, P. AND REES, M.J.
≪Gasdynamics of relativistically expanding gamma-ray burst sources - kinematics, energetics, magnetic fields, and efficiency≫.
ApJ, **415**, pp. 181–190 (1993).

MÉSZÁROS, P. AND REES, M.J.
≪Collapsar jets, bubbles, and fe lines≫.
ApJ, **556**, pp. L37–L40 (2001).

MIRABAL, N., HALPERN, J.P., AN, D., THORSTENSEN, J.R. AND TERNDRUP, D.M.
≪Grb 060218/sn 2006aj: A gamma-ray burst and prompt supernova at z = 0.0335≫.
ApJ, **643**, pp. L99–L102 (2006).

MIRABEL, I.F. AND RODRIGUEZ, L.F.
≪A superluminal source in the galaxy≫.
Nature, **371**, p. 46 (1994).

MISNER, C.W., THORNE, K.S. AND WHEELER, J.A.
Gravitation (San Francisco: W.H. Freeman and Co., 1973).

MODJAZ, M., STANEK, K.Z., GARNAVICH, P.M., BERLIND, P., BLONDIN, S., BROWN, W., CALKINS, M., CHALLIS, P., DIAMOND-STANIC, A.M., HAO, H. ET AL.
≪Early-time photometry and spectroscopy of the fast evolving sn 2006aj associated with grb 060218≫.
ApJ, **645**, pp. L21–L24 (2006).

MOLINARI, E., VERGANI, S.D., MALESANI, D., COVINO, S., D'AVANZO, P., CHINCARINI, G., ZERBI, F.M., ANTONELLI, L.A., CONCONI, P., TESTA, V. ET AL.
≪REM observations of GRB 060418 and GRB 060607A: the onset of the afterglow and the initial fireball Lorentz factor determination≫.
A&A, **469**, pp. L13–L16 (2007).

NAVA, L., GHISELLINI, G., GHIRLANDA, G., TAVECCHIO, F. AND FIRMANI, C.
≪On the interpretation of spectral-energy correlations in long gamma-ray bursts≫.
A&A, **450**, pp. 471–481 (2006).

NEWMAN, E.T., COUCH, E., CHINNAPARED, K., EXTON, A., PRAKASH, A. AND TORRENCE, R.
≪Metric of a rotating, charged mass≫.
Journal of Mathematical Physics, **6**, pp. 918–919 (1965).

NOMOTO, K., TOMINAGA, N., TANAKA, M., MAEDA, K., SUZUKI, T., DENG, J.S. AND MAZZALI, P.A.
≪Diversity of the supernova - gamma-ray burst connection≫.
ArXiv:astro-ph/0702472 (2007).

NORRIS, J.P. AND BONNELL, J.T.
≪Short gamma-ray bursts with extended emission≫.
ApJ, **643**, pp. 266–275 (2006).

NORRIS, J.P., MARANI, G.F. AND BONNELL, J.T.
≪Connection between Energy-dependent Lags and Peak Luminosity in Gamma-Ray Bursts≫.
ApJ, **534**, pp. 248–257 (2000).

NOUSEK, J.A., KOUVELIOTOU, C., GRUPE, D., PAGE, K.L., GRANOT, J., RAMIREZ-RUIZ, E., PATEL, S.K., BURROWS, D.N., MANGANO, V., BARTHELMY, S. ET AL.
≪Evidence for a canonical gamma-ray burst afterglow light curve in the swift xrt data≫.
ApJ, **642**, pp. 389–400 (2006).

OPPENHEIMER, J.R. AND SERBER, R.
≪On the stability of stellar neutron cores≫.
Physical Review, **54**, pp. 540–540 (1938).

OPPENHEIMER, J.R. AND SNYDER, H.
≪On continued gravitational contraction≫.
Physical Review, **56**, pp. 455–459 (1939).

OPPENHEIMER, J.R. AND VOLKOFF, G.M.
≪On massive neutron cores≫.
Physical Review, **55**, pp. 374–381 (1939).

PACIESAS, W.S., MEEGAN, C.A., PENDLETON, G.N., BRIGGS, M.S., KOUVELIOTOU, C., KOSHUT, T.M., LESTRADE, J.P., MCCOLLOUGH, M.L., BRAINERD, J.J., HAKKILA, J. ET AL.
≪The fourth batse gamma-ray burst catalog (revised)≫.
ApJSS, **122**, pp. 465–495 (1999).

PACINI, F.
≪Rotating neutron stars, pulsars and supernova remnants≫.
Nature, **219**, p. 145 (1968).

PACZYNSKI, B.
≪Gamma-ray bursters at cosmological distances≫.
ApJ, **308**, pp. L43–L46 (1986).

PACZYNSKI, B.
≪Are gamma-ray bursts in star-forming regions?≫
ApJ, **494**, p. L45 (1998).

PACZYNSKI, B. AND XU, G.
≪Neutrino bursts from gamma-ray bursts≫.
ApJ, **427**, pp. 708–713 (1994).

PAGE, K., GOAD, M. AND BEARDMORE, A.
≪GRB 060607: Swift-XRT team refined analysis.≫
GRB Coordinates Network, **5240**, pp. 1–+ (2006).

PANAITESCU, A.
≪The energetics and environment of the short-grb afterglows 050709 and 050724≫.
MNRAS, **367**, pp. L42–L46 (2006).

PANAITESCU, A. AND MESZAROS, P.
≪Rings in fireball afterglows≫.
ApJ, **493**, p. L31 (1998a).

PANAITESCU, A. AND MESZAROS, P.
≪Simulations of gamma-ray bursts from external shocks: Time variability and spectral correlations≫.
ApJ, **492**, p. 683 (1998b).

PANAITESCU, A., MÉSZÁROS, P., GEHRELS, N., BURROWS, D. AND NOUSEK, J.
≪Analysis of the x-ray emission of nine swift afterglows≫.
MNRAS, **366**, pp. 1357–1366 (2006).

PAPAPETROU, A.
Proceedings of the Royal Irish Academy, **51**, p. 191 (1945).

PARKER, L., RUFFINI, R. AND WILKINS, D.
«Metric of two spinning charged sources in equilibrium».
Phys. Rev. D, **7**, pp. 2874–2879 (1973).

PARSONS, A., BARTHELMY, S., BARBIER, L., CUMMINGS, J., FENIMORE, E., FINK, R., GEHRELS, N., HOLLAND, S., HULLINGER, D., HURLEY, K. ET AL.
«Swift-bat detection of grb 050315.»
GCN, **3094** (2005).

PERRIN, J.B.
Rev. du Mois, **21**, p. 113 (1920).

PIAN, E., AMATI, L., ANTONELLI, L.A., BUTLER, R.C., COSTA, E., CUSUMANO, G., DANZIGER, J., FEROCI, M., FIORE, F., FRONTERA, F. ET AL.
«Bepposax observations of grb 980425: Detection of the prompt event and monitoring of the error box».
ApJ, **536**, pp. 778–787 (2000).

PIAN, E., GIOMMI, P., AMATI, L., COSTA, E., DANZIGER, J., FEROCI, M., FIOCCHI, M.T., FRONTERA, F., KOUVELIOTOU, C., MASETTI, N. ET AL.
«Xmm-newton observations of the field of γ-ray burst 980425».
Advances in Space Research, **34**, pp. 2711–2714 (2004).

PIAN, E., MAZZALI, P.A., MASETTI, N., FERRERO, P., KLOSE, S., PALAZZI, E., RAMIREZ-RUIZ, E., WOOSLEY, S.E., KOUVELIOTOU, C., DENG, J. ET AL.
«An optical supernova associated with the x-ray flash xrf 060218».
Nature, **442**, pp. 1011–1013 (2006).

PIRAN, T.
«Gamma-ray bursts and the fireball model».
Phys. Rep., **314**, pp. 575–667 (1999).

PIRAN, T.
«Gamma-ray bursts - a puzzle being resolved.»
Phys. Rep., **333**, pp. 529–553 (2000).

PIRAN, T.
«Gamma-ray bursts-when theory meets observations (plenary talk)».
In J.C. Wheeler and H. Martel (eds.), *20th Texas Symposium on relativistic astrophysics*, volume 586 of *American Institute of Physics Conference Series*, p. 575 (2001).

PIRAN, T.
≪The physics of gamma-ray bursts≫.
Reviews of Modern Physics, **76**, pp. 1143–1210 (2005).

PIRAN, T., SHEMI, A. AND NARAYAN, R.
≪Hydrodynamics of relativistic fireballs≫.
MNRAS, **263**, p. 861 (1993).

PIRO, L.
≪Bepposax grb011121.≫
GCN, **1147** (2001).

PIRO, L.
≪Astrophysics: Short-burst sources≫.
Nature, **437**, pp. 822–823 (2005).

PIRO, L., COSTA, E., FEROCI, M., FRONTERA, F., AMATI, L., DAL FIUME, D., ANTONELLI, L.A., HEISE, J., IN 'T ZAND, J., OWENS, A. ET AL.
≪The x-ray afterglow of the gamma-ray burst of 1997 may 8:spectral variability and possible evidence of an iron line≫.
ApJ, **514**, pp. L73–L77 (1999).

PIRO, L., DE PASQUALE, M., SOFFITTA, P., LAZZATI, D., AMATI, L., COSTA, E., FEROCI, M., FRONTERA, F., GUIDORZI, C., IN'T ZAND, J.M.J. ET AL.
≪Probing the environment in gamma-ray bursts: The case of an x-ray precursor, afterglow late onset, and wind versus constant density profile in grb 011121 and grb 011211≫.
ApJ, **623**, pp. 314–324 (2005).

POZDNIAKOV, L.A., SOBOL, I.M. AND SIUNIAEV, R.A.
≪Comptonization and the shaping of x-ray source spectra - monte carlo calculations≫.
Astrophysics and Space Physics Reviews, **2**, pp. 189–331 (1983).

PREECE, R.D., BRIGGS, M.S., MALLOZZI, R.S., PENDLETON, G.N., PACIESAS, W.S. AND BAND, D.L.
≪The synchrotron shock model confronts a "line of death" in the batse gamma-ray burst data≫.
ApJ, **506**, pp. L23–L26 (1998).

PREPARATA, G., RUFFINI, R. AND XUE, S.S.
≪The dyadosphere of black holes and gamma-ray bursts≫.
A&A, **338**, pp. L87–L90 (1998).

PRICE, P.A., BERGER, E., REICHART, D.E., KULKARNI, S.R., YOST, S.A., SUBRAHMANYAN, R., WARK, R.M., WIERINGA, M.H., FRAIL, D.A., BAILEY, J. ET AL.

«Grb 011121: A massive star progenitor».
ApJ, **572**, pp. L51–L55 (2002).

PROCHASKA, J.X., BLOOM, J.S., CHEN, H.W., HURLEY, K.C., MELBOURNE, J., DRESSLER, A., GRAHAM, J.R., OSIP, D.J. AND VACCA, W.D.
«The host galaxy of grb 031203: Implications of its low metallicity, low redshift, and starburst nature».
ApJ, **611**, pp. 200–207 (2004).

REES, M., RUFFINI, R. AND WHEELER, J.A.
Black holes, gravitational waves and cosmology: an introduction to current research, volume 10 of *Topics in Astrophysics and Space Physics* (New York: Gordon and Breach, Science Publishers, Inc., 1974).

REES, M.J.
«Appearance of relativistically expanding radio sources».
Nature, **211**, p. 468 (1966).

REES, M.J. AND MESZAROS, P.
«Unsteady outflow models for cosmological gamma-ray bursts».
ApJ, **430**, pp. L93–L96 (1994).

REICHART, D.E., LAMB, D.Q., FENIMORE, E.E., RAMIREZ-RUIZ, E., CLINE, T.L. AND HURLEY, K.
«A possible cepheid-like luminosity estimator for the long gamma-ray bursts».
ApJ, **552**, pp. 57–71 (2001).

REIF, F.
Fundamentals of Statistical and Thermal Physics (New York: McGraw-Hill, 1965).

RESPONSE, B.R.B.
http://gammaray. msfc. nasa. gov/ kippen/batserbr/ (1999).

RHOADES, C.E. AND RUFFINI, R.
«Maximum mass of a neutron star.»
Physical Review Letters, **32**, pp. 324–327 (1974).

RICHARDSON, D., BRANCH, D. AND BARON, E.
«Absolute magnitude distributions and light curves of stripped-envelope supernovae».
AJ, **131**, pp. 2233–2244 (2006).

RIESS, A.G., NUGENT, P.E., GILLILAND, R.L., SCHMIDT, B.P., TONRY, J., DICKINSON, M., THOMPSON, R.I., BUDAVÁRI, T., CASERTANO, S., EVANS, A.S. ET AL.

≪The farthest known supernova: Support for an accelerating universe and a glimpse of the epoch of deceleration≫.
ApJ, **560**, pp. 49–71 (2001).

ROMANI, R.W.
≪Model atmospheres for cooling neutron stars≫.
ApJ, **313**, pp. 718–726 (1987).

RUFFINI, R.
≪On the energetics of black holes.≫
In *Black holes (Les astres occlus), p. 451 - 546, and 19 appendices, p. R1 - R176*, pp. 451–546 (1973).

RUFFINI, R.
≪Beyond the critical mass: The dyadosphere of black holes≫.
In H. Sato and N. Sugiyama (eds.), *Frontiers Science Series 23: Black Holes and High Energy Astrophysics*, p. 167 (1998).

RUFFINI, R.
≪Analogies, new paradigms and observational data as growing factors of relativistic astrophysics≫.
In W. Janke, A. Pelster, H.J. Schmidt and M. Bachmann (eds.), *Fluctuating Paths and Fields* (World Scientific, 2001).

RUFFINI, R.
talk presented at the congress "Eleventh Marcel Grossmann Meeting", Berlin, Germany, July 23-29 (2006).

RUFFINI, R.
In R.T. Jantzen, H. Kleinert and R. Ruffini (eds.), *The Eleventh Marcel Grossmann Meeting.* (Singapore: World Scientific, in pressa).

RUFFINI, R.
≪The ergosphere and dyadosphere of black holes≫.
In D.L. Wiltshire, M. Visser and S. Scott (eds.), *The Kerr Spacetime* (Cambridge University Press, in press, in pressb).

RUFFINI, R., BERNARDINI, M.G., BIANCO, C.L., CAITO, L., CHARDONNET, P., DAINOTTI, M.G., FRASCHETTI, F., GUIDA, R., ROTONDO, M., VERESHCHAGIN, G. ET AL.
≪The blackholic energy and the canonical gamma-ray burst≫.
In M. Novello and S.E. Perez Bergliaffa (eds.), *XIIth Brazilian School of Cosmology and Gravitation*, volume 910 of *American Institute of Physics Conference Series*, pp. 55–217 (2007a).

RUFFINI, R., BERNARDINI, M.G., BIANCO, C.L., CAITO, L., CHARDONNET, P., DAINOTTI, M.G., FRASCHETTI, F., GUIDA, R., VERESHCHAGIN, G. AND XUE, S.S.
≪The role of grb 031203 in clarifying the astrophysical grb scenario≫.
In S. Grebenev, R. Sunyaev, C. Winkler, A. Parmar and L. Ouwehand (eds.), *The 6th Integral Workshop - The Obscured Universe*, volume SP-622 of *ESA Special Publication*, p. 561 (2007b).

RUFFINI, R., BERNARDINI, M.G., BIANCO, C.L., CHARDONNET, P., FRASCHETTI, F., GUIDA, R. AND XUE, S.S.
≪Grb 050315: A step toward the uniqueness of the overall grb structure≫.
N.Cim.B, **121**, pp. 1367–1372 (2006a).

RUFFINI, R., BERNARDINI, M.G., BIANCO, C.L., CHARDONNET, P., FRASCHETTI, F., GUIDA, R. AND XUE, S.S.
≪Grb 050315: A step toward understanding the uniqueness of the overall gamma-ray burst structure≫.
ApJ, **645**, pp. L109–L112 (2006b).

RUFFINI, R., BERNARDINI, M.G., BIANCO, C.L., CHARDONNET, P., FRASCHETTI, F., GURZADYAN, V., VITAGLIANO, L. AND XUE, S.S.
≪The blackholic energy: long and short gamma-ray bursts (new perspectives in physics and astrophysics from the theoretical understanding of gamma-ray bursts, ii)≫.
In M. Novello and S.E. Perez Bergliaffa (eds.), *XIth Brazilian School of Cosmology and Gravitation*, volume 782 of *American Institute of Physics Conference Series*, pp. 42–127 (2005a).

RUFFINI, R., BERNARDINI, M.G., BIANCO, C.L., CHARDONNET, P., FRASCHETTI, F. AND XUE, S.S.
≪Grb 980425, sn1998bw and the embh model≫.
Advances in Space Research, **34**, pp. 2715–2722 (2004a).

RUFFINI, R., BERNARDINI, M.G., BIANCO, C.L., CHARDONNET, P., FRASCHETTI, F. AND XUE, S.S.
≪Evidence for isotropic emission in grb991216≫.
Advances in Space Research, **38**, pp. 1291–1294 (2006c).

RUFFINI, R., BERNARDINI, M.G., BIANCO, C.L., VITAGLIANO, L., XUE, S.S., CHARDONNET, P., FRASCHETTI, F. AND GURZADYAN, V.
≪Black hole physics and astrophysics: The grb-supernova connection and urca-1 - urca-2≫.
In M. Novello, S. Perez Bergliaffa and R. Ruffini (eds.), *The Tenth Marcel Grossmann Meeting. On recent developments in theoretical and experimental general relativity, gravitation and relativistic field theories*, p. 369 (Singapore: World Scientific, 2005b).

RUFFINI, R., BIANCO, C.L., CHARDONNET, P., FRASCHETTI, F., GURZADYAN, V. AND XUE, S.S.
≪On the instantaneous spectrum of gamma-ray bursts≫.
IJMPD, **13**, pp. 843–851 (2004b).

RUFFINI, R., BIANCO, C.L., CHARDONNET, P., FRASCHETTI, F., GURZADYAN, V. AND XUE, S.S.
≪Emergence of a filamentary structure in the fireball from grb spectra≫.
IJMPD, **14**, pp. 97–105 (2005c).

RUFFINI, R., BIANCO, C.L., CHARDONNET, P., FRASCHETTI, F., VITAGLIANO, L. AND XUE, S.S.
≪New perspectives in physics and astrophysics from the theoretical understanding of gamma-ray bursts≫.
In M. Novello and S.E. Perez Bergliaffa (eds.), *Cosmology and Gravitation*, volume 668 of *American Institute of Physics Conference Series*, pp. 16–107 (2003).

RUFFINI, R., BIANCO, C.L., CHARDONNET, P., FRASCHETTI, F. AND XUE, S.S.
≪On a possible gamma-ray burst-supernova time sequence≫.
ApJ, **555**, pp. L117–L120 (2001a).

RUFFINI, R., BIANCO, C.L., CHARDONNET, P., FRASCHETTI, F. AND XUE, S.S.
≪On the interpretation of the burst structure of gamma-ray bursts≫.
ApJ, **555**, pp. L113–L116 (2001b).

RUFFINI, R., BIANCO, C.L., CHARDONNET, P., FRASCHETTI, F. AND XUE, S.S.
≪Relative spacetime transformations in gamma-ray bursts≫.
ApJ, **555**, pp. L107–L111 (2001c).

RUFFINI, R., BIANCO, C.L., CHARDONNET, P., FRASCHETTI, F. AND XUE, S.S.
≪On the structures in the afterglow peak emission of gamma-ray bursts≫.
ApJ, **581**, pp. L19–L22 (2002a).

RUFFINI, R., CHARDONNET, P., BIANCO, C.L., XUE, S.S. AND FRASCHETTI, F.
≪Les sursaut gamma≫.
Pour la science, **294**, p. 26 (2002b).

RUFFINI, R., FRASCHETTI, F., VITAGLIANO, L. AND XUE, S.S.
≪Observational signatures of an electromagnetic overcritical gravitational collapse≫.
IJMPD, **14**, pp. 131–141 (2005d).

RUFFINI, R., SALMONSON, J.D., WILSON, J.R. AND XUE, S.S.
≪On the pair electromagnetic pulse of a black hole with electromagnetic structure≫.
A&A, **350**, pp. 334–343 (1999).

RUFFINI, R., SALMONSON, J.D., WILSON, J.R. AND XUE, S.S.
≪On the pair-electromagnetic pulse from an electromagnetic black hole surrounded by a baryonic remnant≫.
A&A, **359**, pp. 855–864 (2000).

RUFFINI, R., VITAGLIANO, L. AND XUE, S.S.
to appear on Physics Reports (in preparation).

RUFFINI, R. AND WHEELER, J.A.
≪Introducing the black hole.≫
Physics Today, **24**, pp. 30–36 (1971).

SAHU, K.C., LIVIO, M., PETRO, L., MACCHETTO, F.D., VAN PARADIJS, J., KOUVELIOTOU, C., FISHMAN, G.J., MEEGAN, C.A., GROOT, P.J. AND GALAMA, T.
≪The optical counterpart to γ-ray burst grb970228 observed using the hubble space telescope≫.
Nature, **387**, pp. 476–478 (1997).

SAKAMOTO, T., BARBIER, L., BARTHELMY, S., CUMMINGS, J., FENIMORE, E., GEHRELS, N., HULLINGER, D., KRIMM, H., MARKWARDT, C., PALMER, D. ET AL.
≪Grb 060218/sn 2006aj: Swift-bat fluence and peak flux.≫
GCN, **4822** (2006a).

SAKAMOTO, T., BARBIER, L., BARTHELMY, S.D., CUMMINGS, J.R., FENIMORE, E.E., GEHRELS, N., HULLINGER, D., KRIMM, H.A., MARKWARDT, C.B., PALMER, D.M. ET AL.
≪Confirmation of the e_{peak}^{src}-e_{iso} (amati) relation from the x-ray flash xrf 050416aobserved by the swift burst alert telescope≫.
ApJ, **636**, pp. L73–L76 (2006b).

SARI, R.
≪The observed size and shape of gamma-ray burst afterglow≫.
ApJ, **494**, p. L49 (1998).

SARI, R. AND PIRAN, T.
≪Variability in gamma-ray bursts: A clue≫.
ApJ, **485**, p. 270 (1997).

SARI, R. AND PIRAN, T.

≪Predictions for the Very Early Afterglow and the Optical Flash≫.
ApJ, **520**, pp. 641–649 (1999).

SAZONOV, S.Y., LUTOVINOV, A.A. AND SUNYAEV, R.A.
≪An apparently normal γ-ray burst with an unusually low luminosity≫.
Nature, **430**, pp. 646–648 (2004a).

SAZONOV, S., LUTOVINOV, A. AND SUNYAEV, R.
Private communication (2004b).

SCHAEFER, B.E.
≪Gamma-Ray Burst Hubble Diagram to z=4.5≫.
ApJ, **583**, pp. L67–L70 (2003).

SCHWARZSCHILD, M.
Structure and evolution of the stars (New York: Dover Publication, 1965).

SCHWINGER, J.
≪On gauge invariance and vacuum polarization≫.
Physical Review, **82**, pp. 664–679 (1951).

SHEMI, A. AND PIRAN, T.
≪The appearance of cosmic fireballs≫.
ApJ, **365**, pp. L55–L58 (1990).

SODERBERG, A.M., BERGER, E. AND SCHMIDT, B.P.
≪Grb060218: optical spectroscopy of grb-sn.≫
GCN, **4804** (2006a).

SODERBERG, A.M., KULKARNI, S.R., BERGER, E., FOX, D.W., SAKO, M., FRAIL, D.A., GAL-YAM, A., MOON, D.S., CENKO, S.B., YOST, S.A. ET AL.
≪The sub-energetic γ-ray burst grb 031203 as a cosmic analogue to the nearby grb 980425≫.
Nature, **430**, pp. 648–650 (2004).

SODERBERG, A.M., KULKARNI, S.R., NAKAR, E., BERGER, E., CAMERON, P.B., FOX, D.B., FRAIL, D., GAL-YAM, A., SARI, R., CENKO, S.B. ET AL.
≪Relativistic ejecta from x-ray flash xrf 060218 and the rate of cosmic explosions≫.
Nature, **442**, pp. 1014–1017 (2006b).

SOLLERMAN, J., JAUNSEN, A.O., FYNBO, J.P.U., HJORTH, J., JAKOBSSON, P., STRITZINGER, M., FÉRON, C., LAURSEN, P., OVALDSEN, J.E., SELJ, J. ET AL.
≪Supernova 2006aj and the associated x-ray flash 060218≫.
A&A, **454**, pp. 503–509 (2006).

STRONG, I.B.
≪Cosmic gamma-ray bursts≫.
In H. Gursky and R. Ruffini (eds.), *Neutron Stars, Black Holes and Binary X-ray Sources*, volume 48 of *Astrophysics and Space Science Library*, pp. 47–58 (1975).

TAVANI, M.
≪Euclidean versus non-euclidean gamma-ray bursts≫.
ApJ, **497**, p. L21 (1998).

TAYLOR, G.B., FRAIL, D.A., BERGER, E. AND KULKARNI, S.R.
≪The Angular Size and Proper Motion of the Afterglow of GRB 030329≫.
ApJ, **609**, pp. L1–L4 (2004).

TIENGO, A., MEREGHETTI, S., GHISELLINI, G., ROSSI, E., GHIRLANDA, G. AND SCHARTEL, N.
≪The x-ray afterglow of grb 030329≫.
A&A, **409**, pp. 983–987 (2003).

TIENGO, A., MEREGHETTI, S., GHISELLINI, G., TAVECCHIO, F. AND GHIRLANDA, G.
≪Late evolution of the x-ray afterglow of grb 030329≫.
A&A, **423**, pp. 861–865 (2004).

TOMA, K., IOKA, K., SAKAMOTO, T. AND NAKAMURA, T.
≪Low-luminosity grb 060218: A collapsar jet from a neutron star, leaving a magnetar as a remnant?≫
ApJ, **659**, pp. 1420–1430 (2007).

TRÜMPER, J.E.
≪Observations of cooling neutron stars≫.
In A. Baykal, S.K. Yerli, S.C. Inam and S. Grebenev (eds.), *NATO ASIB Proc. 210: The Electromagnetic Spectrum of Neutron Stars*, p. 117 (2005).

TSURUTA, S.
Ph.D. thesis, , Columbia Univ., (1964) (1964).

TSURUTA, S.
≪Thermal properties and detectability of neutron stars. i. cooling and heating of neutron stars.≫
Phys. Rep., **56**, pp. 237–277 (1979).

TSURUTA, S. AND CAMERON, A.G.W.
≪Cooling and detectability of neutron stars≫.
Canadian Journal of Physics, **44**, p. 1863 (1966).

TSURUTA, S., TETER, M.A., TAKATSUKA, T., TATSUMI, T. AND TAMAGAKI, R.
≪Confronting neutron star cooling theories with new observations≫.
ApJ, **571**, pp. L143–L146 (2002).

TUELLER, J., BARBIER, L., BARTHELMY, S., CUMMINGS, J., FENIMORE, E., GEHRELS, N., HULLINGER, D., KOSS, M., KRIMM, H., MARKWARDT, C. ET AL.
≪GRB 060607: Swift-BAT refined analysis.≫
GRB Coordinates Network, **5242**, pp. 1–+ (2006).

VAN PARADIJS, J., GROOT, P.J., GALAMA, T., KOUVELIOTOU, C., STROM, R.G., TELTING, J., RUTTEN, R.G.M., FISHMAN, G.J., MEEGAN, C.A., PETTINI, M. ET AL.
≪Transient optical emission from the error box of the γ-ray burst of 28 february 1997≫.
Nature, **386**, pp. 686–689 (1997).

VAN RIPER, K.A.
≪Magnetic neutron star atmospheres≫.
ApJ, **329**, pp. 339–375 (1988).

VAN RIPER, K.A.
≪Neutron star thermal evolution≫.
ApJSS, **75**, pp. 449–462 (1991).

VAUGHAN, S., GOAD, M.R., BEARDMORE, A.P., O'BRIEN, P.T., OSBORNE, J.P., PAGE, K.L., BARTHELMY, S.D., BURROWS, D.N., CAMPANA, S., CANNIZZO, J.K. ET AL.
≪Swift observations of the x-ray-bright grb 050315≫.
ApJ, **638**, pp. 920–929 (2006).

VILLASENOR, J.S., LAMB, D.Q., RICKER, G.R., ATTEIA, J.L., KAWAI, N., BUTLER, N., NAKAGAWA, Y., JERNIGAN, J.G., BOER, M., CREW, G.B. ET AL.
≪Discovery of the short γ-ray burst grb 050709≫.
Nature, **437**, pp. 855–858 (2005).

VON WEIZSÄCKR, C.F.
Phys. Zs., **38**, p. 176 (1937).

VON WEIZSÄCKR, C.F.
Phys. Zs., **39**, p. 633 (1938).

WATSON, D., HJORTH, J., JAKOBSSON, P., XU, D., FYNBO, J.P.U., SOLLERMAN, J., THÖNE, C.C. AND PEDERSEN, K.
≪Are short γ-ray bursts collimated? grb 050709, a flare but no break≫.

A&A, **454**, pp. L123–L126 (2006a).

WATSON, D., HJORTH, J., LEVAN, A., JAKOBSSON, P., O'BRIEN, P.T., OSBORNE, J.P., PEDERSEN, K., REEVES, J.N., TEDDS, J.A., VAUGHAN, S.A. ET AL.
≪A very low luminosity x-ray flash: Xmm-newton observations of grb 031203≫.
ApJ, **605**, pp. L101–L104 (2004).

WATSON, D., VAUGHAN, S.A., WILLINGALE, R., HJORTH, J., FOLEY, S., FYNBO, J.P.U., JAKOBSSON, P., LEVAN, A., O'BRIEN, P.T., OSBORNE, J.P. ET AL.
≪The soft x-ray blast in the apparently subluminous grb 031203≫.
ApJ, **636**, pp. 967–970 (2006b).

WAXMAN, E.
≪Angular size and emission timescales of relativistic fireballs≫.
ApJ, **491**, p. L19 (1997).

WAXMAN, E., KULKARNI, S.R. AND FRAIL, D.A.
≪Implications of the Radio Afterglow from the Gamma-Ray Burst of 1997 May 8≫.
ApJ, **497**, p. 288 (1998).

WEINBERG, S.
Gravitation and Cosmology: Principles and Applications of the General Theory of Relativity (Wiley-VCH, 1972).

WIERSEMA, K., SAVAGLIO, S., VREESWIJK, P.M., ELLISON, S.L., LEDOUX, C., YOON, S.C., MØLLER, P., SOLLERMAN, J., FYNBO, J.P.U., PIAN, E. ET AL.
≪The nature of the dwarf starforming galaxy associated with grb 060218/sn 2006aj≫.
A&A, **464**, pp. 529–539 (2007).

WILLINGALE, R., O'BRIEN, P.T., OSBORNE, J.P., GODET, O., PAGE, K.L., GOAD, M.R., BURROWS, D.N., ZHANG, B., ROL, E., GEHRELS, N. ET AL.
≪Testing the standard fireball model of gamma-ray bursts using late x-ray afterglows measured by swift≫.
ApJ, **662**, pp. 1093–1110 (2007).

WILSON, J.R., SALMONSON, J.D. AND MATHEWS, G.J.
≪A binary neutron star grb model≫.
In C.A. Meegan, R.D. Preece and T.M. Koshut (eds.), *American Institute of Physics Conference Series*, volume 428 of *American Institute of Physics Conference Series*, p. 788 (1998a).

WILSON, J.R., SALMONSON, J.D. AND MATHEWS, G.J.
«A gamma ray burst model».
In A. Mezzacappa (ed.), *Stellar Evolution, Stellar Explosions and Galactic Chemical Evolution*, p. 705 (1998b).

WOOSLEY, S.E.
«Gamma-ray bursts from stellar mass accretion disks around black holes».
ApJ, **405**, pp. 273–277 (1993).

WOOSLEY, S.E. AND BLOOM, J.S.
«The supernova gamma-ray burst connection».
ARAA, **44**, pp. 507–556 (2006).

YAKOVLEV, D.G. AND PETHICK, C.J.
«Neutron star cooling».
ARAA, **42**, pp. 169–210 (2004).

YONETOKU, D., MURAKAMI, T., NAKAMURA, T., YAMAZAKI, R., INOUE, A.K. AND IOKA, K.
«Gamma-ray burst formation rate inferred from the spectral peak energy-peak luminosity relation».
ApJ, **609**, pp. 935–951 (2004).

ZHANG, B., FAN, Y.Z., DYKS, J., KOBAYASHI, S., MÉSZÁROS, P., BURROWS, D.N., NOUSEK, J.A. AND GEHRELS, N.
«Physical processes shaping gamma-ray burst x-ray afterglow light curves: Theoretical implications from the swift x-ray telescope observations».
ApJ, **642**, pp. 354–370 (2006a).

ZHANG, B., ZHANG, B.B., LIANG, E.W., GEHRELS, N., BURROWS, D.N. AND MÉSZÁROS, P.
«Making a short gamma-ray burst from a long one: Implications for the nature of grb 060614».
arXiv:astro-ph/0612238v1 (2006b).

ZHANG, W., WOOSLEY, S.E. AND MACFADYEN, A.I.
«Relativistic Jets in Collapsars».
ApJ, **586**, pp. 356–371 (2003).